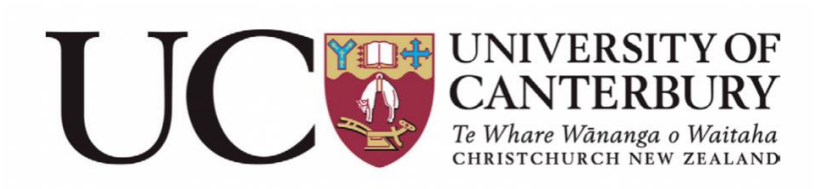

Seismic Performance of Bolted Column Splice Connections in Steel Moment Frames

By

Fahimeh Tork Ladani

Thesis

submitted for the degree of

Doctor of Philosophy

in

Civil and Natural Resources Engineering

At the

University of Canterbury
Christchurch, New Zealand

2019

To my parents,

the most beautiful beings in my life

Abstract

Column splices are common in multi-storey steel construction. When buildings are designed for ultimate limit state, discontinuity in column stiffness due to splice stiffness properties is not often taken into account. Unlike welded splices, bolted connections display some degree of movement before they reach their ultimate strength. Although this phenomenon has received a lot of attention in beam-column connections, the stiffness and ductility characteristics of column splices and their importance on seismic response are less understood. These characteristics are important and should be incorporated in frame seismic analysis to prevent the possibility of an undesirable local or global failure.

A series of cyclic moment and shear tests were performed on bolted and welded column splice connections to understand and quantify their mechanical behaviour. The bolted connections covered a variety of construction methods. Specimens were tested quasi-statically. Flexural and shear performance, with a focus on strength and stiffness properties, were separately investigated via hysteresis loop measurements of rotation and translational shear displacement at the splice. Simple modelling approaches were proposed to predict the backbone behaviour the specimens, and were verified by experimental results.

Non-linear time history analysis of two generic moment frames were conducted to explore the effect of splice shear and rotational flexibility on frame dynamic response. The frames were analyzed for two suites of earthquakes representing Design Basis Earthquake and Maximum Credible Earthquake hazard levels. Rotational properties of column splices were modelled with gap material, while shear-deformation was modeled as bilinear, both consistent with observed experimental results. Parametric studies were undertaken to assess variation with shear elastic

stiffness, post-slip rotational stiffness, and column splice location, and drift profiles were compared against the frame with rigid column splices.

It was observed in the experiments that all splice connections developed greater strength than expected in design, but showed widely varying rotational stiffnesses. Non-linear time history analyses showed some increase in drift response of the stories containing column splices. The response was also found to be sensitive to splice distribution through the frame stories. While bolted column splices may alter dynamic frame response, they do not appear to cause global failure mechanisms in the frames studied, provided they have sufficient strength. In the end, the key findings of this research were translated to implications on local and global design /analysis procedure for moment frames.

Acknowledgements

First, I would like to thank my supervisory team, Professor Gregory MacRae and Professor Geoff Chase for getting me off to a good start. I want to appreciate Professor MacRae for all I learned from him, while demonstrating patience during the course of this research, and Professor Chase for his prompt solutions, enthusiasm and positive energy, which flew into my research and beyond. These have enabled the completion of this thesis.

Secondly, I would like to thank the Natural Hazard Research Platform for funding this project, Structural Engineering Laboratory at the Civil Engineering Department, and John Jones Steel Ltd who supported the experimental program. In addition, I extend my appreciations to the staff and fellow PhD students at the Mechanical Engineering Department who hosted me during the last year of my studies and made it the best time at UC. Especially, sincere gratitude goes to Adam Latham for his intense IT support during the last month.

I also would like to express my heartfelt thanks to my former manager and colleagues Mr Murray Triggs, Mr Trevor Wilson, Mrs Jan Stanway, and Mr Noel Evans whose continuous support and encouragement never let me become distracted from accomplishing my research goals. If it was not for them, I would have not been able to resume my PhD through to completion.

When it comes to friends, I admit how grateful I am for having the most wonderful ones, in particular, Elizabeth Smith and Helen Wells, who were patient with me during rough days and provided me with lots of care.

Last but foremost, I owe my profound appreciation to my parents, who helped me stretching my wings to reach my goals no matter how high. To my family, thank you very much for your presence and unconditional support and care, especially my sister, Dr Faezeh Tork Ladani, for your never-ending encouraging messages in this process and your personal and professional advice throughout life. You have been a mentor and true friend for me.

Contents

List of Figures

List of Tables

Chapter 1. **Introduction**

1.1. **Background**

Column splices are essential parts of multi-story steel frame construction. Limitations on transporting long column pieces to sites and producing sufficiently long members for multi-storey buildings, and the economic advantages of reducing section size with height are some reasons for the ubiquity of column splices in steel construction (Bjorhovde et al., 1996), (*Joints in Steel Construction; Simple Connections (Publication P212)*, 2002), (Bedair, 2011), (Stillmaker et al., 2015), (Ricker, 2000), (Putkey, 1993). There are different methods of constructing column splices, mainly delineated as bolted or welded connections, each of which may offer advantages or drawbacks in construction, cost, and/or performance (Li et al., 2017), (Li et al., 2016), (Katta, 2019), (C. J. Carter et al., 2000), (C. Carter et al., 2000).

One method of constructing column splices is to assemble the column parts in direct contact, so compressive force is directly transferred through the contact area. These splices are referred to as bearing splices (Snijder and Hoenderkamp, 2006), (Padilla, 2014). Contact area can be provided by means of end plates bolted together, or sections in direct contact. Alternatively, non-bearing splices may be constructed (Snijder and Hoenderkamp, 2006), (Padilla, 2014), where there is no contact between the two column parts. This choice means the splice plates themselves must transfer all demands (*Eurocode 3: Design of steel structures- part 1-8: Design of joints*, 2005). Difficulty in quality control in the fabrication of bolted connections is one reason designers often specify non-bearing column splices versus bearing approaches (Mann and Morris, 1984), (Bjorhovde et al., 1996). Figure 1-1 shows the distinction between bearing and non-bearing column splices.

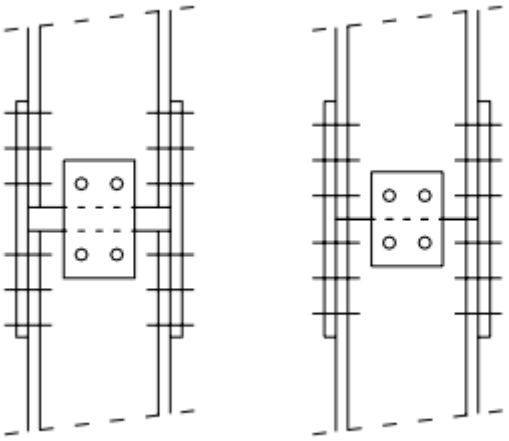

Figure 1-1 *Bearing (right) vs non-bearing (left) column splices* (Snijder and Hoenderkamp, 2006)*, where the non-bearing splice has a gap between the column ends (left).*

Generally, design standards for seismic regions state column splices in moment frames be placed within the middle third of columns (*NZS3404:Part 1, Steel Structures Standard*, 1997), (*AISC 341–10. Seismic provisions for structural steel buildings*, 2010). This specification is rooted in the traditional belief flexural demands in columns in moment frames are small in the middle third region (Bruneau and Mahin, 1991), (Arno and Lnashai, 2002), (Shen et al., 2010). However, inelastic time history analyses for steel moment frames have shown when the higher modes of these structures are excited, significant moments may develop in the middle third of columns in both seismic and gravity frames (Popov et al., 1989), (Park and Paulay, 1975), (Priestley et al., 2007), (Macrae et al., 2004), (Flores et al., 2014). Typically, higher mode contributions to response occur most commonly in tall structures, which are also those requiring column splices. Hence, this assumption means column splice connections are assumed to undergo little demand, when in fact the demand on them could be large.

Figure 1-2 shows several examples of steel column splices. These examples show many types of splices. In particular, Figure 1-2-E shows how splice types can be mixed in one structure.

The entire set shows a range of splice plate design, indicating little consistency. This variation in construction is due, in part, to the lack of stress placed on column splice design in structural design codes due to assumptions on likely column splice demands.

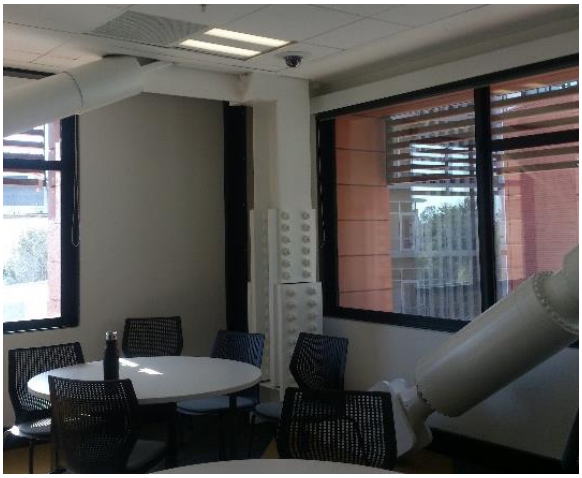

(A) Non-bearing column splice in a corner column in a braced frame with seismic dampers

(B) close view of photo **(A)** showing details of the column splice components

(C) Bolted column splice in a braced frame located close to top floor

(D) Three plate column splice, with flange splice plates on both sides of flanges

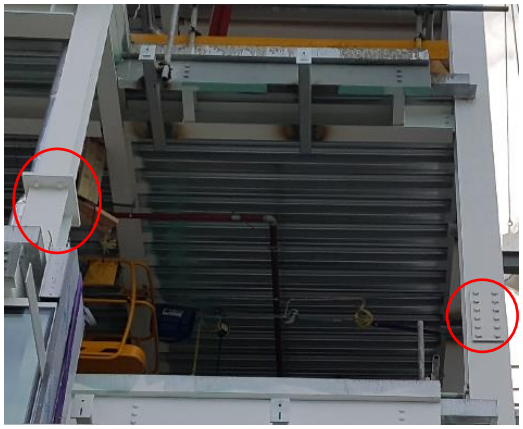

(E) Two types of column splice connections, lap splice and end-plate splice, in one frame

(F) Lap splice connection in photo **(E)** in a braced frame, from a different angle

Figure 1-2 Column splice in steel construction post 2011 Canterbury earthquake, Christchurch

Seismic demand of column splices as part of moment frames have been studied in only a limited amount of literature. This more limited explicit study is unusual, given their ubiquity in use and previously reported seismic damage in column splice connections (Nakashima et al., 1998). In particular and importantly, while spliced columns are studied, the splices themselves and their cyclic fatigue, response and degradation are ignored. This lack of study is due to the assumption splices themselves are rigid. However, this lack of study also creates a significant knowledge gap, given observed damage, which had been largely ignored.

1.2. Studies of Columns/Beams with Splices and Splices

(Gupta and Krawinkler, 1999) studied seismic behaviour of typical steel moment frames with ductile connections, with respect to different seismicity. They found local seismic demands can vary by a combination of a large quantities of factors, and pushover analysis may severely underestimate the demands in certain locations. They observed under certain earthquakes, interior columns could deform in single curvature at a story drift of 0.06 radians, creating a moment demand of approximately 45% of column plastic moment capacity. Fracture of rigid

column splices was not explicitly modelled in these analyses. Thus, this study considers overall column behaviour.

(Hall, 1998), (Almufti et al., 2012), (Hutt, 2017) studied seismic response of steel moment frames with different heights (6, 20, 20 and 50 story buildings). Fracture of welded column splices was modelled in the frame models. All studies concluded most of the fractures occur in beam-column joints, and fractures are less likely in column splices. While these studies assess column splices, they only assess ultimate capacity and not stiffness or degradation.

However, (Hadjiyiangou, 2017), (Akbas et al., 2011) and (Shen et al., 2010) observed flexural demands in column splices in steel moment frames can approximately reach nominal strength of the smaller spliced member under design earthquakes. The studies use a demand-chain concept in which column splice demands were measured in relation to beam hinge rotation. Fracture of column splices were not included in these models. These studies are not conclusive, especially because demands in columns depend on both frame and ground motion properties (Akbas et al., 2014), which means the potential risk is both site and design specific.

None of the aforementioned studies has explicitly considered column splice stiffness properties in their analyses, nor have they considered its change or degradation over cycles or demand. For example, splice rotation is likely to occur in bolted, rather than welded splices, and this effect could change moment distribution in frame members. This last aspect adds a further set of variables to the consideration of frame and ground motion properties. Specifically, the impact of splice type, splice design, and splice performance on structural behaviour, none of which are considered in prior work.

Recently, research was conducted in the United States to investigate seismic performance of welded column splices in steel moment frames. During the 1994 Northridge earthquake, brittle fracture was observed in welded beam-column connections (Mahin, 1998), (Miller, 1998), (Kaufmann et al., 1997). These connections were even susceptible of having brittle behaviour prior to this time, as indicated by (Bruneau and Mahin, 1991). Consequently, fragility assessment of the partial joint penetration welded column splices used in pre-Northridge construction was undertaken. As part of this research program, experimental and numerical studies were conducted to develop fracture mechanics models for these connections to incorporate in moment frame analyses (Shaw et al., 2015), (Stillmaker et al., 2015), (Stillmaker et al., 2017), (Galasso et al., 2015). However, they did not explicitly report on splice stiffness properties in response, since their studies were limited to welded column splices, which have a rigid behaviour with brittle failure due to the weld, which does not offer cyclic ductility.

(Shaw et al. 2015) conducted five full scale tests on partial penetration welded column splices with different detailing. The specimens were tested under cyclic loading, and moment and shear forces were generated at the splice location. The study was also extended by a series of finite element fracture mechanics simulations. The results showed reliable performance of the tested specimens, suggesting partial penetration welded column splices, if high toughness materials and large weld penetration are used, could be adopted in intermediate and special moment frames. The study was further investigated by (Stillmaker et al. 2015) to provide a simple design guideline for implementation or assessment of partial penetration welded joints in steel frames. These researches again lack splice stiffness properties.

The development of fracture-mechanics models for welded column splices enabled (Stillmaker et al. 2017) to investigate the impact of column splice fracture on seismic response of moment

frames. The researchers implemented a gapping and reseating model which represents partial penetration welded column splices. They conducted nonlinear time history analyses of 4 and 20 story moment frames under 100 ground motions with a probabilistic approach. The research concluded column splice fracture does not have a significant effect on frame deformations or possibility of a global collapse. However, the results are limited to steel frames with welded column splices, and consider their brittle, ultimate failure. In contrast, bolted splices can have cyclic degradation and stiffness behaviours were not considered in these and similar studies.

Overall, there are not any specific provisions for the stiffness of column splices in seismic design codes, particularly for more ductile bolted column splices. In addition to seismic response, column splice stiffness may impact the buckling behaviour of columns. Research conducted in Europe has found different configurations and imperfection in the construction of column splices could affect the bucking behaviour of spliced columns (Girão Coelho et al., 2012), (Simão et al., 2012), (Simão et al., 2010), (Girão Coelho et al., 2010), (Snijder and Hoenderkamp, 2008), (Snijder and Hoenderkamp, 2006), (Hoenderkamp and Snijder, 2008). Their research proposed recommendations for spliced columns to maintain stability. Splice rotational stiffness was also found to be one of the contributing parameters to column bucking behaviour (Simão et al., 2012), reinforcing earlier results discussed concerning the impact of splice type, design and implementation.

In particular, (Snijder and Hoenderkamp, 2008), (Snijder and Hoenderkamp, 2006) and (Hoenderkamp and Snijder, 2008) conducted experimental and analytical studies on load bearing capacity of spliced columns. The research proposed stiffness and strength requirements for column splices to avoid premature buckling in spliced columns. The experiments showed an adverse effect of splices on load bearing capacity of slender columns. (Lindner, 2008)

studied performance of columns with flange cover plate splices in bearing contact under axial compression loads. Finite element analysis with full scale experiments were conducted to study the effect of imperfect contact between column sections (within acceptable tolerances) and eccentricity of column sections. A buckling curve for columns with splice at midspan was derived which showed up to ~10% decrease in Euler buckling capacity compared to the uniform column. However, these studies are all considering more global behaviours and not the specific behaviour of the splice, which influences them.

Similarly, (Simão et al., 2012), (Simão et al., 2010) and (Girão Coelho et al., 2010) studied stability of a framed spliced column in sway and non-sway systems using an energy-based formulation. This study concluded splice stiffness can considerably influence the overall system behaviour. Other contributing factors were found to be the ratio of second moment of area of the spliced members, location of splice and end restraint condition of the column. While these studies provide a criterion for column splice stiffness design in columns with different end restraints, they did not provide an approach to quantify column splice rotational stiffness.

Unlike welded column splice connections, which have received more research attention recently, coherent research on seismic performance of bolted column splices has not been performed to date. Scattered experimental studies on flexural, shear and axial behaviour of bolted splice connections in beams/columns can be found in the literature, but they primarily focus on limited cases and more spliced-member behaviours, rather than the splice itself. In addition, they primarily focus on ultimate capacity under monotonic loading, rather than cyclic performance. This knowledge gap is significant because bolted splices in columns are common.

Of these studies, (Edwards et al., 1929) performed tests on seven mixed welded-bolted splices under pure bending about their minor and major axes. The form of these splices is different from what is commonly used in current practice. The load deformation of the specimens were compared against a uniform column of the smaller member size. It was observed the initial stiffness of the spliced columns could decrease by up to 50%. A simple analysis method was proposed to estimate ultimate strength capacity of the connections, which showed good agreement with the test results. Thus, the outcome focused on ultimate behaviour.

Further, (Beedle and Christopher, 1963) and (Douty and McGuire, 1965) reported some experiments on beam bolted lap and end plate splices under pure bending about their major axes. The studies showed appropriately designed and detailed bolted splices could exhibit full plastic capacity of the beam members, with large plastic rotation capacities. Again, these studies focus on ultimate capacity of these connections under monotonic loading.

(Yura et al., 1982) conducted tests on spliced rectangular bars under tensile loads to investigate the effect of number and thickness of fillers plates on the ultimate strength of the connection. Smaller ultimate capacity and larger deformation were observed for the connections having undeveloped filler plates (i.e. if filler plates are not extended beyond the splice plates). Furthermore, it was found that introducing an undeveloped filler plate to the connection could reduce the slip coefficient by ~17%. The slip coefficient was further decrease by adding additional filler plates. These observations emphasize the conjecture that column splices, typically of different member sizes, may behave differently to beam splices which are of similar member sizes.

(Green and Kulak, 1987) tested six bolted web splices, under shear loading, and developed a method of analysing the ultimate capacity of the connections, based on the equilibrium of forces. As part of the methodology, they studied shear behaviour of high strength bolts in tension and compression jigs. It was found the ultimate strength of bolts in compression jigs are 10% larger than that in tension jigs. This difference was attributed to the presence of pry forces in tension jigs. The best agreement between the test results and estimation method was reached when the ultimate strength of bolts in tension jigs were used, along with the assumption shear force acts at the centreline of the splice, rather than centroid of the opposite bolt group. The splices in this research were missing flange cover plates, limiting the scope of the results to web plate only splices, which are uncommon, thus limiting generality.

(Borello et al., 2011), (Denavit et al., 2011), (Borello et al., 2009) conducted compression tests on slip critical connections and investigated parameters affecting behaviour of the connection, such as the number of filler plates, their thickness, and development status (i.e. if filler plates are extended beyond the splice plates, and bolted to spliced members). The study indicated using filler plates reduces the slip load, and to a smaller degree, the ultimate capacity of the connection. However, using developed filler plates can nullify the adverse effects. This study reinforces the findings by (Yura et al. 1982) in real scale column splice connections under compression forces. The outcome of these studies is limited to overall compression behaviour of spliced columns, and does not cover flexural or shear behaviours.

1.3. **Knowledge Gaps and Summary of Specific Relevant Prior Art**

As can be understood, the limited numbers of studies focusing on the splice connection itself were limited in scope, and thus not comprehensive. More specifically, while these previous experimental studies cover a range of axial compression, shear and bending loading, they

mainly focused on ultimate capacities of these splice connections, rather than stiffness, as sub-ultimate capacity behaviour, including cyclic stiffness and mechanics, and degradation over repeated cycles. In addition, in all the experiments reported, monotonic loading was applied to the specimens. As a result, the effect of cyclic loading on the performance of these connections could not be captured, limiting their applicability to seismic cases, particularly where significant aftershocks and degradation behaviour might be expected, and would be necessary to understand in making post-event decisions or the potential level of damage, retrofit, and possible reuse/demolition.

These limitations are significant if we are to understand ongoing splice behaviour during and after seismic events. Furthermore, all of the flexural experiments on bolted splices were conducted on spliced members with the same section sizes. Therefore, the effect of variation in sizes of spliced members, which can be common, and using filler plates on flexural performance of splices are unknown.

Hence, these experimental splices were not representative of actual column splices in practice, where section size changes regularly, and will impact splice stiffness response behaviour. Finally, the research conducted to date, does not cover shear and flexural performance of bolted lap splices about their minor axes. These behaviours are typical as an earthquake can strike from any angle, causing response in multiple directions about both major and minor axes (Nudel et al., 2015). Hence, there is a further significant gap in the correct knowledge of splice behaviour, where it is simply assumed splices will perform well.

Overall, this lack of comprehensive knowledge about seismic demands and behaviour of column splices in moment frames has led to different design requirements in different seismic

design codes. The current New Zealand standard for designing steel structures, NZS 3404, requires column splices in special moment frames to provide at least 50% of reduced flexural strength of the smaller column as well as 25% of its design shear capacity. In addition, column splices are required to be designed for the moment demand associated with the capacity design derived actions for columns (NZS 3404, clause 12.9.1.2.2). However, this approach may not satisfy the capacity design philosophy considering the full capacity of the smaller column at the splice, and could introduce weaknesses in the frame. In contrast, more stringent requirements, such as fully applying capacity design to the splice from the smallest columns, could lead to impractical or uneconomical designs.

On the other hand, current US standard for seismic design of structural steel, AISC 341-10, requires flexural capacity of column splices in special moment frames to be full strength of the smaller column, along with the shear capacity to sustain formation of plastic hinges at both ends of the column (AISC 341-10 2010). This requirement influenced the construction practice for column splices from partial penetration welding, common prior to the 1994 Northridge earthquake, to full penetration welding. This requirement has been perceived as excessively stringent by recent studies (Stillmaker, 2016).

1.4. **Specific Research Need**

From this overview of the state of the art in column splice design, analysis, and implementation, it can be concluded that bolted splices exhibit some degree of flexibility and ductility in comparison to welded splice connections. However, the mechanical behaviour of bolted column splices is not well understood, and has thus never been incorporated in the analysis of multi-story buildings. Therefore, it is unclear if the flexibility of column splices could alter the

dynamic response of buildings, and in particular, whether it presents any risk to seismic performance.

To prevent undesired failure or sway mechanism of steel moment frames, research is needed to quantify the performance of these connections. In particular, it should include development of analytical models for analysis and design, which are currently lacking and design codes are left to rely on safety factors. This research should also investigate the sensitivity of frame dynamic responses to more realistic behaviour of bolted column splices. All of these outcomes would advance knowledge and understanding of the long-term behaviour and safety of this commonly used structural connection.

1.5. **Objective and Scope**

Analytical and experimental studies are conducted to address the specific need and knowledge gap presented and discussed in the previous section. Experiments are conducted to study the cyclic performance of splice connections in universal column sections under major and minor axis bending. Bolted and welded connections are tested in bending to quantify a realistic range for stiffness values of these connections. In addition, bolted splices are tested in shear to quantify shear performance of these connections, which has also not been examined previously. The results of the experiments are compared with component-based analytical models, created in this thesis, which we derived to provide useful analytical design equations for practitioners rather than exact mechanics of all behaviours. Lastly, nonlinear time history analyses are conducted to investigate dynamic responses of mid- and high-rise steel regular moment frames *with special consideration of column splice flexibility*. In the end, this study aims to answer the following questions:

1- What is the difference in cyclic performance of different types of splices under shear and bending?
2- Can we develop simple models to predict splice behaviour?
3- Is there any interaction between web and flange splices under shear or bending, and how could we design robust splice connections?
4- What level of shear and moment demands would be expected in column splices in steel moment frames, and what are the chances of any failure of these connections?
5- How sensitive is seismic response of a frame to strength and flexibility properties of column splices?
6- How sensitive is the seismic response of a frame to the location of splices within the story?

1.6. **Preface**

Chapter 2 starts with the experimental program and the specimens studied. The chapter provides detailed information about the mechanism of the testing frame to facilitate cyclic loading, loading regime and instrumentation. It is followed by an outline of specimens tested in this research, column splice connection design principles, and background information about their fabrication. Finally, it describes how the testing data from the instrumentation was translated into the information utilised for modelling of column splices in macro-models (frame analysis).

Chapter 3 presents the results from ten moment tests and three shear tests. The specimens are made of universal column sections. The results include moment-rotation or shear- translational deformation hysteresis loops for bending or shear loading, respectively. The results are followed by discussions and key observations for each experiment. This information provide

an insight into the mechanism of these connections, and could be helpful towards developing analytical backbone models replicating the behaviour of these connections.

Chapter 4 presents the analytical approaches used to predict the behaviour of splice connections in bending and shear. The approaches vary for different types of bearing lap splices, non-bearing lap splices, end plate splices, and welded splices in bending. In addition, the specimens in shear have different mechanisms from those in moment tests. Several assumptions are adopted, as appropriate, to simulate the backbone behaviour of these connections. These assumptions may pose limitations on the application of these models for general purposes. The chapter will be closed by a comparison of predicted backbone models with the test results.

Chapter 5 includes nonlinear time history analyses conducted on two generic steel moment frames incorporating column splice characteristics. The chapter outlines details about the frames studied and how splices were modelled based on the experimental results. Sensitivity of frame responses to parameters like column splice stiffness and location within a story is investigated and presented.

Chapter 6 presents the implications of this research from different perspectives. It discusses how the findings from this research could be implemented in global frame analysis and design. From a local perspective, design recommendations are proposed for robust column splice connections to ensure desirable frame responses.

Chapter 7 concludes this thesis with a summary about the scope of research and key findings considering the limitations.

Chapter 8 proposes avenues to extend this research in the future.

1.7. Summary

This chapter provided background information on research to date on the seismic performance of column splices in steel moment frames. It also presented the gaps in the literature and dearth of studies in the area where there may be potential unidentified and unquantified risk. In doing so, it identified where the need for more research lies, develops the problem addressed in this thesis, and provides the scope and objectives of the work in this thesis.

Chapter 2. **Experimental Study**

2.1. **Introduction**

Flexural and shear flexibility of column splices may affect both the structural dynamic response and the possibility of an undesirable local or global failure. It is thus necessary to investigate the performance of column splice connections under demands such a splice may experience during earthquake shaking. This evaluation should lead towards quantifying risk and providing data and tools to improve and optimise design.

For this reason, a series of shear and moment tests were conducted to study the performance of bolted splices in particular, as they present a common usage and a particular knowledge gap. Bolted splice connections are commonly used in New Zealand practice due to faster construction on site. A welded specimen was also tested in bending to compare the behaviour of the bolted connections versus a rigid (welded) connection. This chapter provides detailed information about the test program and the specimens studied. Detailed design calculations of column splice connections and their shop drawings are provided in Appendix A. The test results and observations are presented in Chapter 3.

2.2. **Method**

2.2.1. ***Specimens***

Universal Column sections were used for all experiments. The total length of the specimens were 2.4m consisting of two 1.2m long members. Bearing and non-bearing splices were both tested. Bearing splices were fabricated with bolted end plates and bolted lap-splice plates.

Bearing splice specimens were made of 310UC158 and 310UC118 column sections, Grade 300. The pair provides complete bearing area at the contact surface of the sections. Non-bearing splice specimens were made of 310UC158, 310UC118 and 250UC89.5 column sections, Grade 300. This selection enabled the investigation of the performance of connections with different numbers of filler plates, which can vary in design and application and may impact splice mechanics and performance (Yura et al., 1982), (Lee and Fisher, 1968), (Dusicka and Lewis, 2010). Nominal section and material properties of universal columns are provided in Appendix A, Table 1. The loading diagram of specimens are illustrated in Section 2.2.4 for both moment and shear experiments.

Major Axis Bending

Table 2-1 lists the details of the specimens tested about their major axes. The table includes the plan and elevation drawings of splice connections and bolt layouts, with nominal sizes and material properties of the splice plates and bolts. More specific details and shop drawings of the splice plates are provided in Appendix A. The choices represent a range of possible constructions and capture variations within the New Zealand standard (*NZS3404:Part 1, Steel Structures Standard*, 1997).

Specimens #1-3: Specimen #1 targeted the minimum design bending and shear actions prescribed in the New Zealand Steel Structures Standard, NZS3404 clause 12.9.2.2, for seismic columns in ductile moment frames. These specifications are 50% of the reduced moment capacity of the smaller section at the splice joint ($0.5\phi M_r$) and 25% of the reduced shear capacity ($0.25\phi V_n$). Specimen #2 had the same flange splice components, but was not spliced at the web. Specimen #3 splice was stronger and targeted 70% of the reduced moment capacity ($0.7\phi M_r$) of the smaller section and 25% of the reduced shear capacity ($0.25\phi V_n$). Since the bolt

holes reduce the area of flanges, the nominal section capacity of column sections decreases at the splice location to approximately $0.75\phi M_p$ for these specimens.

Specimens #4-6: Specimens #4, #5 and #6 are non-bearing splices. Specimens #4 and #5 were similar to Specimen #1, but have a gap of 10mm at the splice joint. Therefore, they possess same design capacities as Specimen #1. Specimen #6 has a non-bearing splice joint, but is of different section sizes. The connection design targeted 50% and 25% of the reduced moment and shear capacities (ϕM_p and ϕV_n) of the smaller column member.

Specimens #7-8: Specimens #7 is an end plate bolted connection designed for approximately 50% of the reduced moment capacity. Specimen #8 is a fully butt-welded joint to develop the full moment capacity of the smaller member. These last two specimens provide common comparators, as semi-rigid (end plate splice) and rigid (weld) column splice connections.

Specimens #1-3 investigates the flexural performance of cover plate column splice connections with different ultimate capacities. Specimens #4-6 investigates the effect of filler plates on the flexural performance of cover plate splices. In addition, specimens #4-6 provide comparison between bearing (specimens #1-2) and non-bearing (specimens #4-6) column splice connections. Specimens #7 and #8 provide comparison between the three common methods of construction column splice connection, which are cover plate bolted splices, end plate bolted splices and welded splices.

Design principles and fabrication information for the specimens can be found in Sections 2-2-2 and 2-2-3. Design calculations for the specimens can be found in Appendix A.

Table 2-1 Details of specimens – major axis moment (Table continued on the next page)

Specimen	Top and side views	Column Sections	Flange cover plate		Web cover plate		Flange bolts			Web bolts		
			Thickness (mm)	Grade	Thickness (mm)	Grade	Size	Number	Grade	Size	Number	Grade
#1	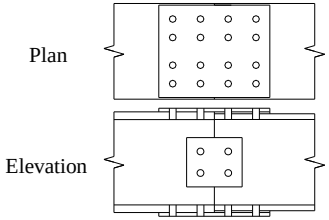	310UC158 310UC118	12	300	6	350	20	32	8.8	20	4	8.8
#2	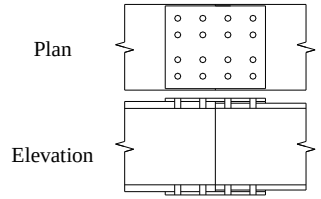	310UC158 310UC118	12	300	-	-	20	32	8.8	20	-	-
#3	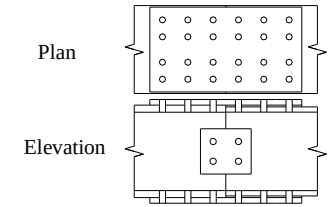	310UC158 310UC118	20	300	6	350	20	48	8.8	20	4	8.8
#4	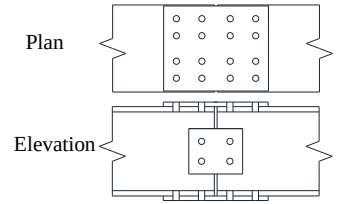	310UC118 310UC118	12	300	6	350	20	32	8.8	20	4	8.8

#5	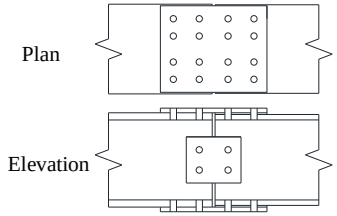	310UC158 310UC118	12	300	6	350	20	32	8.8	20	4	8.8
#6	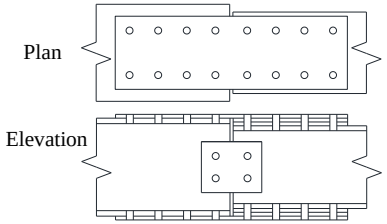	310UC96.8 250UC89.5	12	300	6	350	20	32	8.8	20	4	8.8
#7	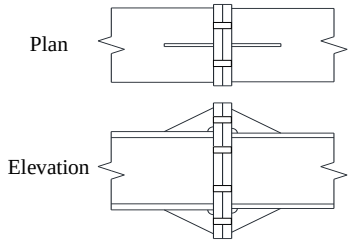	310UC158 310UC118	32	350	-	-	24	8	8.8	-	-	-
#8	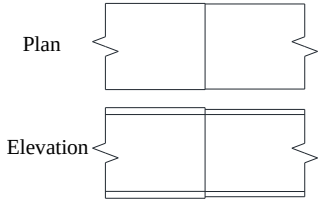	310UC158 310UC118	-	-	-	-		-	-		-	-

Minor Axis Bending

Specimens #9-10: Specimen #9 was designed to be the same as Specimen #1, but tested about its minor axis. Specimen #10 is similar to Specimen #9, but has twice as many bolts as Specimen #9 for greater capacity. The specimens are made from sections of 310UC158 and 310UC118, Grade 300. Together these specimens assess the flexural performance of lap splice connections about their minor axes.

Details of these specimens can be found in Table 2-2. The table includes the plan and elevation drawings of splice connections and bolt layouts, with nominal sizes and material properties of the splice plates and bolts. Shop drawings of splice plates are also provided in Appendix A, along with design calculations. Design and fabrication information for the specimens can be found in Sections 2-2-2 and 2-2-3.

Table 2-2 Details of specimens – Minor axis moment

Specimen	Side and top views	Column Sections	Flange cover plate		Web cover plate		Flange bolts			Web bolts		
			Thickness (mm)	Grade	Thickness (mm)	Grade	Size	Number	Grade	Size	Number	Grade
#9	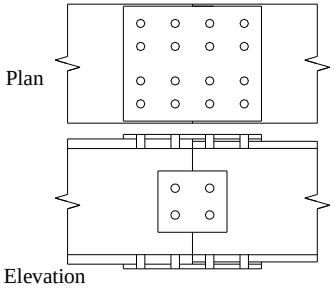	310UC158 310UC118	12	300	6	350	20	32	8.8	4	4	8.8
#10	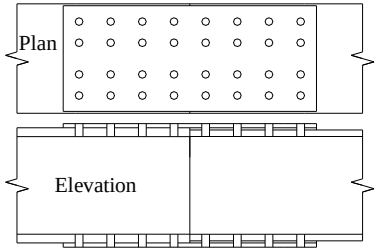	310UC158 310UC118	12	300	-	-	20	64	8.8	-	-	-

Major Axis Shear

Specimens #11-13: High shear tests were performed to investigate the shear behaviour of lap splices about the major axis, and the contributions of web and flange splice plates in carrying the shear. Specimens #11 and #12 were similar to Specimens #1 and #2, respectively. Specimen #13 is similar to Specimen #11 but the flange splice plates were eliminated.

Table 2-3 shows the details of the specimens, which includes the plan and elevation drawings of splice connections and bolt layouts, with nominal sizes and material properties of the splice plates and bolts. Fabrication information for the specimens can be found in Section 2-2-3. Shop drawings of these splice plates are similar to Specimen #1, which can be found in Appendix A.

Table 2-3 Details of specimens – Major axis shear

Specimen	Top and side views	Column Sections	Flange cover plate		Web cover plate		Flange bolts			Web bolts		
			Thickness (mm)	Grade	Thickness (mm)	Grade	Size	Number	Grade	Size	Number	Grade
#11	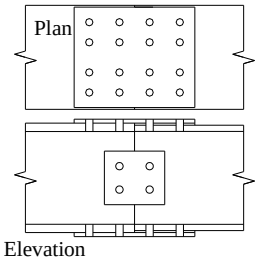	310UC158 310UC118	12	300	6	350	20	32	8.8	20	4	8.8
#12	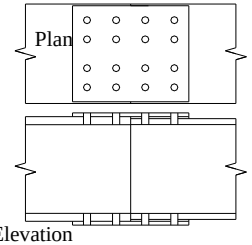	310UC158 310UC118	12	300	-	-	20	32	8.8	20	-	-
#13	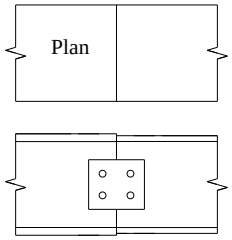	310UC158 310UC118	-	-	6	350	-	-	4	8.8		

2.2.2. *Design principles*

Bolted Cover Plate Splice

Specimens #1 to #6 were designed based on the model proposed in the Connection Design Guide 13, which is in accordance with Australian Standard AS 4100. The model assumes moment demand is transferred through the flange splice plates acting in tension and compression, while the web splice plates transfer shear demand. No interaction between the web and flange splices is considered (Hogan and Munter, 2007).

In this model (Hogan and Munter, 2007), the capacity of bolts at flanges is determined based on the minimum value of shear capacity of bolt, local bearing capacity and end plate tear-out of flange and splice plate. The capacity of flange splice plate is determined as the minimum of yield capacity on gross area or fracture capacity on net area excluding the holes. The design shear capacity of the web cover plate, $0.5f_y t_i d_i$, is also required to be greater than the design shear action. In this case, f_y,t_i and d_i are the yield stress, thickness and width of the web plate, respectively.

Splice connections with Category 8.8/TF bolts are used to limit slip at service level loads. For the flange splice configuration of Specimens #1 and #2, slip is estimated to occur at $0.19M_p$ without considering the capacity reduction factor, 0.7, at serviceability limit state (Hogan and Munter, 2007). Slip moment was calculated assuming the friction coefficient is 0.35 for rolled steel surfaces, and tension per M20 bolt at installation (proof load) is 145kN (Hogan and Munter, 2007). Slip is predicted at $0.29M_p$ for the flange splice configuration of Specimen #3, based on the above description.

Based on the design model, the specimens are expected to develop the capacities for each component as listed in Tables 2-4 and 2-5. All estimations are based on the reduced design capacities of the components. Design calculations can be found in full in Appendix A.

Bolted End Plate Splice

Specimen #7, the end plate splice, was designed in accordance with "HERA REPORT R4-100.1:2003" (Hyland et al., 2003). The model follows the principles set by BCSA and SCI in their publication (*Joints in Steel Construction: Moment Resisting Joints to Eurocode3 (Publication P398)*, 1995). To develop sufficient rigidity in the connections with end plates thinner than 20mm, the model requires the plate and bolt strength not to be governed by formation of four plastic hinges in the equivalent T-stub (See Appendix A for illustrations). In addition, the maximum bolt offset from the section flange, web or gusset plate is recommended to be less than 60mm.

In this case, the top or the bottom bolt group/plate tension capacity limits the moment capacity of the connection, while the bolt group at the other side is assumed to transfer shear actions. Three potential failure modes, which include formation of either two or four plastic hinges in equivalent T stub or bolt failure, incorporate bolt-prying effects in the assessment (Hyland et al., 2003). End plate strength limits are pull-out flexure, pull-out shear, transverse shear, bearing and tear-out at the bolt holes extended beyond flanges (Hyland et al., 2003). The estimated capacity of Specimen #7 based on the design model is listed in Table 2-4. Full design calculations and equations can be found in Appendix A.

Welded Splice

No specific design was carried out for Specimen #8. The abutted joint was welded through the full thickness of web and flanges by a certified welder.

Table 2-4 Reduced design capacity of connections tested under moment about major axis (ϕ=*0.9* per NZS3404)

Specimen	Design capacity of flange splice				Design capacity of web splice			
	Plate component		Bolt component		Plate component		Bolt component	
	Capacity	Failure mode	Capacity	Failure mode	Capacity	Failure mode	Capacity	Failure mode
#1	$0.5\phi M_p$	Plasticity in the net area	$0.44\phi M_p$	Shear in bolt	$0.58\phi V_y$	Shear failure	$0.35\phi V_y$	Shear in bolt
#2	$0.5\phi M_p$	Plasticity in the net area	$0.44\phi M_p$	Shear in bolt	-	-	-	-
#3	$0.84\phi M_p$	Plasticity in the net area	$0.67\phi M_p$	Shear in bolt	$0.58\phi V_y$	Shear failure	$0.35\phi V_y$	Shear in bolt
#4	$0.5\phi M_p$	Plasticity in the net area	$0.44\phi M_p$	Shear in bolt	$0.58\phi V_y$	Shear failure	$0.35\phi V_y$	Shear in bolt
#5	$0.5\phi M_p$	Plasticity in the net area	$0.44\phi M_p$	Shear in bolt	$0.58\phi V_y$	Shear failure	$0.35\phi V_y$	Shear in bolt
#6	$0.57\phi M_p$	Plasticity in the net area	$0.49\phi M_p$	Shear in bolt	$0.76\phi V_y$	Shear failure	$0.45\phi V_y$	Shear in bolt
#7	$0.74\phi M_p$	Plastic hinges in T-stub, Mode 2 failure	$0.56\phi M_p$	Tension in bolt	$5.3\phi V_y$	Transverse tearing in bolt hole 1st	$0.99\phi V_y$	Shear in bolt
#8	Full penetration butt weld				Full penetration butt weld			

Table 2-5 Reduced design capacity of connections tested under moment about minor axis (ϕ=*0.9* per NZS3404)

Specimen	Design capacity of flange splice			
	Plate component		Bolt component	
	Capacity	Failure mode	Capacity	Failure mode
#9	$0.67\phi M_{py}$	Plasticity due to bending	$0.49\phi M_{py}$	Shear in bolt
#10	$0.67\phi M_{py}$	Plasticity due to bending	$1.28\phi M_{py}$	Shear in bolt

2.2.3. *Specimen Fabrication*

For the specimens using 310UC158 and 310UC118 columns (Specimens #1, 2, 3, 5, 7, 8, 9, 10, 11, 12, 13), the dimensional difference of the section heights is 12mm, which is filled by two 6mm-filler plates of mild steel on each side of flanges. Two web splice plates of thickness of 6mm were used on both sides of the webs. Since the difference in the web thicknesses was less than 3mm on each side, no filler was used to fill the gaps. The plates bent with bolt

tightening and closed the gaps. Specimen #6 consisted of 310UC96.8 and 250UC89.5 columns. The dimensional difference of the section heights is 48mm, which was filled with two 12mm filler plates on each side of flanges.

High strength zinc-plated bolts, fully threaded through the length, were used to connect the flange splice plates. A few of the flange bolts were partially threaded due to a construction oversight as described in Table 2-6. Web bolts were from the same material, but partially threaded. Standard flat round washers for high strength structural M20 bolts are 3.1-4.6mm thick and their outside diameter is 37-39mm (Blacks Fasteners, n.d.). Some of the washers supplied with the bolts were later found to be approximately 1-2mm thick and 37mm of outside diameter. The holes were 2mm oversized (22mm for M20 bolts) and cut using drill bits. Table 2-6 provides more information about fabrication for each specimen.

New Zealand steel standard (NZS3404 1997), clause 14.3.6.3 specifies "all oil, dirt, loose scale, loose rust, burrs, fins and any other defects on the surfaces of contact preventing solid seating of the parts in the snug-tight condition shall be removed". In Specimen #1, the contact surfaces were contaminated with drilling oil and loose particles. No attempt was made to clean the surfaces before assembling the parts, as a result of construction oversight. For the rest of the specimens with lap splice plates, the contact surfaces were cleaned with a wire brush to remove the loose mill scale and then wiped with solvent to remove any contamination with drilling oil.

Specimen #1 was assembled horizontally. A gap of 0.45mm was observed between the abutted columns over the bottom flanges. The rest of the specimens were assembled vertically to ensure the members are abutted during the fabrication of bearing specimens. Figure 2-1 shows the typical surface preparation and assembling of the specimens.

(A) Connection surfaces cleaned prior to assembly

(B) Assembling bolted connections, bolts were tightened from centre towards edges

Figure 2-1 Specimen preparation

The bolts in Specimen #1 were tightened with a torque wrench set to apply 145Nm. However, the recommended torque by the fabrication company to reach approximately 65% of the proof load is 372Nm. For the rest of the similar specimens, the bolts were proof tightened with 1/3 of a full turn as recommended by the manufacturer, expecting to obtain 145kN tension in the bolts.

Specimen #7 is an end-plate bolted splice. The M24 bolts are partially threaded with 40mm unthreaded length. The end-plates experienced distortion due to welding. This distortion caused a gap of 1-1.5mm between the plates. The bolts were proof tightened with 1/3 of a full turn as recommended by the manufacturer to obtain 210kN tension in bolts.

Table 2-6 Fabrication details of specimens

Specimen	Flange Bolts	Washers	Surface Preparation	Contact Area Condition
#1	Fully threaded	Substandard	Contaminated with drilling oil	0.45mm gap between bottom flanges
#2	Fully threaded	Substandard	Cleaned	Full contact
#3	Fully threaded	Substandard	Cleaned	0.6mm gap over half of top flange 1.5mm gap over half of bottom flange
#4	Fully threaded	Substandard	Cleaned	Non-bearing -10mm gap
#5	Top flange: all bolts 20mm unthreaded length Bottom flange: 4No. 20mm unthreaded length, rest fully threaded	Substandard	Cleaned	Non-bearing -10mm gap
#6	Fully threaded	Substandard	Cleaned	Non-bearing -10mm gap
#7	40mm unthreaded	Standard	Cleaned	1-1.5mm gap throughout contact area
#8	NA	NA	NA	NA
#9	Fully threaded	Substandard	Cleaned	Full contact
#10	Fully threaded- 3No. 20m unthreaded length	Substandard	Cleaned	1mm gap over half of top flange
#11	Fully threaded	Standard	Cleaned	Full contact
#12	Fully threaded	Standard	Cleaned	Full contact
#13	Fully threaded	Standard	Cleaned	Full contact

2.2.4. *Test Setup*

Pure moment test

Figure 2-2-A shows the diagram of the moment test setup and its components using the Dartec 10MN universal testing machine. Four columns, not shown in Figure 2-2-A, support the rigid roof of the Dartec, which can be fixed at any height. The columns can be seen in Figure 2-2-B, which shows the actual test setup used in this study. A hydraulic actuator at the bottom of the machine applies vertical forces.

The top and bottom setup beams are attached to the Dartec by four 51mm (2 in) bolts of high strength steel, AISI 4140. While the bottom beam can move up and down with the actuator, the top beam is fixed to the Dartec roof and is stationary. Special connections were designed to facilitate the cyclic loading. The connections accommodate two rollers each side of the

specimens at the loading and supporting points. The rollers are pinned to two plates with slotted holes. This design restrains the ends of the rollers from vertical movements, while providing freedom for the test specimen to move horizontally. Figure 2-3-A shows a close view of these connections.

Three M36 (36mm diameter) Grade 10.9 threaded rods are located at each side of the specimen to clip the rollers on the specimen. The threaded rods are tightened sufficiently to keep the rollers on the specimen, avoiding pre-tensioning of threaded rods and restraining horizontal movement of the specimen. The connections are fixed to the top and bottom beams with rigid pedestals. Eight M24 high strength bolts connect the pedestal blocks to the setup beams.

When the actuator moves up, the end bottom rollers push up the specimen ends and the middle top rollers, apply downwards force on the specimen. When the actuator moves down, the forces are applied in the opposite direction through the opposite rollers. In this state, the threaded rods are engaged to transfer the forces. This setup provides constant moment between the loading points without a significant shear force. The displacements of the specimen were measured at four bearing points, as well as the centre to measure the deformation profile of the specimen.

Although the right end rollers were restrained from rolling, it was observed the specimen could slip on these rollers under heavy loads. Therefore, a link was provisioned to stop the slippage while allowing the end to rotate. Figure 2-3-B shows a close view of the link.

Figure 2-4 shows a simple diagram of loading and end supports the test rig provides for moment testing. This loading thus tests the splice explicitly under pure moment. The overall column behaviour is not the interest of this study.

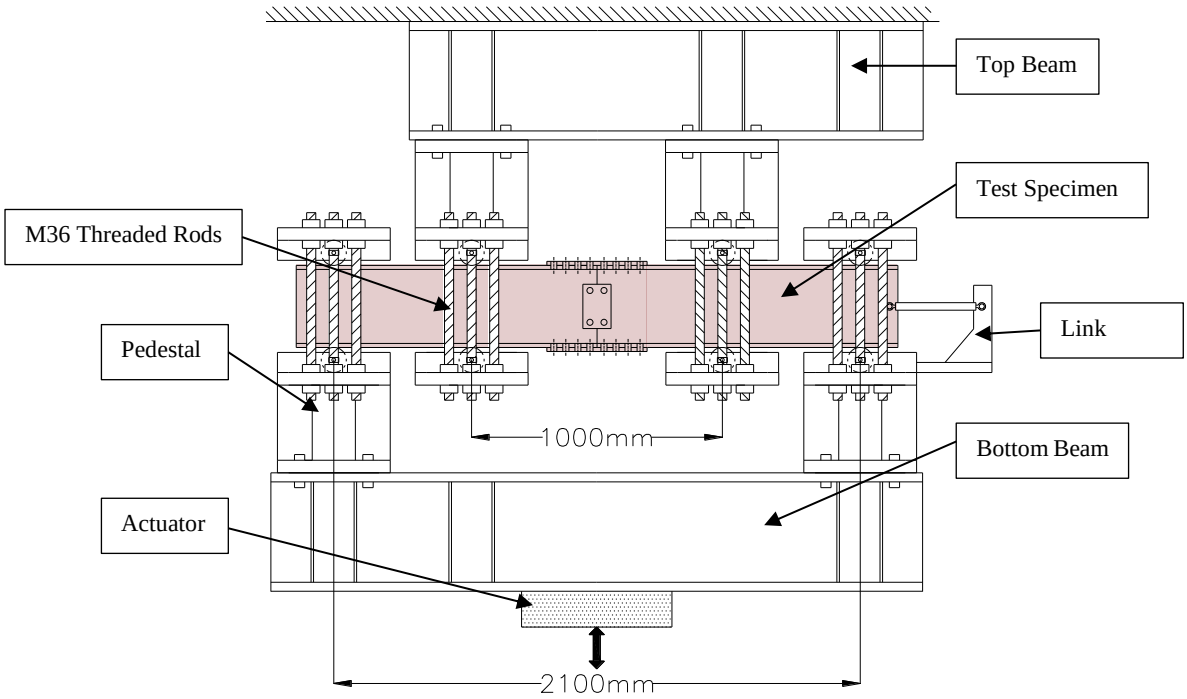

(A) Moment test rig and components

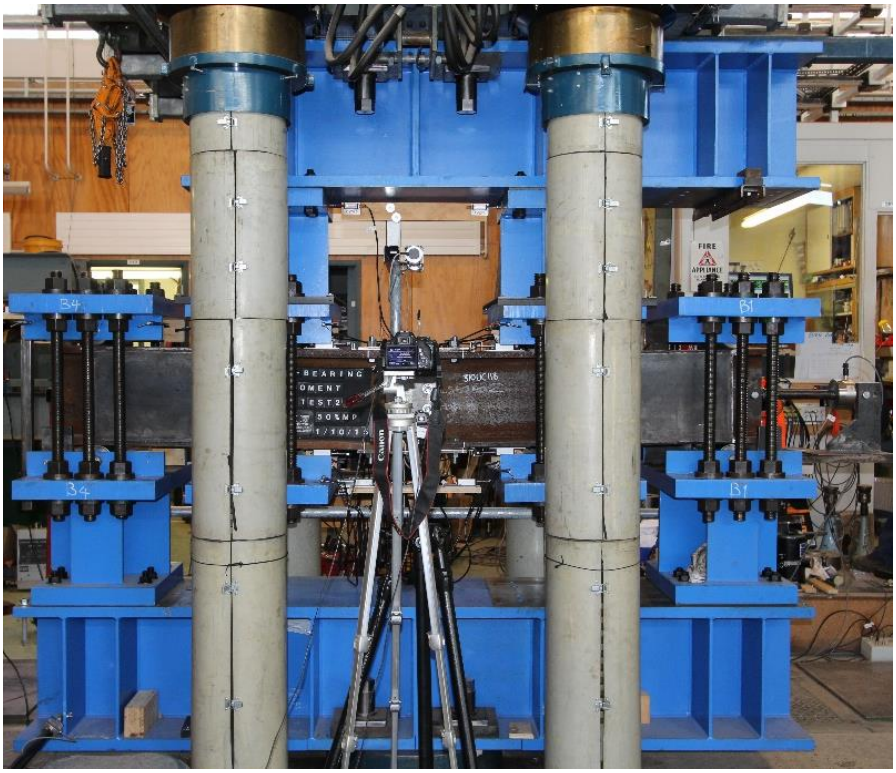

(B) Moment test rig in blue under Dartec machine, a camera obscures the splice in this view

Figure 2-2 Pure moment test setup using Dartec loading machine with input motion at the base double arrow shown.

(A) Close view of connections facilitating cyclic loading

(B) Close view of end link restraining horizontal movement while allowing rotations

Figure 2-3 Close view of test rig components

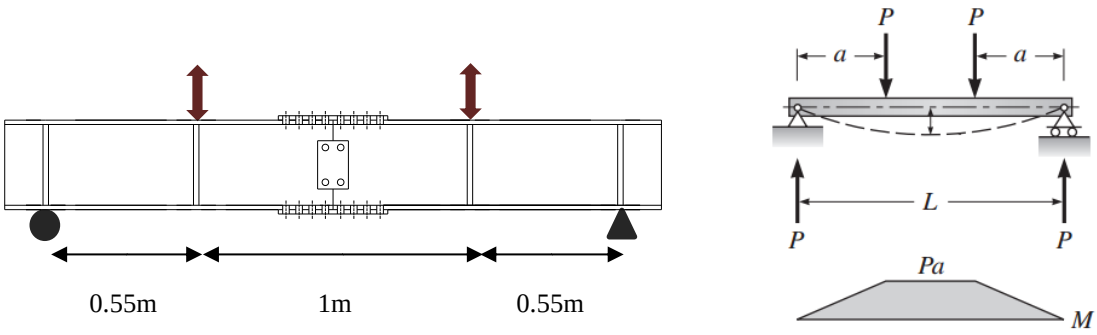

Figure 2-4 Moment test loading diagram and specimen dimensions. Double arrows indicate cyclic loading

High Shear Test

Figure 2-5 shows the configuration of the high shear test setup using the Dartec machine. The setup is similar to the moment test setup. The components and the mechanism of the system are as explained previously in Section 2-2-4. The only difference here is that the support and loading points were shifted horizontally on the right side as can be seen in the figure. The outcome is a loading diagram yielding high shear demand at the splice location. Figure 2-6 shows a simple diagram of loading and end supports the test rig provides for shear testing.

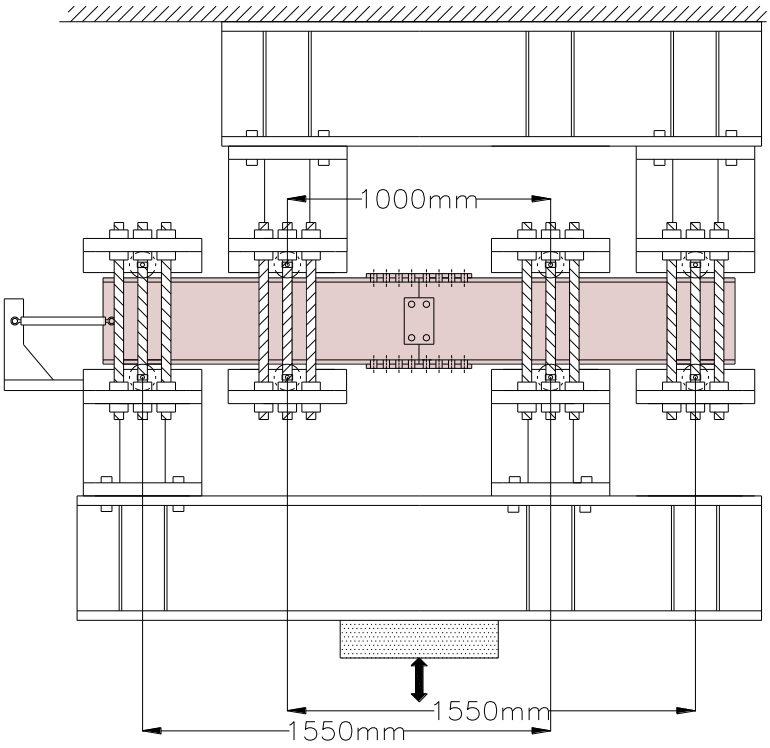

(A) High shear test rig (components are similar to those in Figure 2-2-A). Loading and support points are swapped on the right side compared to moment test rig in Figure 2-2-A.

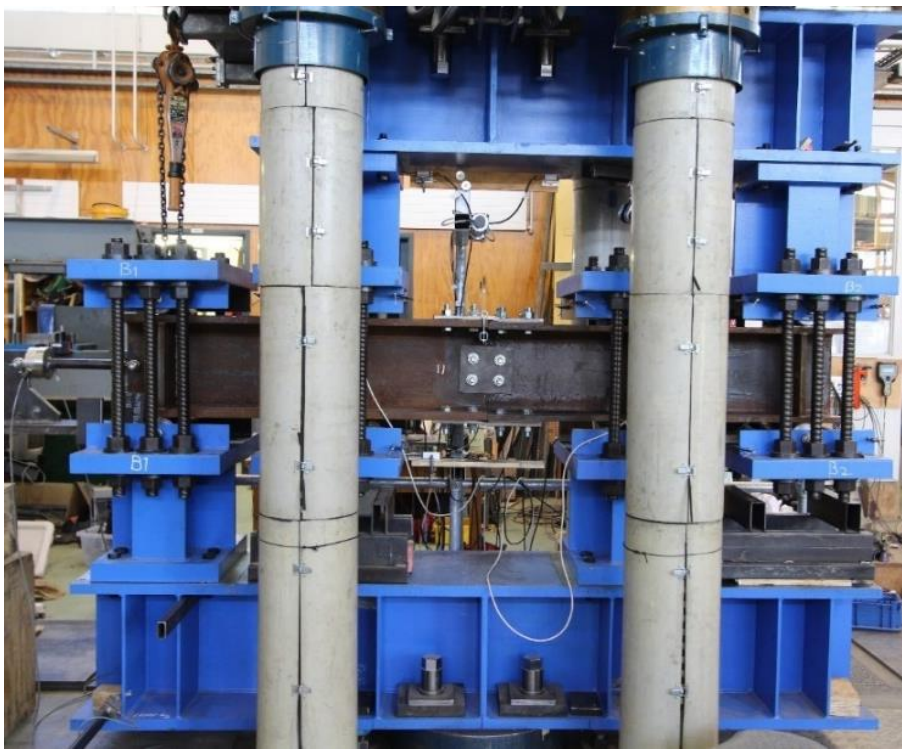

(B) High shear test rig in blue under Dartec machine

Figure 2-5 (A) High shear test setup using Dartec loading machine with input motion at the base double arrow shown.

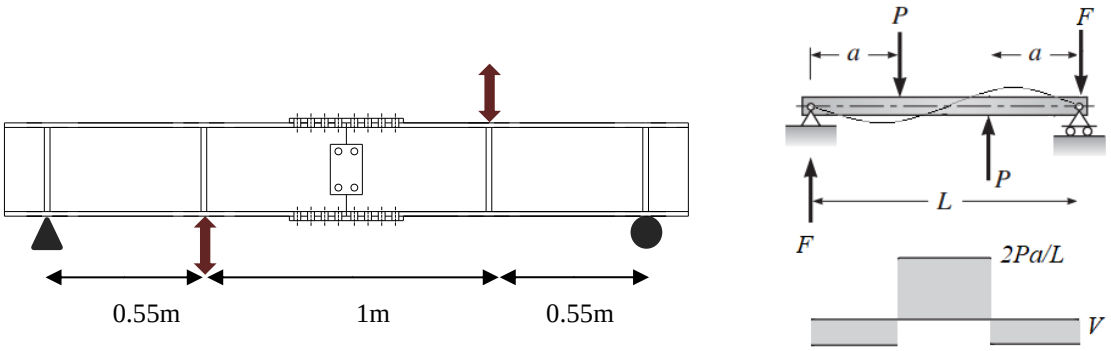

Figure 2-6 Shear test loading diagram and specimen dimensions. Double arrows indicate cyclic loading

2.2.5. *Loading Regime*

The loading in this study was controlled by the displacement of the actuator. This displacement is different from the displacement at the centre of the specimens. Since the bolts attaching the setup to the Dartec could not be post-tensioned due to their large diameter, the joints experienced some slack when the actuator was in tension. This slack or free motion was as large as 0.8mm at the bottom actuator joint at an actuator force of approximately 2000kN. Therefore, the specimens themselves were subjected to smaller displacements in the direction corresponding to actuator tension.

Displacement controlled loading was applied slowly to the Dartec actuator. The loading regime is shown in Figure 2-7. At each level of displacement, three full cycles were repeated followed by a full cycle with half of the previous displacement amplitude. This range of motions was chosen to ensure yielding and failure in a well-incremented set of steps. This loading regime is similar to ACI Report T1.1-01 (ACI Innovation Task Group 1, 2001) and was adopted by (Borzouie, 2016) to test steel column base connections. No axial load was applied to the specimens during the moment or shear tests, due to limitation of resources. The absence of

compression force in the specimens may have some implications on the results, which are discussed in Chapters 3.

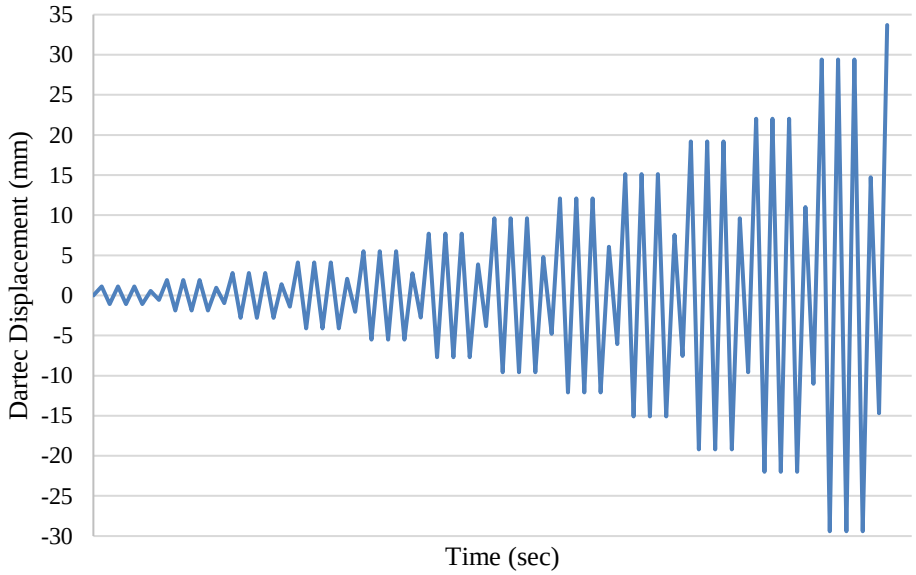

Figure 2-7 Displacement regime for Dartec tests

2.2.6. ***Instrumentation***

Moment Test

Two linear potentiometers were attached horizontally to the top and bottom flanges to measure the gap between the spliced members, as shown in Figure 2-8. When moment demand overcomes the initial friction in the splice connection, a gap starts to grow on one side. When the direction of the moment reverses the gap closes and starts to grow on the opposite side. The data from these potentiometers provides the rotation at the splice joint at each load step.

Other instrumentations were string potentiometers to measure the displacement of the specimens at the centre and the ends. The string potentiometers were attached to an independent frame from the moving parts. The two middle loading points in the setup were constrained between the top and bottom rollers, which are both fixed to the Dartec roof. The data provides

the displacement profile of the specimens. The displacement of the setup frame at the bottom beam ends was also monitored with additional string potentiometers. This data was not directly used in this study, but is recorded to be able to account for any motion in the results.

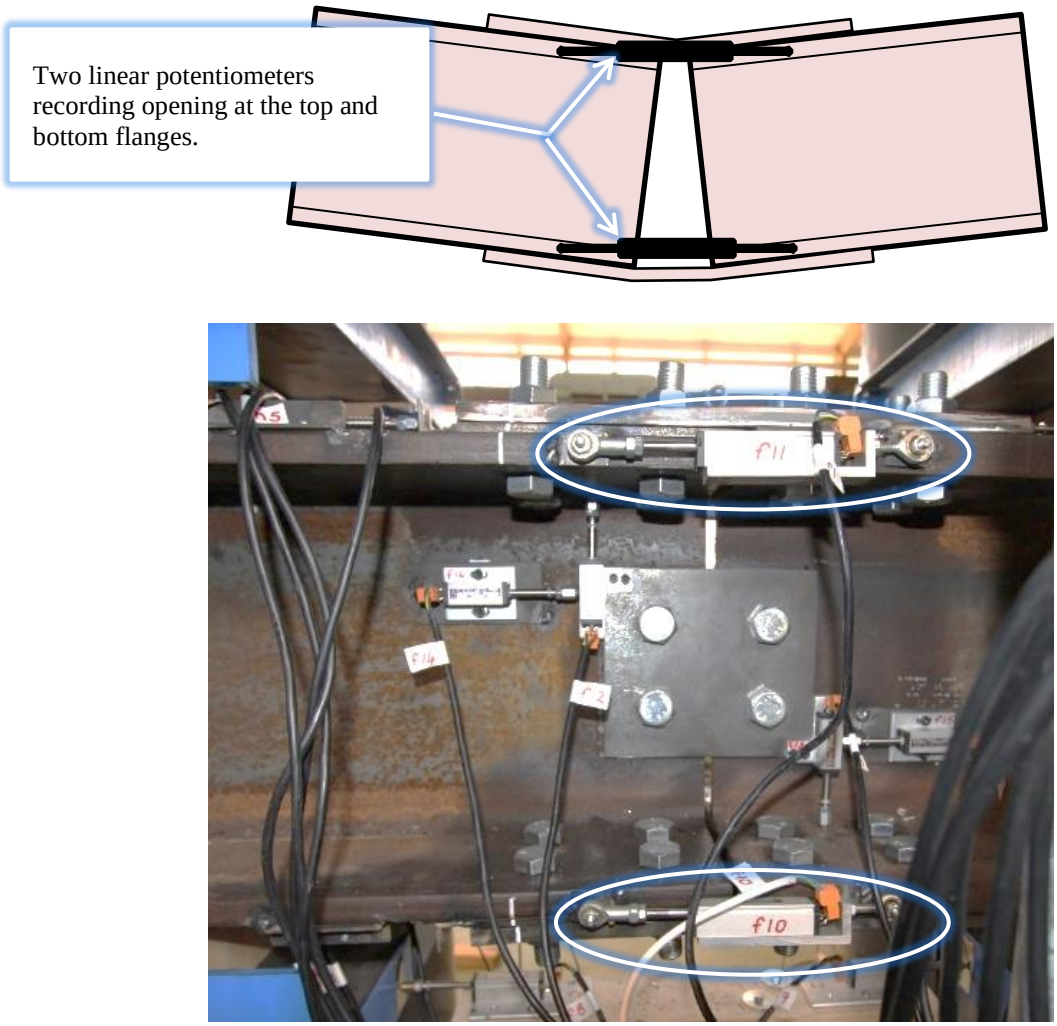

Figure 2-8 Instrumentation at lap splice connection in moment tests of Figure 2-2 to measure joint rotation

Shear Test

A linear potentiometer was used to measure the relative vertical (shear) displacement between the spliced members at the web. The ends of the potentiometer were attached to two small fin plates welded to the webs of the spliced members at the joint, as shown in Figure 2-9. The

potentiometer String potentiometers were used to monitor the displacement of the setup frame at beam ends.

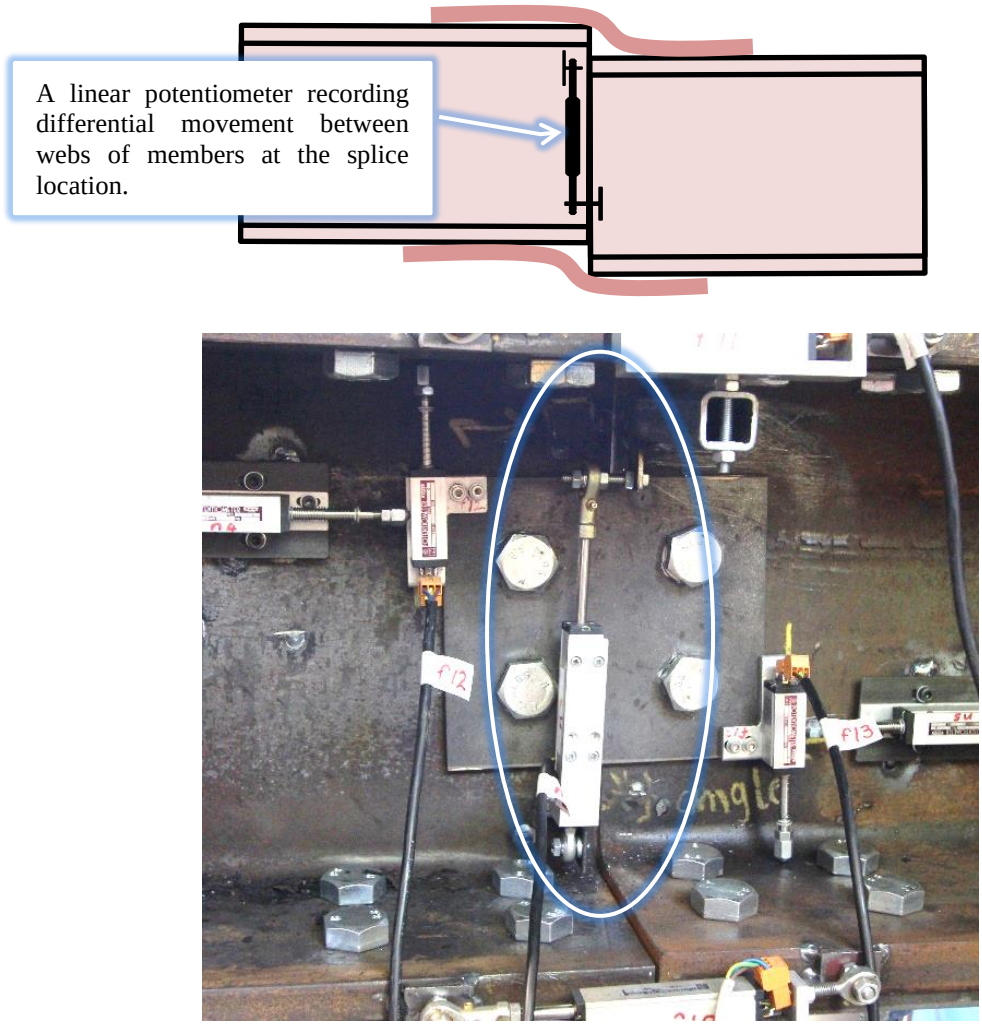

Figure 2-9 Instrumentation at splice connection in shear test of Figure 2-5 to measure joint shear distortion (vertical displacement)

2.2.7. *Interpreting Instrument Readings*

Moment Test

Figure 2-10-A shows the bending moment diagram resulting from the applied loads in the moment tests. The applied load from the Dartec actuator is divided between the two loading points, therefore, $F_{Dartec}=2\times P$. The moment at the connection is defined:

$$M_{splice}(kNm) = \left(\frac{F_{Dartec}}{2}\right)(kN) \times 0.55(m)$$ ***Equation 2-1***

The rotation of the connection, which is illustrated in an exaggerated manner in Figure 2-10-B, was calculated as per Equation 2-2. In non-bearing splices, where the spliced member ends are abutted at the joint, the deformation at one side can be assumed equal to zero.

$$\theta = \frac{\Delta_2 - \Delta_1}{d}$$ ***Equation 2-2***

These calculations translate measurements into resulting loads and rotations (M-θ) for specimens tested under moment. These results are presented in Sections 3-2-1 and 3-2-2.

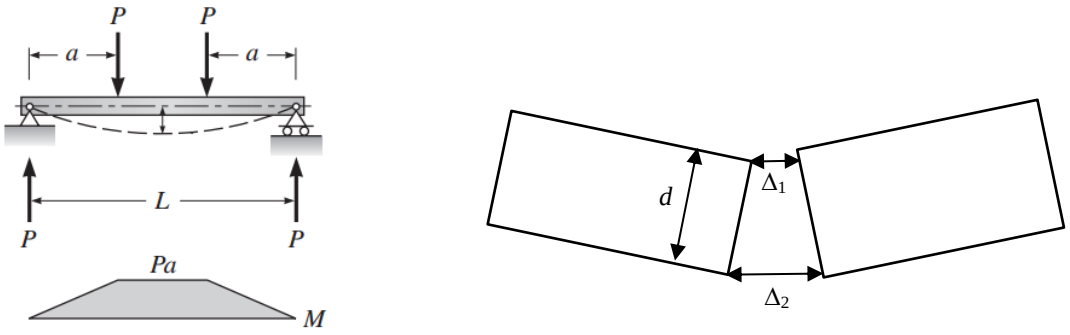

(A) Bending moment diagram **(B)** Rotation at splice connections

Figure 2-10 Moment test: Definition of splice rotation (θ) and bending moment

Shear Test

Figure 2-11-A shows the shear diagram resulting from the applied loads in the shear tests. The shear force and distortion at the connection are defined:

$$P(kN) = F_{Dartec}(kN) \times 1.05(m)/1.55(m)$$ ***Equation 2-3***

$$V_{splice} = 2 \times (F_{Dartec} \times 1.05/1.55) \times 0.55/2.1$$ ***Equation 2-4***

$\gamma = \frac{\Delta}{d}$ ***Equation 2-5***

Again, these calculations turn measurements into resulting internal shear load and deformation (V-γ), for connections tested in shear. These results are presented in Section 3-2-3.

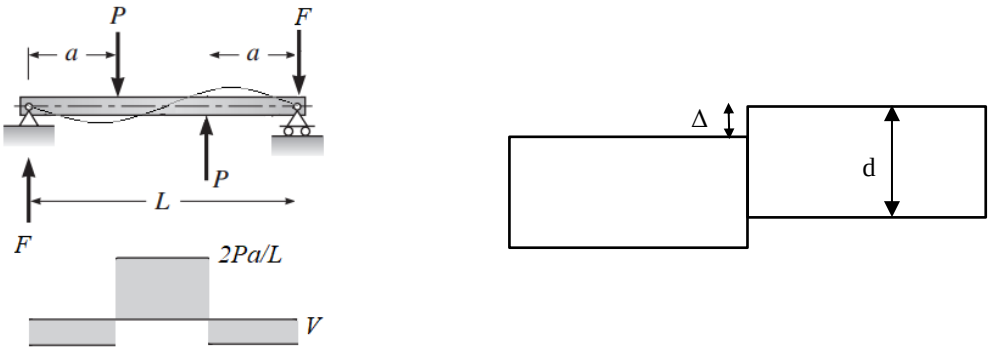

(A) Shear force diagram **(B)** Shear deformation at splice connection

Figure 2-11 Shear test: Definition of splice shear-distortion (γ) and shear force

2.2.8. *Material Testing*

Tensile testing was performed on bolts and coupons from the splice plates and column specimens. While bolt properties are explicitly used in predictive backbone models of specimens in Chapter 4, plate and column material properties are not directly included in the models. These tests were performed to ensure their properties are within the expected range of nominal properties.

2.3. Summary

In this chapter, the test setup, connection design methods and fabrication of the test specimens were discussed in detail. Detailed design calculations along with shop drawings of the

specimens are provided in Appendix A. Nominal material and section properties of universal column sections used in this experimental program are listed in Appendix A Table 1. Chapter 3 provides the results of the experiments and comparisons with the design information described here.

Chapter 3. **Experimental Results**

3.1. **Introduction**

This chapter presents, the results of cyclic moment and shear experiments conducted on Specimens #1 to #13 described in Chapter 2. The results include hysteresis loops and key observations of each experiment. This information is novel since past similar experiments only focused on the monotonic or ultimate behaviour of these splice connections, ignoring the nonlinear change in stiffness. In particular, the measured hysteresis loop data are used to assess the **cyclic strength and stiffness properties** of the connections, which are essential for seismic assessment of global frame responses, and understanding splice behaviour and durability over multiple cycles and events.

Qualitative and quantitative observations from these tests will enable development and verification of predictive backbone models representing the behaviour of these connections, which is provided in Chapter 4. The understanding leading to these models enables its implementation in guiding design. Finally, results are presented from component material testing conducted to verify the mechanical properties of specimen components.

3.2. **Results and Discussions (Specimens #1 to #13)**

3.2.1. ***Moment Tests - Major Axis Bending (Specimens 1-8)***

Specimen #1 (Bearing lap splice, 12mm flange plates with web splice)

This test was conducted to study the cyclic flexural performance of a typical bolted column splice connection designed for the minimum strength per (*NZS3404:Part 1, Steel Structures*

Standard, 1997). The design calculations can be found in Appendix A. Figures 3-1-A and 3-1-B show the hysteresis behaviour and deformation of the connection close to failure. The connection developed ~76% of the nominal plastic moment capacity of the smaller section associated with ~8% rotation at the joint.

Slip at bearing splice connections mainly occurs at the tension flange, allowing the spliced members rotate relative to each other. For the specimen, if the bolts are centred in the 2mm oversized holes, the rotation anticipated before bolt bearing occurs is approximately 4mm/327mm = 0.012 or 1.2%, as there are two holes either side of the splice and 2mm oversize yielding 4mm motion. Here, 327mm is the height of the larger member. Figure 3-1-A shows the actual rotation before load increased significantly was about 2%, which is larger, but likely due to the bolts tilting and not being perfectly centred. Small fabrication gaps between the contact flanges may have also contributed to the larger value.

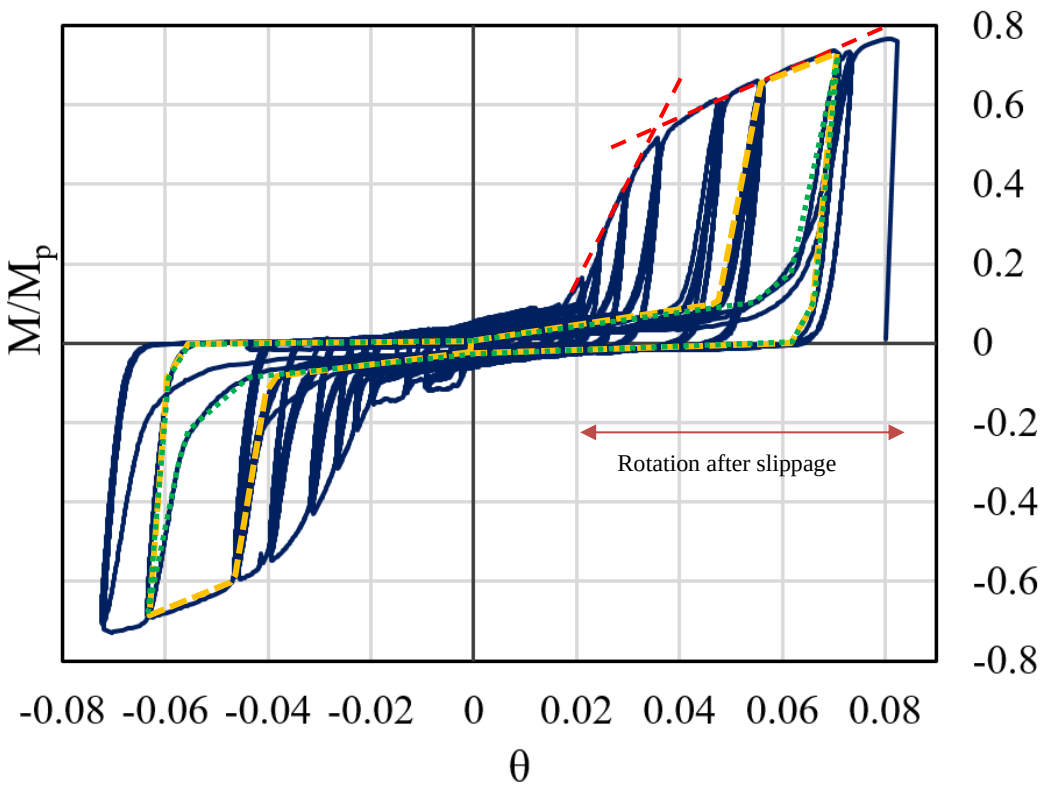

(A) Moment ratio (M/M_p) vs rotation θ, red dash lines show backbone slope changes

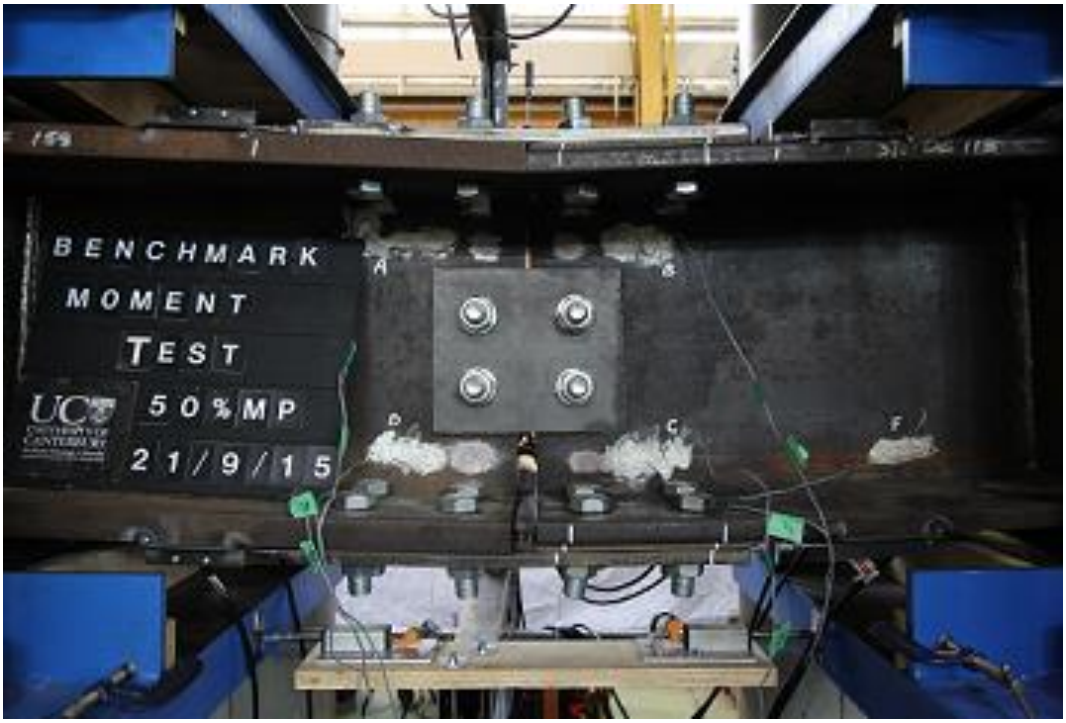

(B) Localized deformation in Specimen #1

Figure 3-1 (A) Moment ratio vs rotation at the splice in Specimen #1, M_p is plastic capacity of smaller member and rotation is the ratio of joint opening to section height **(B)** Localized deformation in Specimen #1

In addition, after dismantling the specimen, the bolt threads were observed to have penetrated into the edges of the bolt holes, as seen in Figure 3-2-A. The minor diameter of Grade 8.8 M20 bolts used in the experiments was approximately 3mm smaller than the nominal diameter (Blacks Fasteners, n.d.). Therefore, the threads are ~1.5mm high, and the rotation anticipated after bolt bearing (against bolt hole) occurs is approximately 2×(2+1.5)mm/327mm = 0.021 or 2.1%, which better matches the 2% value seen in the hysteresis loop of Figure 3-1.

The bolts were snug-tightened, due to construction oversight, with a hand torque wrench set to apply 145Nm. This value was less than the torque recommended by the fabrication company to obtain approximately 65% of the proof load, which was 372Nm. The likely axial force of each bolt was thus approximately 65% × (145kNm/372kNm) × 145kN (proof load) =

65%×145/372×145 = 36.7kN. Having eight bolts at each side of the flange splices, the total normal force on the contact surface would be 8×36.7=294kN.

The friction force, assuming a coefficient of 0.1, which is much less than the standard value of 0.35 from NZS3404 for cleaned as-rolled surfaces, is 29.4kN. This lower value is used because the contact surfaces of this specimen were contaminated with drilling oil and loose particles, resulting in a smaller initial slip force. The associated moment predicted from the flange bolts is 29.4kN×0.327m = 9.6 kNm, which is only 1.7%M_p. The actual strength before the bolts started bearing on bolt holes was less than 0.1M_p. This result is consistent with the low predicted strength of 1.7%M_p.

The design strength of the specimen was 0.44ϕM_p for the bolts and 0.50ϕM_p for the plates from Table 2-4. Of these two values, the bolts control the splice design strength, as they are weaker. The peak strength measured was approximately 0.76M_p, as shown in Figure 2-1. This value is about 69% greater than the 0.50ϕM_p from the plate design, and 90% greater than the 44%ϕM_p from the bolt design.

The loops in Figure 3-1-A corresponding to the second and third cycles of each loading increment after the slippage stage show slackness and gapping due to bolt hole elongation. This behaviour has been illustrated for three cycles of the same amplitude. The yellow dashed lines correspond to the first cycle and the green dashed lines correspond to second and third cycles. The maximum elongation in the splice plates and the shear deformation in the bolts were observed to be approximately 4mm and 5mm, respectively. These values allow a 2×(4+5)mm/327mm = 0.055 rotation after slippage. This latter result is consistent with the post-slippage displacement of approximately 6% seen in Figure 3-1-A.

The connection exhibited bilinear behaviour post slippage, shown with red dashed lines in Figure 3-1-A. The slopes of these lines represent the rotational stiffnesses of the connection. The initial stiffness from the figure is approximately $0.5M_p/0.02=25M_p$, which can be expressed as a function of a column flexural stiffness (EI/L). For a 3m long column of 310UC118 section, a stiffness of $25M_p$ is approximately equivalent to $0.6EI/L$. For 310UC118, I=329e6 mm^4 and M_p=548.8e6 Nmm. Hence, knowing E=200,000 MPa, the result $25M_p / (EI/L) = 0.6$ is obtained. Universal column section properties can be found in Appendix A, Table 1.

Similarly, the secondary stiffness is approximately $0.14EI/L$, which is 23% of the initial stiffness. The post-slip stiffness of the connection can be mainly attributed to bolt shear stiffness and plate bearing stiffness, in series. The stiffness of the connection decreases when the bolts yield in shear.

Based on the small-angle approximation, for angles smaller than 0.176 radian (10 degrees), $tan\theta \sim \theta$ (Holbrow et al., 2010). Thus, the maximum rotation of the connection is approximately 0.08, which is smaller than half of 0.176 radian. Therefore, the rotation of the connection can be expressed in radians.

The bolts in the tension splice plate of the smaller member failed in shear and the bolts were ejected explosively. This failure occurred as the elastic flexural energy in the splice plates was released as the bolts failed. While the bending/prying of the splice plates puts tension on the bolts, this tension did not seem to adversely affect the splice flexural strength. The washers used in the specimen bent, squashed and tore in large cycles, as can be seen in Figure 3-2-B.

Figure 3-2-C shows damage in the flange splice plat, where all the holes yielded in bearing and the plate yielded along the inner rows of bolt holes. The resulting deformation allowed the inner bolts to tilt more. It is also clear the hole ovallization is larger for the inner rows, near the centre of splice, compared to edge rows. The average elongation observed was 3.9 mm and 1.3 mm for the inner and edge rows, respectively.

Figure 3-2-D shows the damage in the web holes. Although it is assumed web splices do not contribute in transferring bending moment (Hogan and Munter, 2007), it can be seen they damaged in large rotations, which could potentially affect their shear performance. Figure 3-2-E shows 1mm distortion in the column flange at the location of splice. Figure 3-2-F shows the separation of the splice plate and the filler plate close to connection failure. The damage could be attributed to prying actions, and piled up material behind the bolts due to bearing.

(A) Threads in holes due to bearing of bolts

(B) Bending and tear in washers

(C) Damage in flange splice plate along inner rows of bolts, mill scale flaking around damaged areas

(D) Hole elongation in web of smaller member

(E) Distortion in the flange of smaller member

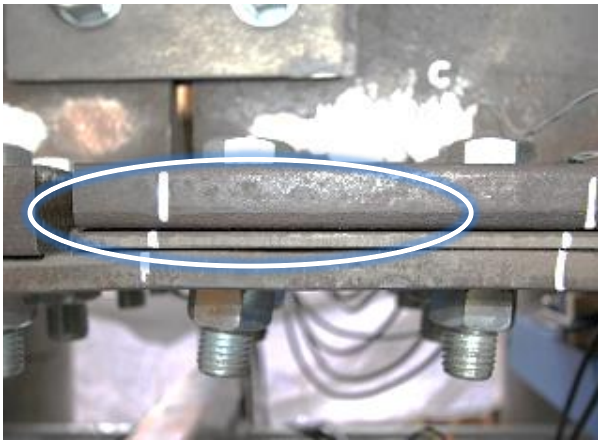

(F) Separation between connection plates

Figure 3-2 Specimen #1: Damage observations

During the experiment, a gap was observed between the abutted members at the end of each cycle. This gap grew larger by the increase in loading amplitude. In other words, the member experienced residual axial elongation at the location of splice. This phenomenon has been observed in the cyclic performance of reinforced concrete shear walls as well (Eom and Park, 2010) There is no tendency for it to move together as Poisson ratio effect mean more deformation is expected on the tension flange. Also, there is no axial compressive force which may cause the gap to close, as there may be in a realistic column.

Flaking of mill scale and ovallization of holes were observed at both flange and web cover plates. The smaller member also damaged in the vicinity of the connection in the form of plasticity in flanges close to the holes and distortion of flange plates.

Key outcomes of Specimen #1 (Tension Bearing (TB) bolts):

- The specimen developed 76% of the nominal plastic capacity of the smaller section, which is larger than the design capacity calculated as 40% of the nominal section plastic capacity.
- The cyclic behaviour of the connection is of a gap system with incremental damage.
- The stiffness behaviour includes four distinct phases: 1) pre-slippage with almost rigid behaviour; 2) post-slippage with almost zero stiffness; 3) bolt hole ovalization prior to bolts yielding in shear; and 4) bolt hole ovalization post bolt yielding. The splice stiffness values corresponding to the third and fourth phases are approximately $0.6EI/L$ and $0.14EI/L$.
- Premature slip occurred due to oil contaminated surfaces and bolts not being fully tensioned.
- The rotation due to slip in 2mm oversized holes was ~0.02 rad and the ultimate rotation capacity was ~0.08 rad.

Specimen #2 (Bearing lap splice, 12mm flange splice, no web splice)

This test was conducted to study the effect of eliminating the web splice in Specimen #1 on flexural performance of the connection. Figures 3-3-A and 3-3-B show the hysteresis behaviour and localized deformation of the column at the splice connection. The ultimate strength is approximately $0.73M_p$, which is 4% less than that of Specimen #1. The small variation could be because of the specific configuration of the web splice, which involves small lever arm for

the web splice bolts. Specimen #2 is also more flexible than Specimen #1, which is likely result of the absence of web splice. The initial and secondary stiffness values of Specimen #2 are approximately 14.5M_p and 4.3M_p, respectively.

Initially, the friction force in Figure 3-3-A is ~0.25M_p, which is very close to the estimated value calculated as follows. The bolts in Specimen #2 were tightened to obtain 145kN tension. The friction force, assuming a coefficient of 0.35 (NZS3404 1997), is 0.35×145kN×8 bolts = 406kN. The associated moment from the flange bolts is 406kN×0.327m = 133kNm, which is equal to 0.24M_p. The slip force is greater than that of Specimen #1 due to different surface preparations and higher tension in the bolts. However, the slip force dropped to less than 0.1M_p in larger displacement cycles. The connection rotational capacity before sudden failure is 0.084, which is 5% more than for Specimen #1.

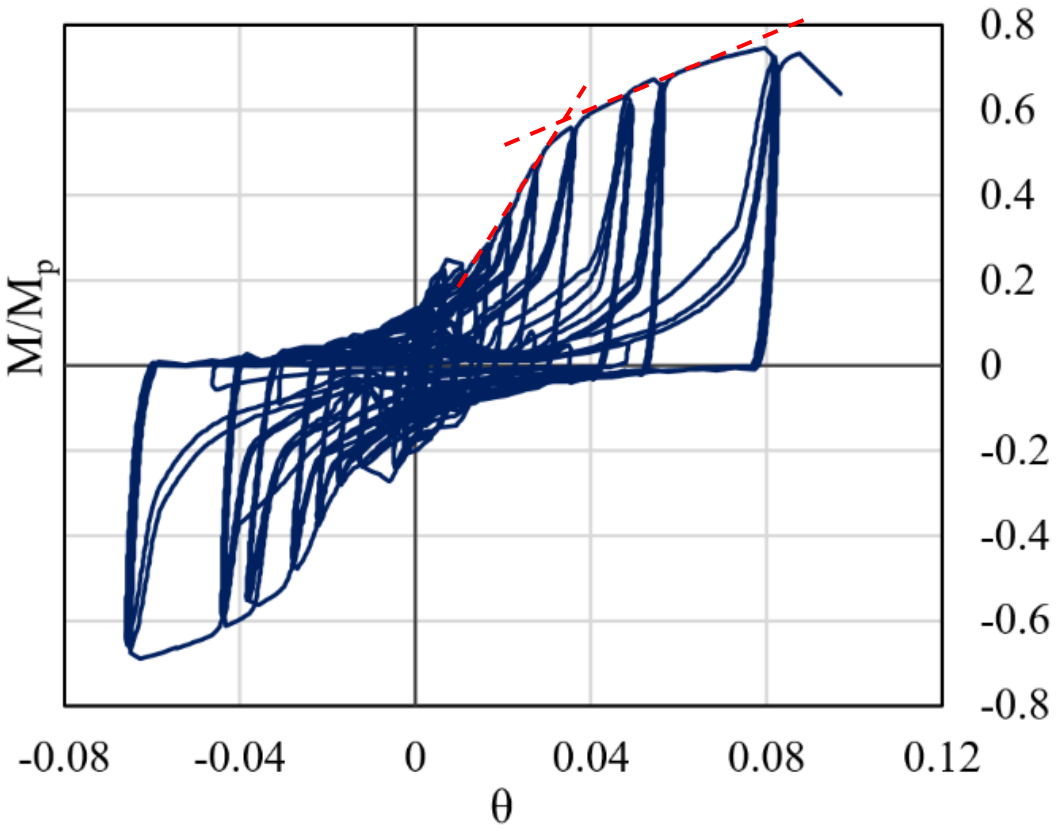

(A) Moment ratio (M/M_p) vs rotation θ, red dash lines show backbone stiffness changes

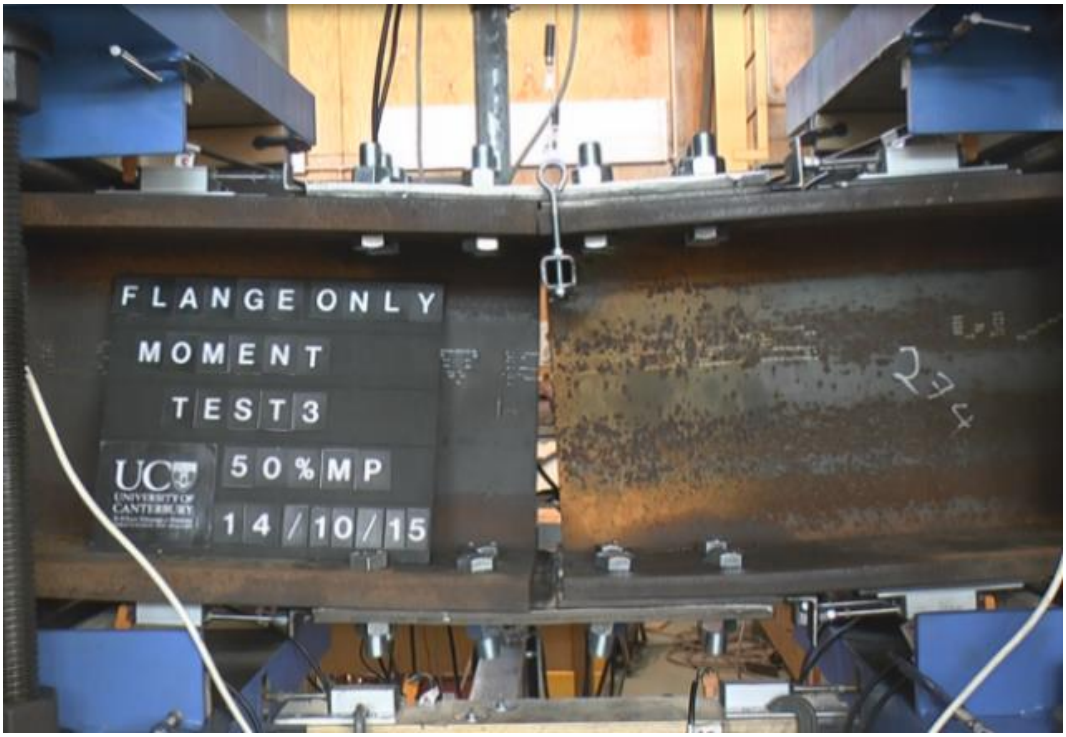

(B) Localized deformation in Specimen #2

Figure 3-3 (A) Moment ratio vs rotation at the splice in Specimen #2, M_p is plastic capacity of smaller member and rotation is the ratio of joint opening to section height **(B)** Localized deformation in Specimen #2

The failure mode was similar to that of Specimen #1 with bolts being fractured and explosively ejected from the splice. Small strength degradation can be observed in the hysteresis loop before the failure occurred. Figure 3-4-A shows damage in the splice plate, which is similar to the damage observed in Specimen #1. The inner rows of holes in the splice plate elongated 2.7mm on average, but no elongation was observed for the edge rows. Figure 3-4-B shows yield lines in the flange of the smaller member. Residual bearing deformation under the bolt heads can also be observed around the hole edges.

Figure 3-4-C shows abrasion and galling of the hole edge in a filler plate, which was also observed in Specimen #1. Figure 3-4-D shows the gap at the spliced joint during the experiment at the end of a cycle post slippage (at zero displacement), as also observed for Specimen #1. Figures 3-4-E and 3-4-F show the extent of deformation in one of the bolts at failure. It can be

seen that there is significant local shear deformation and the upper portion of the bolt has translated. Similar deformation was observed in bolts of Specimen #1.

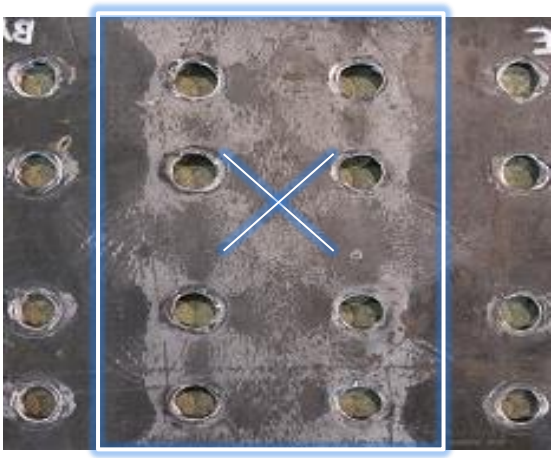

(A) Damage in flange splice plate along inner rows of bolts, diagonal yield lines between four centre bolts

(B) Yield lines in the flange in 310UC118 section, and residual bearing deformation under bolt heads

(C) Abrasion and built-up material/galling at hole edges in filler plates in the direction of movement

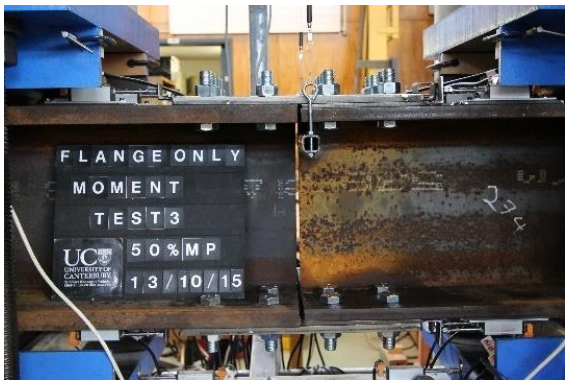

(D) Gap/elongation at splice joint at zero load

(E) Deflection of bolts at failure

(F) Overall deformation and the tilt in the upper portion of bolts at failure

Figure 3-4 Specimen #2: Damage observations

Key outcomes of Specimen #2 (Tension Friction (TF) bolts):

- The specimen developed 73% of the nominal plastic capacity of the smaller section. The ultimate strength is smaller than Specimen #1 due to the absence of a web splice.
- The splice post-slippage stiffness values are approximately 0.35*EI/L* and 0.10*EI/L*, which are smaller than Specimen #1. This reduction was due to absence of a web splice.
- Slip occurred at ~25% of nominal section plastic capacity. This value is larger than Specimen #1 due to fully tensioned bolts and cleaned contact surfaces.
- The rotation due to slip in 2mm oversized holes was ~0.01 rad, which is smaller than Specimen #1 due to the tensioned bolts. The ultimate rotation capacity was ~0.084 rad, which is larger compared to Specimen #1 due to absence of web splice.

Specimen #3 (Bearing lap splice, 20mm flange splice)

Specimen #3 was designed for higher strength than Specimen #1 (See Table 2-4), to compare the overall performance of splices designed for larger ultimate capacity. Figures 3-5-A and 3-5-B show the hysteresis behaviour and localized deformation at the splice connection. The connection ultimate strength capacity is greater than M_p even though holes were present in the column flanges. This overstrength could be attributed to strain hardening in the flanges and the contribution of the splice plates. In addition, the connection exhibits larger stiffness compared to Specimen #1. The initial and secondary stiffness of the connection is approximately $40M_p$ and $10M_p$, respectively, which is 60% and 100% larger than those for Specimen #1.

Initially, the friction force in this case is approximately $0.35M_p$, which is close to the estimated value calculated as follows. The friction force, assuming a coefficient of 0.35 (NZS3404 1997), is $0.35 \times 145\text{kN} \times 12$ bolts = 609kN. The associated moment from the flange bolts is

609kN×0.327m = 199kNm, which is equal to 0.36%M_p. This outcome could indicate the bolts may not have been fully proof loaded due to larger length.

The connection has a smaller rotational capacity (0.07 Rad) compared to the other two specimens (0.08-0.09 Rad) possibly because the thicker (20mm) flange splice plates had less bolt hole deformation under the forces imposed by the bolts. Thicker flange plates may have also contributed to larger initial stiffness of the connection (ratio of moment to rotation) post slippage than seen in Specimens #1 and #2.

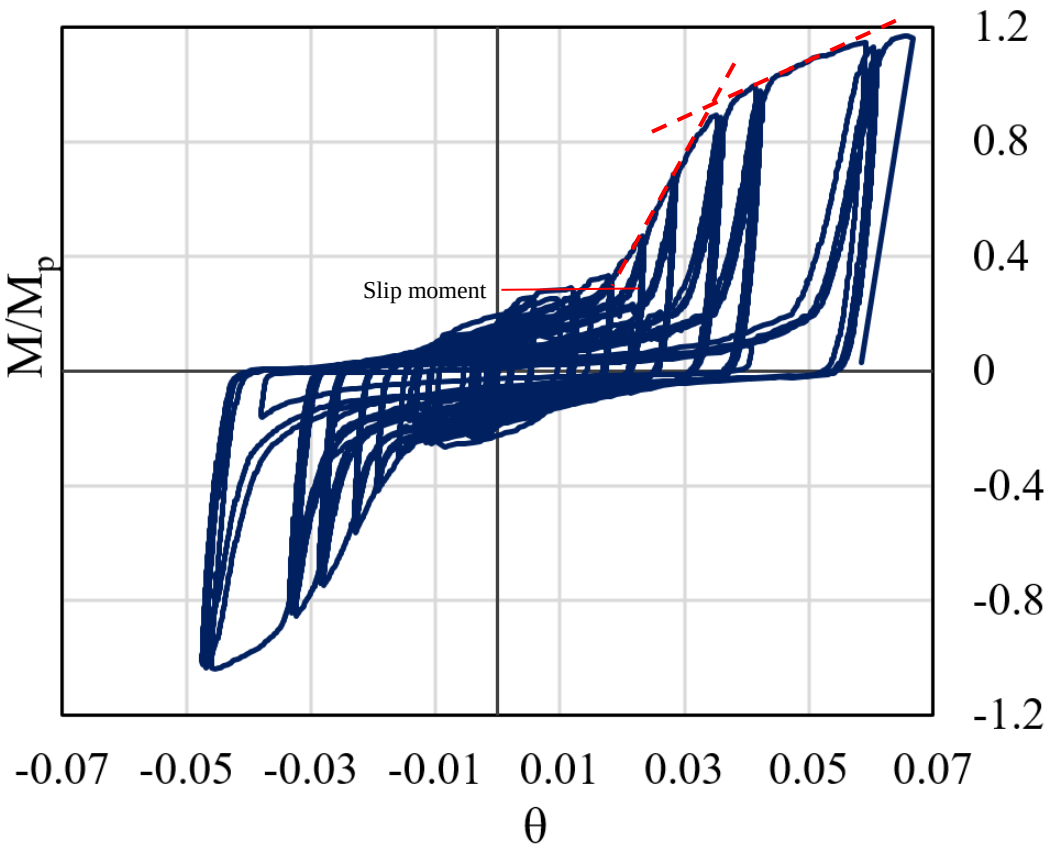

(A) Moment ratio (M/M_p) vs rotation θ, red dash lines show backbone stiffness changes

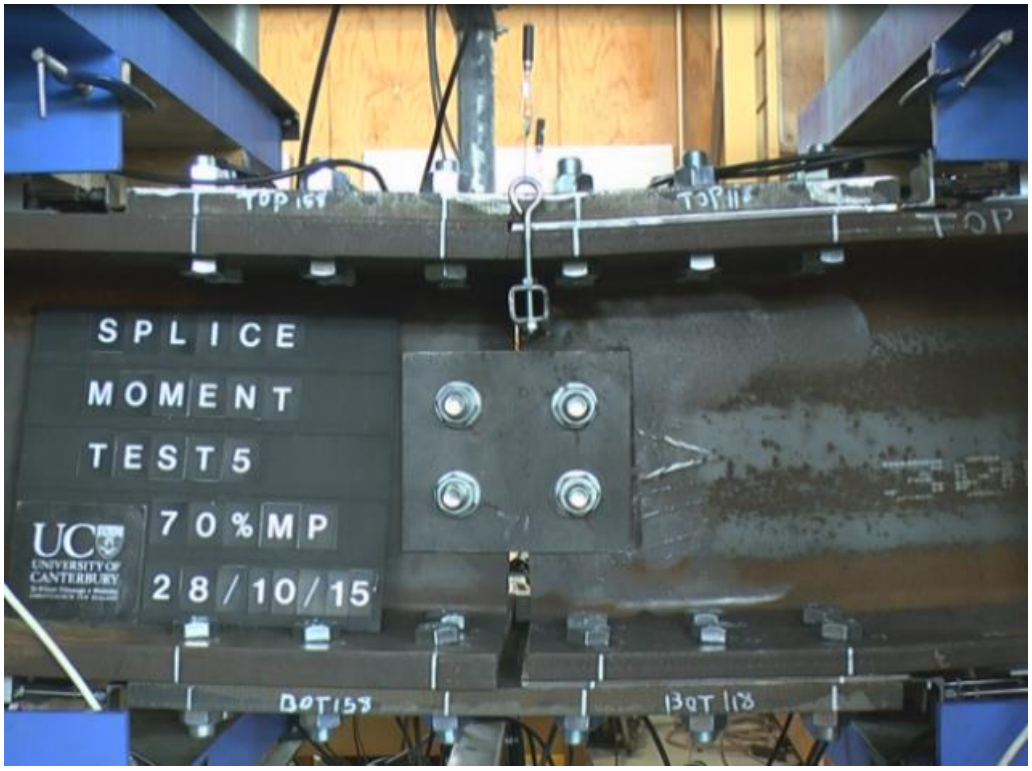

(B) Localized deformation in Specimen #3

Figure 3-5 (A) Moment ratio vs rotation at the splice in Specimen #3, M_p is plastic capacity of smaller member and rotation is the ratio of joint opening to section height **(B)** Localized deformation of Specimen #3

Figures 3-6-A and 3-6-B show damage in the smaller member. The column flanges and web were damaged more than in Specimen #1. The 6mm web plate material is of Grade 350, rather than the Grade 300 11.9mm thick beam web. Interestingly, the web plates were damaged less than the web itself. In addition, the smaller section yielded in bending adjacent to the splice joint which indicates that the splice developed the moment capacity of the specimen.

Figures 4-6-C and 4-6-D show damage in flange and web splice plates. No significant elongation was observed at the holes in the flange splice plate. Bolt thread traces on bolt hole edges and ovalization in splice plates were observed towards the ends of the splice, whereas the same was observed in the column holes towards the centre of the splice. This result indicates forces in tension, and that compression forces were mainly transmitted through the contact area

and not through flange. This behaviour was observed in the other specimens, as well. Failure occurred with bolts being fractured and ejected explosively.

(A) Flexural yield lines in flange of smaller member outside the splice zone as well as diagonal yield lines in the splice zone

(B) Elongated holes and yield lines in web, and distortion of flange in smaller member was measured 5mm at the joint centre

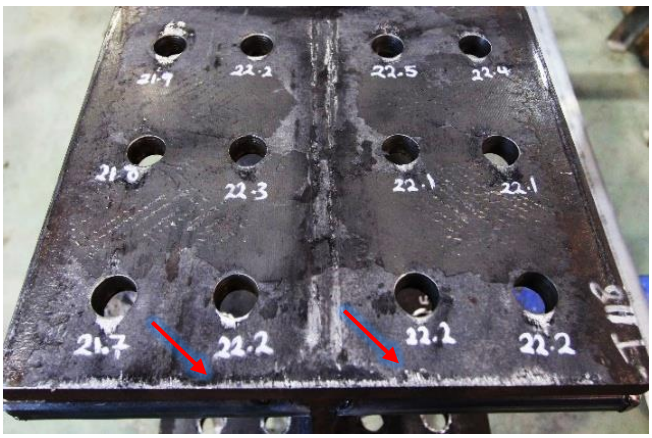

(C) Abrasion at the edge of flange at the joint centre, diagonal yield lines between holes and elongation of bolts holes (numbers show elongated diameter, initially 22mm)

(D) Elongation of holes in web splice plate (numbers show elongated diameter from initial 22mm hole)

Figure 3-6 Specimen #3: Damage observations

Key outcomes of Specimen #3 (Tension Friction (TF) bolts):

- The specimen developed ~115% of the nominal plastic capacity of the smaller section. The design strength was calculated as 60% of the nominal section plastic capacity.

- The splice post-slippage stiffness values are approximately 0.96*EI/L* and 0.24*EI/L*. These larger values are due to thicker flange splice plates and more number of bolts.
- Slip occurred at ~35% of nominal section plastic capacity. This value is larger than Specimen #2 due to the greater number of bolts in the specimen.
- The rotation due to slip in 2mm oversized holes was ~0.01 rad, which is similar to Specimen #2. The ultimate rotation capacity was ~0.067 rad, which is smaller than Specimen #2 is due to the greater number of bolts and resulting reduced bolt hole ovalization.

Specimen #4 (Non-bearing lap splice, no filler plate)

Splice plates in Specimen #4 are similar to those in Specimen #1, but the specimen consists of two 310UC118 members. Therefore, no filler plates were required for fabrication. A gap of 10mm was provided between the members at the joint to create a non-bearing splice. The purpose of this test was to study the effects of eliminating filler plates and introducing a gap at the joint on flexural performance.

Figure 3-7-A and 3-7-B present the hysteresis behaviour and localized deformation at the splice connection of Specimen #4. The behaviour of the connection appears different in the reverse direction. The difference could be because of cyclic shear loading in the bolts, whereas in the bearing lap splices, bolts only deform in one direction. The initial friction force in this case is slightly larger than for Specimens #1 and #2 because of the absence of filler plates in the connection. The estimated slip force, using the same principles as previously adopted, was the same as Specimens #1 and #2, which is 0.23M_p. The ultimate strength is 0.81M_p, which is greater than for Specimen #1 of 0.76M_p, possibly because smaller bending developed in the bolts.

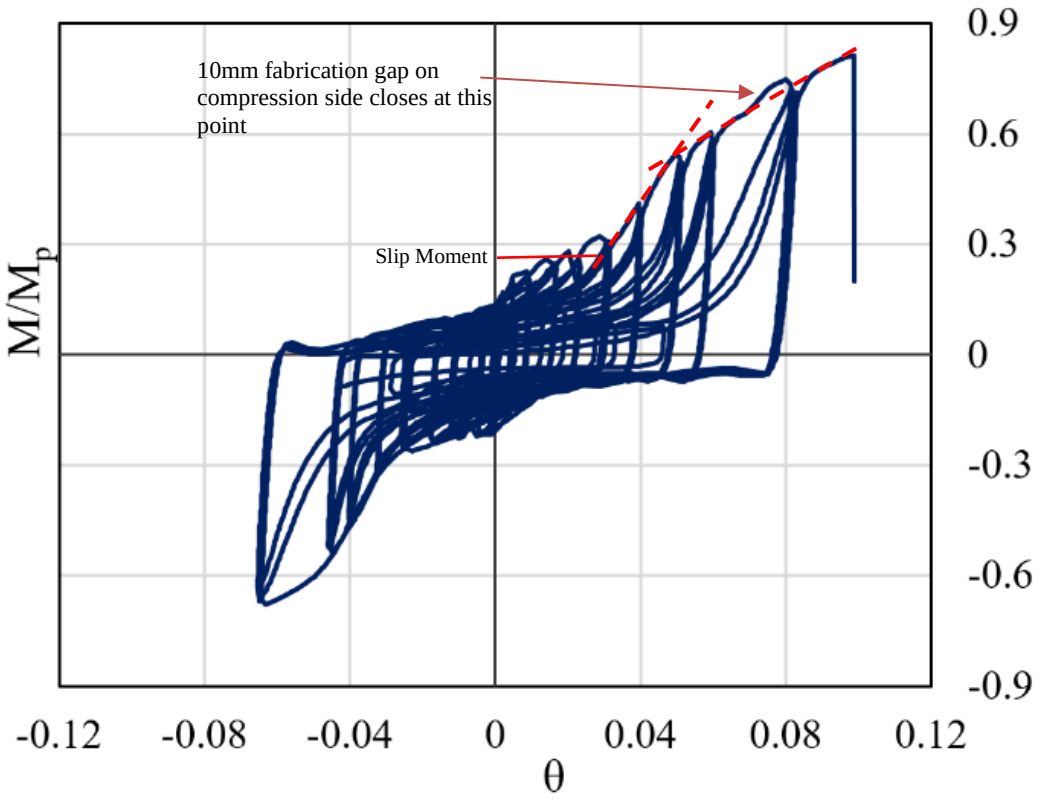

(A) Moment ratio (M/M_p) vs rotation θ, red dash lines show backbone stiffness changes

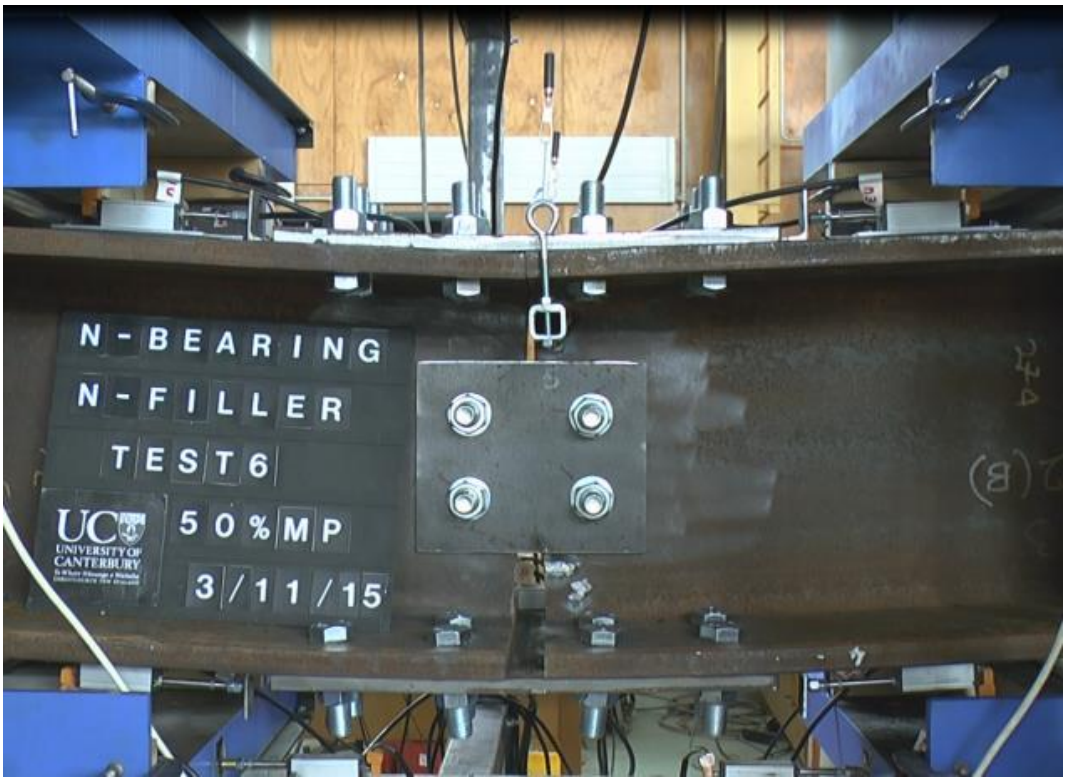

(B) Localized deformation in Specimen #4

Figure 3-7 (A) Moment ratio vs rotation at the splice in Specimen #4, M_p is plastic capacity of spliced members and rotation is the ratio of joint opening to section height **(B)** Localized deformation in Specimen #4

If the bolts are centred in the 2mm oversize holes, the rotation anticipated before bolt bearing occurs is approximately 2×(2+1)mm/315mm = 0.019 or 1.9%, where 315mm is the section height of the spliced members. While each member can move 2mm relative to the splice plate on the tension side, they can only move 1mm on the compression sides. The total rotation when the compression flanges contact each other occurs at (10+10)mm/315mm=0.063 or 6.3%, which is close to where the kink can be seen in Figure 3-7-A. Note that 10mm is the fabrication gap between the spliced members.

The initial and secondary stiffnesses of the connection are approximately $15M_p$ and $6M_p$, respectively. The initial stiffness of the connection is 60% of that for Specimen #1. The connection has larger rotational capacity compared to the other two specimens because slip occurs on both the compression and tension sides. Figure 3-8 shows damage in Specimen #4, similar to those previously observed for Specimens #1, #2 and #3. Failure of the connection occurred with the fracture of bolts on the tension side, and was explosive. The members were in contact on the compression side when failure occurred.

(A) Deformation in fractured bolts, bolts were put together after failure

(B) Ground mill scale due to friction

(C) Distortion of flange in smaller member

(D) Yield lines in the flange of smaller member

Figure 3-8 Specimen #4: Damage observations

Key outcomes of Specimen #4 (Non-Bearing, Tension Friction (TF) bolts):

- The specimen developed 81% of the nominal plastic capacity of the smaller section. The ultimate strength is larger than Specimen #1 due to the absence of filler plates in the flange splice, resulting in smaller bending in the bolts and larger bolt shear capacity.
- The splice post-slippage stiffness values are approximately 0.36*EI/L* and 0.14*EI/L*, which are smaller than Specimen #1. This reduction is due to movement in both tension and compression flanges. The stiffness is slightly smaller in the reverse direction due to cyclic shear in bolts.
- Slip occurred at ~25% of nominal section plastic capacity. This value is similar to Specimen #2, with similar contact surfaces, bolt number and bolt tensioning method.
- The rotation due to slip in 2mm oversized holes was ~0.02 rad, which is larger than Specimen #2 due to rotation in both tension and compression flange splices. The ultimate rotation capacity was ~0.1 rad, which is larger compared to splices in butted columns.

Specimen #5 (Non-bearing lap splice, one filler plate)

This test was conducted to investigate how a filler plate in a non-bearing splice connection would affect flexural performance. This assessment is achieved by comparing the performance of Specimen #5 with Specimen #4. Comparison to Specimen #1 also assesses how the presence of a gap between the spliced members would change the flexural performance.

The hysteresis loop and localized deformation of the connection are illustrated in Figure 3-9. The rotational stiffness of the specimen post slippage is similar to Specimen #4. The smaller stiffness compared to Specimen #1 may be due to the freedom of the members to move on the compression side before the spliced members meet each other. The initial friction force in the specimen is also slightly smaller for Specimen #4. This reduction is due to the presence of the filler plates, which can reduce the effective friction forces (Yura et al., 1982).

Generally, similar patterns of damage were observed in the specimen components as in the previous tests. Figure 3-10-A shows translation of unthreaded bolt at the intersection with the unthreaded part. Figure 3-10-B shows traces of bolt bearing on both inner and outer hole edges in the flange splice plate. This observation indicates the splice plates were engaged in transferring both tension and compression forces, which was seen in Specimen #4 as well.

The connection failed explosively on the side with no filler plates, in contrast to Specimens #1 to #4, where failure occurred where filler plates were used. Due to construction oversight, four of the bolts in the smaller member had partially unthreaded shanks and their shear planes did not pass through the threads. Thus, failure occurred on other side of the connection, in which the bolts were fully threaded. This analysis may also explain the slight increase in the ultimate strength compared to Specimen #4, as the strength was dominated by the bolt shear strength.

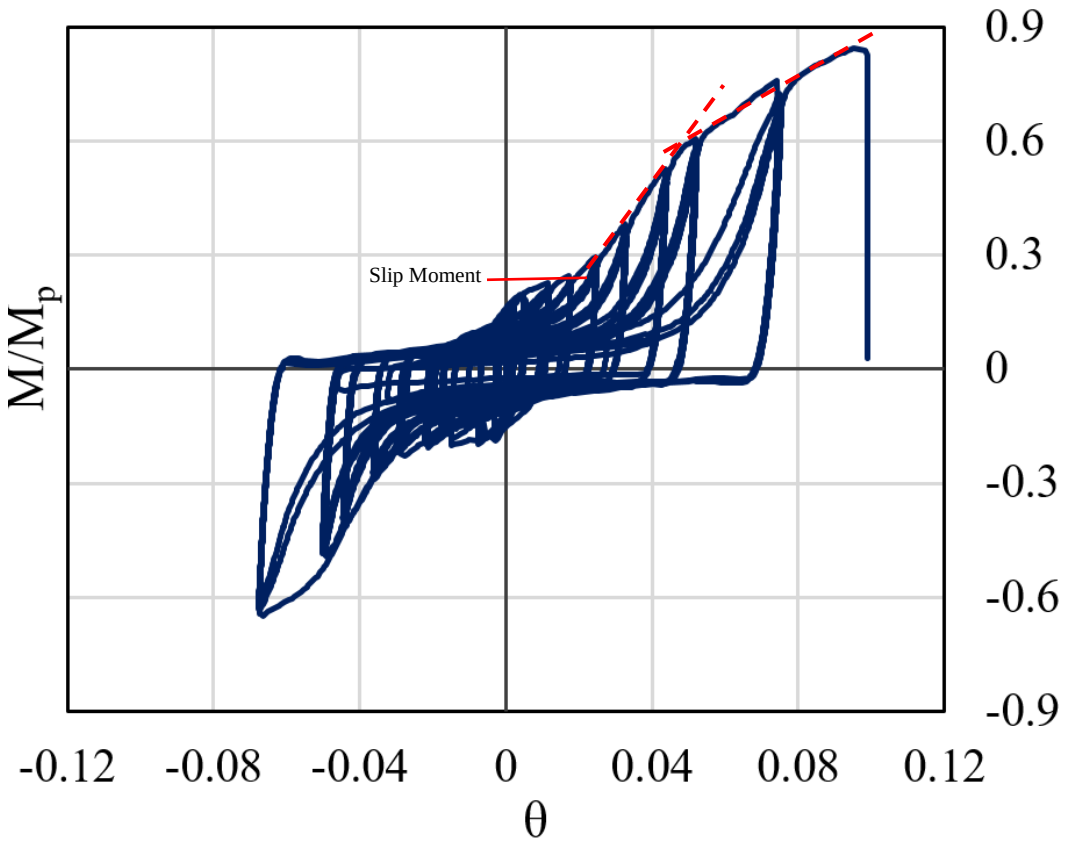

(A) Moment ratio (M/M_p) vs rotation θ, red dash lines show backbone stiffness changes

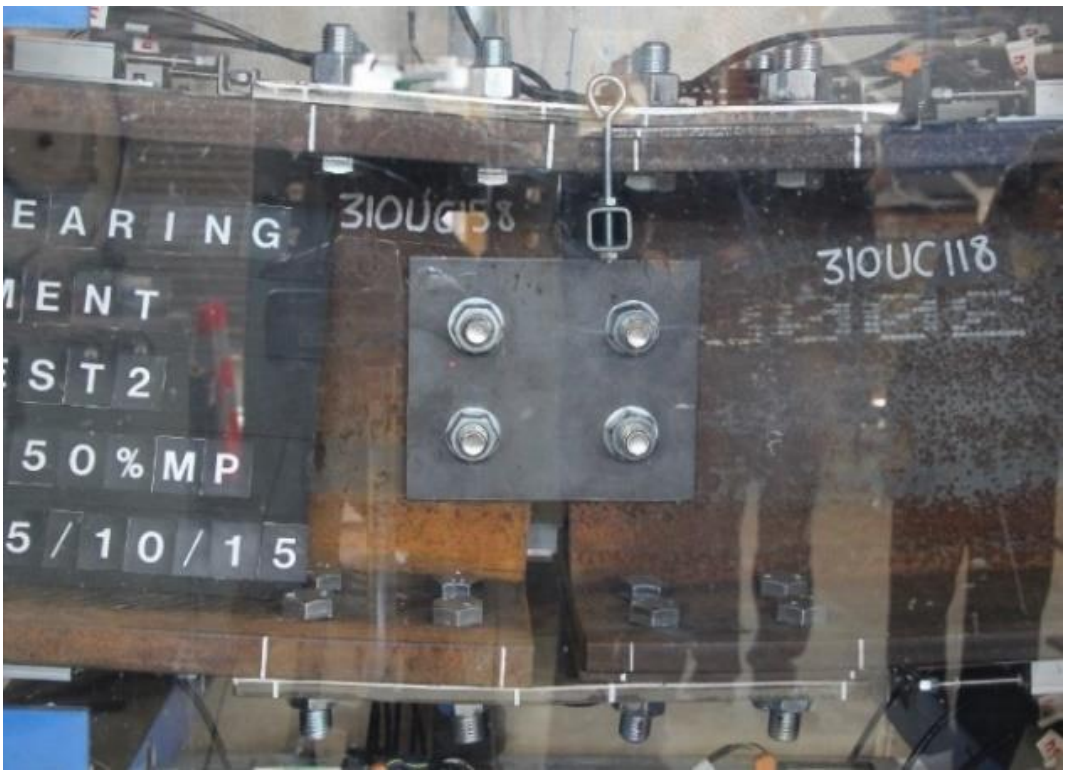

(B) Localized deformation in Specimen #5

Figure 3-9 (A) Moment ratio vs rotation at the splice in Specimen #5, M_p is plastic capacity of smaller spliced member and rotation is the ratio of joint opening to section height **(B)** Localized deformation in Specimen #5

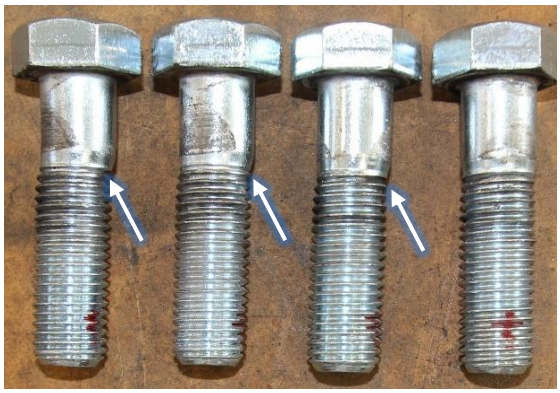

(A) Translation of bolt upper part at the intersection of threaded and unthreaded shank

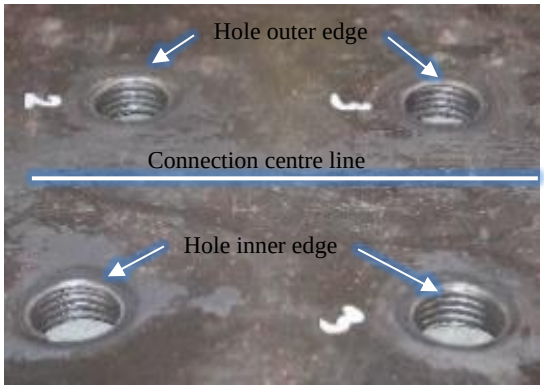

(B) Traces of bolt bearing on both tension and compression sides of holes

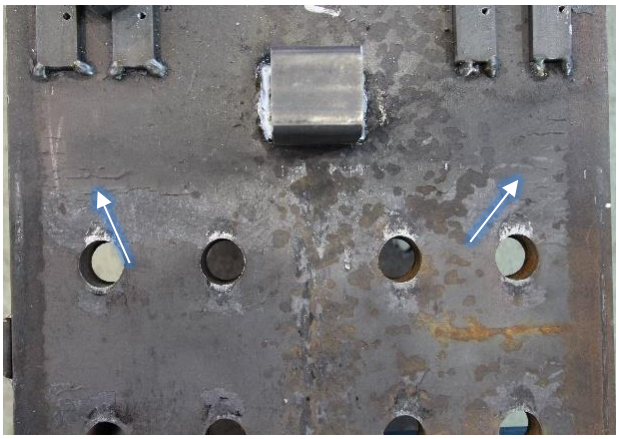

(C) Flexural yield lines in the column adjacent to the splice joint

(D) Abrasion in the middle of splice plate, generated when plate was in tension

Figure 3-10 Specimen #5: Damage observations

Key outcomes of Specimen #5 (Non-Bearing, Tension Friction (TF) bolts):

- The overall capacity and behaviour of the connection is very similar to Specimen #4. The 6 mm filler plate used in Specimen #5 is not sufficiently thick to change the connection behaviour significantly.
- Comparison to Specimen #1 shows the gap may have led to a modest reduction in stiffness due to the added freedom to move.

Specimen #6 (non-bearing splice, two filler plates)

This test was conducted to investigate the effect of two filler plates in a non-bearing splice connection on the flexural performance of the connection. This assessment is achieved through

comparing the performance of Specimen #6 with Specimens #4 and #5. The hysteresis loop and localized deformation of the connection is illustrated in Figure 3-11. The ultimate capacity of the connection is $0.88M_p$ at a rotation of 0.13 or 13%.

The friction force, assuming a coefficient of 0.35 (NZS3404 1997), is 0.35×145kN×8 bolts = 406kN. Given the section height for the larger member is 0.308m, the associated moment from the flange bolts is 406kN×0.308m = 125 kNm, which is equal to $36\%M_p$. If the bolts are centred in the 2mm oversize holes, the rotation anticipated before bolt bearing occurs is approximately 2×(2+1)mm/260mm = 0.023 or 2.3%, as there are two holes either sides of the splice plate on both tension and compression sides. 260mm is the section height of the smaller member at the joint.

The performance of the connection shows good agreement with the estimated slip force. The slip deformation from the figure is approximately 0.03, which is larger than the estimated value. The reason is likely to be bolt tilting due to freedom length between the filler plates. The connection developed larger deformation at failure (0.13), compared to Specimens #4 and #5 (0.1rad), is likely because flange of smaller member met and indented the web of larger member at the compression side. The hysteresis loop shows spikes at smaller rotations, which can be attributed to more filler plates and slip between them.

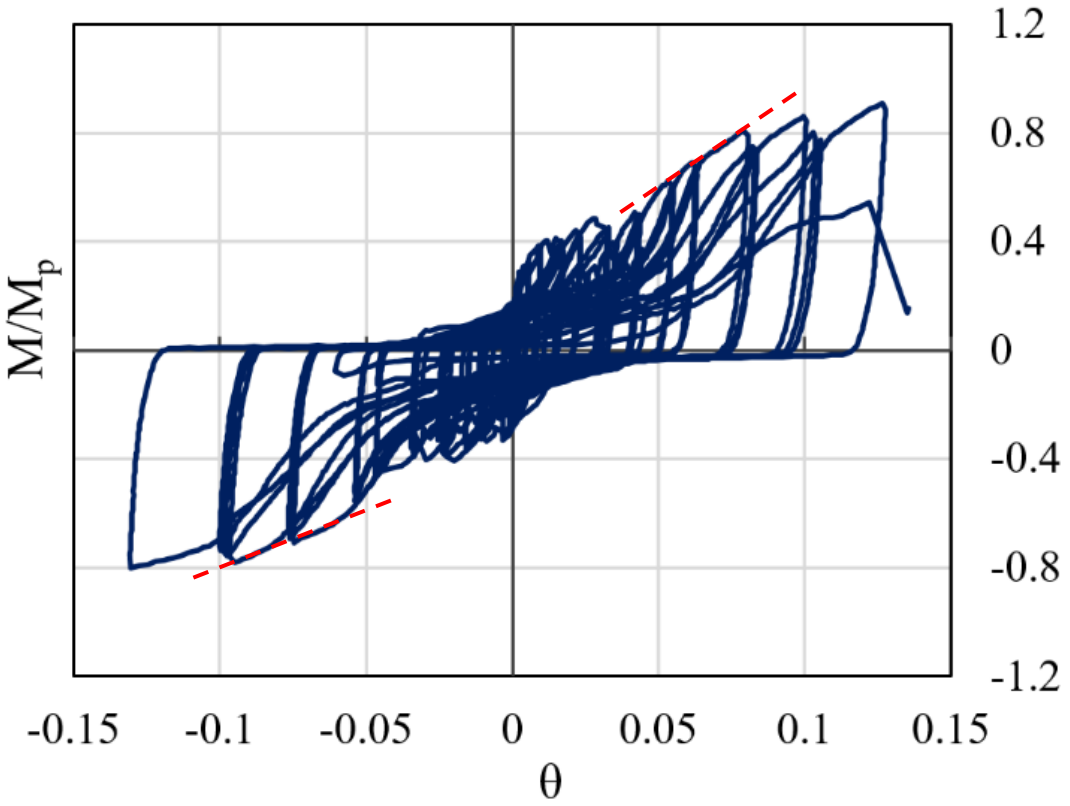

(A) Moment ratio (M/M_p) vs rotation θ, red dash lines show stiffness degradation in reverse loops

(B) Localized deformation of Specimen #6

Figure 3-11 (A) Moment ratio vs rotation at the splice in Specimen #6, M_p is plastic capacity of smaller spliced member and rotation is the ratio of joint opening to section height **(B)** Localized deformation of Specimen #6

The strength for rotations larger than 5% was less in the second and third cycles at each increment, due to stiffness degradation. In addition, the loops showed smaller stiffness in the reversed loading direction for rotations larger than 0.05%. Stiffness in the reversed direction reduced from $8M_p$ to $4M_p$. The connection failed at the side of the smaller member explosively.

Figure 3-12-A shows the filler plates moved relative to each other, and the compression flange met the web of the other member. Bending in flange plate at the bolts close to the centre show prying forces developed in the bolt. Bolt end rotation is observed at the bolt heads in Figures 3-12-A and B. Figure 3-12-C shows galling damage at the edge of a hole in the smaller member.

Figure 3-12-D shows damage was mainly concentrated at the centre of the splice plate. Hole elongation is also larger for the central bolts. Figures 3-12-E and F show different abrasion patterns on the two sides of the splice plate. In the absence of filler plates, friction damage appears greater near the bolts. The filler plates may have reduced the total effective friction on the surfaces. Finally, Figure 3-12G shows the indentation damage resulted from the bearing of the smaller member on the web of the larger member. Figure 3-13H shows the typical deformation of the bolts in the smaller member.

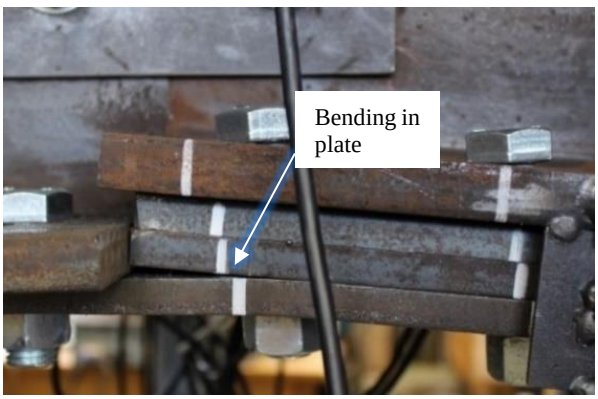

(A) Relative movement of filler plates, bending in splice plate at the central bolt at compression flange

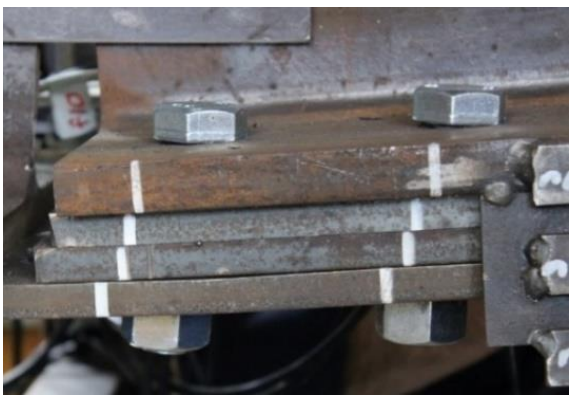

(B) Rotation of the bolt ends at tension flange

(C) Hole edge damage in flange of smaller member

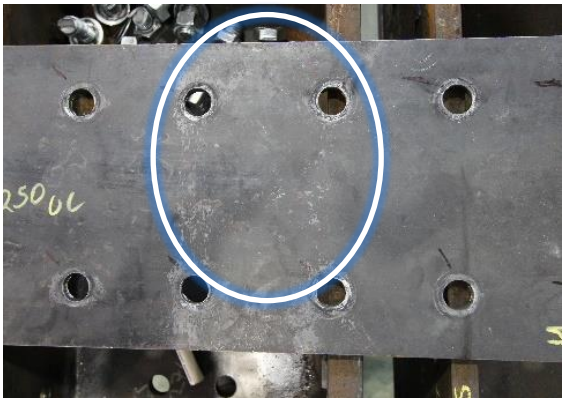

(D) Damage in the centre of splice plate

(E) Abrasion on contact surface of splice plate covering smaller member

(F) Abrasion on contact surface of the splice plate covering larger member

(G) Yielding in web due to bearing of smaller member flange on web of larger member

(H) Typical deformation in bolts connecting smaller member, prior to fracture

Figure 3-12 Specimen #6: Damage observations

Key outcomes of Specimen #6 (Non-Bearing, Tension Friction (TF) bolts):

- The specimen developed 88% of the nominal plastic capacity of the smaller section. The ultimate strength is larger than the design capacity calculated as 44% of the nominal section plastic capacity.

- The connection strength in the second and third cycles of each increment was approximately 10% smaller than the first cycle.
- The splice post-slippage stiffness value is approximately 0.29*EI/L*. The stiffness is half of this value in the reverse direction due to cyclic shear in bolts.
- Slip occurred at ~40% of nominal section plastic capacity.
- The rotation due to slip in 2mm oversized holes was ~0.03 rad. The ultimate rotation capacity was ~0.13 rad, which is larger compared to splices in Specimens #4 and #5.

Specimen #7 (End-plate splice)

This test was conducted to study the difference in the flexural performance of a bolted lap splice connection relative to an end-plate splice connection designed for similar ultimate capacity. The cyclic behaviour and the localized deformation of the connection close to failure is shown in Figure 3-13. The rotational capacity of the specimen is considerably smaller than the lap splice connections. The elastic rotation is approximately 0.001 or 0.1%, which could be due to elastic elongation of bolts.

The ultimate deformation of the connection is approximately 1.56%, which is associated with approximately 6mm elongation in the farthest bolts assuming zero deformation in the end plates. The ultimate strength is approximately $0.78M_p$ compared to the $0.56\phi M_p$ calculated in Chapter 2. The stiffness of connection post-yield can be approximated at $24M_p$. As expected, the failure occurred at bolts in tension, and bolts ejected explosively.

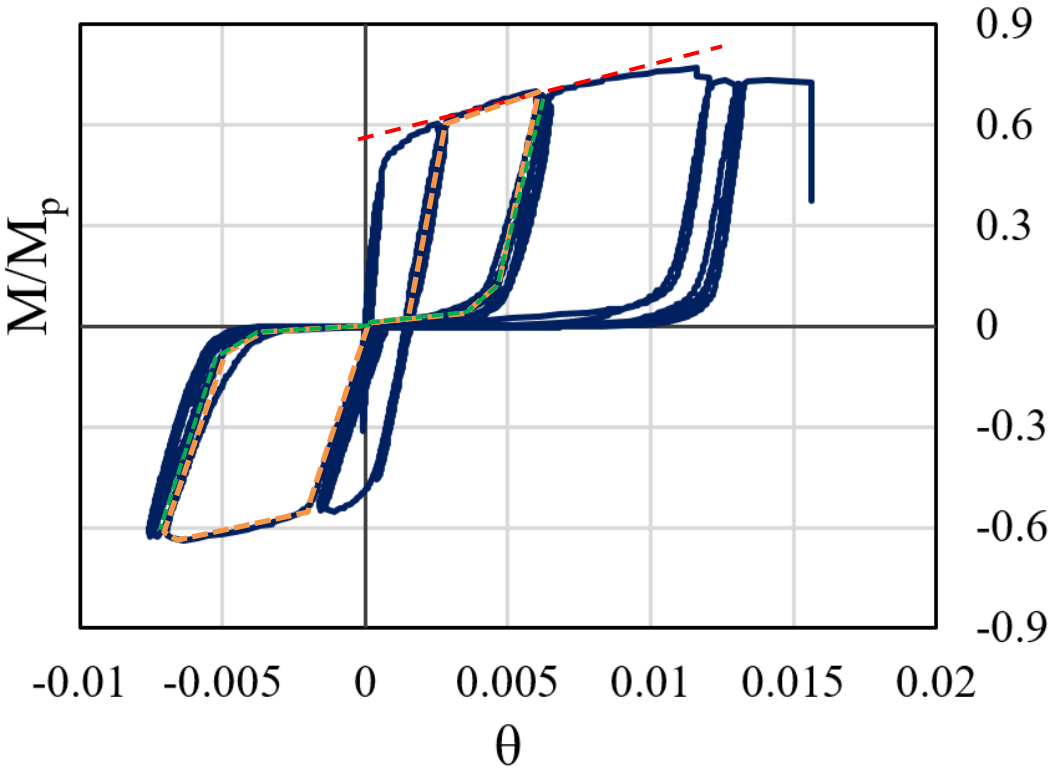

(A) Moment ratio (M/M_p) vs rotation θ, red dash line shows equivalent post elastic stiffness

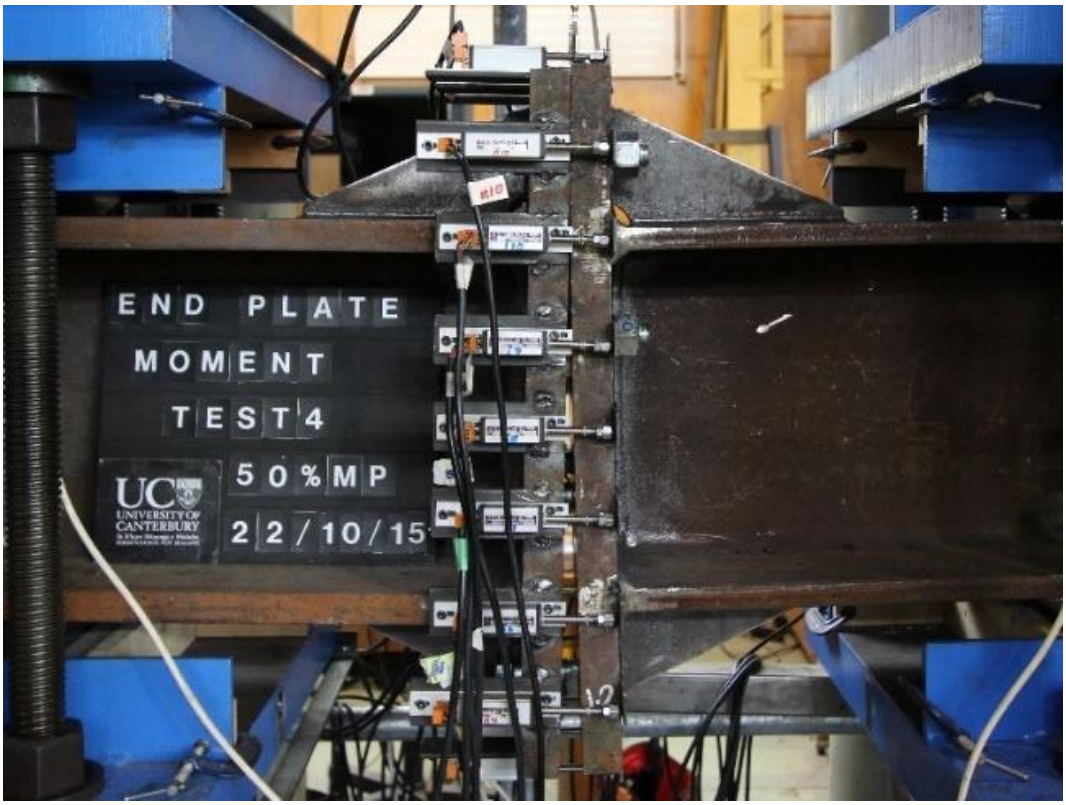

(B) Localized deformation of Specimen #7, potentiometers along the connection height measure opening

Figure 3-13 (A) Moment ratio vs rotation at the splice in Specimen #7, M_p is plastic capacity of smaller spliced member and rotation is the ratio of joint opening to section height **(B)** Localized deformation of Specimen #7

(A) Bolt slackness due to residual elongation

(B) Elongation in bolt

(C) Necking in bolt

(D) Failure at the end of unthreaded shank

Figure 3-14 Specimen #7: Damage observations

The connection presented a gapping system mainly due to the residual elongation of the bolts. This behaviour can be seen in Figure 3-13-A. The yellow dashed lines are corresponding to the first cycle, and the green dashed line are corresponding to the second and third cycle at the same amplitude.

Figure 3-14-A shows a slacken bolt during the experiment due to plastic elongation. Figure 3-

14-B shows a bolt in the second bottom row elongated approximately 5mm compared to a bolt in the top row. Figures 3-14-C and 3-14-D show different failure modes in the fractured bolts.

Key outcomes of Specimen #7 (Tension Friction (TF) bolts):

- The specimen developed 78% of the nominal plastic capacity of the smaller section. The ultimate strength is larger than the design capacity calculated as 50% of the nominal section plastic capacity.
- The connection showed characteristics of a gap system with incremental damage due to residual elongation of bolts.
- The splice presented a very high stiffness of 12*EI/L* initially. The splice stiffness value after bolt tensile yielding is approximately 0.57*EI/L*.
- The ultimate rotation capacity was ~0.015 rad, which is significantly smaller compared to rotations in lap plate splices.
- The overstrength capacity of the end plate splice is 56%, which is smaller than overstrength of lap plate splices, ~100%.

Specimen #8 (Welded splice)

This test was conducted to compare the behaviour of full penetration butt-welded splices with bolted splices. To compare the behaviour of the welded connection with bolted splice connections, the moment-displacement loops for Specimens #7 and #8 were overlaid in Figure 3-15-A. The displacement was measured at the centre of the specimen (at the splice centre). Specimen #8 demonstrates elastoplastic performance, with ultimate strength of $1.2M_p$. The end plate connection performs similar to the rigid welded connection at small displacements as can be seen in the figure. Figure 3-15-B shows Specimen #8. The test was stopped after yielding in the smaller members due to restrictions of the test rig. No visual damage was observed in

the weld after the experiment. However, flexural yield lines were visible in the flanges of the smaller member.

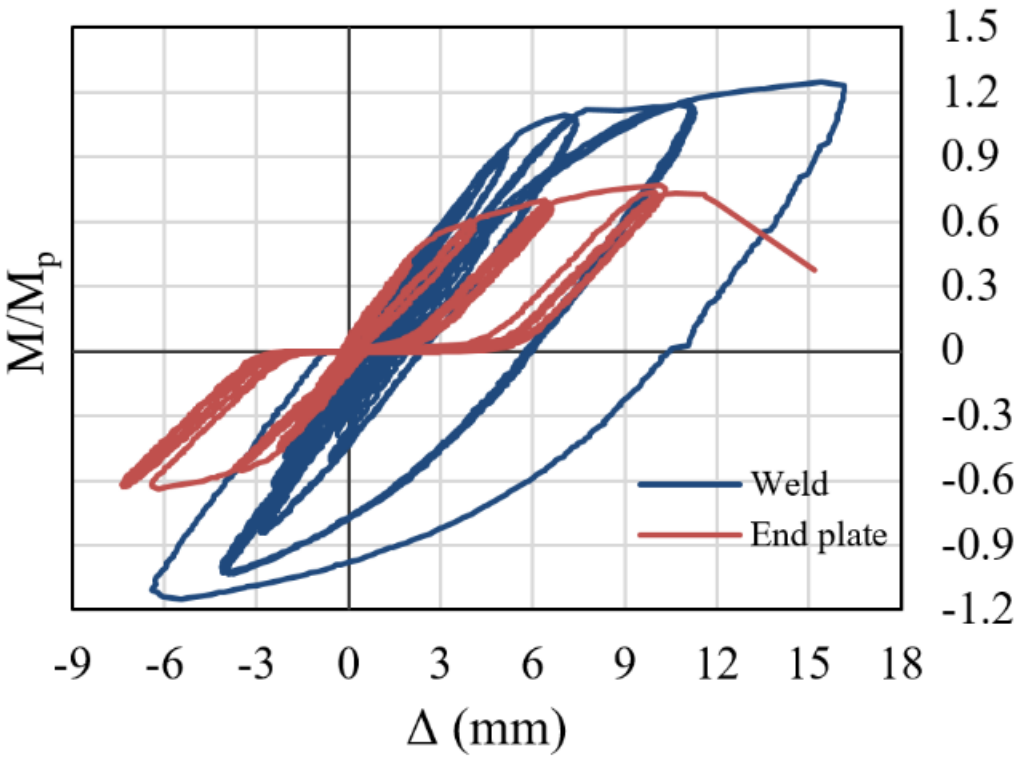

(A) Moment ratio (M/M_p) vs displacement Δ

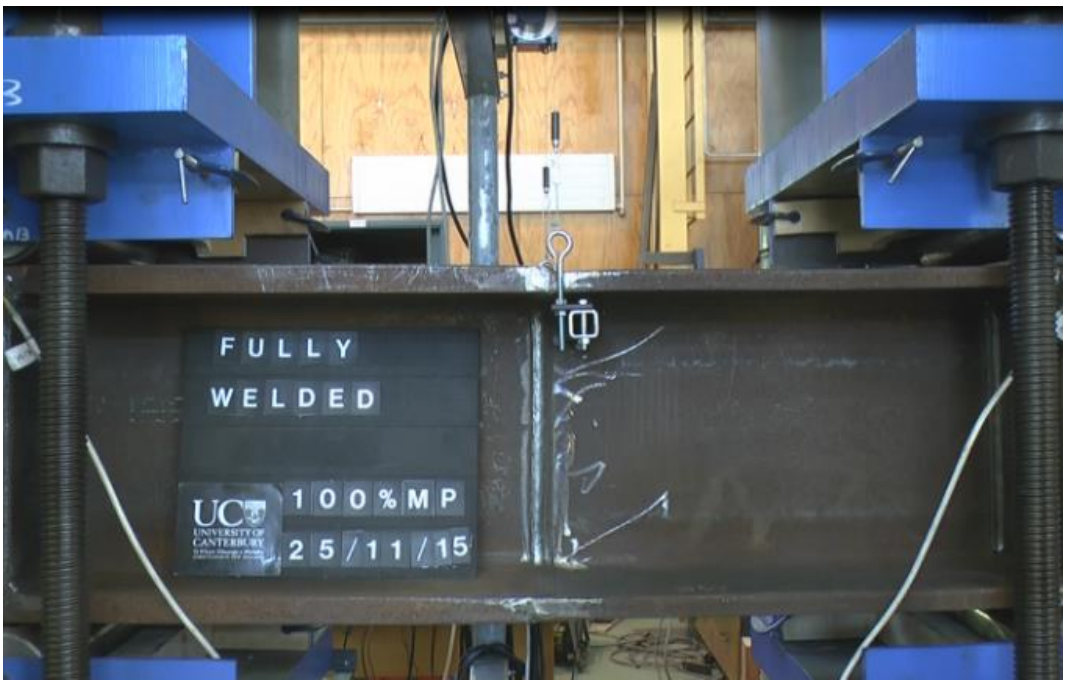

(B) Global deformation in Specimen #8

Figure 3-15 (A) Moment ratio vs displacement at the splice in Specimens #7 and #8, both connections have similar stiffness at displacements up to ~2mm **(B)** Global deformation of Specimen #8

Key outcomes of Specimen #8:

- The specimen developed 120% of the nominal plastic capacity of the smaller section.
- The connection showed characteristics of an elastoplastic system.
- The splice presented a very high initial stiffness of 12*EI/L*.
- No obvious damage was observed in the weld after the experiment.
- The test was stopped due to flexural yielding in the smaller member.

3.2.2. *Moment Tests - Minor Axis Bending (Specimens 9-10)*

Specimen #9 (Bearing lap splice similar to Specimen #1)

The purpose of this test was to study the flexural performance of Specimen #1 about its minor axis, rather than its initial major axis. Figure 3-16 shows the hysteresis loop and localized deformation of the specimen at the connection. The connection developed approximately 120% of the computed minor axis plastic moment capacity of the smaller member. The ultimate rotation of the connection is approximately 11.4%.

The rotation associated with slip is estimated to be $2 \times 1\text{mm}/289\text{mm}=0.007$, assuming the members rock against each other. A total of 289mm is the distance between the pivot point, at the end of flange, to the furthest bolt. The moment-rotation relationship increases relatively linearly post slippage, with a stiffness of approximately $7.5M_{py}$ equivalent to $3.4M_p$.

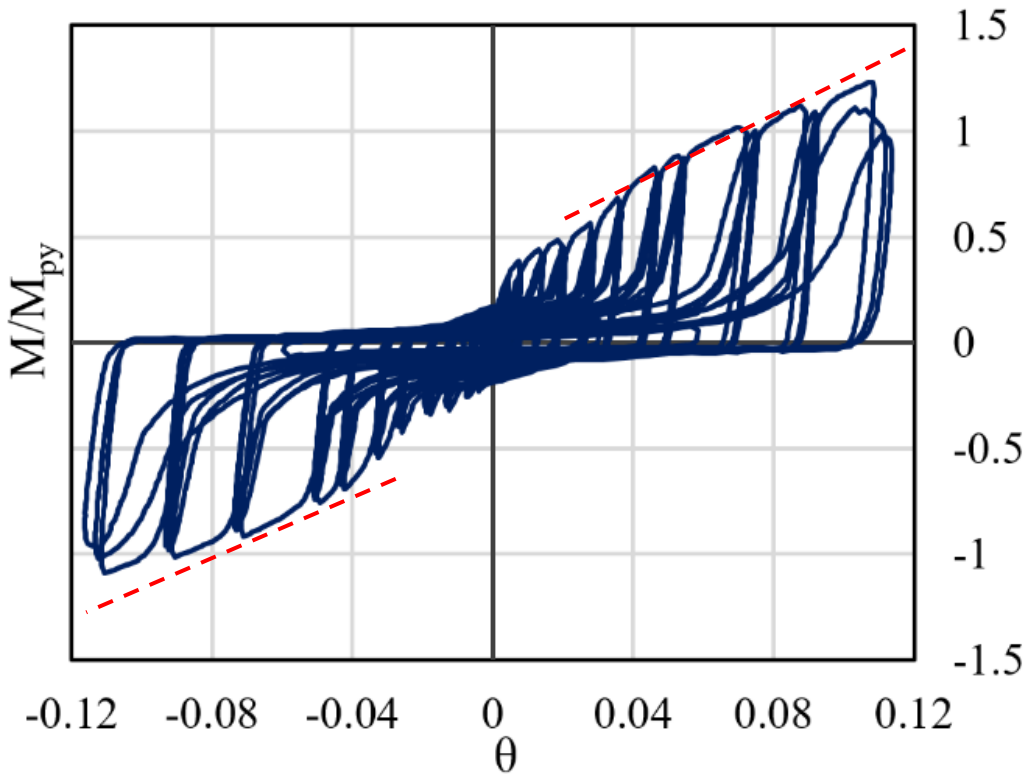

(A) Moment ratio (M/M_{py}) vs rotation θ, red dash lines show backbone slope

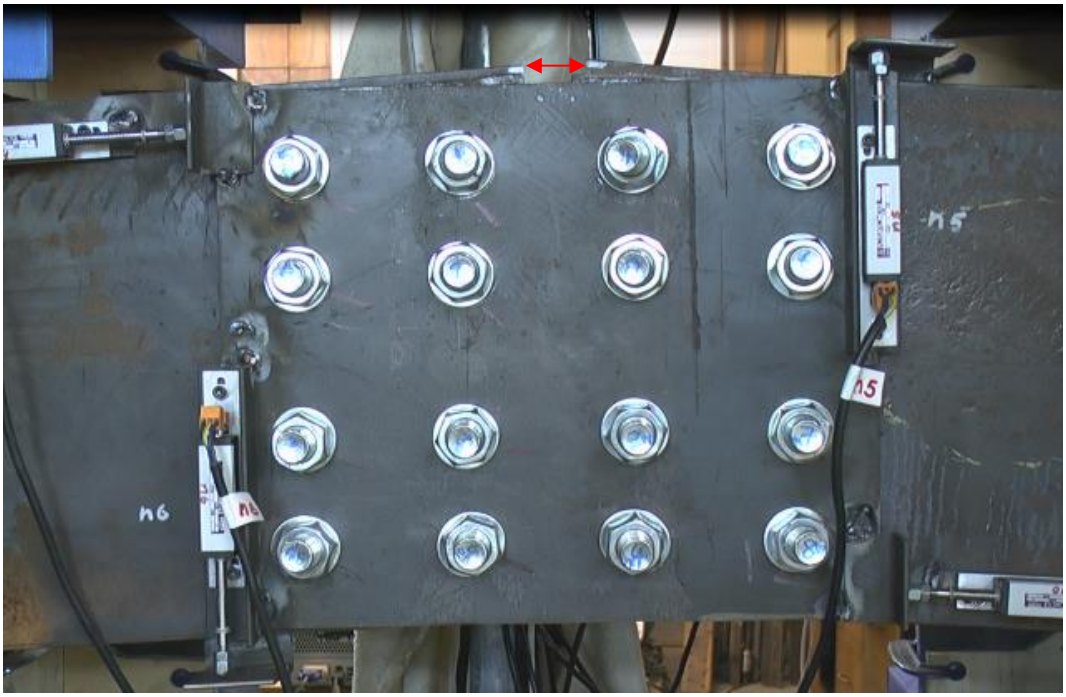

(B) Localized deformation of Specimen #9 at splice connection

Figure 3-16 (A) Moment ratio vs rotation at the splice in Specimen #9, M_{py} is plastic capacity of smaller spliced member about minor axis and rotation is the angle of joint opening **(B)** Localized deformation of Specimen #9 bending about minor axis

Figure 3-17-A shows the connection after failure of two bolts farthest from the centre of

rotation, and their deformation is shown in Figure 3-17-B. It appears bolt deformation is mainly generated by pure shear forces. Connection failure was not noted, as the fractured bolts dropped quietly. While forces are ideally transferred in the plane of the splice plates, out of plane deformations were observed in both flanges and splice plates, as seen in Figure 3-17-C. This deformation could be a result of local buckling in the compression zone.

Residual bearing deformation and rounded flange corners were observed. Bearing deformation of spliced member flanges is evident in Figure 3-17D. It is evident the filler plates make an insignificant contribution in transferring compressive forces. Figure 3-17-E shows flange splice plate distortion.

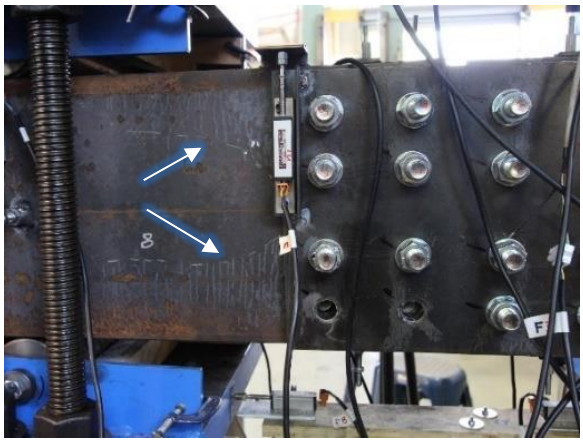

(A) Failure of bolts in shear, and flexural yield lines on flange adjacent to splice plate

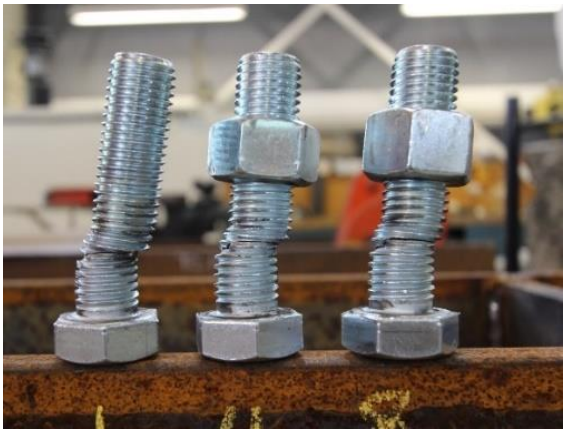

(B) Shear failure in bolts (bolts were put together after failure)

(C) Distortion in flange due to local buckling, flange deformed ~5mm out of alignment

(D) Bearing deformation in flanges due to compression

(E) Distortion in flange splice plate due to buckling in flanges

Figure 3-17 Specimen #9: Damage observations

Key outcomes of Specimen #9 (Tension Friction (TF) bolts):

- The specimen developed 120% of the nominal plastic capacity of the smaller section about its minor axis. The ultimate strength is larger than the design capacity calculated as 44% of the nominal section plastic capacity.
- The connection showed characteristics of a gap system with incremental damage.
- The connection initially reached a strength of $0.4M_{py}$ at 0.01 rad rotation, after which it presented a steady stiffness of approximately $0.3EI_y/L$.
- The ultimate rotation capacity was ~0.11 rad.

Specimen #10 (Bearing lap splice with longer splice plate than Specimen #9)

The purpose of this test was to study the influence of doubling the number of flange bolts on the flexural behaviour in comparison to Specimen #9. The ultimate strength of the connection similar to Specimen #9. However, the ultimate rotational capacity of the connection is smaller.

Figure 3-18 shows the hysteresis loop and localized deformation of Specimen #10 at the splice connection. The rotation associated with slip equals to 2×1mm/398mm=0.005, where 398mm is the distance from pivot point to the furthest bolt, given the members rock against each other. The connection showed ductile behaviour with buckling in the splice plates.

The connection did not exhibit complete gapping behaviour, likely due to residual friction in

the connection after splice plate buckling. Therefore, it was able to provide energy dissipation throughout the experiment unlike the connections discussed previously. No failure or obvious deformation occurred in the bolts. The test was stopped since the specimen had already reached its plastic moment capacity. The stiffness of the connection at large deformations is approximately $5M_{py}$, which is 67% of the stiffness obtained for Specimen #9.

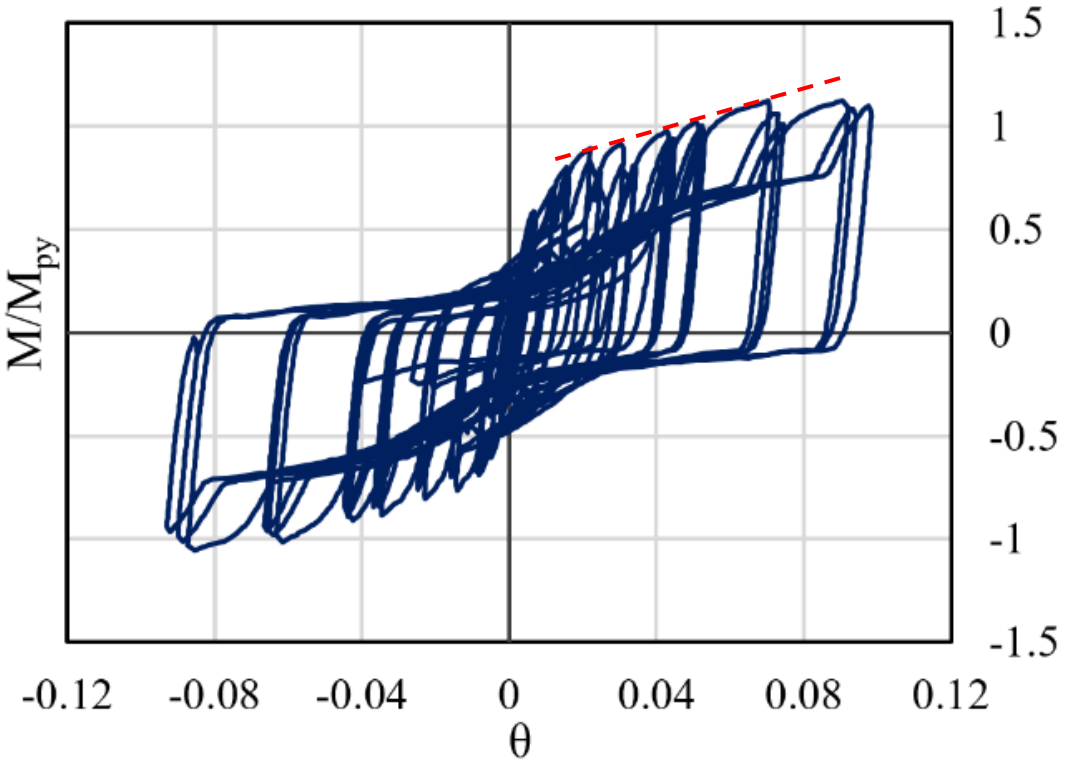

(A) moment ratio (M/M_{py}) vs rotation θ, red dash line shows backbone slope

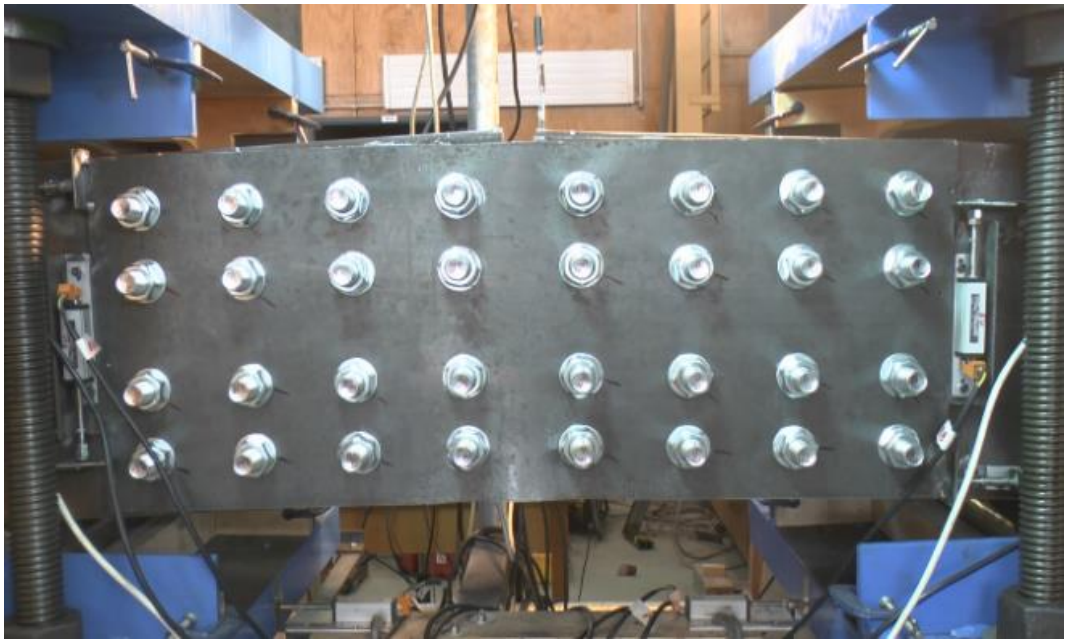

(B) Localized deformation of Specimen #10

Figure 3-18 (A) Moment ratio vs rotation at the splice in Specimen #10, M_{py} is plastic capacity of smaller spliced member about minor axis and rotation is the angle of joint opening **(B)** Localized deformation of Specimen #10 bending about minor axis

After the experiment, two bolts close to the centre were loose and could be undone by hand. A fracture initiated at a hole in the central row close to the edge, as can be seen in Figure 3-19-B. Flange splices yielded along the inner bolt rows as can be seen in Figure 3-19-C. The column flanges experienced damage in the form of yielding near the holes, out of plane distortion, and rounded corners at the contact area. These observations can be seen in Figures 3-19-D to F.

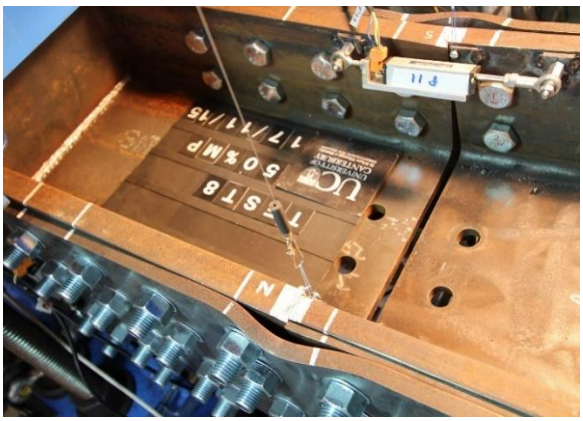

(A) Buckling of splice plate in compression

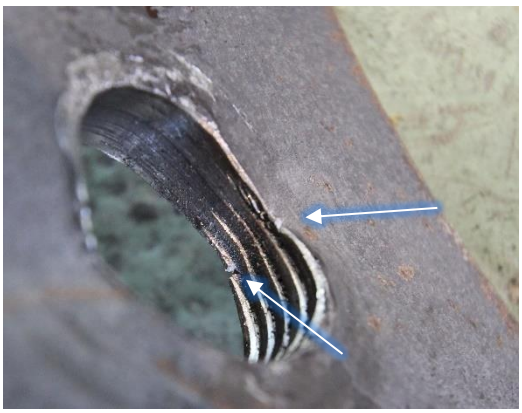

(B) Initiation of rupture at hole edge

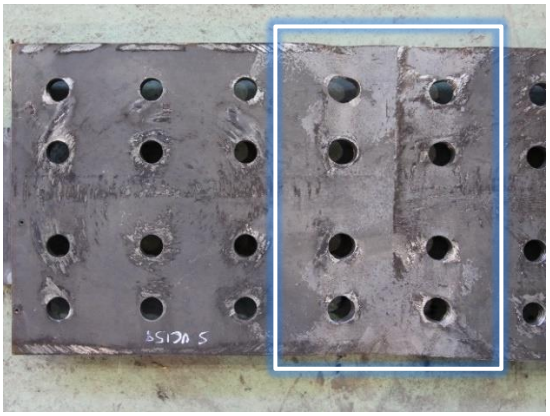

(C) Damage along central bolt rows in flange splice plate

(D) Distortion of flanges in smaller member

(E) Yield lines near the central holes in flange

(F) Rounded flange end in smaller member

Figure 3-19 Specimen #10: Damage observations

Key outcomes of Specimen #10 (Tension Friction (TF) bolts):

- The specimen developed ~115% of the nominal weak axis plastic moment capacity of the smaller section. The ultimate strength is larger than the design capacity calculated as 60% of the nominal section plastic capacity. The ultimate capacity of the connection is smaller than Specimen #9, despite the greater number of bolts.
- The connection did not show the complete characteristics of a gap system and retained some friction.
- Local buckling occurred at the compression side of the flange splice plates, which changed the characteristics of the hysteresis loops post buckling.

- The connection reached a strength of $0.87M_{py}$ at approximately 0.02 rad, then presented a stiffness of approximately $0.2EI_y/L$. The connection can initially develop larger strength at smaller rotations, but its stiffness at larger rotations is smaller than Specimen #9.
- The ultimate rotation capacity of ~0.1 rad was achieved with no bolt failure. The test was stopped due to flexural yielding of the section.

3.2.3. *Shear Tests - Major Axis Shear (Specimens 11-13)*

Specimen #11 (Flange and web splice)

This test was conducted to study the cyclic shear performance of Specimen #1 about its major axis. Figure 3-20 shows the hysteresis loop and localized shear deformation of the connection. The connection developed 120% of the calculated shear capacity of the smaller member with ultimate shear deformation of 0.043 or 4.3%. The connection presented dissipation characteristics, which are mainly attributed to plasticity in the flange splice plates.

The connection exhibited different stiffness in the reverse direction. Shear distortion of the splice, γ, was defined as the relative shear displacement of the members at the joint normalized by the section height, 327mm. Thus, the stiffness of the connection in the positive direction can be calculated as $0.3V_y/(0.327\text{m}\times0.02)=45.9V_y$ kN/m. The stiffness can be expressed as a function of A_vG/L where A_v is the area of smaller web. For a 3m long column of 310UC118 section, the stiffness is equivalent to $0.31A_vG/L$ (kN/m), knowing G=80 GPa and A_v=3303 mm^2 (see Appendix A for section dimensions). The stiffness in the reverse direction is larger, equal to $76V_y$ kN/m.

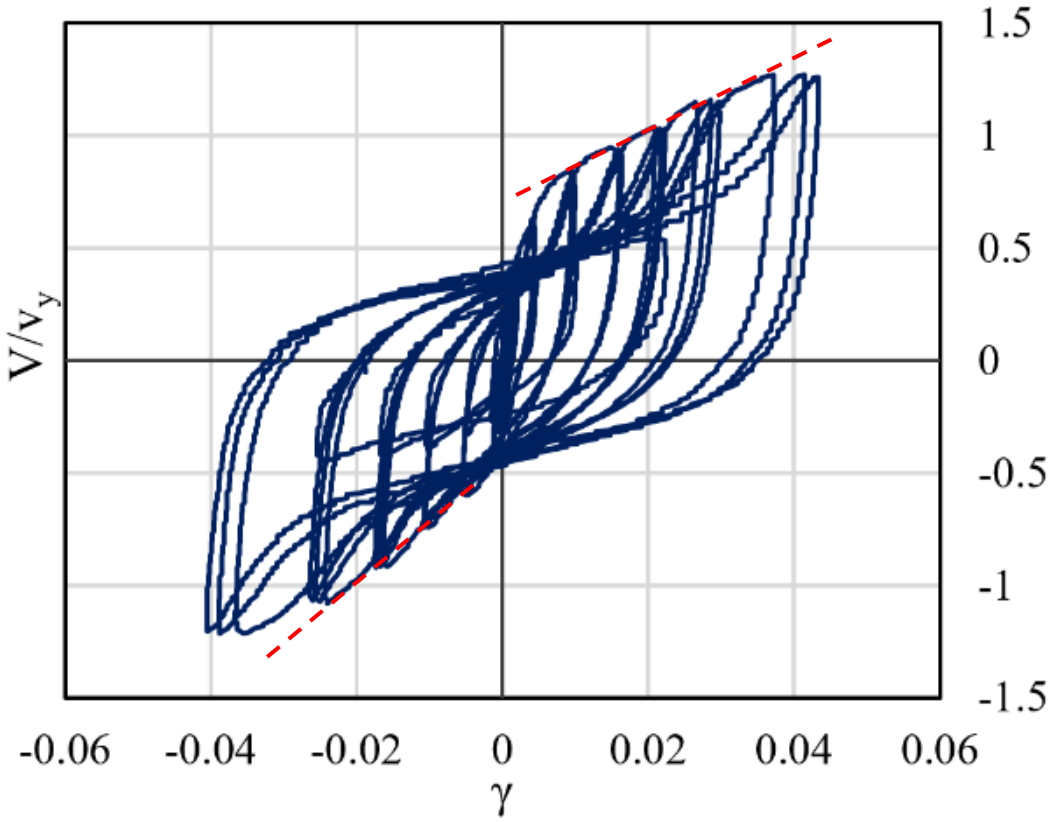

(A) Shear ratio (V/V_y) vs shear distortion γ, red dash lines show backbone slopes

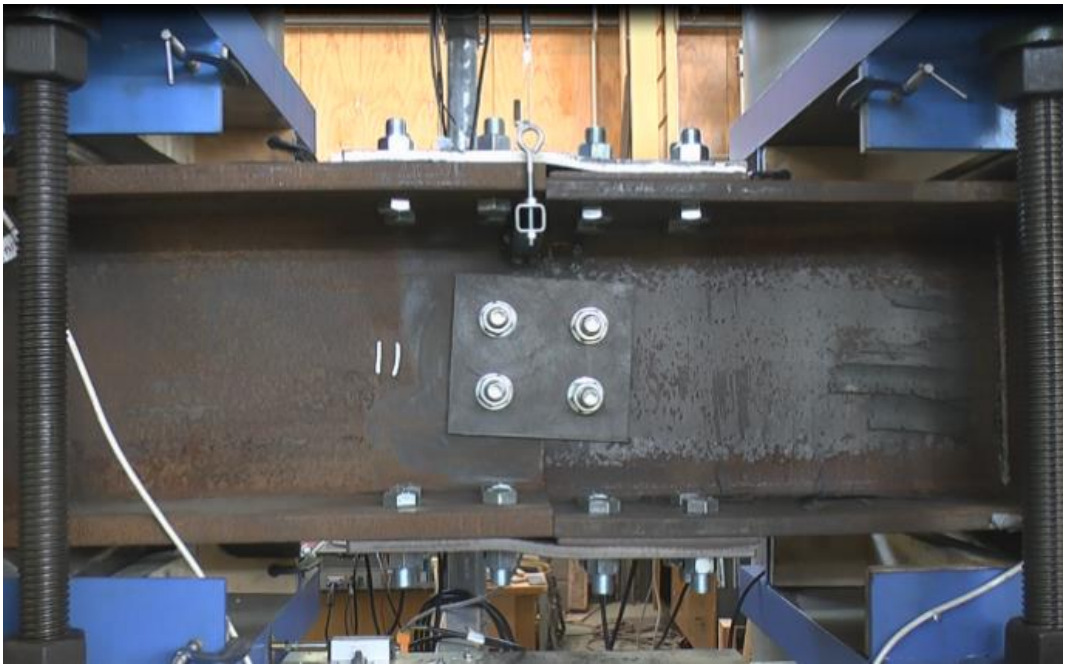

(B) Localized deformation in Specimen #11

Figure 3-20 (A) Shear vs distortion at the splice in Specimen #11, V_y is shear capacity of smaller spliced member and rotation is ration of shear displacement to section height **(B)** Specimen #11 under shear about major axis

The test was stopped after significant shear yielding started in the smaller member, but no connection failure occurred. Figure 3-21 shows specimen component damage for each element.

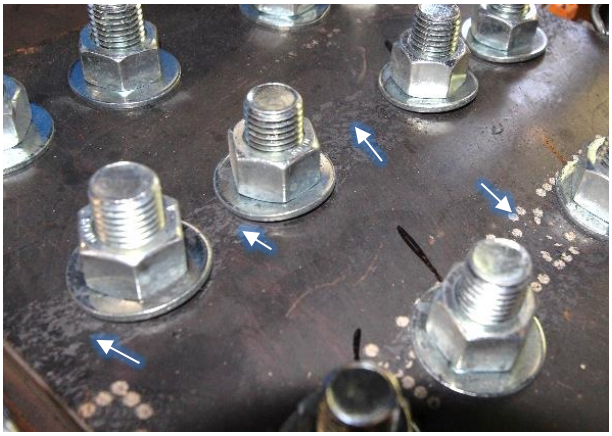

(A) Yielding along inner bolt rows in flange splice plate, and bending in washers

(B) Abrasion around flange bolt holes

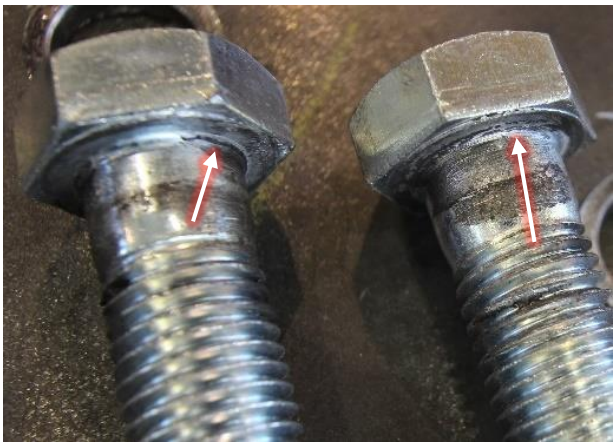

(C) Cracking in bolt head joint

(D) Yield line in flange of smaller member

(E) Abrasion around web holes due to movement

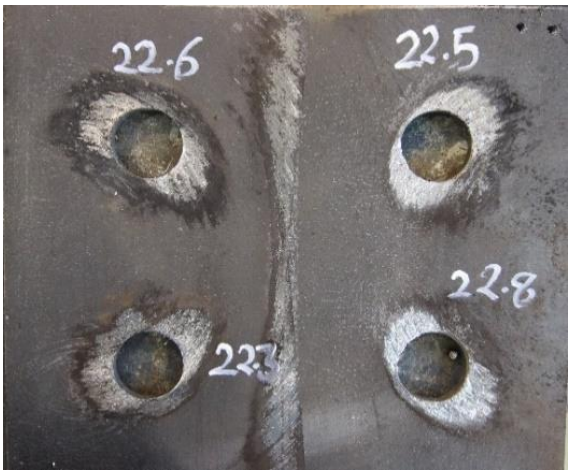

(F) Abrasion in web splice plate

Figure 3-21 Specimen #11: Damage observations

Key outcomes of Specimen #11 (Tension Friction (TF) bolts):

- The specimen developed 120% of the nominal shear capacity of the smaller section. The ultimate strength is larger than the design capacity of the web splice, which was calculated as $0.3V_y$.
- The connection showed characteristics of a bilinear system.
- The connection yielded at approximately 0.6% shear distortion, with a strength of $0.75V_y$, resulting in an elastic stiffness of 2.6 A_vG/L. The post yielding stiffness is $0.31A_vG/L$.
- The stiffness of the connection in the reverse direction is larger, equal to $0.51A_vG/L$.
- The connection reached an ultimate shear distortion capacity of 4%. The test was stopped due to shear failure of the section.

Specimen #12 (Flange splice with no web plates)

This test was conducted to study the effect of web splices in shear performance. It is similar to Specimen #11, but has no web splice. Figure 3-22 shows the hysteresis loop and localized deformation. The ultimate capacity of the connection is ~15% smaller than Specimen #11, but the ultimate shear deformation is approximately double. The hysteresis behaviour shows smaller dissipation capacity compared to Specimen #1, which could be attributed to the absence of web splice plate. The stiffness of the connection is approximately $23V_y$ and $40.8V_y$ (kN/m) in positive and negative directions which is approximately half of those for Specimen #11.

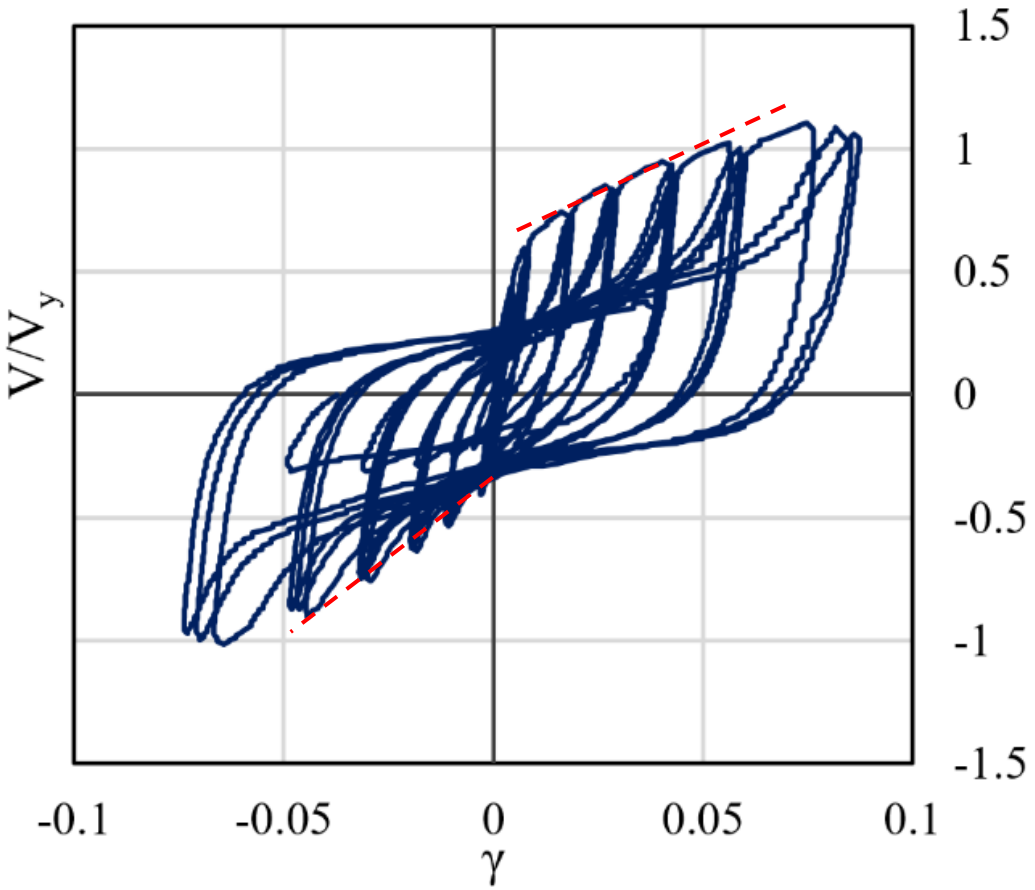

(A) Shear ratio (V/V_y) vs shear distortion γ, red dash lines show backbone slopes

(B) Localized deformation in Specimen #12

Figure 3-22 (A) Shear vs distortion at the splice in Specimen #12, V_y is shear capacity of smaller spliced member and rotation is ration of shear displacement to section height **(B)** Specimen #12 under shear about major axis

The test was stopped after significant shear yielding started in the smaller member. The damage in the flange splices was more extensive than the damage in Specimen #11. Figures 4-23 show damage in the components of the connection. Bending in the bolts at the inner rows were noticeable and can be seen in Figure 3-23-F.

(A) Flexural plasticity in splice plate and bending in washers

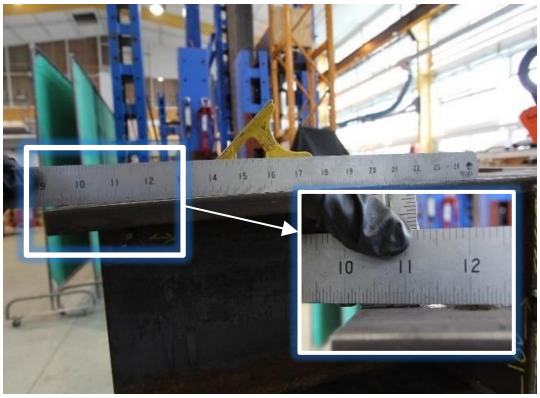

(B) Distortion in flange of smaller member

(C) Elongation in inner row holes

(D) Yielding in flange of smaller member

(E) Abrasion near inner row holes in filler plate

(F) Bending in inner row bolts

Figure 3-23 Specimen #12: Damage observations

Key outcomes of Specimen #12 (Tension Friction (TF) bolts):

- The specimen developed 110% of the nominal shear capacity of the smaller section.
- The connection showed characteristics of a bilinear system.
- The connection yielded at approximately 1% shear distortion, with a strength of $0.6V_y$, equivalent to an elastic stiffness of 1.2 A_vG/L. The post yielding stiffness is $0.15A_vG/L$, which is half of that in Specimen #11.
- The stiffness of the connection in the reverse direction is larger, equal to $0.25A_vG/L$.
- The connection reached an ultimate shear distortion capacity of 9%, which is approximately two times larger than Specimen #11.

Specimen #13 (Web splice)

This test was conducted to study the effect of eliminating flange splices in the shear performance of Specimen #11. Figure 3-24 shows the hysteresis behaviour and localized shear deformation at the connection. The connection developed 52% of the shear capacity of the smaller member at a shear deformation of 10%. The shear force capacity of the connection is approximately half of that of Specimen #1, and the shear deformation capacity is more than twice of Specimen #1 as shown in Figure 3-24-A. The connection energy dissipation is less than 50% of that of Specimens #1 and #2. The stiffness of the connection is approximately $12V_y$ (kN/m), which is only 28% of the smaller stiffness in Specimen #11.

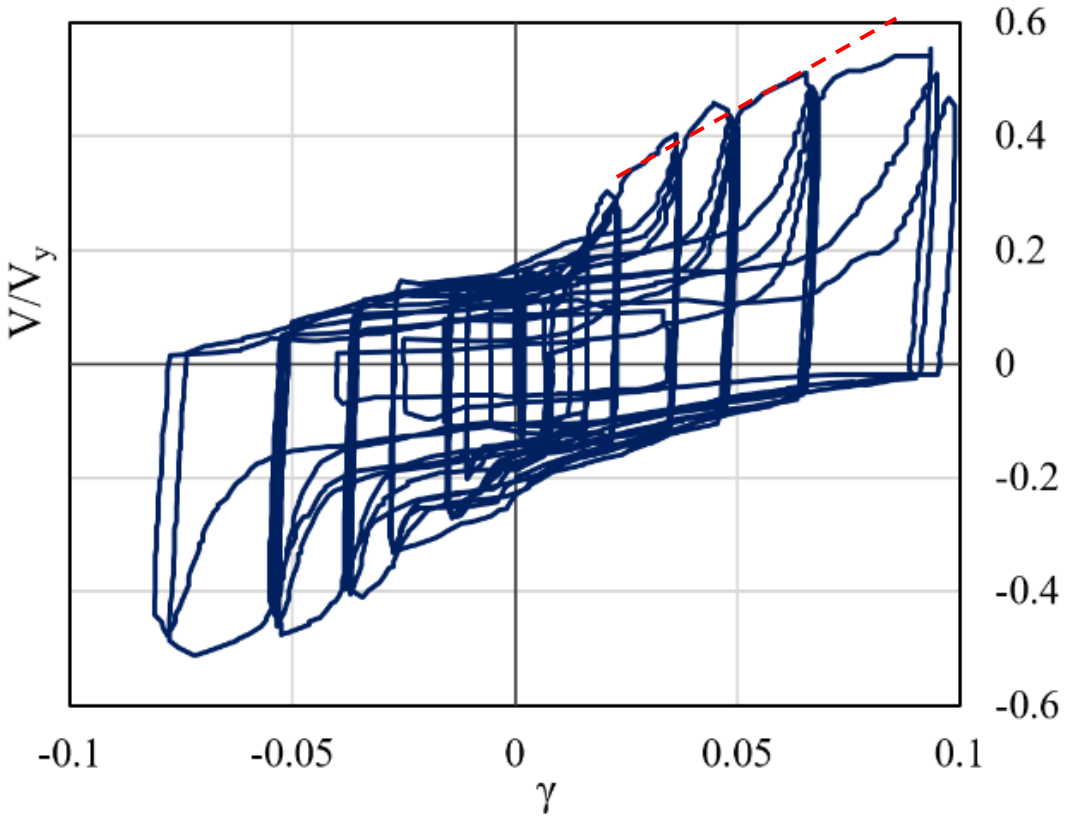

(A) Shear ratio (V/V_y) vs shear distortion γ, red dash line shows backbone slope

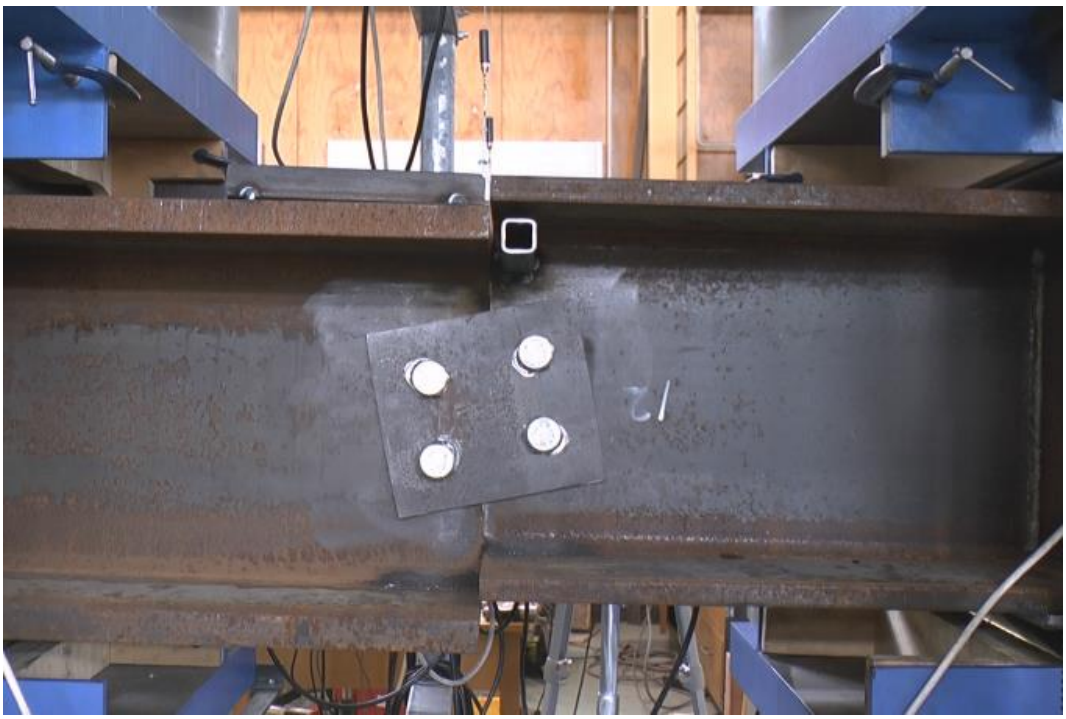

(B) Localized deformation in Specimen #13

Figure 3-24 (A) Shear vs distortion at the splice in Specimen #13, V_y is shear capacity of smaller spliced member and rotation is ration of shear displacement to section height **(B)** Specimen #13 under shear about major axis

The test was stopped after failure in one of the bolts. Figure 3-25 shows damage in the web splice. This damage is similar, but more extensive than seen in the web of Specimen #11.

(A) Bolt failure in web splice

(B) Hole elongation in the web of the smaller member

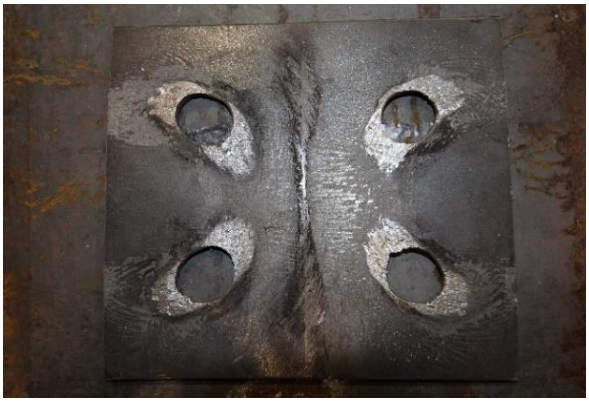

(C) Abrasion in web splice plate

(D) Yield lines in web splice due to bolt bearing

Figure 3-25 Specimen #13: Damage observations

Key outcomes of Specimen #13 (Tension Friction (TF) bolts):

- The specimen developed 52% of the nominal shear capacity of the smaller section. The ultimate strength is larger than the design capacity of the web splice, which was calculated as $0.3V_y$.
- The connection showed characteristics similar to a gap system.

- The bolts initially slipped at $0.15V_y$, generating a shear distortion of approximately 1%. The backbone stiffness of the connection post slippage was $0.08A_vG/L$, which is the smallest compared to Specimens #11 and #12.
- The connection reached an ultimate shear distortion capacity of 10%.

3.2.4. *General Limitations (All Tests)*

All the specimens tested under moment were fabricated with Engineers washers thinner and slightly smaller than the standard size structural washers due to an oversight. Washers are used in bolted connections to distribute bearing pressure under the nuts smoothly (Portland Bolt, 2015). It also used in friction connections to ensure consistent bolt tensioning outcome (Allen and Iano, 2013). It is expected the thickness of the washers had a minor impact on the overall performance of the connections post slippage.

3.2.5. *Implications of Axial Loading on Connection Performance*

Flexural Performance

For bearing lap splices, the absence of compression force would result in smaller moment at which slip occurred. In contrast, slip would occur at smaller moments for non-bearing connections in the presence of compression load. However, the flexural stiffness of these connections may not change as a result of compression loads. While compression loading could reduce the flexural capacity of non-bearing splices, it can increase the flexural capacity of bearing splices. Similarly, for bolted end-plate splices, provided end-plates not yield in compression, compression loading could increase its flexural capacity, with no significant compromise in the connection flexural stiffness.

Shear Performance

Compression loads would generate frictional resistance at the contact surface of bearing splices without compromising shear stiffness. The capacity of bearing connections may increase depending on the contact surface roughness and axial load. For non-bearing splices, axial load could induce second order moments in flange splices if shear deformations are considerable. The interaction of shear and axial actions would also reduce the capacity of both web bolts and splice plates in non-bearing splice connections. Both shear capacity and stiffness of non-bearing splice connections would be compromised if compression forces are sufficiently large.

3.3. Material Testing of Components

Column sections

Samples were taken from the webs and flanges of test specimens. Dimensions of the test coupons are provided in Appendix B. The objective of these tests was to ensure that the specimens were supplied from the expected grade, 300MPa. The results of these tests do not appear explicitly in the predictive backbone models described in Chapter 4, but may be used to discuss suitability of models. Table 3-1 shows the average values of yield and ultimate tensile stresses for these component tests versus the specified nominal values (*Design with Steel: Dimensions and Properties Handbook*, 2013). Overall, test values were up to 10% greater than the nominal values in flanges for yield strength. However, the web in 250UC89.5, however, exhibited smaller yield strength than the nominal specification. The ultimate strength of all samples were larger than the nominal values by up to 20%.

Table 3-1 Yield stress properties of column sections

Column	Sample	Yield Stress (MPa)		Ultimate Stress (MPa)	
		From Component Testing	Nominal	From Component Testing	Nominal
310UC158	Flange	285	280	470	440
	Web	315	300	475	440
310UC118	Flange	320	280	510	440
	Web	330	300	485	440
310UC96.8	Flange	325	300	480	440
	Web	355	320	480	440
250UC89.5	Flange	310	280	495	440
	Web	315	320	450	440

Bolts

Table 3-2 shows the average values of ultimate tensile capacities of the bolts used in the splice testing. The nominal values in the table are the design strengths suggested in (Hogan and Munter, 2007). The actual shear capacities of the bolts were derived from tensile testing per the calculations seen in the table. The actual shear capacities of the bolts were derived from multiplying the ultimate tensile strength from component tests, by the ratio of design shear capacity of threaded area (ϕV_{fn}) to design tensile capacity (ϕN_{tf}) of the bolt. These values are 92.6kN and 163kN for M20, and 133kN and 234kN for M24 (Hogan and Munter, 2007). The ultimate strengths were up to 10% greater than the nominal specified values.

Table 3-2 Material properties of bolts

Bolt Diameter	Ultimate Tensile Strength (kN)		Ultimate Shear Strength (kN)		Ultimate Axial Deformation (mm)
	From Testing	Nominal	Derived From Tensile Testing	Nominal	
M20	235	204	235*92.6/163=133	116	7.3
M24	309	293	309*133/234=176	166	4.9

Photos of the test rig and failed bolts can be found in Appendix B.

Flange and web Splice Plates

Table 3-3 shows the yield and ultimate tensile stresses of the plates used in the splice testing. It can be seen the yield and ultimate strength of 6mm plate is considerably larger than the

nominal specified properties. While these values are not directly used in the predictive models, it is important to ensure that they were supplied from the expected grades, used in design calculations.

Table 3-3 Material properties of plates

Plate Thickness	Yield Stress (MPa)		Ultimate Stress (MPa)	
	From Testing	Nominal	From Testing	Nominal
12mm	305	310	445	440
6mm	405	360	560	480

3.4. Summary

In this chapter, cyclic bending and shear performance of the specimens in Chapter 2 were discussed. The hysteresis loop for each specimen was provided, and damage observations were illustrated in photos. Analysis results predicting expected behaviour from fundamental mechanics were compared to design expectations. The overall set of experiments covers the range of major and minor axis loading, and splice design types. In addition, material testing was conducted to verify mechanical properties of components. Key results were tabulated for each test specimen, as presented and in relevant context to the goal of the specific experiment.

It was found connections developed larger strength than their design capacities. Generally, bolted lap splice connections and end plate connection exhibited characteristics of a gap system under moment loading. Splices developed a range of stiffnesses depending on their design and construction method. For the splices tested in this study, welded connection was the most rigid, while bolted lap splices showed the greatest flexibility and ductility. End-plate splice was relatively rigid in small deformations. The results of these experiments will be used to verify analytical models developed for each specimen in Chapter 4.

Chapter 4. **Development of Equations to Predict Splice Behaviour**

4.1. **Introduction**

This chapter describes the prediction of force versus deformation behaviour of tested splice connections in bending and shear. The goal of this chapter is to present simple modelling approaches suitable for practitioners for analysing these connections. The specific goal is to capture the load-deformation "backbone" for loading. This backbone provides the fundamental connection information needed by designers. While more sophisticated numerical approaches could simulate the full loading and unloading cyclic performance of these connections, they are not timely or cost-effective in design practice, and do not necessarily provide significant further practical information for designers. The novelty of these approaches is their accuracy and adequacy for design purposes, which will be discussed in Chapter 5, given their relative computational and mathematical ease of use for practitioners.

This chapter starts with the development of the prediction models, followed by comparison of the results with the tested data. The predicted backbone behaviours are based on the mechanical properties of components provided in Chapter 3. Several symbols have been adopted throughout this chapter for the analyses of these connections. A complete list of these symbols can be found at the end of this chapter (Section 4-5) summarizing these symbols in a single place.

4.2. **Development of Predictive Methods**

Different assumptions and approaches were adopted in predicting the behaviour of different types of splices under bending and shear loading. For moment about the major axis, they are

classified as bearing lap splices, non-bearing lap splices, end plate splices, and welded splices, which are individually discussed in Section 4.2.1. For minor axis bending and major axis shear, the predictive approaches are discussed in Sections 4.2.2 and 4.2.3, respectively.

4.2.1. ***Major Axis Bending***

Bearing Lap Splices

Figure 4-1 shows the exploded view of a column (shown horizontally) under bending moment and the free body diagram of the smaller member of the specimen. The compression force, F_c, was assumed to be a point load acting at the top edge of the smaller member flange, as shown in the figure. This member was assumed to rotate about this point, known as the pivot point. It was assumed the plate on the compression side only maintains the column member in place, but does not contribute in transferring compression forces. The tensile force at the section is equal to total shear in the flange bolts assuming all bolts undergo the same amount of deformation. Since the flange bolted length is short, this assumption is reasonable (Kulak et al., 1987), (Hogan and Munter, 2007) prior to yielding occurring in the plate at the net area, along the inner rows of holes. When yielding starts, the holes closer to the centre of connection would elongate more than the bolts further from the centre.

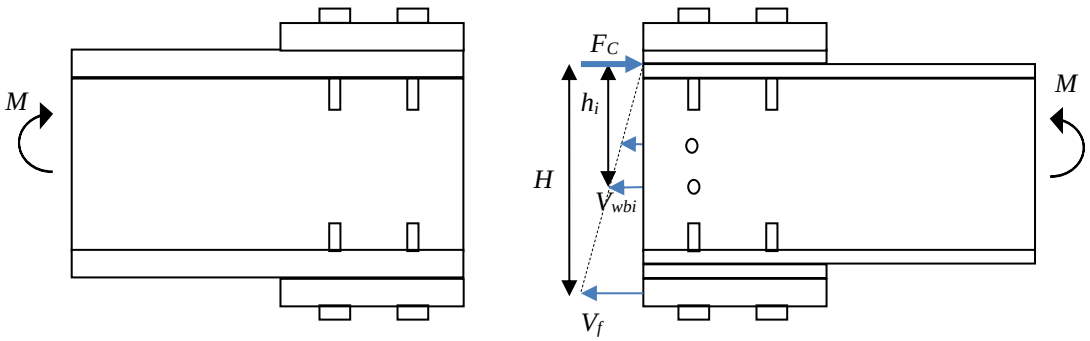

Figure 4-1 Free body diagram of lap splice in bending

The force displacement model used to characterize the behaviour of the splice plate in tension was derived from (Fisher, 1965):

$$R = R_{ult} \times (1 - e^{-\mu\Delta})^{\lambda} \qquad \textit{Equation 4-1}$$

Where R_{ult} is ultimate shear strength of bolt, and Δ is the deformation of the bolt-plate system, e is the mathematical constant that is the base of the natural logarithm, and μ and λ are the parameters that (Crawford et al. 1971) later determined to be 10/inch and 0.55, respectively. These parameters were found from six single bolt shear tests. The bolts were ¾ inch A325, fully tensioned and tested in double shear, in 13/16 inch holes. The plates were from ASTM A36 steel. While the thickness of the plates were not explicitly mentioned, it is understood the thicknesses were ½ inch and 7/8 inch. The bolts were the critical components in the tests. The deformation, Δ, was assumed to be the sum of shear deformation of bolt and bearing deformation of bolt and adjacent plates (Crawford et al. 1971).

Equation 4-1 is very general and does not explicitly consider parameters such as bolt diameter, bolt length, failure mode (bolt failure or plate tear-out), thicknesses of the plates, or the number of shear planes. In spite of these limitations, the LRFD Manual (*Manual of Steel Construction, Load and Resistance Factor Design*, 2001) uses Equation 4-1 to estimate bolt load deformation in an eccentrically loaded connection for bolt group design. Hence, it is widely used in practice.

For the splice model in bending, the total deformation of the flange in tension, Δ_t, consists of the axial deformation of the splice plate, shear deformation of the bolts, and ovalization of the bolt holes. The mathematical model of the shear force of the flange bolts relative to their deformation can be expressed as below:

$$V_f = n_{bolt} \times R_{ult} \times (1 - e^{-0.394\Delta_t})^{0.55}$$ ***Equation 4-2***

where Δ_t has units of mm. In this case, μ, from Equation 4-1, is 10(/inch) /25.4(mm/inch) = 0.394/mm, and n_{bolt} refers to the number of bolts on the tension splice plate each side of the connection.

It was assumed the connection reaches its ultimate flexural capacity when bolts reach the ultimate shear deformation capacity of the bolt/plate system, which is 8.6mm (Salmon et al., 2009). The tensile force in the flange splice plate was assumed to be acting at the centre of its thickness, as shown in Figure 4-1. Bolt shear in the compression side of the splice was ignored in predicting the load-deformation backbone because the compression plate only holds the column members in place. Finally, prying actions, in particular due to bending of splice plates, were not taken into account, since it may only affect the first rows of flange bolts from the centre of the connection.

For connections with web splices, shear forces of the web bolts were calculated assuming the members rock relative to each other about the pivot point. Therefore, the web bolt shear-deformation relationship can be expressed:

$$V_{wb} = R_{ult} \times \left(1 - e^{-0.394\left(\frac{h}{H}\Delta_t\right)}\right)^{0.55}$$ ***Equation 4-3***

where *h* is the web bolt lever arm (distance to the centre of rotation), and *H* is the lever arm of the tension flange force to the centre of rotation. These symbols are illustrated in Figure 4-1.

From the equilibrium of moments about the pivot point, the moment-rotation relationship of the connection can be directly calculated for any bolt deformation:

$$M = V_f H + \sum V_{wb_i} h_i \qquad \textbf{\textit{Equation 4-4}}$$

For simplicity in the above procedure, slippage in the standard oversized holes was ignored. Slippage can be added through an extra procedure, after the moment-rotation of the connection is found ignoring hole oversize. Rotations then will be increased at the onset of slippage by the associated slip rotation at the predicted slip force. The method to calculate slip force and rotation was explained in Section 3.1.1. This procedure is depicted in Figure 4-2. The blue line is the original force-deformation relationship ignoring the oversized holes. The dashed orange line is force-deformation post slippage, which is shifted for the estimated slippage for the bolt hole oversize.

In addition, friction connection behaviour prior to slippage can be assumed fully rigid. This assumption has widely been used in previous literature, thus acceptable (Borzouie, 2016), (Borzouie et al., 2015), (Borzouie et al., 2016), (Ramhormozian et al., 2017). The final idealized backbone model is shown in solid red line.

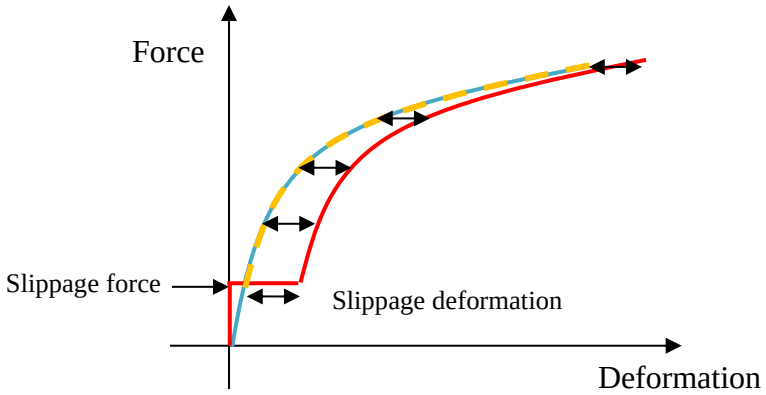

Figure 4-2 Simplified approach of incorporating slippage in force-deformation prediction of friction connections

Non-Bearing Lap Splices

For non-bearing lap splices, the flange splice plates initially work in tension and compression as a couple to resist the moment. When deformations on the compression side are sufficiently large to close the fabrication gap, the mechanism will be similar to a bearing lap splice. From this point of contact, the moment-rotation of the connection can be calculated as described for bearing lap splices in Equations 4-2 to 4-4.

The slippage due to oversized holes for non-bearing lap splices is different to those for bearing lap splices. The difference occurs because the columns have room to move on the compression side as well as the tension side. The method to estimate the slippage force and rotation can be found in Section 3.1.1 describing Specimens #4 to #6.

End-Plate Splice

The model to predict the behaviour of the end plate splice assumes the end-plates remain rigid with no major deformation in tension. This assumption is acceptable when end-plates do not experience pull-out distortions due to bolt tension. Thus, all splice rotation can be attributed to bolt axial deformation. Figure 4-3 shows the free body diagram of the specimen.

The free body diagram assumed compression was a point load acting at the top of the smaller member flange, as shown in Figure 4-3. The pivot point was chosen at the top of the flange rather than the top of end plate for two reasons. First, obtaining a perfect contact area between the end plates due to distortions from welding is unlikely. Second, one gusset plate could be insufficient for wide flange splices to provide evenly distributed bracing for end-plates, thus, failing to prevent them from rotating.

The members were assumed to rock about the top of the smaller member flange. Thus, the bolts imitate tension rods in a rocking system. To model this connection behaviour, the bolt axial force-deformation relationship is required.

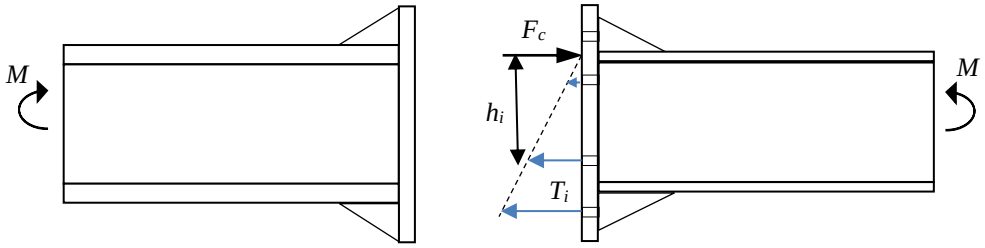

Figure 4-3 Free body diagram of end-plate splice in bending

For preloaded bolts in tension, the bolt axial stiffness parameter can be defined (*EN 1993-1-8: Eurocode 3: Design of steel structures - Part 1-8: Design of joints*, 2005):

$$k_{10} = 1.6\frac{A_s}{L_b}$$ ***Equation 4-5***

Where A_s is the tensile stress area of the bolt and L_b is the bolt length. The length here includes the grip length and half of the heights of the nut and bolt head. This length is assumed to be independent of the proportion of threaded area in the grip. The axial stiffness of the bolt was

calculated: $K_l = Ek_{10}$ (Thai and Uy, 2016), where E is the modulus of elasticity of the bolt material, assumed to be 200GPa.

Knowing the bolt tension-elongation relationship, the moment in the connection can be calculated:

$$M = \sum T_i h_i \qquad \textbf{Equation 4-6}$$

$$T_i = \frac{h_i}{h_{max}} T_{max} \qquad \textbf{Equation 4-7}$$

Where T_i is bolt tension at any deformation, and h_i is the distance of the bolt from the pivot point. T_{max} is the tension in the bolts furthest from the pivot point at the considered deformation (the bottom row of bolts in Figure 4-3). Due to proof loading of the bolts, the connection is expected to perform rigidly up to the moment calculated, per Equations 4-6 and 4-7, when T_{max} is equal to the bolt proof load of 210kN, assuming the end-plates perform rigidly.

The Welded Splice

For a four point bending beam, as shown in Figure 4-4, the elastic deformation at the centre of the beam was calculated considering flexural deformation alone (Oberg et al., 2016):

$$\Delta_e = \frac{Pa}{24EI}(3l^2 - 4a^2) \qquad \textbf{Equation 4-8}$$

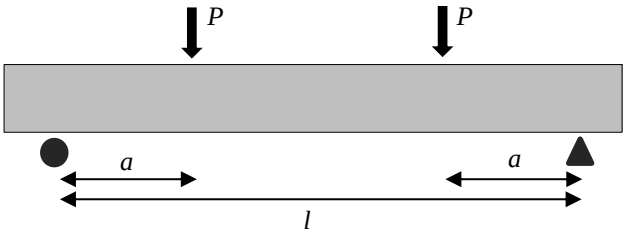

Figure 4-4 Four-point bending loading diagram

After yielding starts, it was assumed additional deformation mainly occurs in the plastic region, between the loading points, with a constant moment of $a.(P\text{-}P_y)$. The additional deformation can be calculated assuming an imaginary loading diagram, as shown in Figure 4-5, yielding:

$$\Delta_p = \frac{a \times (P - P_y) l^2}{8 E_p I} \qquad \textit{Equation 4-9}$$

Where, P_y is the load causing yielding moment in the beam. E_p was considered to be 1/30 of the elastic modulus post yielding (Bruneau et al., 2011).

Figure 4-5 Imaginary additional loading diagram of beam after yielding started between the loading points

4.2.2. *Minor Axis Bending*

Plastic analysis was implemented to estimate, *M*, the ultimate flexural capacity of the connections about the minor axis. This method is similar to the procedure used in (Salmon et al., 2009) to analyse bolted connections under eccentric shear. However, it respects the fact column members contact each other in bearing and contribute in transferring compression. The compression in this case is assumed to be transferred through a portion of flanges developed

ultimate tensile stress, f_u. Therefore, the pivot point was assumed to be at the bottom of the plastic region, as shown in Figure 4-6.

The column members are assumed to rotate about an instantaneous centre of rotation and the deformations of the bolts are proportionate to their distance from the centre of rotation. In addition, it was assumed tension is transferred through the splice plates and bolts, and compression is mainly transferred through contact between flanges. The centre of rotation, labelled as CoR in Figure 4-6, was considered to be on the centre line of the bolt groups on each side of the connection, and aligned with the pivot point in the longitudinal direction of the specimen. The location of the centre of rotation can be found through a trial and error procedure to satisfy the equilibrium of forces acting on the column members.

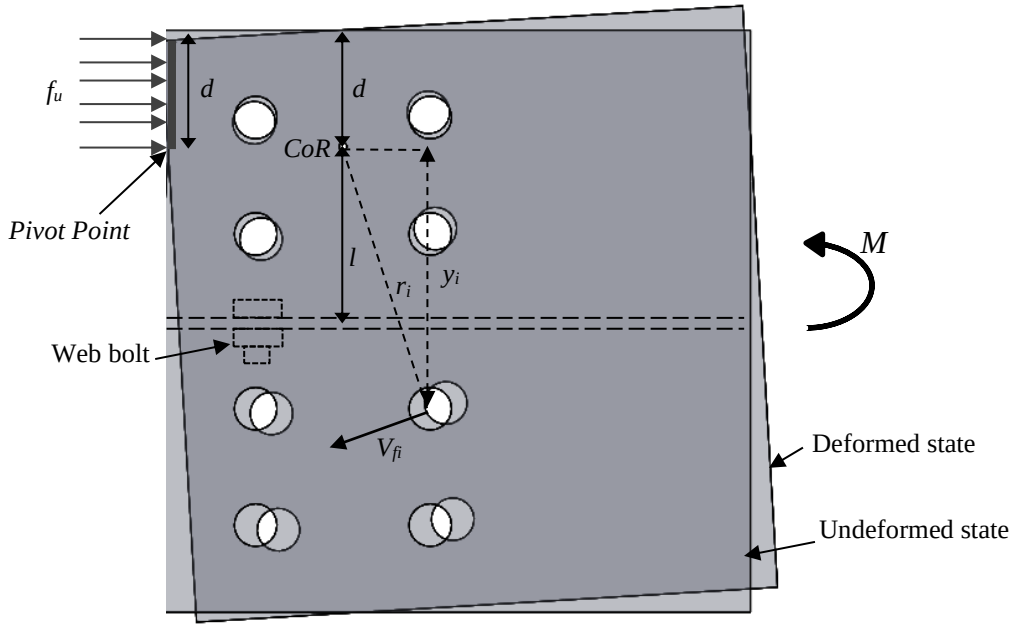

Figure 4-6 Free body diagram and deformed state of halved flange splice connection under bending about minor axis, where CoR is the instantaneous centre of rotation

Once the centre of rotation is found, the moment can be calculated for any deformation of the bolts, using:

$$M = f_u \times t_f \times \frac{d^2}{2} + \sum V_{fbi} r_i + \sum V_{wbi} \times l$$ ***Equation 4-10***

$$\Delta_{t_i} = \frac{r_i}{r_{max}} \Delta_{t_{max}}$$ ***Equation 4-11***

where f_u and t_f in Equation 4-10 are the ultimate tensile stress and flange thickness, respectively. V_{wbi} and V_{fbi} are bolt shear in web and flange, and Δ_{t_i} is the deformation of each bolt-plate. Geometrical parameters, *r*, *l* and *y* are all defined in Figure 4-6, and *d* is the depth of flange in bearing calculated through the trial and error procedure.

The rotation of the connection was estimated assuming 2mm oversized holes, yielding:

$$\theta = \frac{2 \times (2 + \Delta_{t_{max}})}{(y_{max})}$$ ***Equation 4-12***

The mechanism of forces and rotation prior to slippage is different. To estimate the moment resistance at slippage, it was assumed the centre of rotation is located at the centroid of the bolt group and the friction force at each bolt is proportional to its distance from the centroid of the bolt group. The slip was assumed to initiate when the bolt furthest from the centroid of the bolt group reaches the slip force, defined: $\mu_f \times T_{proof-load}$, where, μ_f is surface friction coefficient and $T_{proof-load}$ is the proof load tension in the bolt.

4.2.3. ***Major Axis Shear***

Flange splice mechanism in shear

It is traditionally accepted web splices carry shear forces in a beam or column (Hogan and Munter, 2007). However, the experiments in Chapter 3 showed flange splices could contribute

in transferring shear, even at small deformations when slippage occurs in the web splice. Thus, in this analysis, it is assumed flange and web splices act in parallel when the connection goes under major axis shear forces. The flange plates bend from the centre of the connection to the first row of holes at the other side of the connection shown as *L* in Figure 4-7. The web splice resists shear through bearing of the bolts against the hole edges, while the web splice plates rotate as a rigid body, as can be seen in Figure 4-8.

As can be seen in Figure 4-7, the edges of column flanges provide displacement constraints for flange splice plates when these plates bend towards them. It was assumed the plates deform like a beam with fixed and guided end supports. The axial stiffness of flange bolts is significant compared to the plate bending stiffness. Therefore, tensile deformation of flange bolts was ignored in the calculations. Bending deformation observed in the central bolts in Specimen #12 (Refer to Figure 3-23-F) was not taken into account in the prediction methods. This behaviour occurred due to prying actions at large displacements. Finally, shear deformations of the flange plates were ignored in the analysis, since it was negligible compared to the associated bending deformation in the post elastic state.

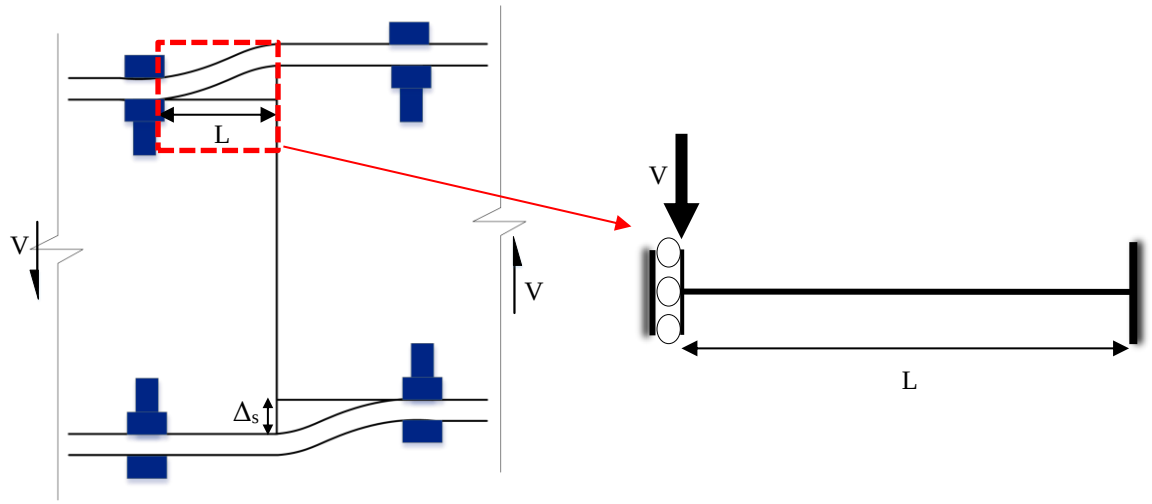

Figure 4-7 Bending deformation in flange splices due to connection shear

The force – flexural deformation of the flange splice plates can thus be expressed:

$$\Delta_s = \frac{VL^3}{12EI} \qquad \textit{Equation 4-13}$$

$$I = \frac{bt^3}{12} \qquad \textit{Equation 4-14}$$

where *L* is the length of the flange from the nut/head to the centre of the connection, as shown in Figure 4-7. *I* is the moment of inertia of the plate without holes, and *b* and *t* are the width and thickness of flange splice plate, respectively. The nut across flat distance was 32mm in these experiments.

Bending deformation of the splice plates were modelled at three stages:

1) beginning of yielding at the supports;

2) full formation of plastic hinges at the supports; and

3) the maximum displacement observed in the shear tests.

When the plates start yielding, the modulus of elasticity was reduced to 1/30 of the elastic modulus (Bruneau et al., 2011). In addition, the ultimate strength of the plates was increased by the ratio 410MPa/300MPa=1.39 at the ultimate deformation, knowing the material has reached the ultimate tensile capacity due to excessive deformation.

Web splice mechanism in shear

Figure 4-8 shows the mechanism of movement and deformation of the holes in the web splice plates post slippage. When the shear force overcomes the friction force in the web splice, the web plate starts rotating, since the plate has larger shear stiffness compared to the bearing stiffness of the bolt holes. Therefore, the shear deformation of the web splice is generated mainly through shear deformation of bolts and bearing deformation of bolt holes.

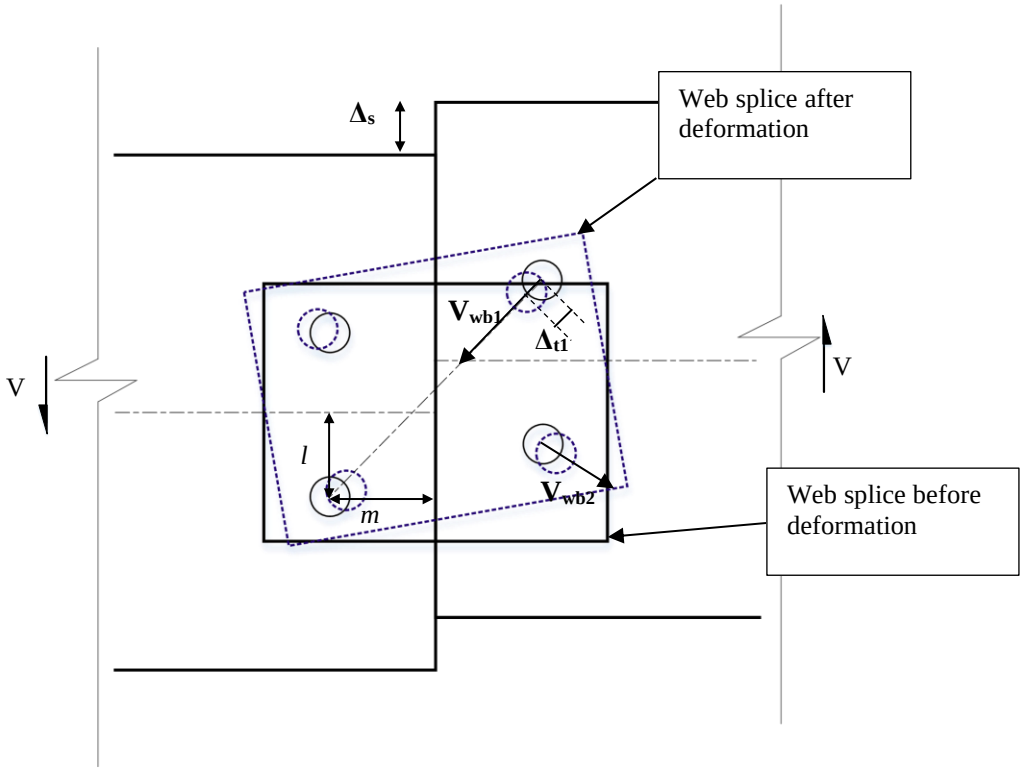

Figure 4-8 Movement of web plates due to shear, and bolt forces

The deformations of the bolts relative to the shear deformation of the connection can be calculated:

$$\Delta_{t_1} = \sqrt{(l + \frac{\Delta_s}{2})^2 + m^2} - \sqrt{l^2 + m^2} \qquad \textit{Equation 4-15}$$

$$\Delta_{t_2} = \sqrt{l^2 + m^2} - \sqrt{(l - \frac{\Delta_s}{2})^2 + m^2} \qquad \textit{Equation 4-16}$$

$$V = V_{wb_1} \times \sin\left(tan^{-1}\left(\frac{\left(l+\frac{\Delta_s}{2}\right)}{m}\right)\right) + V_{wb_2} \times \sin\left(tan^{-1}\left(\frac{\left(l-\frac{\Delta_s}{2}\right)}{m}\right)\right) \qquad \textit{Equation 4-17}$$

$$V_{wb_i} = R_{ult} \times (1 - e^{-0.394\Delta_{t_i}})^{0.55} \qquad \textit{Equation 4-18}$$

where Δ_s is the shear deformation of the connection, and the geometrical parameters *l* and *m* are defined in Figure 4-8.

The web splice initially resists shear force through friction. To have equilibrium of moments and forces acting on the web splice plate, bolt shear forces would be acting in the directions shown in Figure 4-9. From the equilibrium of moments about the centre of splice:

$$F_h \times 2l = F_v \times m$$ ***Equation 4-19***

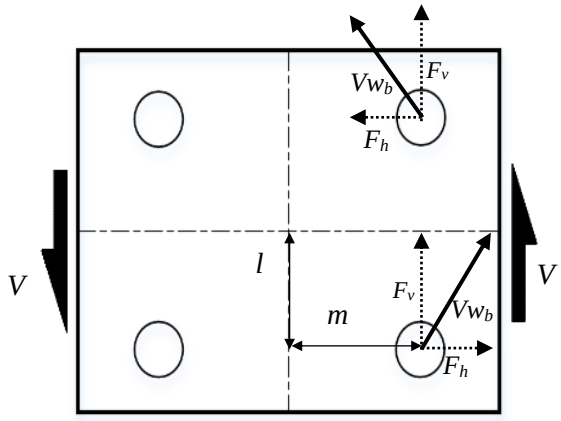

Figure 4-9 Friction forces in web bolts

Substituting F_h, horizontal component of bolt shear force, as a function of F_v, vertical component of bolt shear force, in Equation 4-20, the shear force associated with slip, V_{slip}, would be derived as follows:

$$V_{wb}{}^2 = F_v{}^2 + F_h{}^2$$ ***Equation 4-20***

$$F_v = \frac{V_{wb}}{\sqrt{1+\frac{m^2}{4l^2}}}$$ ***Equation 4-21***

$$V_{wb} = \left(\mu_f \times T_{proof-load}\right)$$ ***Equation 4-22***

$$V_{slip} = 2 \times F_v = \frac{2\mu_f T_{proof-load}}{\sqrt{1+\frac{m^2}{4l^2}}}$$ ***Equation 4-23***

Where μ_f is the friction coefficient, assumed to be the design value of 0.35 from NZS3404 for clean as-rolled surfaces. The tension in the bolts was assumed 145kN per the manufacturers Handbook (Blacks Fasteners Handbook). Since two web splice plates were used both sides of the webs, shear force is twice as much as Equation 4-23.

4.3. Comparison of Experimental Behaviour with Backbone Envelope Prediction

Major Axis Bending

Specimens #1 to #3 (Bearing splice connections)

The ultimate strength of the flange and web bolts in shear, R_{ult}, was considered 133.5kN and 186kN, respectively, in all prediction methods. These values are the average result from the sample material tests shown in Table 3-2.

Figure 4-10 shows the prediction of behaviour versus the experimental results for Specimen #1. The model shows very good agreement with the experimental result. The experiment showed larger deformation capacity than the prediction. The model assumed failure occurred once the bolt deformation reached 8.6mm. This value could be slightly conservative comparing it with the ultimate deformation capacity from the bolt shear tests by (Crawford and Kulak, 1971), which was about 9mm. Plastic deformations along the central rows of holes could also attributed to the underestimated rotation. However, the overall backbone matches well in Figure 4-10.

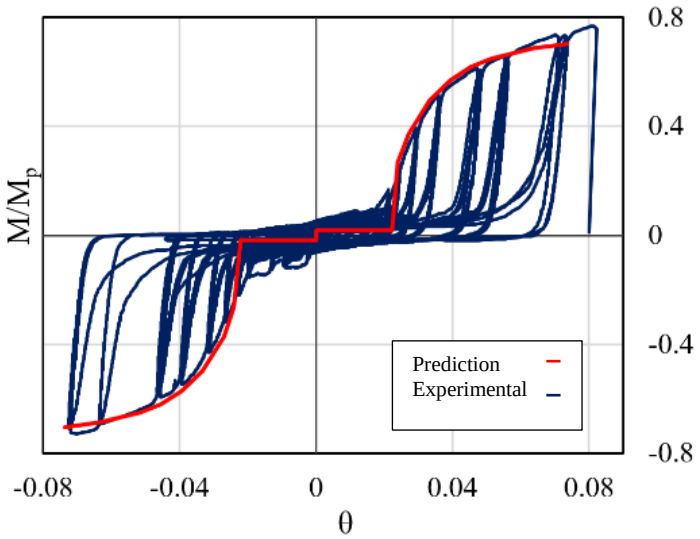

Figure 4-10 Prediction and experimental results for Specimens #1 and #2 under major axis bending

The bolts in this experiment were in single shear, connecting plates with thicknesses of 25mm (flange) and 12mm (flange splice). These values are very close to those tested to derive the force-deformation relationship of the bolts. The plates were of grade 300MPa, whereas the relationship of Equation 4-1 was derived from grade 250MPa steel plates. Finally, cyclic loading in this experiment could have altered the shear behaviour of bolts compared to the mechanics assumed in Equation 4-1.

Figure 4-11 shows the prediction of Specimen #2 is in good agreement with the experimental result at smaller displacements, but conservative at larger displacements. The prediction for Specimen #1 shows ~10% increase in the ultimate moment capacity compared to Specimen #2, due to the web bolts, but the experiments show similar capacities for both Specimens #1 and #2. This result could indicate bearing connections could have slightly less capacity than friction connections, as bolts could experience undesired actions due to tilting and/or other unaccounted eccentric loading.

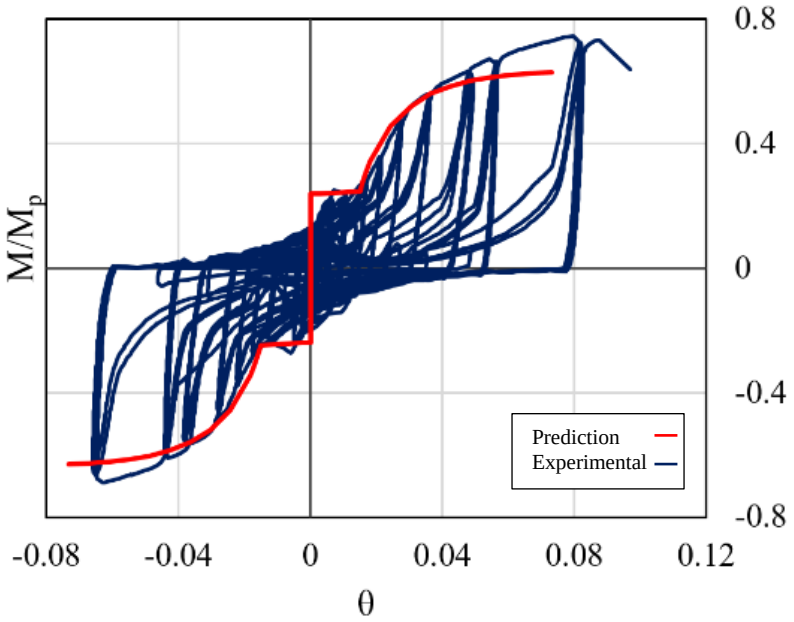

Figure 4-11 Prediction and experimental results for Specimens #2 under major axis bending

Figure 4-12 shows the prediction for Specimen #3 overestimates flexural capacity of the connection at small displacements, while underestimating the capacity at larger deformations. This result could be due to the use of thicker splice plates compared to the other two experiments (20mm thick versus 12mm thick, Section 3.2.1). In addition, Specimen #3 is a longer connection, which could lead to uneven distribution of forces amongst the bolts. Furthermore, larger prying actions are expected in this connection due to the thicker splice plates. These reasons could also explain why the estimated friction capacity is larger than the experimental capacity, since prying actions could lead to loss of tension in bolts not accounted for in the fundamental mechanics models. Finally, contribution of web splices to the total moment capacity of the connection in the prediction was approximately 5%.

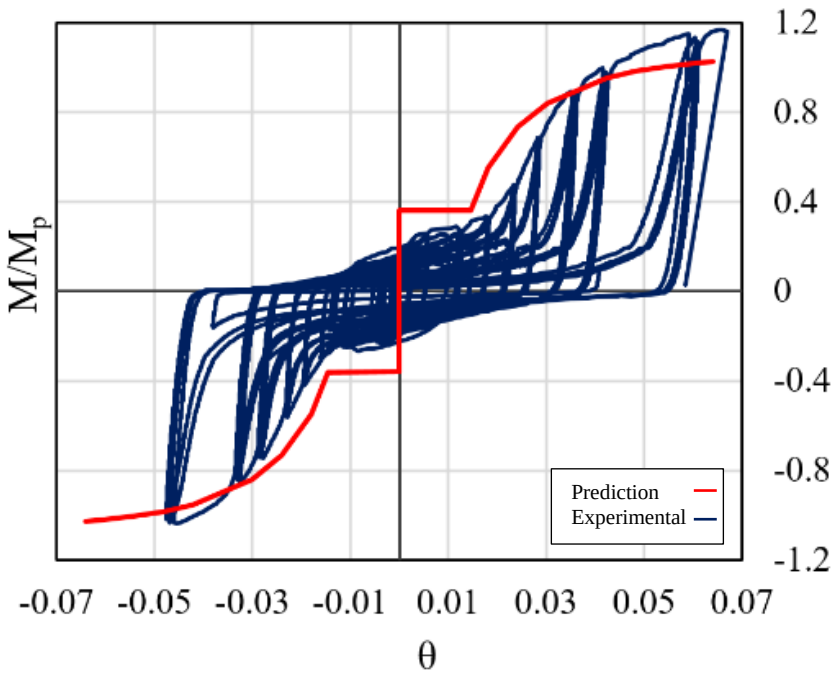

Figure 4-12 Prediction and experimental results for Specimens #3 under major axis bending

Key outcomes of Specimens #1 to #3, Major axis bending of bearing lap splices:

- The model presented to estimate the backbone behaviour of bearing lap splices shows very good agreement with the experimental results. The model is capable of capturing the fundamental behaviours, including slip and nonlinear effects, required for design and analysis.
- The bolt/plate deformation model used for backbone predictions can provide more accurate representation when the spliced plates are of similar geometry and material properties. Hence, the predicted backbones for Specimens #1 and #2 show a better match compared to Specimen #3, which is still good enough for design purposes.
- The ultimate ductility of the connection was predicted at bolt failure corresponding to an 8.6mm bolt/plate deformation.
- The contribution of the web splice in resisting moment at the ultimate deformation was as high as ~10% of the total flexural capacity.

- Most errors are at very large motions where response is highly nonlinear. These motions are less likely in general application of column splices in moment frames, and good accuracy overall indicates the models' efficacy and potential for design.
- Differences show a range of possible behaviours due to changes or variability in material behaviour, dimensions, and/or construction not accounted for by first principles design equations and impossible to know ahead of time in practice.

Specimens #4 to #6 (Non-bearing splice connections)

Figure 4-13-A shows the prediction for Specimen #4 is initially in good agreement with the experiment, but underestimating the capacity of the connection at large displacement, similar to previous specimens. The kink in the model corresponds to the point when the members come into contact in compression. Again, small to medium motions are very accurate, with a loss of accuracy only at large highly nonlinear regions.

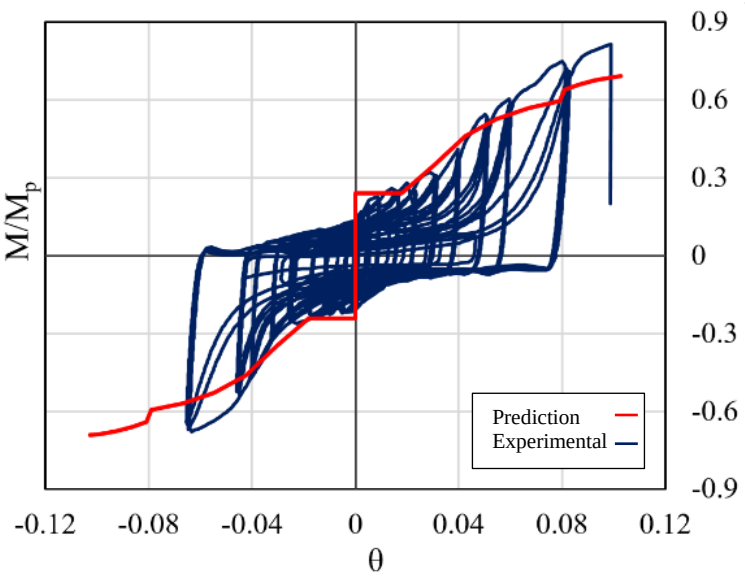

(A) Specimen #4, Non-bearing with no filler plate

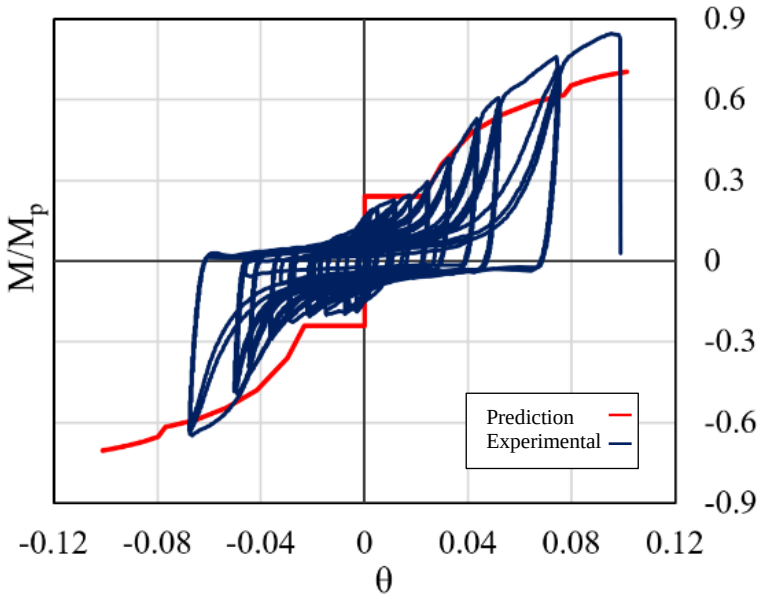

(B) Specimen #5, Non-bearing with 6mm fillers

Figure 4-13 Prediction and experimental results for Specimens #4 and #5 under major axis bending

Figure 4-13-B shows the prediction of Specimen #5 is similar to Specimen #4, as the bolt force-deformation relationship does not take the filler plates into account. The fillers could reduce the capacity of bolts because of additional freedom and potential bending in bolts. The only difference in these two models is the larger distance of flange splice plates in Specimen #5 due to the filler plates.

Figure 4-14-A shows the prediction for Specimen #6 is non-conservative, post slippage. As described in Chapter 3 (Figures 3-12-B and H), bending and tilting occurred in the bolts, leading to a different failure mechanism than bolt single shear mechanism. Therefore, the mathematical model used for bolts in the prediction could be non-realistic. Figure 4-14-B shows the prediction of the specimen assuming 15% reduction in bolt shear force, due to the thick loose fillers. The reduction value was selected per clause C9.3.2.5, NZS3404. No bearing was considered in this specimen since the smaller member touches the web of the other member and contact area does not form between flanges.

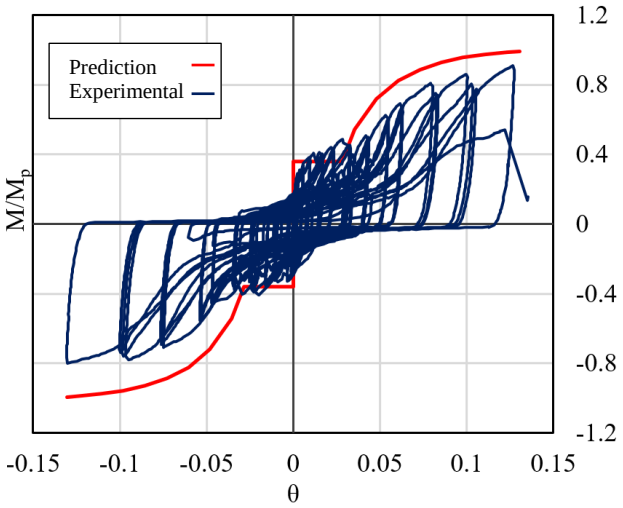

(A) Specimen #6, non-bearing lap splice with no reduction in bolt shear due to thick loose fillers

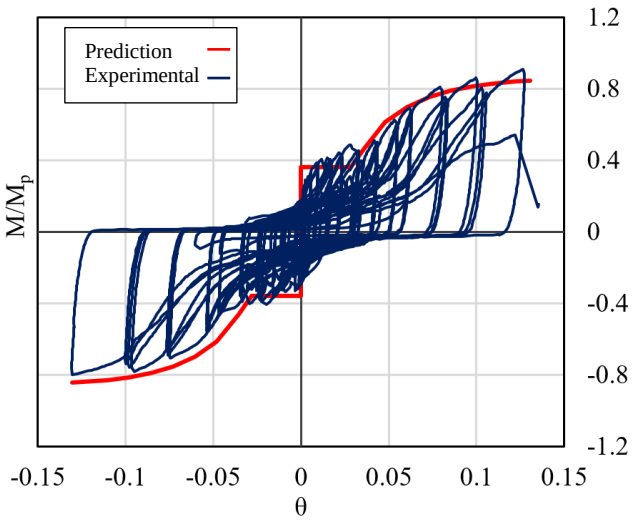

(B) Specimen #6, non-bearing lap splice with 15% reduction in bolt shear due to thick loose fillers

Figure 4-14 Prediction and experimental results for Specimen #6 under major axis bending

Summary: Specimens #4 to #6, Major axis bending for non-bearing lap splices

- The model presented to estimate the backbone behaviour of bearing lap splices shows very good agreement with the experimental results. The model is capable of capturing the fundamental behaviours, including slip and nonlinear effects, required for design and analysis.
- The ultimate ductility of the connection was predicted at bolt failure corresponding to an 8.6mm bolt/plate deformation.

- Most errors are at very large motions where response is highly nonlinear. These motions are less likely in general application of column splices in moment frames, and good accuracy overall indicates the models' efficacy and potential for design.
- While the 6mm filler plate had insignificant impact on the ultimate flexural capacity, 2x12mm filler plates in Specimen #6 caused an ~15% reduction in the ultimate capacity of the connection.

Specimen #7

For Specimen #7, it was assumed the bolts were threaded along the whole length, which was 89mm. This assumption is reasonable since axial stiffness of the unthreaded part is more than threaded part, and plasticity tends to form in the threaded part. The axial deformation of the bolt in the unthreaded length is not significant after yielding started in the threaded length. The M24 bolts were tightened using the part turn method from the snug tight condition to achieve 210kN bolt tension, per the manufacturer's recommendation (Blacks Fasteners Handbook). The tensile area of the threaded length is 353mm^2 for the M24 bolts. The bolt proof load stress, yield stress and ultimate tensile stress is provided in the manufacturer's handbook as 600MPa, 660MPa and 830MPa, respectively. Multiplying these values by the nominal tensile area, the proof load, yield load, and tensile breaking load were calculated as 212kN, 233kN and 293kN, respectively.

The average bolt tensile breaking force obtained from the component tests was 309kN, as listed in Table 3-2. This is 5.5% greater than the manufacturer specified strength above. The bolt elongation corresponding to yielding was therefore multiplied by 309/293=1.055 to represent the actual property of the bolts.

Figure 4-15 presents the force-deformation curve of one of the bolts from component testing representing the average behaviour. The average elongation of the bolts from component testing was observed to be approximately 1mm at yielding and 5mm at failure. Since the reliability of the testing machine deformation gauge was uncertain, it was decided to use the estimated initial stiffness of the bolt from the manufacturers data. As such, the force-deformation of the bolt can be idealized as shown in black in Figure 4-15. The elongation of the bolts at proof load was calculated from the idealized curve to be ~0.16mm.

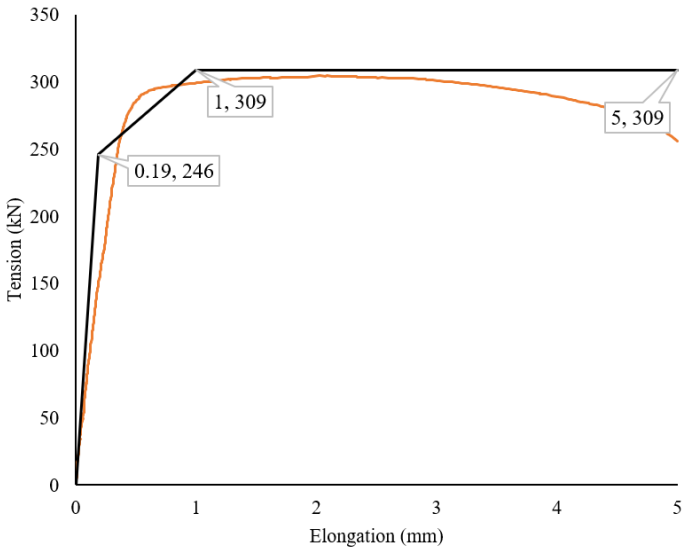

Figure 4-15 Experimental and idealized axial load-deformation of M24 bolts

Figure 4-16-A shows the prediction for Specimen #7 assuming the end plates are perfectly in contact. As can be seen, the model leads to non-conservative results. However, it predicts the ultimate flexural capacity reasonably. A similar model was developed for the specimen considering the 1mm gap observed between the end plates after the construction. It can be seen in Figure 4-16-B the model has good agreement with the experimental results when including 1mm gap.

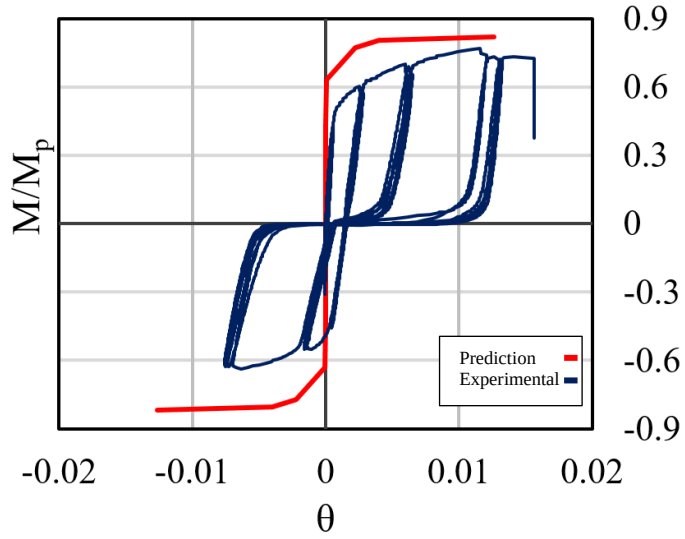

(A) Specimen #7, end plate splice

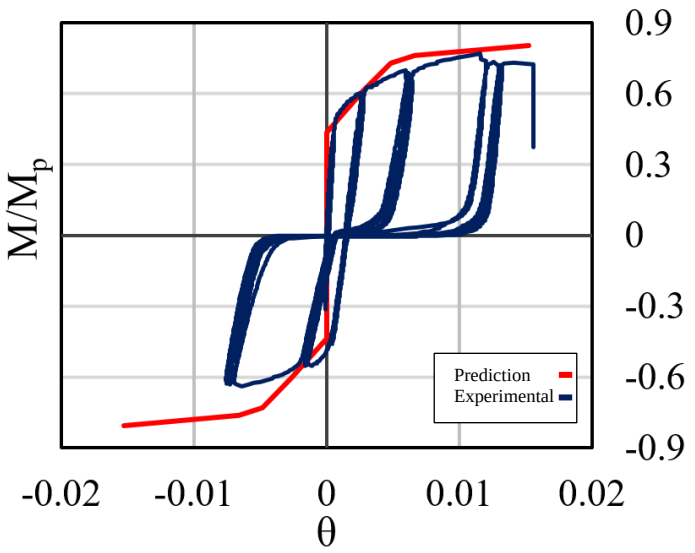

(B) Specimen #7 considering 1mm construction gap

Figure 4-16 Prediction and experimental results for Specimen #7 under major axis bending

Summary: Specimen #7, Major axis bending for end plate splice

- The overall behaviour of the connection is sensitive to the end plate contact condition. The model considering 1mm construction gap between the end plates shows good agreement with the experimental results, despite the potential impacts of small variability in construction in creating differences between model and experimental performance.

- The predicted ultimate capacity and ductility of the connection is very close to the experimental value, irrespective of end plate contact condition.

Specimen #8

Figure 4-17 shows moment versus displacement at the centre of the column for the weld splice connection. For simplicity, it was assumed the member is one unit from 310UC118 column section. The model shows good agreement between the prediction and experimental results for the welded splice connection.

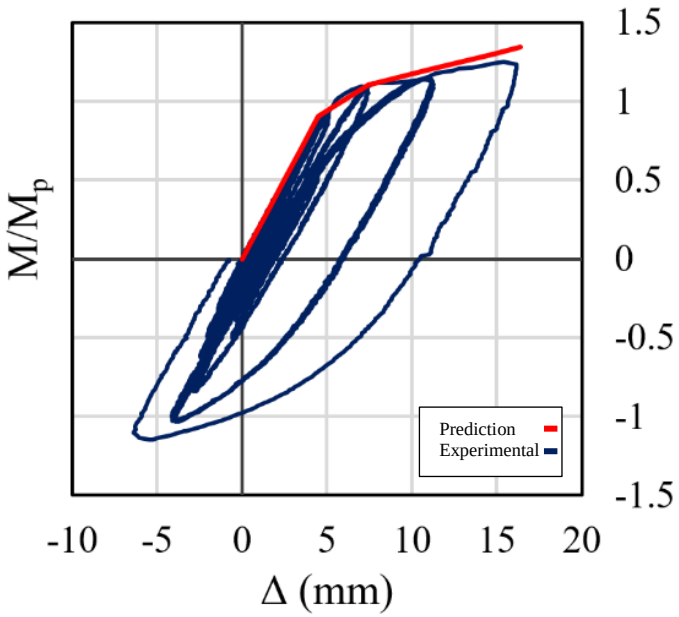

Figure 4-17 Prediction and experimental results for Specimen #8 under major axis bending

Summary: Specimen #8, Major axis bending for welded splice

- The model shows very good agreement with the nonlinear behaviour of the specimen under four-point bending. The nonlinearity in the specimen is due to material nonlinearity at plastic hinges, and not the welded splice mechanics. This agreement also shows the rigidity of the welded splice connection.

Minor Axis Bending

Specimen #9 and #10

Figures 4-18A and B show very good agreement between the prediction and experimental results for the specimens bent about their minor axes. There is no prying mechanism in these connections, and the bolts were expected to experience shear actions only. Specimen #9 has a web splice, which transferred ~10% of the bending actions at the ultimate deformation of the connection. Due to the complicated nature of analysing these connections to find the centre of the rotation, only two points were analysed post slippage and the behaviour of the connection in between the points were extrapolated linearly. The overall approach provides an accurate predicted backbone curve.

For the longer connection (#10), the critical component in bending was the splice plate. The flange splice plates did not have sufficient capacity to develop the potential moment capacity of the bolt group. Since the plate underwent large plastic deformations, inelastic bucking occurred in the plates. Therefore, the ultimate capacity of the connection was governed by the ultimate tensile capacity of the portion of the plate in tension, and not the bolt group. The ultimate rotation was assumed to happen at an equivalent bolt deformation of 8.6mm, although almost all the deformation can be attributed to the plastic deformations as hole elongation.

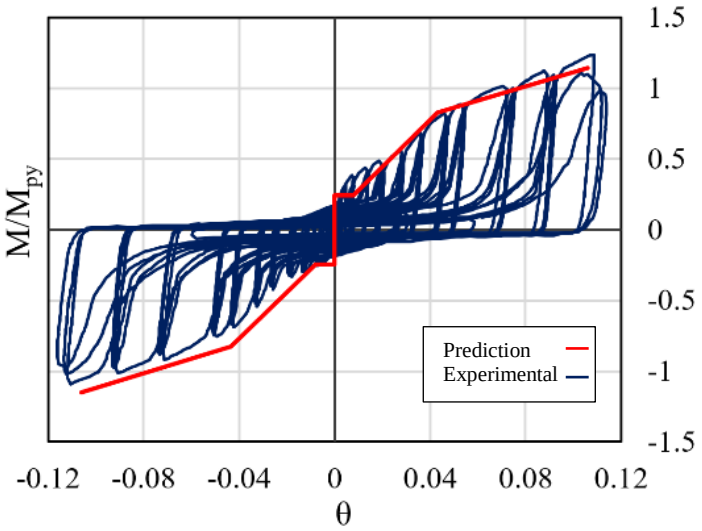

(A) Specimen #9, Bearing lap splice

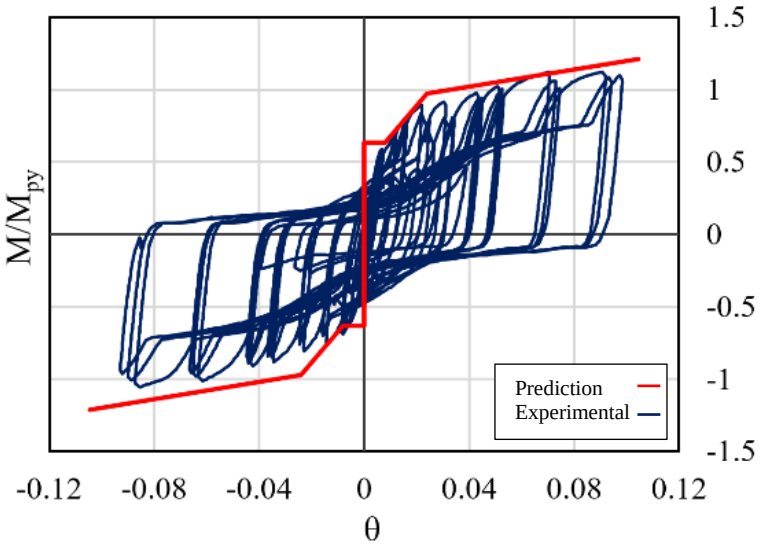

(B) Specimen #10, Bearing lap splice

Figure 4-18 Prediction and experimental results for Specimens #9 and #10 under minor axis bending

Summary: Specimens #9 and #10, Minor axis bending for lap bearing splices

- The estimated backbone behaviour of bearing lap splices under weak axis bending show very good agreement with the experimental results. The model is capable of capturing the fundamental behaviours, including significant nonlinearities, required for design and analysis.

- The ultimate ductility of Specimen #9 was predicted at bolt failure corresponding to an 8.6mm bolt/plate deformation. However, the ultimate capacity of Specimen #10 was governed by splice plate capacity.
- The contribution of web splice in resisting moment at the ultimate deformation of Specimen #9 was ~10% of the total flexural capacity.

Major Axis Shear

Specimens #11 to #13

Figures 4-19 show good agreement between the prediction and experimental results overall. However, the results are non-conservative for very small displacements. Since no failure occurred at the connections during the experiments, the prediction was performed as far as the ultimate deformations observed in the experiments.

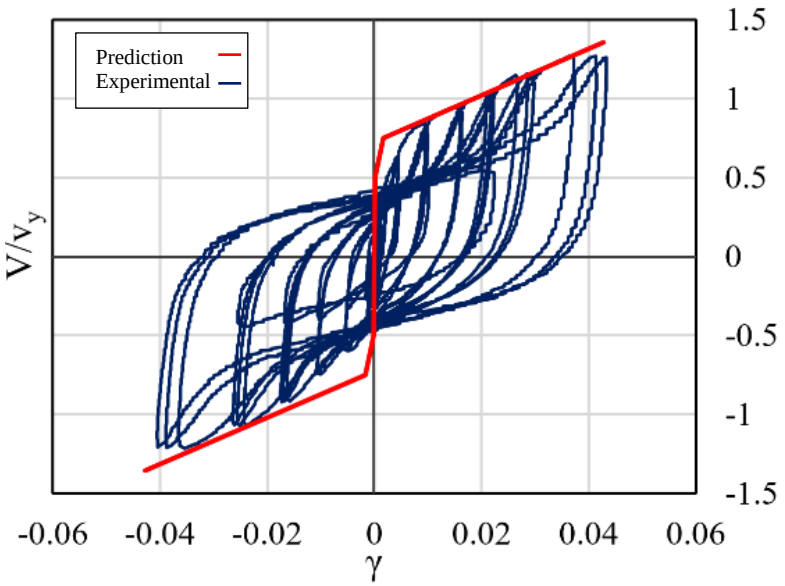

(A) Specimen #11, flange and web splice

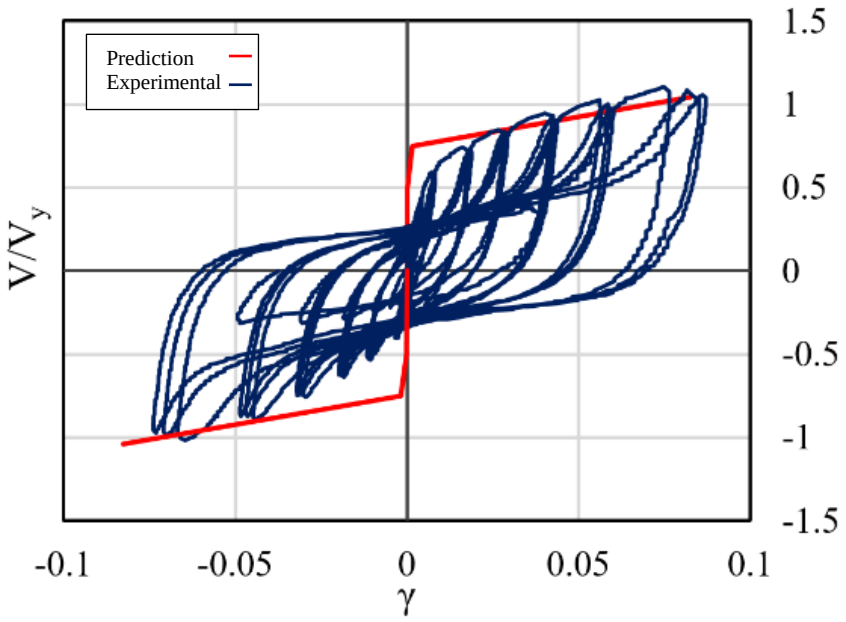

(B) Specimen #12, flange splice only

Figure 4-19 Prediction methods versus experimental results for Specimens #11 and #12 under minor axis shear

Several factors could cause the discrepancy between the experimental results and prediction at small displacements. Experimentally, the flanges were observed to move with the splice plates. Therefore, realistically, the flanges act as spring supports.

In addition, no axial or bending deformation was considered for the bolts. Slippage could also occur at the flanges, which could alter the length of the plate bending and reducing the bending stiffness. All of these factors may play a role, but the results are otherwise good predictors for design.

For Specimen #11, since the web holes are 2mm oversized, it was assumed the web splice would not transfer shear prior to a shear deformation of 4mm is achieved. Since the shear deformation associated with bending flange splice plates is smaller than 4mm, the shear strength of the web plates was only added to the shear capacity of the flange plates at the ultimate deformation.

The actual ultimate shear strength of the web bolts was estimated to be 129×(235/163)=186kN, assuming the shear planes do not pass through the threads. 129(kN) is the design shear strength of plane shank of Grade 8.8 M20 bolt and 163(kN) is its design axial strength. Finally, 235(kN) is the actual tension capacity of M20 bolts, as listed in Table 3-2.

The dimensional difference of the webs in the shear experiments was 6mm, resulting in a 3mm gap on each side, between the splice plates and web. This gap was closed during bolt tightening due to bending of the 6mm splice plates, which may have resulted in smaller pretension than the desired proof load. In addition, due to bending in the splice plates, abrasion occurred at the centre of splice plates (See to Figure 3-25-C). It was observed in Specimen #13 that friction did not completely diminish at larger cycles, which could be attributed to continual abrasion. The associated friction resistance was observed to be between $0.1V_y$ to $0.2V_y$, which is about 30% of the total strength of the connection. The friction coefficient for abrasive blasted surfaces in NZS3404 is 0.53 compared to the 0.35 used in the analyses; where the actual value may be in between these values.

Figure 4-20 shows the prediction and experimental results for Specimen #13, assuming slip occurred at $0.16V_y$ rather than predicted value, $0.32V_y$, per Section 4.2.3. The model is conservative at large displacements, which could be due to an unrealistic model of the bolts. This issue might be expected since the thicknesses of the web and splice plates, and grade of steel material is not similar to the setup used to develop the bolt model in Equation 4-1.

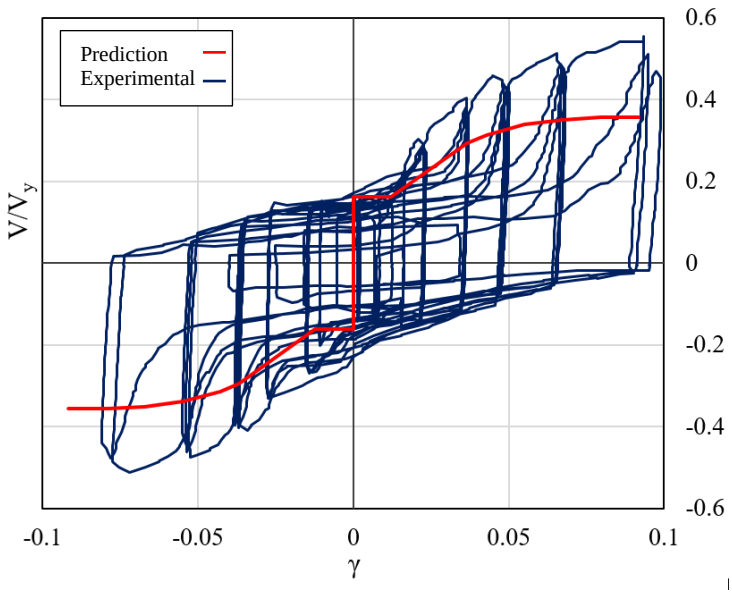

Figure 4-20 Specimen #13, web splice under major axis shear

Summary: Specimens #11 to #13, Major axis shear for lap bearing splice

- The backbone prediction models show a good overall match to fundamental linear and nonlinear behaviours from the experiments.
- The contribution of flange splice in transferring shear force was quantified using a beam formula for unsupported length of flange.
- For web splice modelling, it was assumed the web is spliced on one side only, and the web bolts are in single shear. Therefore, the bolt/plate deformation model used for predictions may have overestimated the bolt/plate deformations, leading to error.
- The ultimate ductility of Specimen #13 was predicted at bolt failure corresponding to an 8.6mm bolt/plate deformation.
- The web splices in Specimens #11 and #13 bent with bolt tensioning due to the 3.9mm difference in web thickness either sides of the splice. This construction issue led to continual abrasion throughout the experiment, which has not been considered in the modelling and results in error in these specimens.

- Model results are highly sensitive to design versus construction differences in the material properties, dimensions, other factors, which also contribute to observed errors.

4.4. **Summary**

This chapter discussed several modelling approaches in detail, which were then applied to predict the nonlinear force-deformation backbone behaviour of test specimens under different loadings. The models are essentially analysing the spliced members for equilibrium of forces from the connectors, considering geometrical compatibility of the moving parts. For lap plate splices, the model substantially relies on bolt shear/bearing deformation relationship with bolt shear for splice deformation estimations. The relationship used in this study is general, and does not specify plate thickness, plate material grade, presence of filler plates and effect of bolt cyclic loading.

Predicted results were compared with the experimental results for validation. Predictions yielded generally good to very agreement with the linear and nonlinear experimental data, serving as an overall validation of the models and methods presented in this chapter for use in design and analysis. Most errors were at very large deformations in highly nonlinear regimes of behaviour, primarily due to assumptions not holding perfectly into these regimes and/or variabilities in dimensions, construction, materials properties, or other parameters that can arise and create differences between design and experimental construction, particularly in nonlinear response regions. The overall results are more than suitable for design specification and analysis in practice to better understand the potential splice behaviour. This capability and insight are not currently avoidable in practice, and are thus a novel contribution.

4.5. List of Symbols in Chapter 4

A_s: Bolt tensile stress area

b: Flange splice width

CoR: Centre of rotation

e: Mathematical constant, base of the natural logarithm

E: Young modulus

E_p: Post elastic modulus (Plasticity modulus)

f_u: Ultimate tensile stress

F_c: Concentrated compression force at the centre of rotation for bearing lap splice

h: Web or end plate bolt lever arm, refer to Figure 4-1, Figure 4-3

H: Tension flange force lever arm, refer to Figure 4-1

k_{10}: Axial stiffness parameter of a preloaded bolt

K_l: Bolt axial stiffness

L_b: Bolt length, includes the grip length and half of the heights of the nut and head

M: Ultimate moment capacity

n_{bolt}: Number of bolts each side of flange splice

P_y: Load causing yielding moment in the beam Figure 4-4

R: Bolt shear at a certain bolt shear displacement in Crawford et al. equation

R_{ult}: Ultimate bolt shear strength

t: Flange splice thickness

t_f: Flange thickness

T_i: Bolt tension

T_{max}: Bolt tension furthest from the pivot point at a certain deformation

$T_{proof-load}$: Tension proof-load in bolt

V_f: Total bolt shear in tension flange splice

V_{wbi}: Bolt shear in web for each bolt

V_{fbi}: Flange bolt shear

V: Shear capacity of connection

Δ: Deformation of bolt-plate system in Crawford et al equation has units of inch

Δ_e: Elastic deformation of beam centre under four-point bending, Figure 4-4

Δ_p: Post elastic deformation of beam centre under four-point bending, Figure 4-5

Δ_s: Shear deformation of connection

Δ_t : Deformation of bolt-plate system, sum of shear deformation of bolt and bearing deformation of plate in units of mm

μ: Bolt shear strength parameter (1/inch)

μ_f: Friction coefficient

λ: Bolt shear strength parameter equal to 0.55 proposed by Crawford et al.

Chapter 5. **Frame Analysis Considering Column Splice Flexibility**

5.1. **Introduction**

This chapter quantifies the effect of column splices on the dynamic response of generic steel moment frames, using results of prior chapters. Non-linear time history analyses of moment frames were conducted to evaluate the effect of the shear and flexural stiffness properties of these connections on overall frame response. The frames studied here are 9 and 20 story moment frames from the SAC Steel Project (SAC Steel Project).

Column splices were explicitly modelled using nonlinear shear and rotational springs. A rigid plastic model in combination with a gap model was used to simulate the flexural behaviour of the column splice connections pre and post slippage, based on experimental results. A bilinear model was used for shear springs, which represents the shear property of bolted column splice connections accounting for the interaction of flange splices in transferring shear. This behaviour was observed in the experiments and discussed in Section 3-2-3. Parametric studies on shear and flexural properties were conducted to assess the possibility of global or local failure mechanisms within expected ranges of column splice properties observed in the experiments.

The earthquakes used are the medium and high suite earthquakes of the SAC suite, known as LA1-LA40, representing Design Basic Earthquake (DBE) and Maximum Credible Earthquake (MCE) levels of shaking. The results of this chapter along with the findings from the experimental studies in Chapter 3 lead to design implications presented in Chapter 6.

5.2. **Method**

5.2.1. ***Steel Moment Frame Modelling***

Two generic moment frames of 9 and 20 stories were analysed. These frames are identical to the pre-Northridge designs from the SAC steel project (Gupta and Krawinkler, 1999). The frames were modelled in Opensees (Open System for Earthquake Engineering Simulation) with non-linear beam and column members, capable of considering distributed plasticity along the members (Mazzoni et al., 2007). This overall modelling approach is well-accepted and standard.

The SAC three-dimensional buildings consist of a central gravity system surrounded by perimeter moment frames. For simplicity, a two-dimensional moment frame representing half of the structure in the earthquake direction was modelled in this study. The allocated seismic mass of the frame at each floor level was half of the total seismic mass for that floor, knowing two moment frames were resisting earthquake lateral forces in the direction of earthquake. Seismic mass for each floor was applied at the beam-column nodes based on their tributary area. The basement floors of the structures were modelled as normal stories, but laterally restrained against movement. The seismic acceleration was applied at all laterally restrained degrees of freedom.

To simulate the P-delta effects of the internal gravity frames on the two-dimensional moment frame, half of the floor weights were applied to the frame. This consideration is necessary since the rigid floor slab transfers the P-delta effects to the flexible moment frames (Gupta and Krawinkler, 1999). For the two-dimensional SAC 9 and 20 story frames in this study, the weights were directly applied at beam-column nodes. This loading allocation may result in

slightly non-conservative moment demands for the exterior columns, since the attached beam end moments were not modelled (for rigid beam-column connections).

Second-order P-Delta effects were modelled for columns members using a P-Delta transformation in Opensees. Column splices were modelled with *ZeroLength* elements with stiffnesses in translational shear and rotational degrees of freedom. The element was set rigid in the axial direction using *equalDOF* in the corresponding direction. Two cases for splice location within the column height were considered, the bottom and top of the middle third of columns, which are referred to as lower bound and upper bound in this chapter. These locations are the lower and upper bound of the middle third range of columns in which splices are to be placed in seismic regions (*NZS3404:Part 1, Steel Structures Standard*, 1997).

The beam and column members were modelled centre to centre, and doubler plates were not modelled. The beam and column members were modelled with non-linear fibre elements allowing interaction of moment-curvature and axial force-deformation characteristics. Each section plate (web and flanges) consisted of 16 fibres through the width and 4 fibres through the thickness. Steel material properties were chosen to be representative of a bilinear material with kinematic hardening resulting in a hardening slope ratio of 1/30=3.3%. The yielding stress of steel for beam and column members were 248MPa (36ksi) and 345MPa (50ksi), respectively.

Rayleigh damping was adopted to represent the overall damping characteristics of the buildings (Clough and Penzien, 1993). Therefore, the damping matrix of frame $[C]$, is a linear combination of the mass and stiffness matrices, $[M]$ and $[K]$, defined:

$$[C] = \alpha[M] + \beta[K] \qquad \textbf{\textit{Equation 5-1}}$$

Where the Rayleigh damping coefficients, α and β are calculated from:

$$\begin{Bmatrix}\alpha\\ \beta\end{Bmatrix} = \frac{2\zeta}{\omega_i+\omega_j}\begin{Bmatrix}\omega_i\omega_j\\ 1\end{Bmatrix} \qquad \textit{Equation 5-2}$$

Where ω_i and ω_j are the frequencies of the two vibration modes selected for the damping ratio ζ chosen for these vibration modes.

In this study, a damping ratio of 0.02 was considered for both frames. For the 20 story frame, the first and fifth mode of the frame were assumed to control the damping response of the frames (Gupta and Krawinkler, 1999). These modes were selected to be the first and second mode for the 9 story frame. The Newmark-Beta integration method was used to compute the time history analyses. The Newmark-Beta parameters, γ and β, were set to 0.5 and 0.25, respectively.

The main objective of the frame analyses presented here is to investigate the response of the frames in relation to flexibility of column splices. Therefore, a benchmark model was created with rigid splices for each of the 9 and 20 story frames. This model could be a representation of welded splices with unlimited capacity. In the following sections, properties of these frames are provided with further details.

5.2.1.1. ***Nine story moment frame***

Figure 5-1 illustrates the two-dimensional 9 story moment frame geometry and the location of splices in the frame. Column splices are located every second floor, at floors 2, 4, 6 and eight.

Column splices are schematically shown with solid black rectangles. Two cases of column splice locations within the floor height were studied. These locations are one and two thirds of the column height. Beams and columns are all from W sections, and their sizes can be found in Table 5-1. The exterior column, to which beams are connected by pinned joints, is oriented about its minor axis.

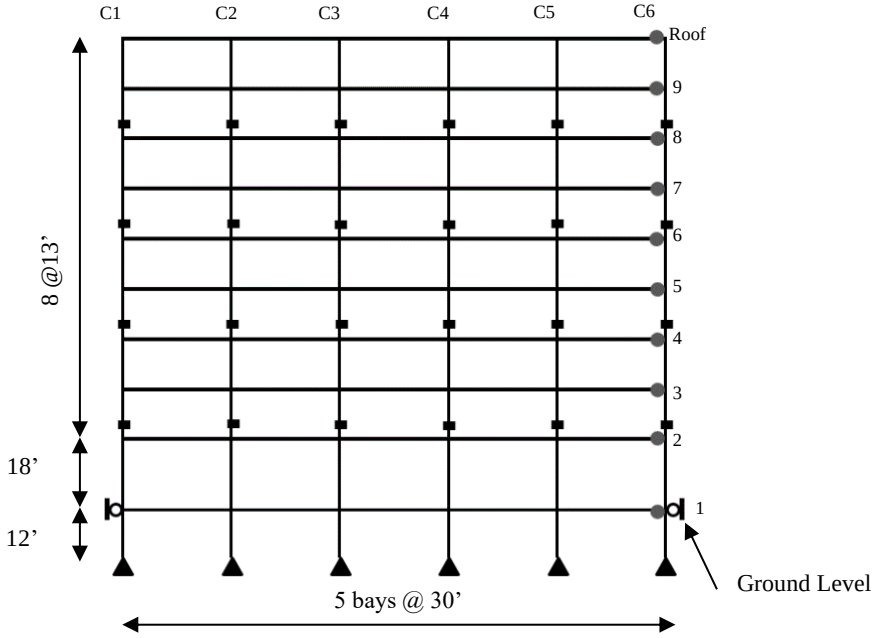

Figure 5-1 Pre-Northridge nine story SMRF from SAC steel project

Table 5-1 Section sizes of pre-Northridge nine-story SMRF from SAC steel project

story/Floor	COLUMNS		GIRDER
	Exterior (C1, C6)	Interior (C2 to C5)	
-1/1	W14X370	W14X500	W36X160
1/2	W14X370	W14X500	W36X160
2/3	W14X370, W14X370	W14X500, W14X455	W36X160
3/4	W14X370	W14X455	W36X135
4/5	W14X370, W14X283	W14X455, W14X370	W36X135
5/6	W14X283	W14X370	W36X135
6/7	W14X283, W14X257	W14X370, W14X283	W36X135
7/8	W14X257	W14X283	W30X99
8/9	W14X257, W14X233	W14X283, W14X257	W27X84
9/Roof	W14X233	W14X257	W24X68

* Column 1 (C1) has exterior column section oriented about strong axis.
** Column 6 (C6) has exterior column section oriented about weak axis.
*** Columns 2, 3, 4 and 5 have interior column sections.

5.2.1.2. ***Twenty story moment frame***

Figure 5-2 illustrates the two-dimensional 20 story moment frame geometry and the location of column splices are shown with solid black rectangles. Column splices are generally located every third floor, at floors 2, 5, 8, 11, 14, 17 and 19. Two cases considered in the analyses for column splices, which are one and two thirds of the column height. Columns are from square hollow sections and beams are from W sections. Member sizes can be found in Table 5-2. The beams of the basement floor have simple connections.

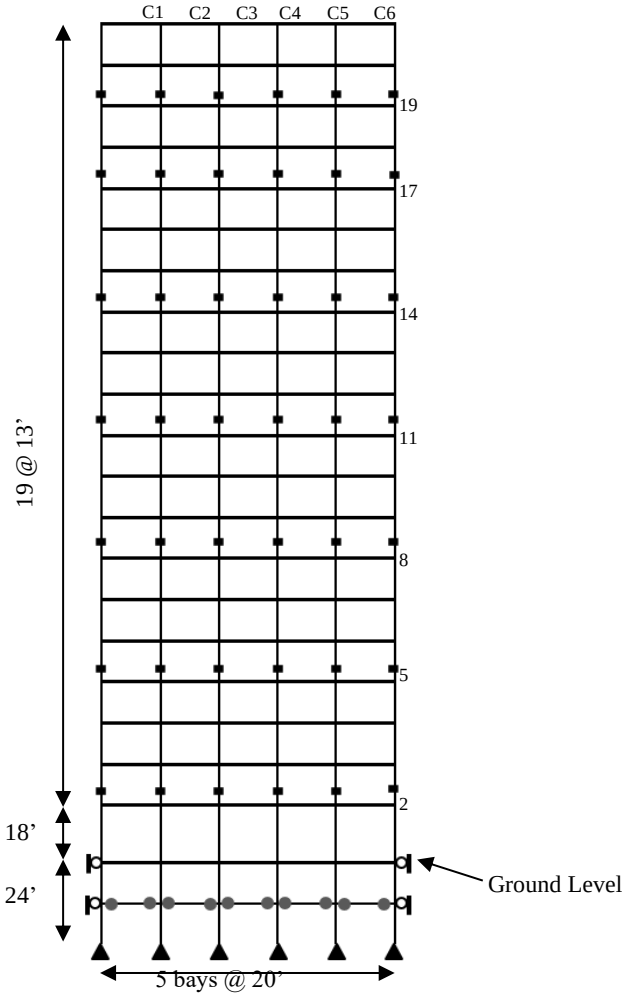

Figure 5-2 Pre-Northridge twenty story SMRF from SAC steel project

Table 5-2 Section sizes of the pre-Northridge twenty-story moment frame from the SAC project

story/Floor	COLUMNS		GIRDER
	Exterior (C1, C6)	Interior (C2 to C5)	
-2/-1	15x15x2.00	W24X335	W14X22
-1/1	15x15x2.00	W24X335	W30X99
1/2	15x15x2.00	W24X335	W30X99
2/3	15x15x2.00, 15x15x1.25	W24X335, W24X335	W30X99
3/4	15x15x1.25	W24X335	W30X99
4/5	15x15x1.25	W24X335	W30X99
5/6	15x15x1.25, 15x15x1.00	W24X335, W24X229	W30X108
6/7	15x15x1.00	W24X229	W30X108
7/8	15x15x1.00	W24X229	W30X108
8/9	15x15x1.00, 15x15x1.00	W24X229, W24X229	W30X108
9/10	15x15x1.00	W24X229	W30X108
10/11	15x15x1.00	W24X229	W30X108
11/12	15x15x1.00, 15x15x1.00	W24X229, W24X192	W30X99
12/13	15x15x1.00	W24X192	W30X99
13/14	15x15x1.00	W24X192	W30X99
14/15	15x15x1.00, 15x15x0.75	W24X192, W24X131	W30X99
15/16	15x15x0.75	W24X131	W30X99
16/17	15x15x0.75	W24X131	W30X99
17/18	15x15x0.75, 15x15x0.75	W24X131, W24X117	W27X84
18/19	15x15x0.75	W24X117	W27X84
19/20	15x15x0.75, 15x15x0.50	W24X117, W24X84	W24X62
20/Roof	15x15x0.50	W24X84	W21X50

* The basement floor (-1 level) has simple connections

5.2.2. *Column Splice Modelling*

In this study, column splices are assumed to be flexible in the translational shear and rotational directions, and rigid in the axial direction. Figure 5-3 schematically shows the mechanical model used for the column splices in the frames. Assuming rigid axial behaviour of column splices is reasonable for bearing column splices in compression. However, for non-bearing column splices, this assumption may lead to non-conservative results. No interaction was modelled between the shear and flexural springs. However, the overall modelling approach provides a foundation analysis for assessing the nonlinear impact of splice mechanics.

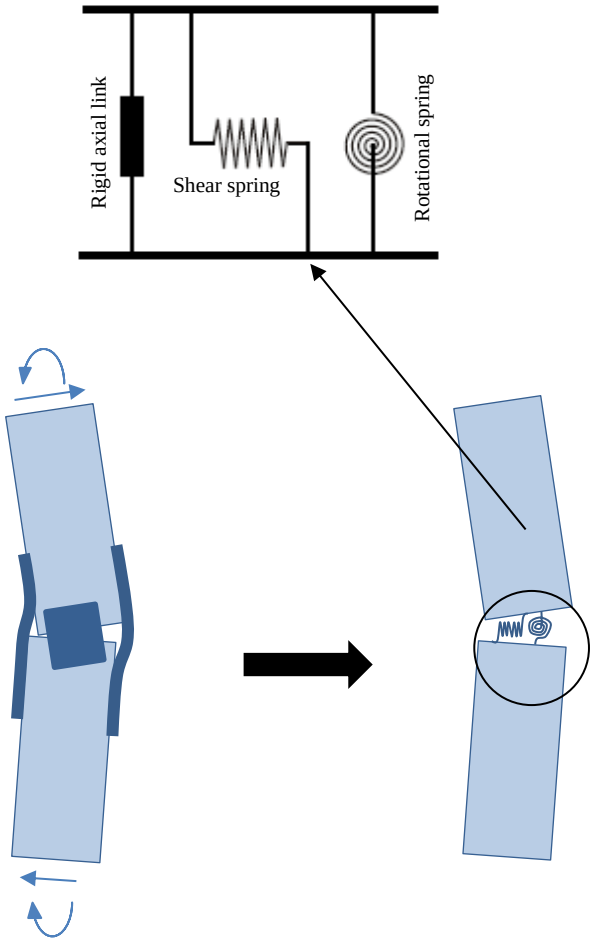

Figure 5-3 Mechanical model for column splices used in 2D frame analysis

5.2.2.1. ***Flexural Springs***

A gap model with incremental damage was adopted to represent the cyclic behaviour of rotational springs. This model can best represent bolted splice connections, both lap splices and end plate splices. In lap splice connections, the gap originates from oversize bolt holes or ovalized holes due to bolt bearing deformations, as seen in Chapter 3. The connection initially has very high stiffness (almost rigid) until demands overcome the friction in the connection, per Figure 5-4-A for one example. For simplicity in modelling, the bilinear stiffness behaviour post slippage was simplified to linear behaviour per Figure 5-4-B. In bolted end plate splices,

when end plates remain reasonably rigid, the bolts can initially elongate elastically under tension. A gap can be formed from residual post-elastic tensile deformations of bolts.

For frame analysis, two moment-rotation models were adopted for column splices bending about their major and minor axis. These models are shown in Figures 5-4-B and 5-4-D, as opposed to the experimental behaviours as can be seen in Figures 5-4-A and 5-4-C. These models are representative of splices for columns with W sections oriented about their major axis (Figure 5-4-B), columns with square hollow sections (Figure 5-4-D), and columns with W section oriented about their minor axis (Figure 5-4-D). Black and red arrows in Figure 5-4-B demonstrate the moment-rotation path prior and after a gap is formed in the system. Several *ElasticPPGap* materials were used in parallel in Opensees (Mazzoni et al., 2007) to generate the desired behaviours.

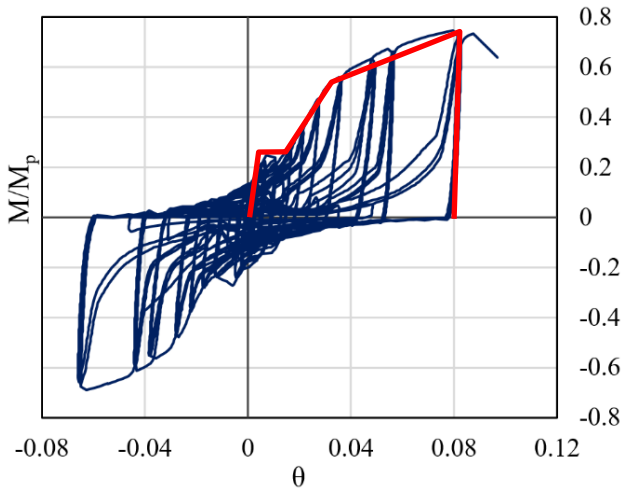

(A) typical example flexural behaviour of lap splice connection in UC section about major axis. Red lines show the backbone behaviour.

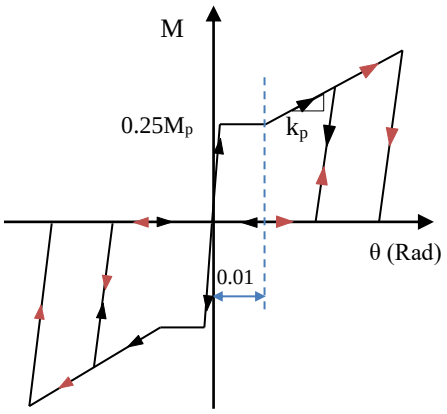

(B) Moment-rotation gap model representing splices for columns with W sections oriented about major axis.

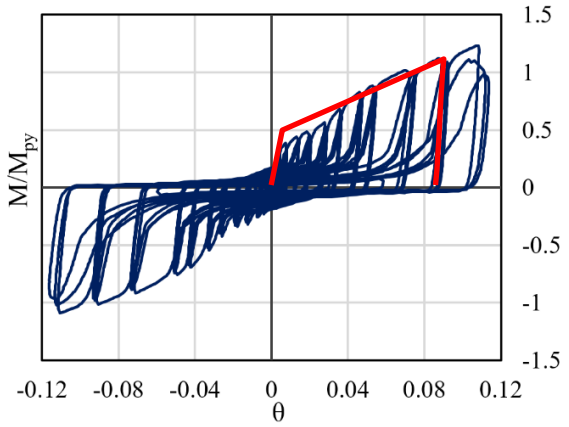

(C) typical example flexural behaviour of lap splice connection in UC section about minor axis. Red lines show the backbone behaviour.

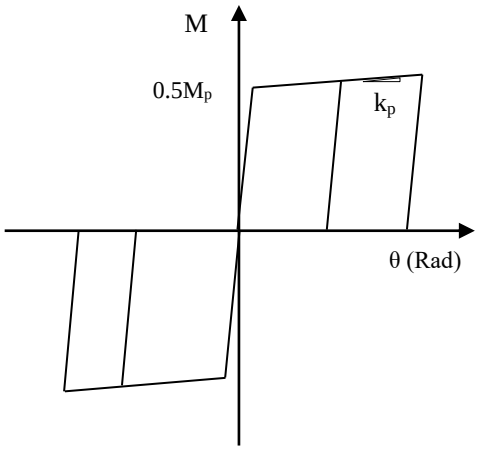

(D) Moment-rotation gap model representing splices for columns with W sections oriented about minor axis and splices for columns with square hollow sections.

Figure 5-4 Moment-rotation gap models for rotational springs used in 2D frame analysis

Slip moment and rotation for the rotational spring, modelled per Figure 5-4-A, were assumed to be constant values of $0.25M_p$ and *0.01rad*, respectively. Previous studies showed the SAC 9 and 20 story moment frames with rotational springs (representing column splices) of elastic stiffness values larger than *5EI/L* behave similar to the frame with rigid rotational springs (Tork Ladani et al., 2015). Therefore, the initial stiffness was selected to be *5EI/L*, knowing friction splice connections perform rigidly prior to slippage. The term *EI/L* is the flexural stiffness of the smaller column at the splice location.

The plateau in Figure 5-4-A corresponds to when friction is overcome and bolts can move freely in oversize holes, which was assumed to create up to *0.01rad* rotation. From this point onwards, it was assumed the spring exhibits a constant stiffness of k_p. This part of the model corresponds to bolts deforming in shear and bolt holes deforming due to bolt bearing. The frames were analysed for two values of k_p equal to *0.3EI/L* and *1.0EI/L*, which covers the upper and lower ranges of the stiffness values seen in the experiments, as discussed in Chapter 3. In

Figure 5-4-B, the initial elastic stiffness was assumed *5EI/L* and the post elastic stiffness, k_p, was assumed *0.5EI/L*.

5.2.2.2. ***Shear Springs***

A bilinear model was adopted to represent the cyclic behaviour of shear springs. The shear force deformation model can be seen in Figure 5-5. In this model, it was assumed shear springs yield at $0.5V_y$, where V_y is the shear capacity of the smaller member at the splice location. The stiffness of the shear springs was assumed to be a function of A_vG/L, where A_v is the shear area of the smaller member and G is the shear modulus. Two values for the initial shear stiffness were considered, $0.35A_vG/L$ and $0.5A_vG/L$. The post elastic stiffness ratio was considered constant for all shear springs and equal to 0.2.

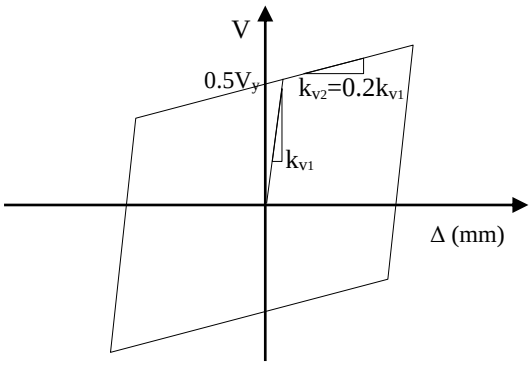

Figure 5-5 Shear-deformation model for shear springs used in frame analysis

5.2.3. ***Ground Motions***

An ensemble of 40 ground motion records, 2 sets of 20, were used for frame analysis. These ground motions represent DBE and MCE hazard levels with 10% and 2% possibility of occurrence in 50 years, corresponding to return periods of 475 and 2475 years, respectively (Somerville et al., 1997). The ground motions are from the SAC steel project, known as LA1 to LA40, and are compatible with potential shakings in Los Angeles, USA (SAC Joint Venture,

2000). The ground motions have already been scaled based on target spectra from the USGS for structural periods of 0.3, 1.0, 2.0 and 4.0 seconds. Further modifications were performed so the ground motions be representative of stiff soil (with shear wave velocity of 600 to 1200ft/sec) (Somerville et al., 1997). Tables 5-3 and 5-4 summarize the characteristics of these ground motions.

Table 5-3 Characteristics of ground motions representing DBE hazard level

Designation	Record Information	Duration (sec.)	Magnitude (M_w)	Fault distance, R (km)	Scale	PGA (in/sec.^{2})
LA01	Imperial Valley, 1940	39.38	6.9	10.0	2.01	178.0
LA02	Imperial Valley, 1940	39.38	6.9	10.0	2.01	261.0
LA03	Imperial Valley, 1979	39.38	6.5	4.1	1.01	152.0
LA04	Imperial Valley, 1979	39.38	6.5	4.1	1.01	188.4
LA05	Imperial Valley, 1979	39.38	6.5	1.2	0.84	116.4
LA06	Imperial Valley, 1979	39.38	6.5	1.2	0.84	90.6
LA07	Landers, 1992	79.98	7.3	36.0	3.20	162.6
LA08	Landers, 1992	79.98	7.3	36.0	3.20	164.4
LA09	Landers, 1992	79.98	7.3	25.0	2.17	200.7
LA10	Landers, 1992	79.98	7.3	25.0	2.17	139.1
LA11	Loma Prieta, 1989	39.98	7.0	12.4	1.79	256.9
LA12	Loma Prieta, 1989	39.98	7.0	12.4	1.79	374.4
LA13	Northridge, 1994, Newhall	59.98	6.7	6.7	1.03	261.8
LA14	Northridge, 1994, Newhall	59.98	6.7	6.7	1.03	253.7
LA15	Northridge, 1994, Rinaldi	14.95	6.7	7.5	0.79	206.0
LA16	Northridge, 1994, Rinaldi	14.95	6.7	7.5	0.79	223.9
LA17	Northridge, 1994, Sylmar	59.98	6.7	6.4	0.99	219.9
LA18	Northridge, 1994, Sylmar	59.98	6.7	6.4	0.99	315.5
LA19	North Palm Springs, 1986	59.98	6.0	6.7	2.97	393.5
LA20	North Palm Springs, 1986	59.98	6.0	6.7	2.97	380.9

Table 5-4 Characteristics of ground motions representing MCE hazard level

Designation	Record Information	Duration (sec.)	Magnitude (M_w)	Fault distance, R (km)	Scale	PGA (in/sec.^{2})
LA21	1995 Kobe	59.98	6.9	3.4	1.15	495.3
LA22	1995 Kobe	59.98	6.9	3.4	1.15	355.4
LA23	1989 Loma Prieta	24.99	7.0	3.5	0.82	161.4
LA24	1989 Loma Prieta	24.99	7.0	3.5	0.82	182.6
LA25	1994 Northridge	14.95	6.7	7.5	1.29	335.3
LA26	1994 Northridge	14.95	6.7	7.5	1.29	364.3
LA27	1994 Northridge	59.98	6.7	6.4	1.61	357.8
LA28	1994 Northridge	59.98	6.7	6.4	1.61	513.4
LA29	1974 Tabas	49.98	7.4	1.2	1.08	312.4
LA30	1974 Tabas	49.98	7.4	1.2	1.08	382.9
LA31	Elysian Park (simulated)	29.99	7.1	17.5	1.43	500.5
LA32	Elysian Park (simulated)	29.99	7.1	17.5	1.43	458.1
LA33	Elysian Park (simulated)	29.99	7.1	10.7	0.97	302.1
LA34	Elysian Park (simulated)	29.99	7.1	10.7	0.97	262.8
LA35	Elysian Park (simulated)	29.99	7.1	11.2	1.10	383.1
LA36	Elysian Park (simulated)	29.99	7.1	11.2	1.10	424.9
LA37	Palos Verdes (simulated)	59.98	7.1	1.5	0.90	274.7
LA38	Palos Verdes (simulated)	59.98	7.1	1.5	0.90	299.7
LA39	Palos Verdes (simulated)	59.98	7.1	1.5	0.88	193.1
LA40	Palos Verdes (simulated)	59.98	7.1	1.5	0.88	241.4

5.2.4. ***Analyses***

The main objective of this chapter is to investigate the possibility of global failure mechanism due to flexibility of bolted column splice connections, or local failure of the connections due to shear or moment failure of the connection. Global response of the frames can be assessed through comparison of frame drift profiles with rigid and flexible column splices. Local failure of the connections can be assessed through comparing shear and moment demands at the splices with the design capacities prescribed in seismic design codes.

The responses of interest in this study are peak story drift ratio, and maximum moment and shear demand at splices. The median, 84^{th} percentile and 16^{th} percentile values for each suite of ground motions are presented as the distributions of responses are lognormal (Limpert et al., 2001), (Limpert and Stahel, 2011). In the following sections, the results are discussed in detail for the 9 and 20 story frames. Results are presented as median (50^{th} percentile) for central value and the 16^{th} and 84^{th} percentiles to show the spread, representing one lognormal standard deviation on either side of the median, middle value (Limpert et al., 2001).

To date, no research has been conducted to study the seismic behaviour of moment frames incorporating the impact of flexible column splice connection behaviour in the analysis. This lack of study limits the possibility of full verification of the methods, approach, and results in this chapter by comparison to results in previous literature. However, indirect verification of frame responses are possible through comparing the previous study by (Gupta and Krawinkler, 1999) with frames including rigid column splice connections.

In particular, the geometry of the frames studied in this chapter are identical to model M1 in (Gupta and Krawinkler, 1999). This model is recognized as the most commonly used model in

structural engineering analyses and thus provides a well-accepted baseline comparator. Appendix C provides comparison of the M1 model analysis results which are in very good agreement with the results of this study. They are presented in Appendix C to preserve the clarity of this chapter. The good match shown there validated proceeding in this analysis as presented here.

5.3. **Results and Discussion**

5.3.1. ***Nine Story Frame***

The first and second mode periods of the 9 story frame with rigid and flexible column splices were analysed, and results are presented in Table 5-5. The frame with rigid column splices has the shortest first and second mode periods. These values are 2.37 sec and 0.89 sec, respectively, which are consistent with the 2.34 sec and 0.88 sec values in the research conducted by (Gupta and Krawinkler, 1999). Frames with the most flexible shear springs have the longest fundamental periods. The increases in the period for the first and second modes are 5% and 4%, respectively. The elastic stiffness of rotational springs is constant for all splices and variation only occurs post slippage. Therefore, no changes can be seen for different values of rotational stiffness, k_p, since the Eigen analysis only considers elastic stiffnesses. Hence, this result should be expected and nonlinear time history analysis should better delineate any differences.

Table 5-5 Period of 9 story frame (sec.) with different splice properties and locations

Location Within Height	**Mode of Vibration**	**Rigid**	**k_p=0.30EI/L k_v=0.50A_vG/L**	**k_p=0.30EI/L k_v=0.35A_vG/L**	**k_p=1.0EI/L k_v=0.50A_vG/L**	**k_p=1.0EI/L k_v=0.35A_vG/L**
One third	**First**	2.37	2.46	2.49	2.46	2.49
	Second	0.89	0.92	0.93	0.92	0.93
Two third	**First**	2.37	2.46	2.49	2.46	2.49
	Second	0.89	0.92	0.93	0.92	0.93

5.3.1.1. ***Comparison of frame response for flexible and rigid splices***

Figure 5-6 shows the median, 16th percentile, and 84th percentile values of absolute peak story drifts in the 9 story frame, for rigid and flexible splices *(k_p=0.3EI/L, k_v=0.50A_vG/L)*, under DBE and MCE hazard level events. Splices were located at one third of the column heights. Flexible splices increased drifts of the stories containing column splices. This increase varies for different stories and hazard levels, but it is the greatest for the second top level splices (levels 6) under DBE events. The increase is ~20% for this splice location, which is a significant difference and increase damage and risk.

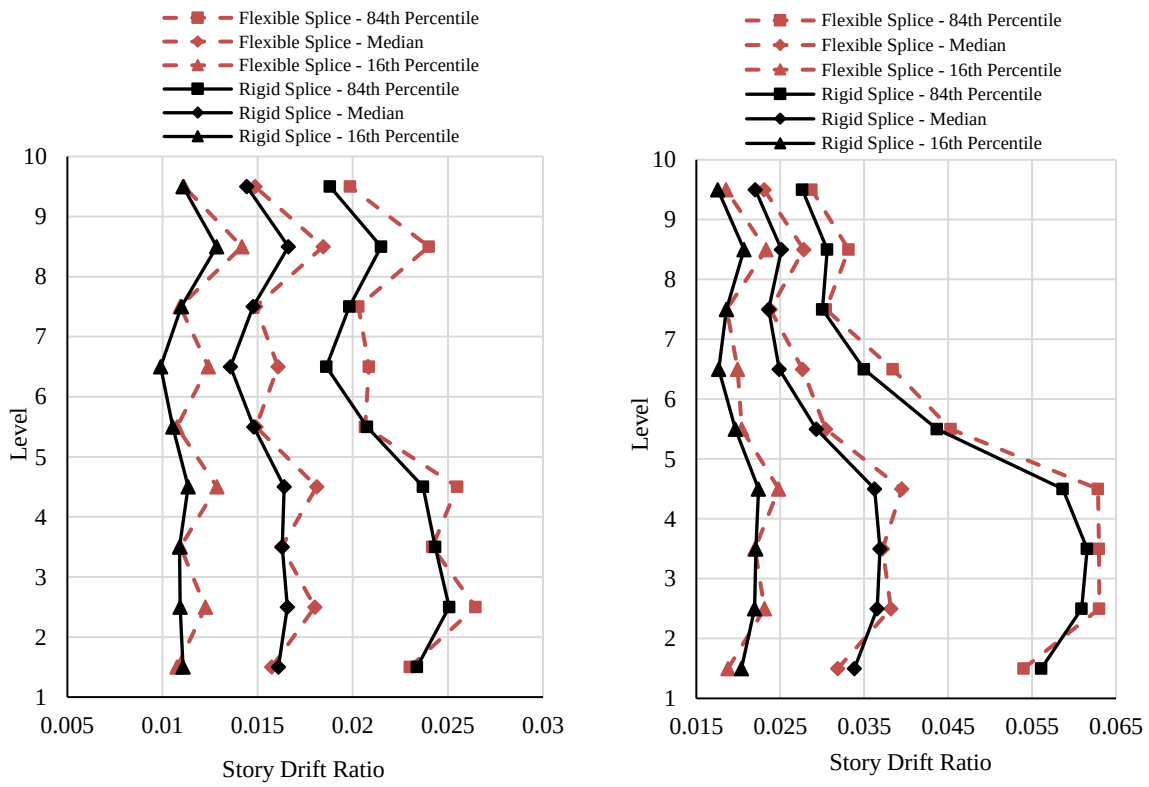

(A) DBE hazard level **(B)** MCE hazard level

Figure 5-6 Comparison of peak absolute story drift ratio in 9 story frame for DBE and MCE hazard levels, Solid lines represent frame with rigid splices and dash lines represent frame with flexible splices (k_p=0.3EI/L, k_v=0.50A_vG/L). Splices were located at one third of story height up the column.

Figure 5-7 shows the median, 16th percentile and 84th percentile values of peak moment demand at the location of splices in the 9 story frames with rigid and flexible splices *(k_p=0.3EI/L,*

$k_v=0.50A_vG/L$) under DBE hazard level events. Column splices were located at one third of column height. For the interior columns, Columns 2 to 4, moment demand is larger if splices are rigid, especially for levels 6 and 8. For the exterior columns, Columns 1 and 6, demands are similar for both rigid and flexible splices.

Moment demands are generally larger for the splices at levels 6 and 8, reaching approximately $0.36M_p$, which is smaller than the minimum prescribed requirement of $0.5\phi M_p$ (ϕ=0.9) in New Zealand Standard NZS3404. Demands are generally the smallest for splices in column 6, which could be due to the pin beam-column connection. Generally, the dispersion or spread of the results are larger for the frame with rigid column splices.

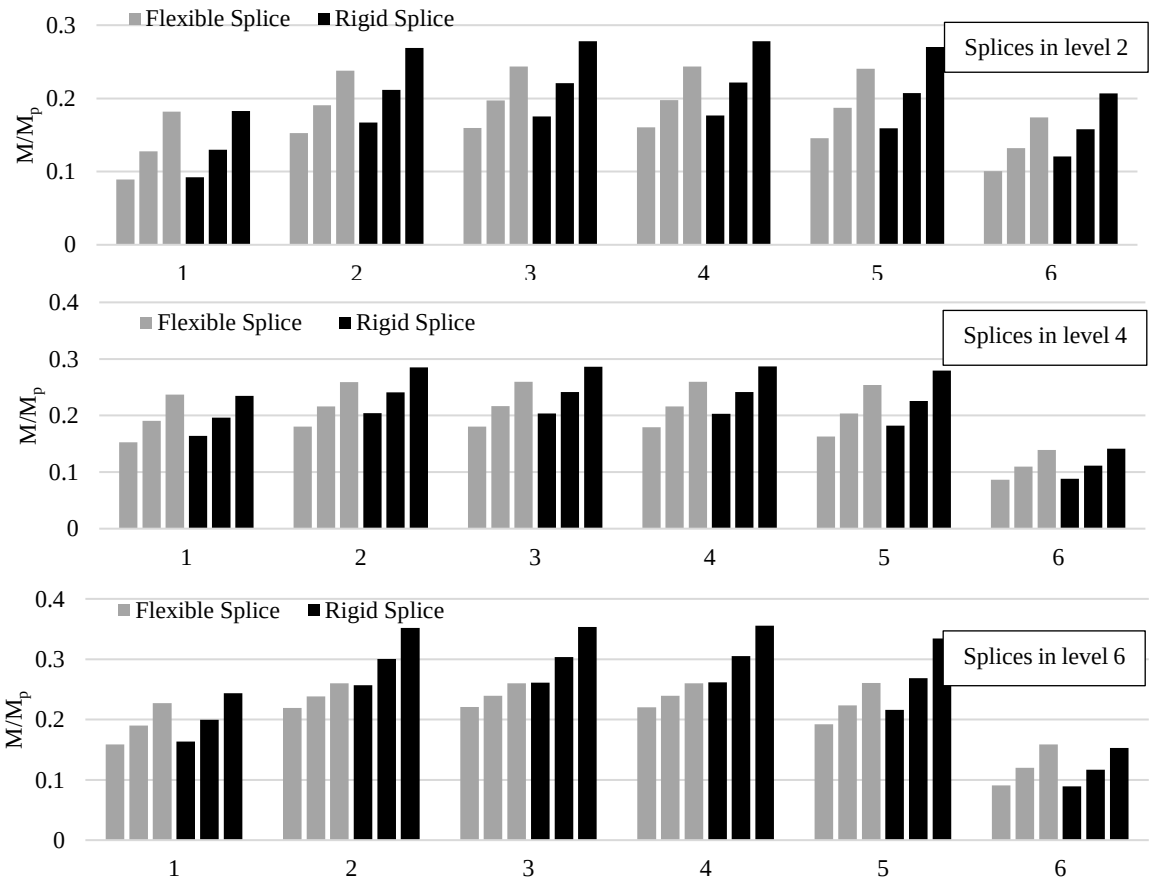

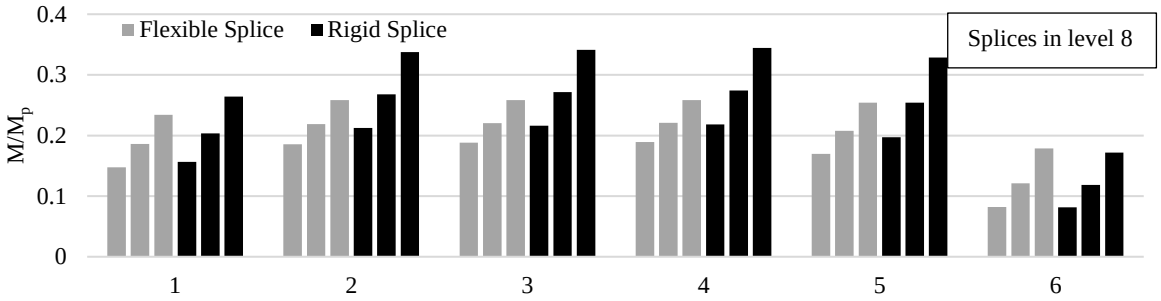

Figure 5-7 Peak moment ratio in 9 story frame in columns 1-6 under DBE hazard level. Grey bars represent flexible splices with (k_p=0.3EI/L, k_v=0.50A_vG/L) (from left to right, 16th percentile, Median, 84th percentile). Black bars represent rigid splices (from left to right, 16th percentile, Median, 84th percentile). Splices were located at one third of story height up the column.

Figure 5-8 shows the median, 16th percentile and 84th percentile values of peak shear demand at the location of splices in the 9 story frames, with rigid and flexible splices *(k_p=0.3EI/L, k_v=0.50A_vG/L)*, under DBE hazard level events. Splices were located at one third of column heights. Shear demands are very similar for rigid and flexible splices. Since column 6 is oriented about the minor axis, it has a higher shear capacity compared to the other columns. Hence, the shear ratio is very small. Shear demand is the highest for splices at level 6, reaching 0.44V_y for rigid splices, which is larger than the minimum code prescribed shear requirement of 0.25ϕV_y (ϕ=0.9).

As it was seen in the shear experiments in Section 3.2.3 and explained in Section 4.2.3, even small shear displacement is sufficient to engage flange splices to resist the shear force. Since no stiffness requirement has been defined for bolted column splice design in the New Zealand design standard, it is likely bolted columns move relative to each other during earthquake motions. In this case, interaction of flange and web splices is inevitable. Thus, not only are bolted column splices designed for these minimum requirements at risk of shear failure, flange splices may also fail due to the interaction of shear and moment demands.

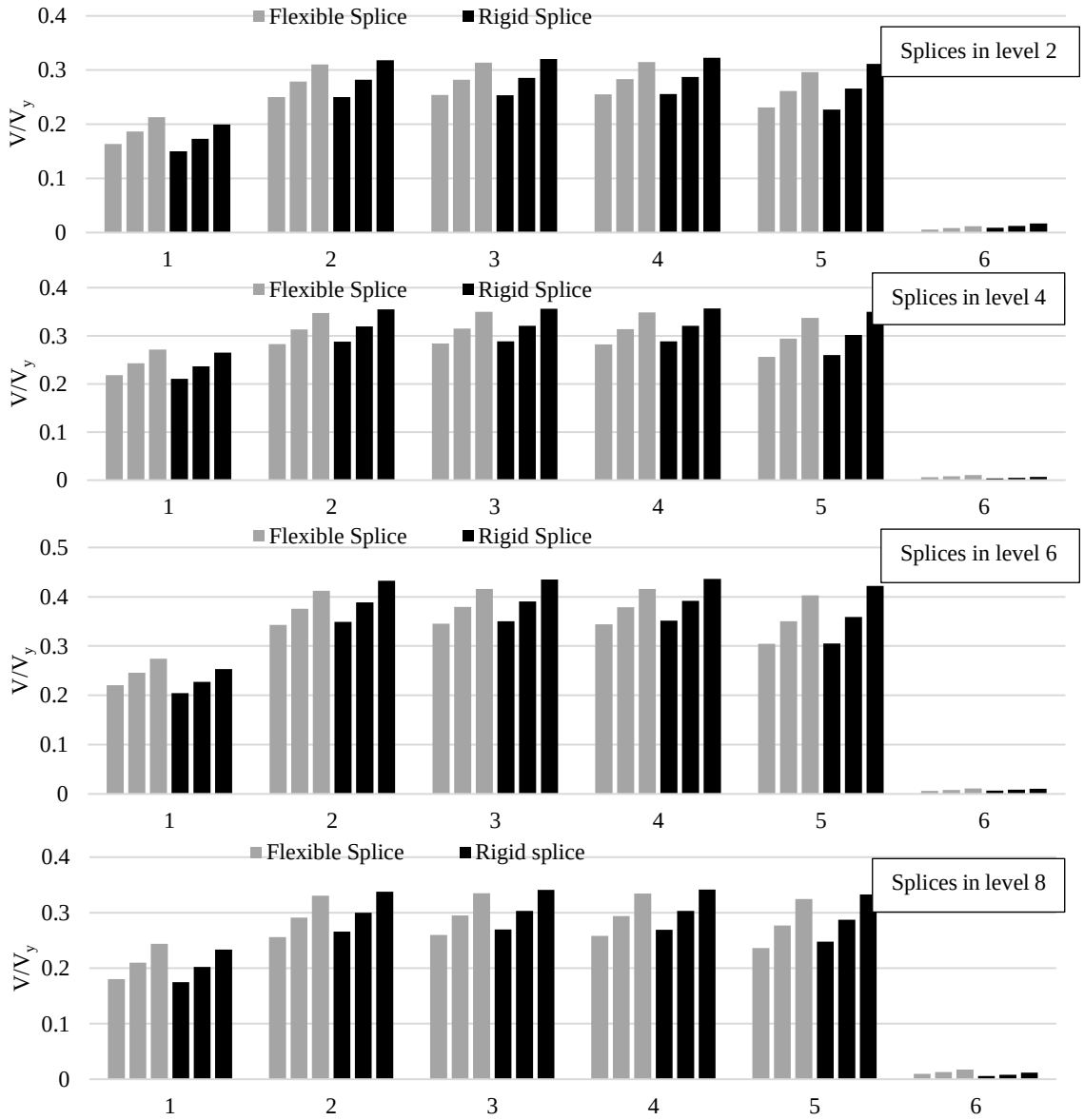

Figure 5-8 Peak shear ratio in 9 story frame in columns 1-6 for DBE hazard level. Grey bars represent flexible splices with (k_p=0.3EI/L, k_v=0.50A_vG/L) (from left to right, 16th percentile, Median, 84th percentile). Black bars represent rigid splices (from left to right, 16th percentile, Median, 84th percentile). Splices were located at one third of story height up the column.

5.3.1.2. ***Effect of Rotational Stiffness***

Figure 5-9 shows the peak story drift ratio for column splices with two different rotational stiffnesses (k_p=*1EI/L* vs k_p=*0.3EI/L*) while keeping the shear stiffness constant (*0.5*A_v*G/L*). The response is not sensitive to the change in rotational stiffness for either DBE or MCE hazard level events. Column splices with smaller rotational stiffness caused insignificant increase in the 84th percentile response under MCE events for the first and second levels.

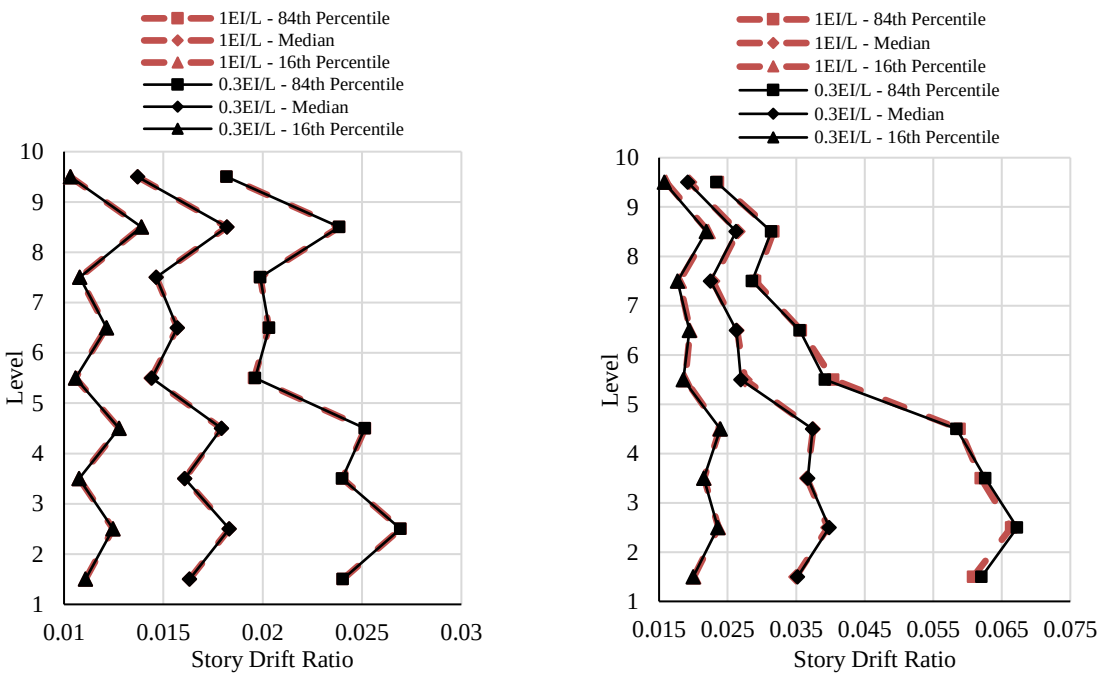

(A) DBE hazard level

(B) MCE hazard level

Figure 5-9 Comparison of peak story drift ratio in 9 story frame with splices of different rotational stiffnesses for DBE and MCE hazard levels, Solid lines represent frame with splices of (k_p=0.3EI/L, k_v=0.50A_vG/L) and dash lines represent frame with splices of (k_p=1EI/L, k_v=0.50A_vG/L). Splices were located at two third of story height up the column.

5.3.1.3. ***Effect of Shear Stiffness***

Figure 5-10 shows the peak story drift ratio for column splices with two different shear stiffnesses (*0.5A_vG/L* vs *0.35A_vG/L*) while keeping the rotational stiffness constant (*k_p=1EI/L*). Increasing the shear flexibility increased drift ratios of the floors contacting splices. The increase is larger for level 6, with ~6% increase in the drift demand under DBE hazard level events. The increase is not as significant under MCE hazard level events.

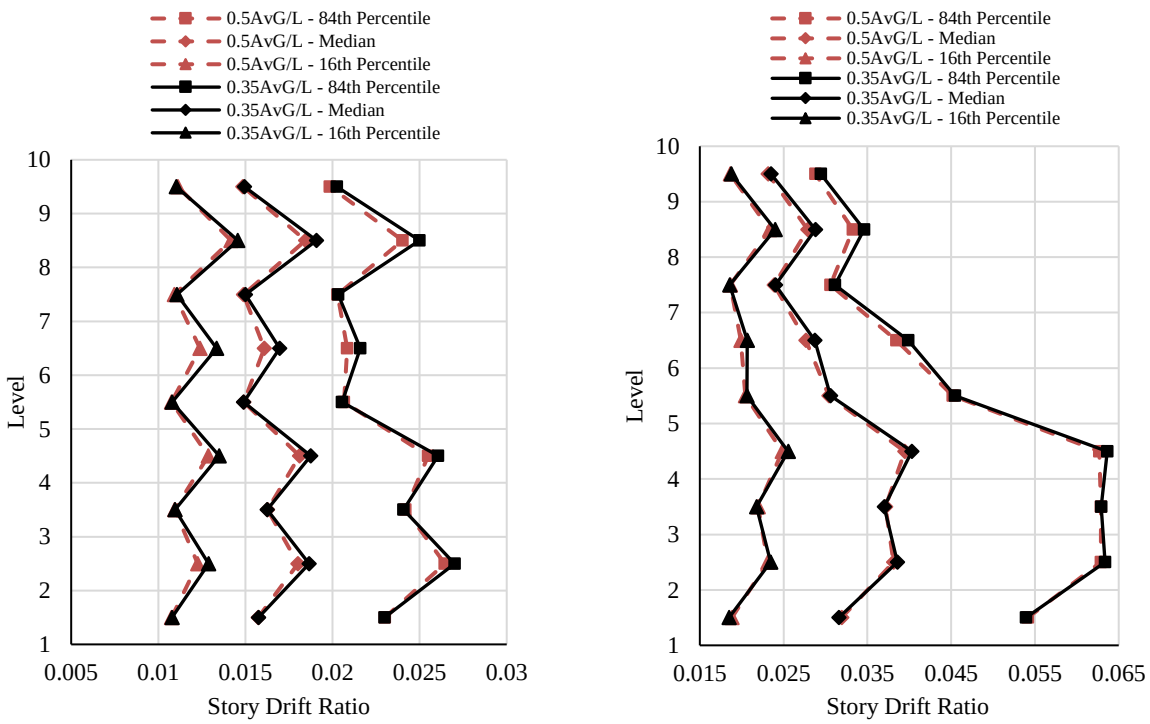

(A) DBE hazard level **(B)** MCE hazard level

Figure 5-10 Comparison of peak story drift ratio in 9 story frame with splices of different shear stiffnesses under DBE and MCE hazard levels. Solid lines represent frame with splices of (k_p=1EI/L, k_v=0.350A_vG/L) and dash lines represent frame with splices of (k_p=1EI/L, k_v=0.50A_vG/L). Splices were located at one third of story height up the column.

5.3.1.4. ***Effect of Splice Location within Same Levels***

Figure 5-11 shows the peak story drift ratio for column splices of the same properties located at two different locations within the level, specifically the top and bottom of the middle third of the columns. Splices close to bottom floor decreased the drift ratios of the bottom two stories, while increasing drift ratios at other levels. The change is larger under MCE level events, on the order of 15%, which is again a significant change in response and risk.

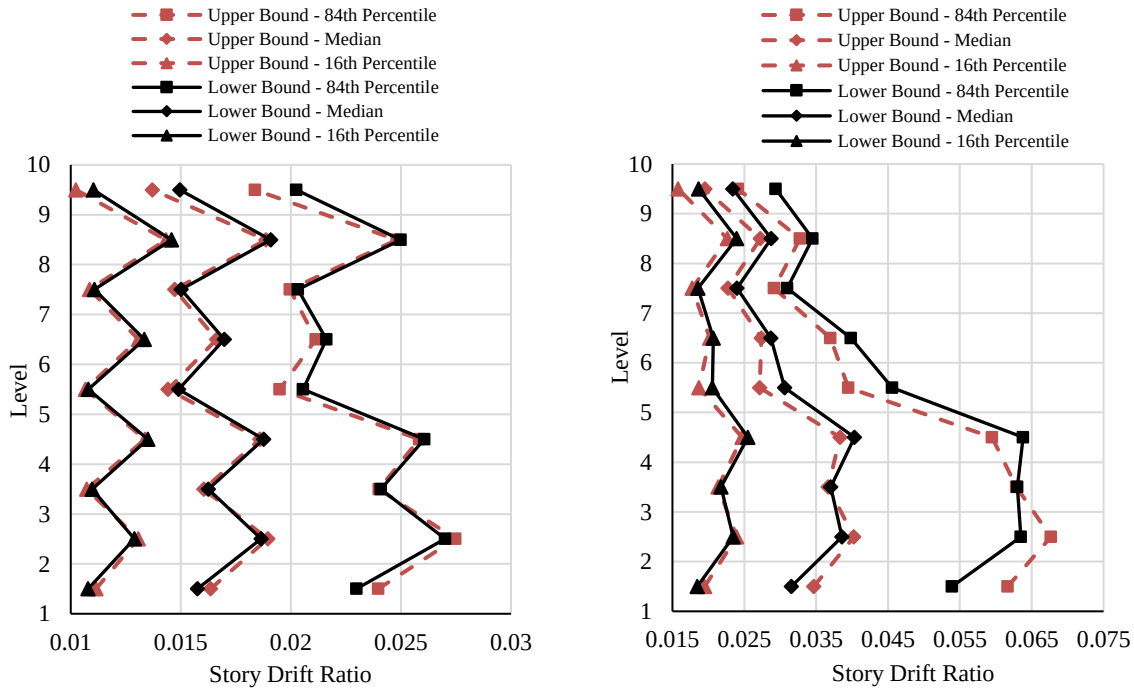

(A) DBE hazard level **(B)** MCE hazard level

Figure 5-11 Comparison of peak story drift ratio in 9 story frame with column splices at different locations (top and bottom of column middle third) for DBE and MCE hazard levels. Solid lines represent frame with splices at one third of story height up column (lower bound) and dash lines represent frame with splices located at two thirds of story height up the column (upper bound). Splices were k_p=0.3EI/L, k_v=0.350A_vG/L.

5.3.1.5. ***Effect of Splice Location within other Levels***

Analyses were conducted to study frame response when column splices were located at other stories. To accomplish this analysis, a frame model was created in which new column splices were introduced at levels 1, 3, 5 and 7, while column splices at levels 2, 4, 6 and 8 were set as rigid and removed. The column cross sections and their changes remained identical to the SAC 9 story model.

Figure 5-12 shows the median, 16th percentile, and 84th percentile values of absolute peak story drifts in the frame, for rigid and flexible splices *(k_p=0.3EI/L, k_v=0.50A_vG/L)*, under DBE and MCE hazard level events. Splices were located at one third of the story height up columns. Unlike the previous model under DBE level events, flexible splices altered drifts of not only the stories containing column splices, but also adjacent floors. This change is an increase of

drift at story 2 (6% and 12% for median and 84th percentile drifts) and decreases at levels 6 and 9 (7% and 13% for median and 84th percentile drifts at level 6). Similar trends can be observed for frame response under MCE level events. But the change is not as significant as at the DBE level. It appears frame responses could be sensitive to the arrangement of column splice locations through the frame height.

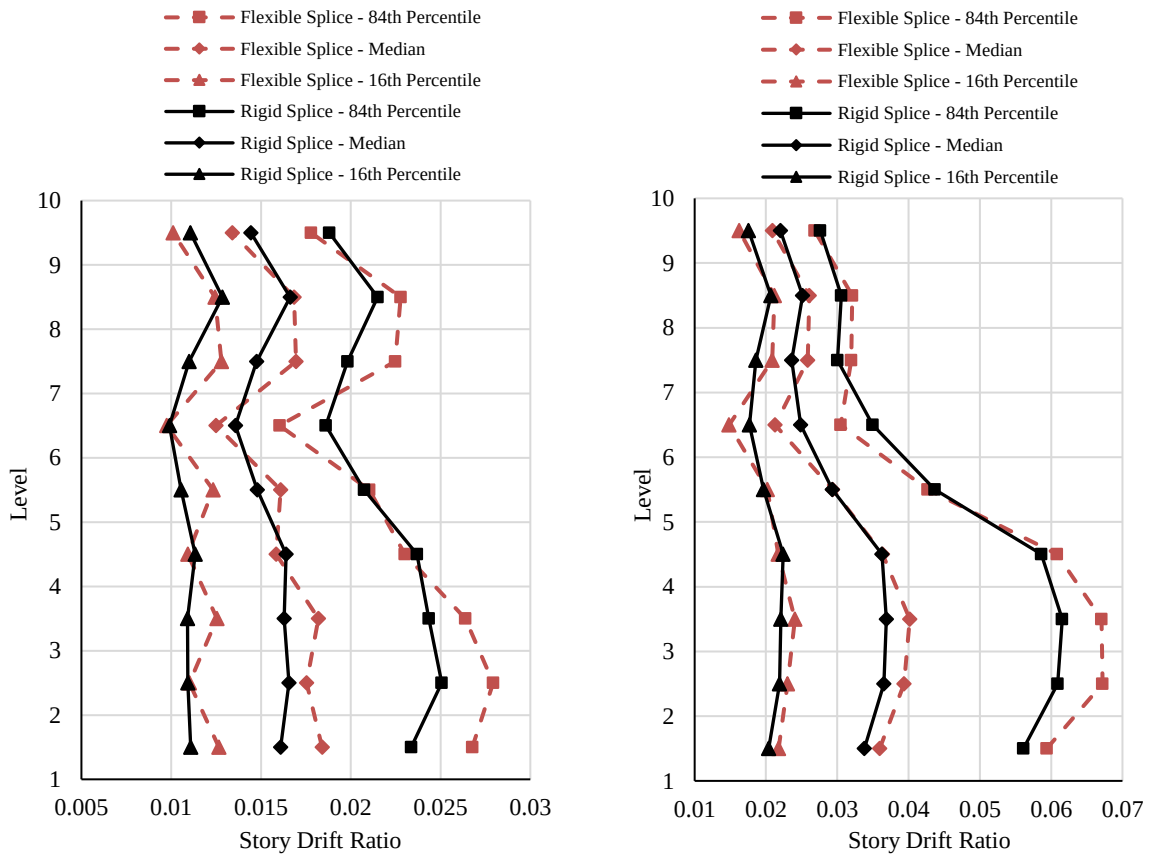

(A) DBE hazard level **(B)** MCE hazard level

Figure 5-12 Comparison of peak absolute story drift ratio in 9 story frame for DBE and MCE hazard levels, Solid lines represent frame with rigid splices and dash lines represent frame with flexible splices (k_p=0.3EI/L, k_v=0.50A_vG/L). Splices were located at one third of story height up the column.

5.3.1.6. ***Time History Responses and Further Discussion***

For the 9 story frames with flexible column splices, maximum shear demand under DBE level events for all cases was smaller than 50% of the smaller member shear capacity at the splice. In addition, maximum splice shear deformation was approximately 11mm, at 0.42V_y. This

result means for all DBE level events, the shear springsmodelling part of the splice were in the elastic range. The maximum moment demand under the same level events, was 29% of moment capacity, M_p, in frames with flexible column splices. The moment corresponds to post slippage stage, which was selected to occur at $0.25M_p$. Therefore, maximum rotation of flexural springs would be approximately 0.01Rad, equal to the selected slip rotation shown in Figure 5-4-A. Results were very similar for either of the specified locations of splices within the floor at one or two thirds of story height up the column.

The maximum shear demand from the MCE level events occurred at 50% of the smaller member shear capacity at the splice in an interior column. This maximum demand was associated with approximately 11mm and 15mm shear displacement for $kv=0.50A_vG/L$ and $kv=0.350A_vG/L$. Similar to DBE level events, shear springs remained in the elastic range in all MCE level events. The maximum moment demand under MCE level events was $0.55M_p$ in an exterior column. Results were very similar for either of the specified locations of splices within the floor.

Figure 5-12 shows moment-rotation response of the three candidate splices, as modelled, subjected to a major input cycle of the MCE level LA36 event. The graphs demonstrate gapping behaviour with incremental damage, as prescribed by the analysis programme and specific model elements chosen.

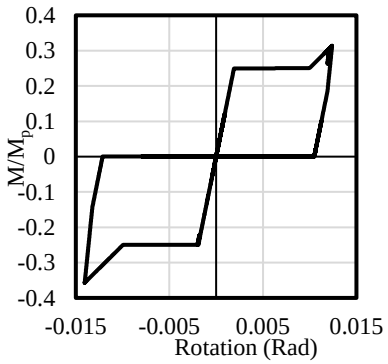

(A) Moment vs Rotation of splice in column 2, level 7

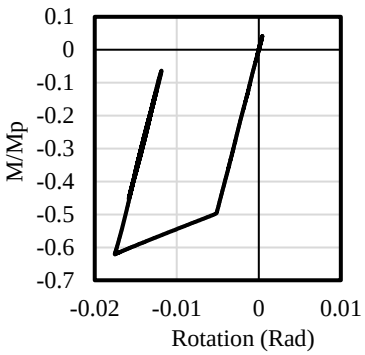

(B) Moment vs Rotation of splice in column 6, level 5

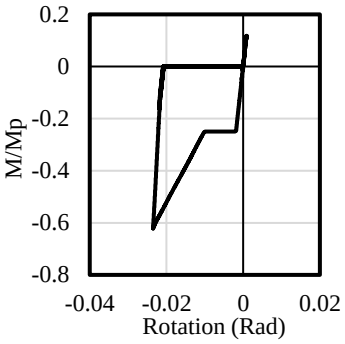

(C) Moment vs Rotation of splice in column 5, level 5

Figure 5-13 Moment vs rotation of column splices in LA36 event. Splices were of (k_p=1.0EI/L, k_v=0.50A_vG/L) and located at the two third of column height. **(A)** Splice in column 2, level 7 **(B)** Splice in column 6, level 5 **(C)** Splice in column 5, level 5

Figures 5-13 shows the time history of roof displacement in LA17 event, selected randomly, for frames with rigid and flexible splices. Although no significant changes were observed in the peak response, the transient response of the frames vary for different splice properties. This variability could indicate flexible splices could alter other responses, such as residual displacements and floor accelerations.

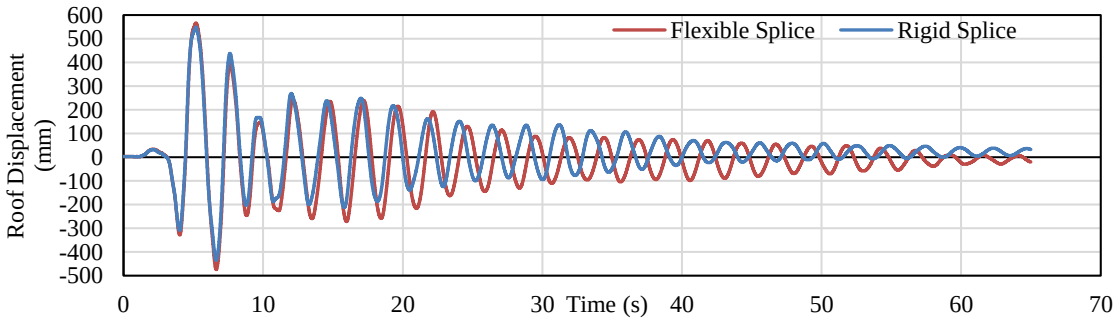

Figure 5-14 Time history of roof displacement in 9 story frame with rigid and flexible (k_p = 0.3EI/L, k_v = 0.50A_vG/L) column splices for LA17 event. Splices were located at one third of story height up the column.

In total, flexible column splices increased drifts of the stories containing column splices, up to ~20%. However, this increase does not appear significant enough to initiate a global frame mechanism. It was observed that story drift responses were more sensitive to shear stiffness than flexural stiffness of the column splices, for the ranges of stiffness studied here. While column splice

location within a floor could alter the story drifts locally within that floor, shifting splices to other stories could overshadow the drift profile of the whole frame. Moment and shear demand in column splices vary with their location, geometry and stiffness properties. While moment demands were consistently smaller than the minimum strength requirement of $0.5\phi M_p$, shear demands exceeded the minimum shear strength requirement of $0.25\phi V_y$. As explained before, due to flexibility of bolted column splices, the risk of failure of flange splices increases with engagement of flange splices in carrying the shear force.

5.3.2. *Twenty Story Frame*

The first and second mode periods of the 20 story frame with rigid and flexible column splices was analysed and results are presented in Table 5-6. Frame with rigid column splices has smallest periods for the first and second modes of vibrations. Frames with the most flexible shear springs, have the longest periods. The increases in the period for the first and second modes are 3% and 4% respectively. Similar to the 9 story frame, the elastic stiffness of rotational springs are constant for all splices and variation only occurs post slippage. Therefore, no changes can be seen for different properties of rotational springs as the Eigen analysis only considers elastic stiffnesses. The period of the frame with rigid column splices is in very good agreement with previous literature, as explained in Appendix C.

Table 5-6 Period of 20 story frame (sec.) with different splice properties and locations

Location Within Height	**Mode of Vibration**	**Rigid**	**k_p=0.30EI/L k_v=0.50A_vG/L**	**k_p=0.30EI/L k_v=0.35A_vG/L**	**k_p=1.0EI/L k_v=0.50A_vG/L**	**k_p=1.0EI/L k_v=0.35A_vG/L**
One third	**First**	4.01	4.11	4.15	4.11	4.15
	Second	1.38	1.42	1.44	1.42	1.44
Two third	**First**	4.01	4.11	4.15	4.11	4.15
	Second	1.38	1.42	1.44	1.42	1.44

5.3.2.1. ***Comparison of frame response for flexible and rigid splices-DBE***

Figure 5-15 shows the median, 16th percentile and 84th percentile values of peak story drifts in the 20 story frame, with rigid and flexible splices *(k_p=0.3EI/L, k_v=0.50A_vG/L)*, under DBE and MCE hazard levels. Splices were located at one third of column heights. Flexible splices increased drifts for the stories containing column splices. The effect of flexibility on drift demands is more significant for stories higher than level 10. The increase in the median response can be as large as 20% and 30% for DBE and MCE level events, which significantly increase response, any potential damage, and risk.

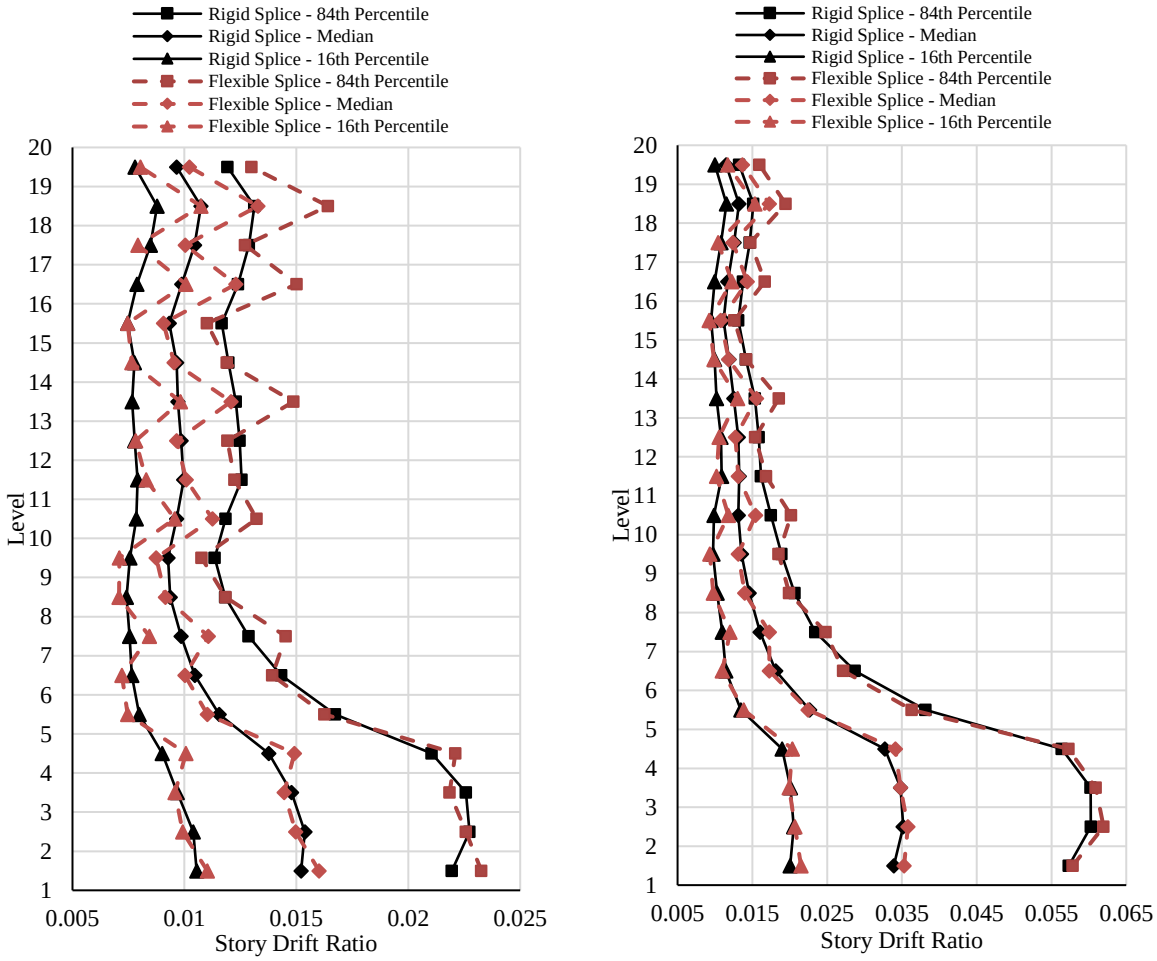

(A) DBE hazard level **(B)** MCE hazard level

Figure 5-15 Comparison of peak story drift ratio in 20 story frame for DBE and MCE hazard levels, Solid lines represent frame with rigid splices and dash lines represent frame with flexible splices (k_p=0.3EI/L, k_v=0.350A_vG/L). Splices located at one third of story height up the column.

Figure 5-16 shows the median, 16th percentile and 84th percentile values of peak moment demand at the location of splices in the 20 story frames, with rigid and flexible column splices *(k_p=0.3EI/L, k_v=0.50A_vG/L)*, under DBE hazard level. Splices were located at one third of column heights. For the interior columns, moment demand is larger if column splices are rigid, especially for the top two upper levels with splices, specifically those splices at levels 16 and 18. For the exterior columns, demands are generally similar for both rigid and flexible splices. However, interestingly, moment demand is larger for frame with flexible splices at level 19 compared to the frame with rigid splices.

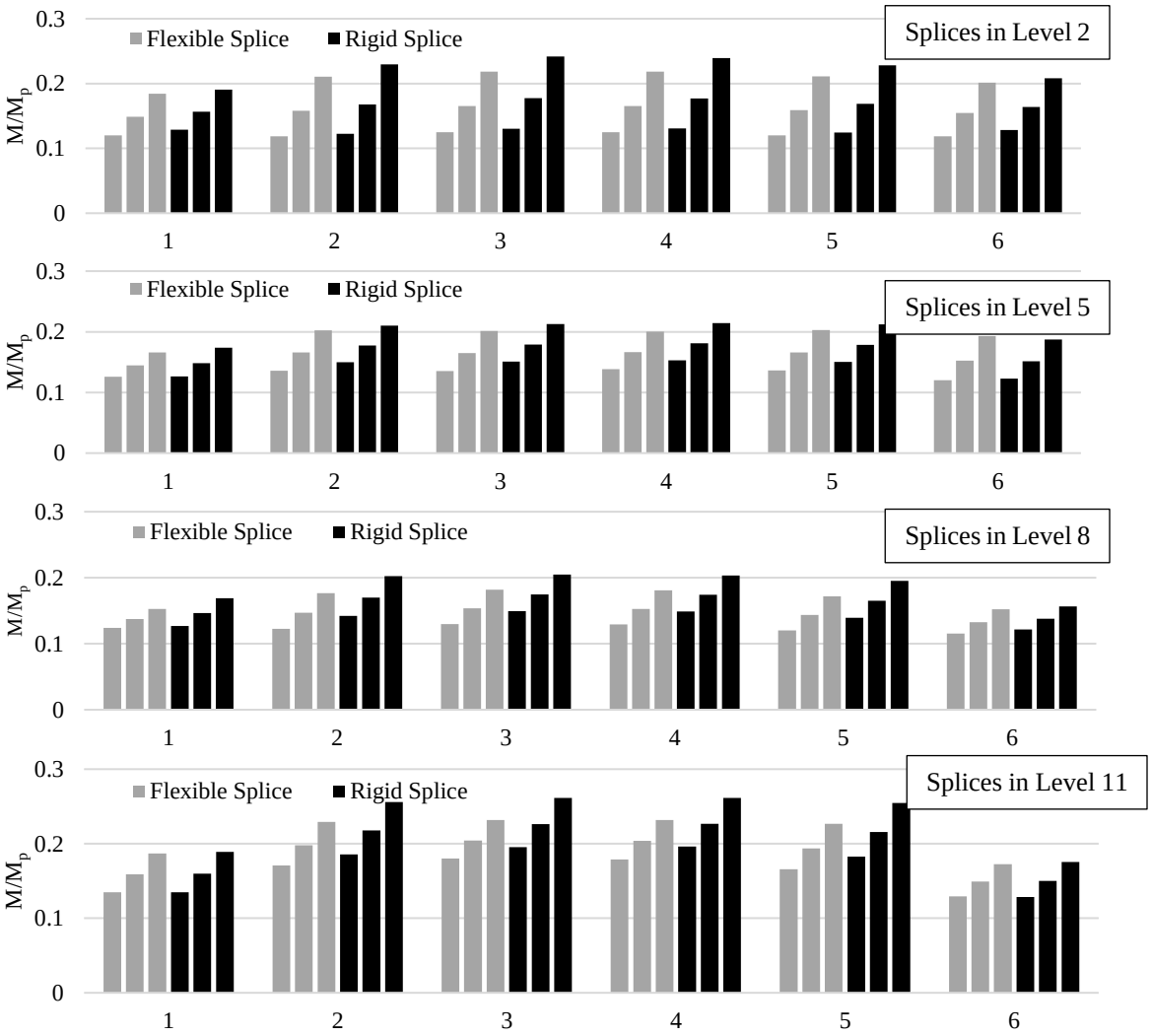

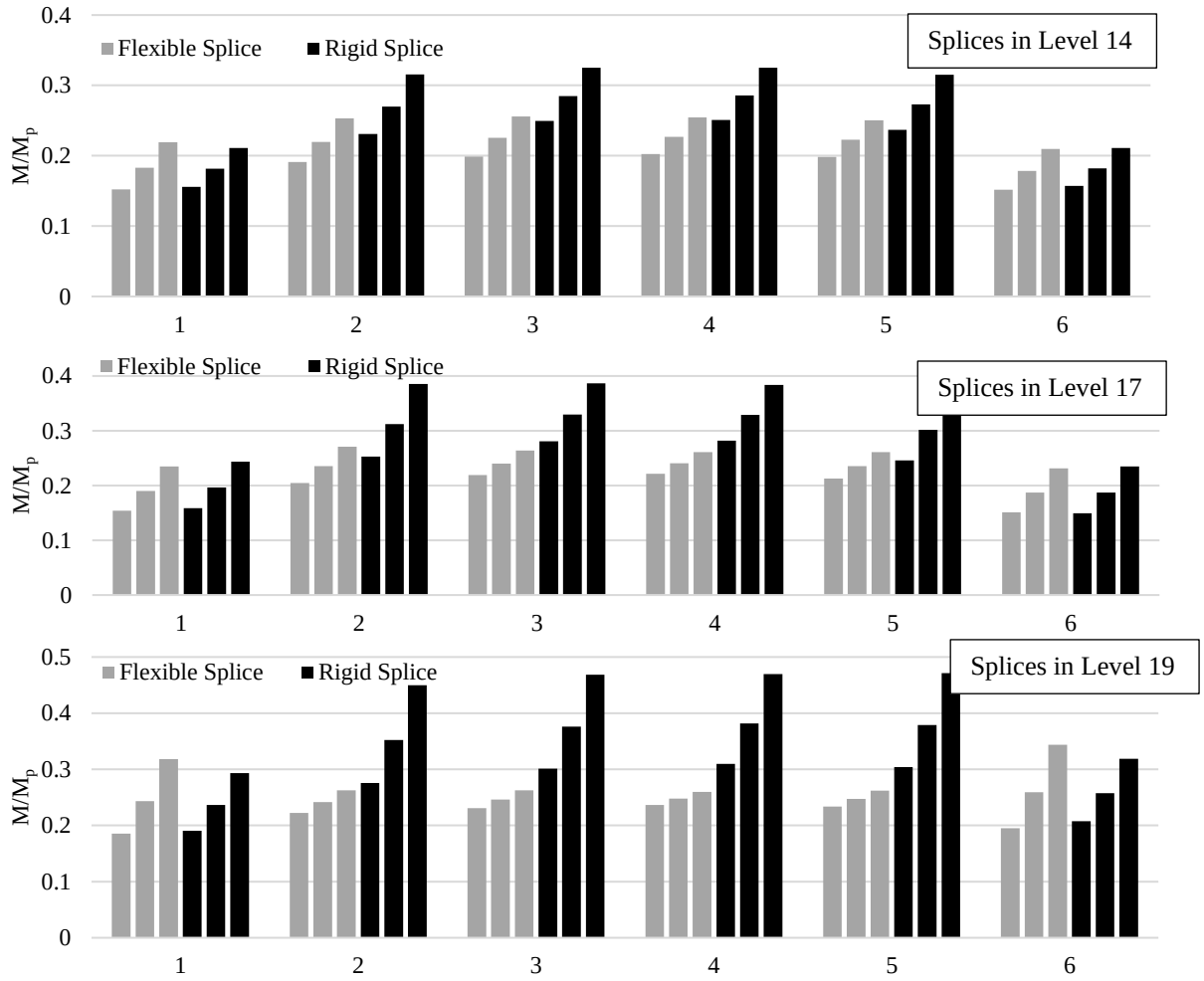

Figure 5-16 Peak moment ratio in twenty-story frame in columns 1-6 under DBE hazard level. Grey bars represent flexible splices with (k_p=0.3EI/L, k_v=0.50A_vG/L) (from left to right, 16th percentile, Median, 84th percentile). Black bars represent rigid splices (from left to right, 16th percentile, Median, 84th percentile). Splices are located at one third of story height up the column.

Moment demands generally increased with height for splices above level 8 in the frame with rigid splices. However, for the frame with flexible splices, demands stayed within the limit of 0.2M_p to 0.3M_p. The maximum demand for a rigid splice was 0.47M_p at level 19 for an interior column, which is larger than the minimum requirement for flexural strength of column splices of 0.5ϕM_p=0.45M_p (ϕ=0.9), prescribed in the New Zealand standard. In contrast, the maximum demand for the frame with flexible splices occurred in exterior column 6, which was 0.34M_p. Generally, the dispersion of the results is larger for the frame with rigid column splices, especially at higher levels, showing flexible splices effectively ameliorate this variability.

Figure 5-17 shows the median, 16th percentile and 84th percentile values of peak shear demand at the location of splices in the 20 story frames, for rigid and flexible splices *(k_p=0.3EI/L, k_v=0.50A_vG/L)*, under DBE hazard level. Splices were located at the bottom of the middle third of columns. Shear demands are very similar for rigid and flexible splices up to level 8. Exterior columns have hollow square sections and have larger shear capacities. Hence, the shear ratio is smaller for these columns. Maximum shear demand for frames with flexible and rigid splices were 0.36V_y and 0.38V_y, respectively, which is again larger than the minimum requirement of 0.25ϕV_y. Shear demands are larger for flexible splices, especially at the top two levels compared to rigid splices.

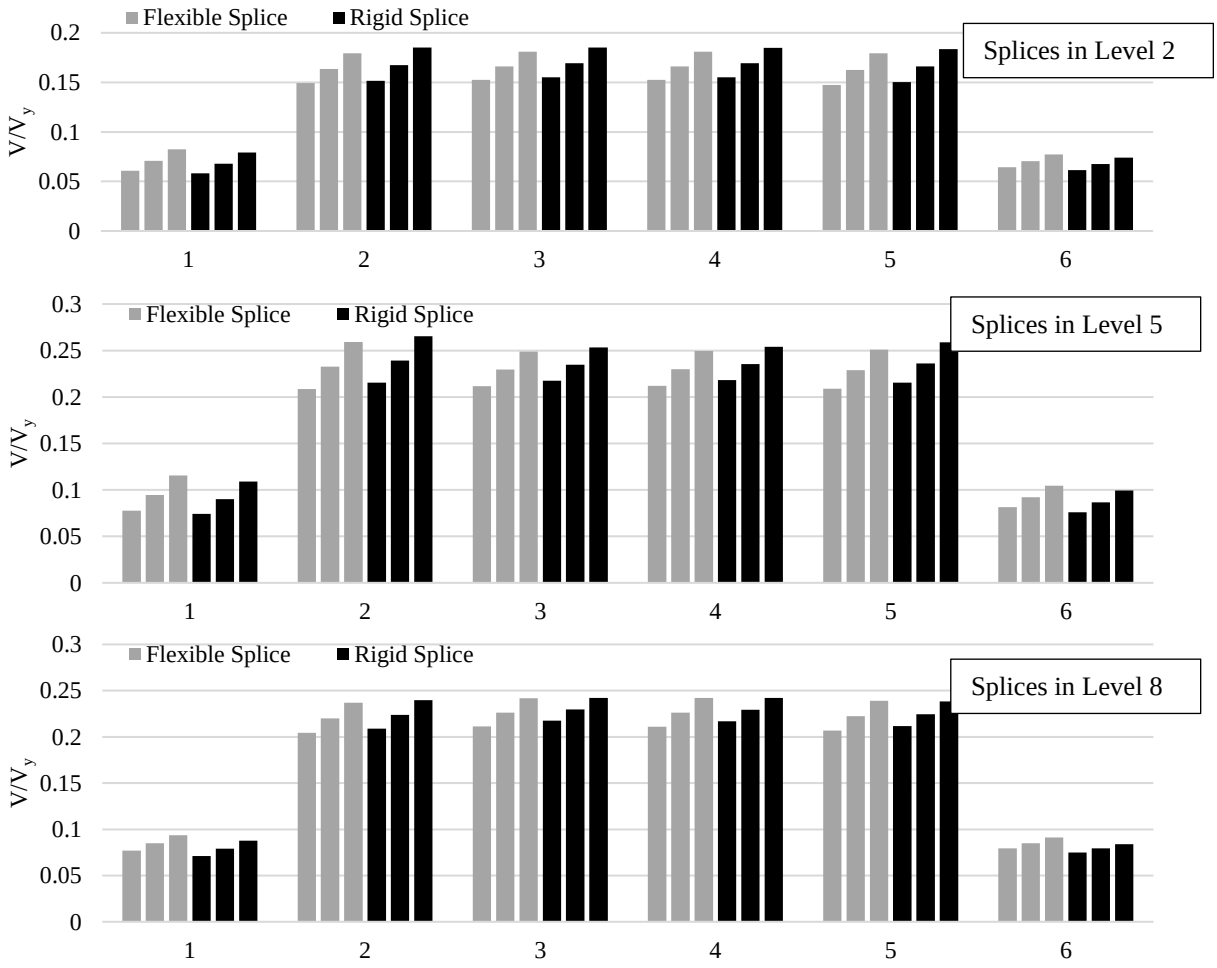

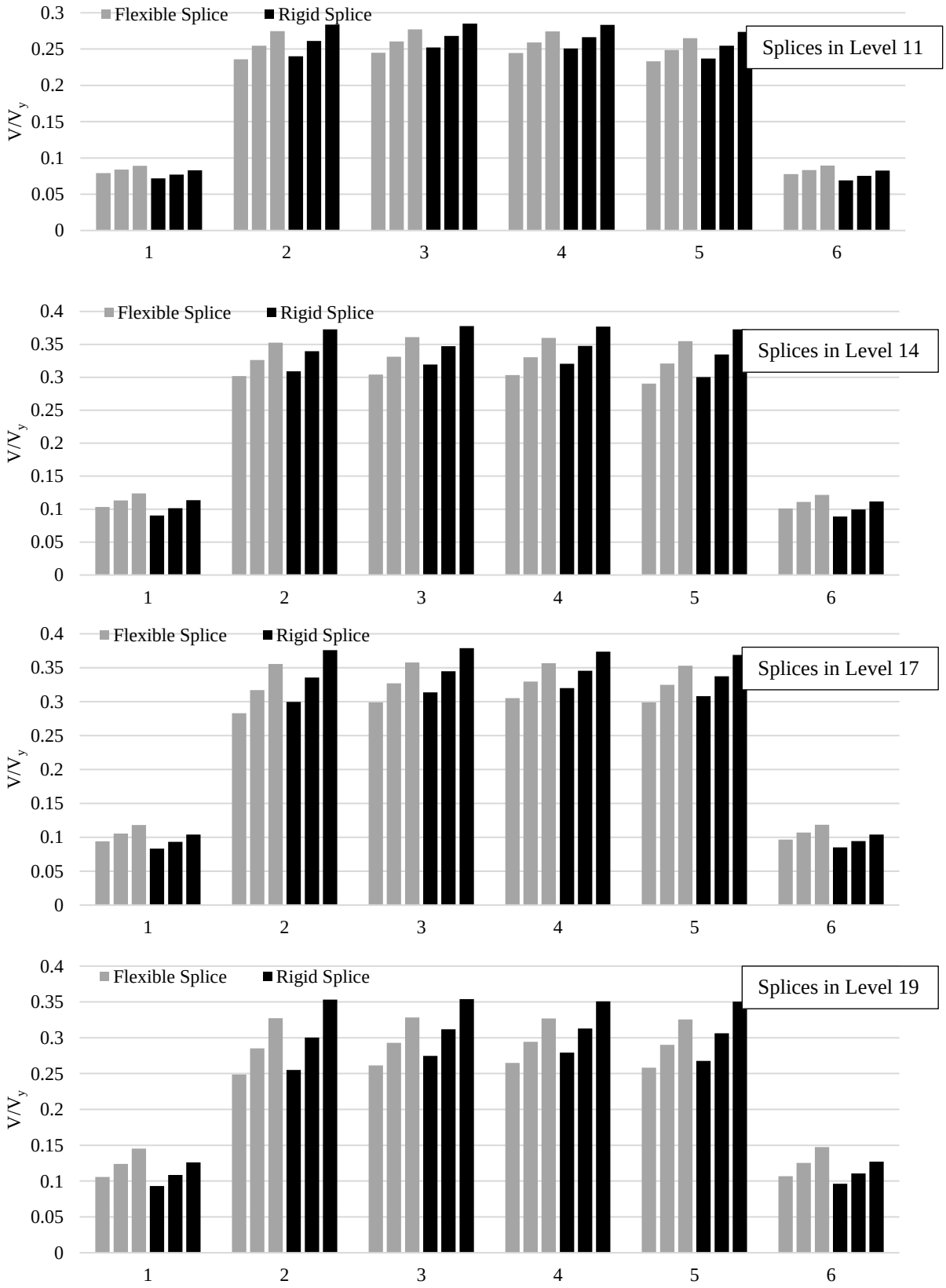

Figure 5-17 Peak shear ratio in twenty-story frame in columns 1-6 for DBE hazard level. Grey bars represent flexible splices with (k_p=0.3EI/L, k_v=0.50A_vG/L) (from left to right, 16th percentile, Median, 84th percentile). Black bars represent rigid splices (from left to right, 16th percentile, Median, 84th percentile). Splices are located at one third of story height up the column.

5.3.2.2. ***Effect of Rotational Stiffness***

Figure 5-18 shows the peak story drift ratio for frames having column splices with two different rotational stiffnesses ($k_p=1EI/L$ vs $k_p=0.3EI/L$), while keeping the shear stiffness constant ($0.5A_vG/L$). The response is not sensitive to the change in rotational stiffness, for DBE level events. For MCE hazard level, column splices with smaller rotational stiffness caused small increases in the 84th percentile response for the first and second levels.

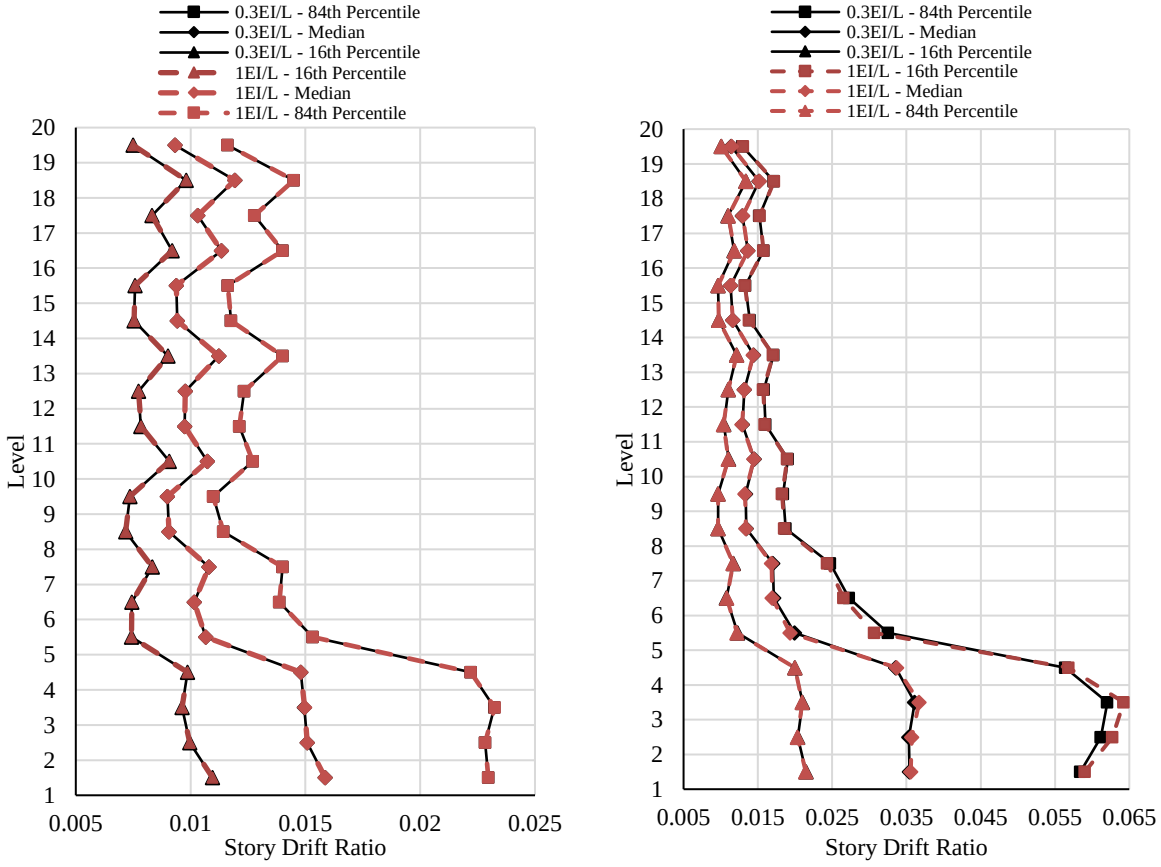

(A) DBE hazard level **(B)** MCE hazard level

Figure 5-18 Comparison of peak story drift ratio in twenty-story frame with splices of different rotational stiffnesses for DBE and MCE hazard levels, Solid lines represent frame with splices of (k_p=0.3EI/L, k_v=0.50A_vG/L) and dash lines represent frame with splices of (k_p=1EI/L, k_v=0.50A_vG/L). Splices were located at two thirds of story height up the column.

5.3.2.3. ***Effect of Shear Stiffness***

Figure 5-19 shows the peak story drift ratio for frames having column splices with two different shear stiffnesses ($0.5A_vG/L$ vs $0.35A_vG/L$), while keeping the rotational stiffness constant ($k_p=1EI/L$). Increasing the shear flexibility increased drift ratios of the floors containing splices. The increase is greater for levels higher than level 13, with a maximum 9% increase in the drift demand of level 16 under DBE hazard level events. The increase is not as significant as seen under MCE hazard level events.

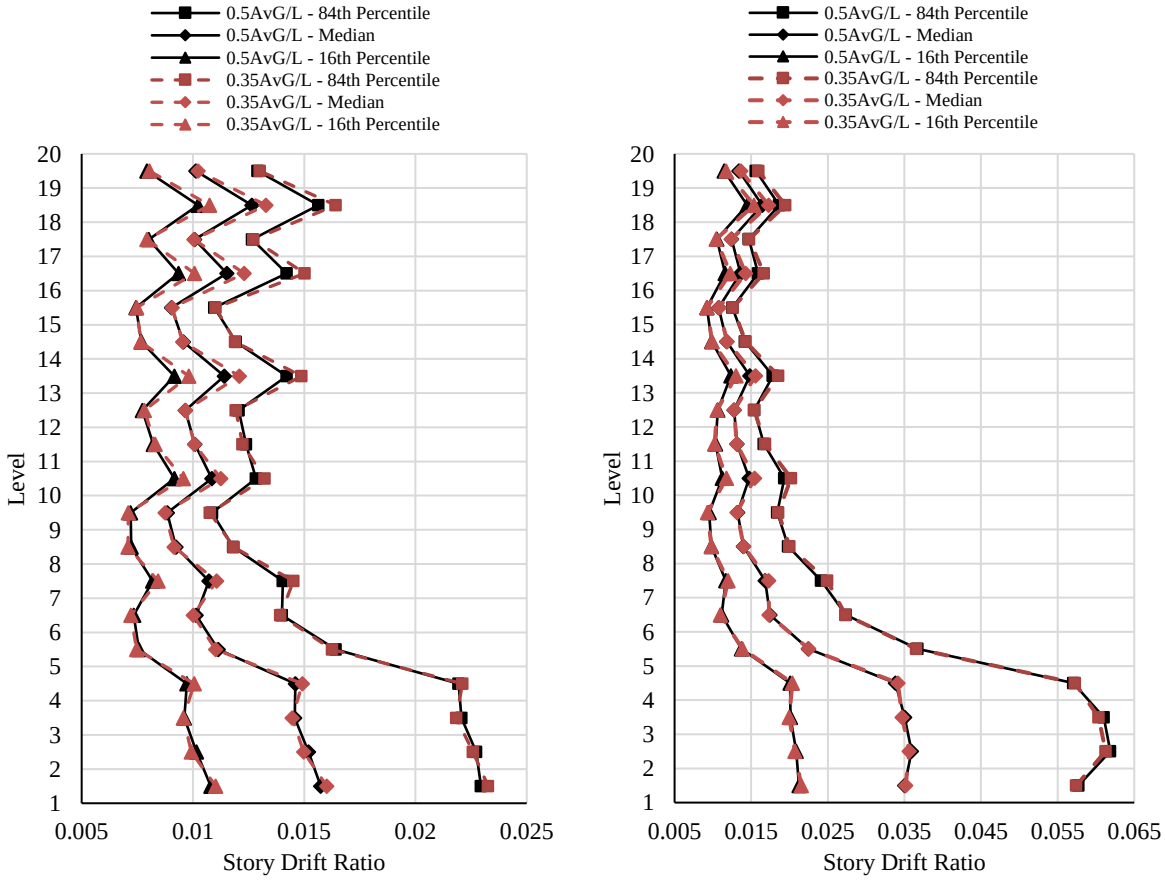

(A) DBE hazard level **(B)** MCE hazard level

Figure 5-19 Comparison of peak story drift ratio in twenty-story frame with splices of different shear stiffnesses under DBE and MCE hazard levels, Solid lines represent frame with splices of (k_p=1EI/L, k_v=0.350A_vG/L) and dash lines represent frame with splices of (k_p=1EI/L, k_v=0.50A_vG/L). Splices were located at one third of story height up the column.

5.3.2.4. ***Effect of Splice Location***

Figure 5-20 shows the peak story drift ratio for column splices of the same properties located at two different locations within the level. More specifically, the top and bottom of the middle third of the columns. Splices close to the bottom floor decreased drift ratios of the bottom two stories, while increasing drift ratios at other levels. The change is larger under MCE level events, on the order of 15%, which is a significant increase.

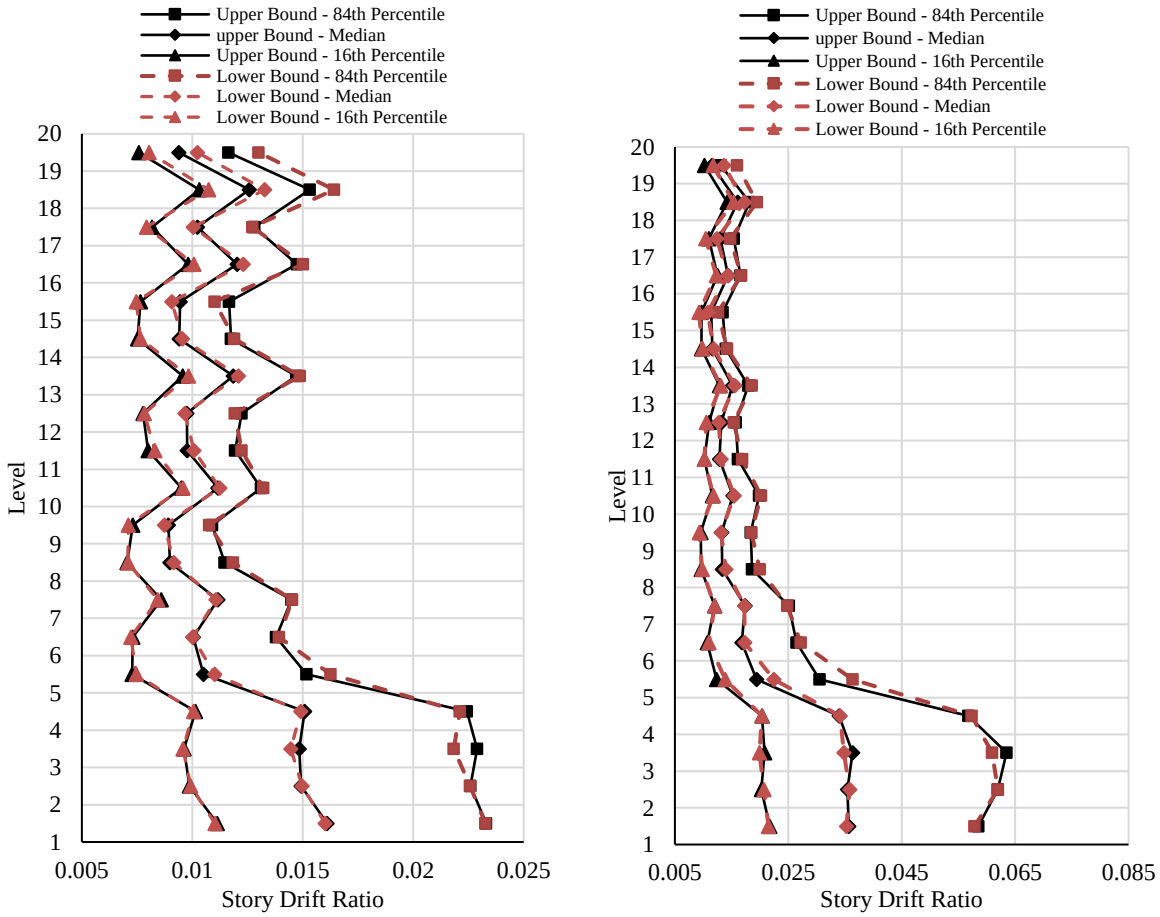

(A) DBE hazard level **(B)** MCE hazard level

Figure 5-20 Comparison of peak story drift ratio in nine-story frame with column splices at different locations (top and bottom of column middle third) for DBE and MCE hazard levels. Solid lines represent frame with splices at one third of story height up the column (lower bound) and dash lines represent frame with splices at two thirds of story height up the column (upper bound). Splices were k_p=0.3EI/L, k_v=0.350A_vG/L.

5.3.2.5. ***Time History Responses and Further Discussion***

Similar to the 9 story frame, shear demands in column splices under all DBE and MCE level events were smaller than $0.5V_y$. This result means shear spring modelling part of the splice connection were all within their elastic range and did not experience residual deformations. Maximum moment demands observed in the DBE and MCE level events were $0.39M_p$ and $0.7M_p$, respectively. Since the first mode period of the 20 story frames is larger than 4 sec, the frame would not experience large earthquake demands in its fundamental mode of vibration for the sets of ground motions used, as can be seen in Figure 5-21. Instead, higher mode effects caused larger demands at higher levels.

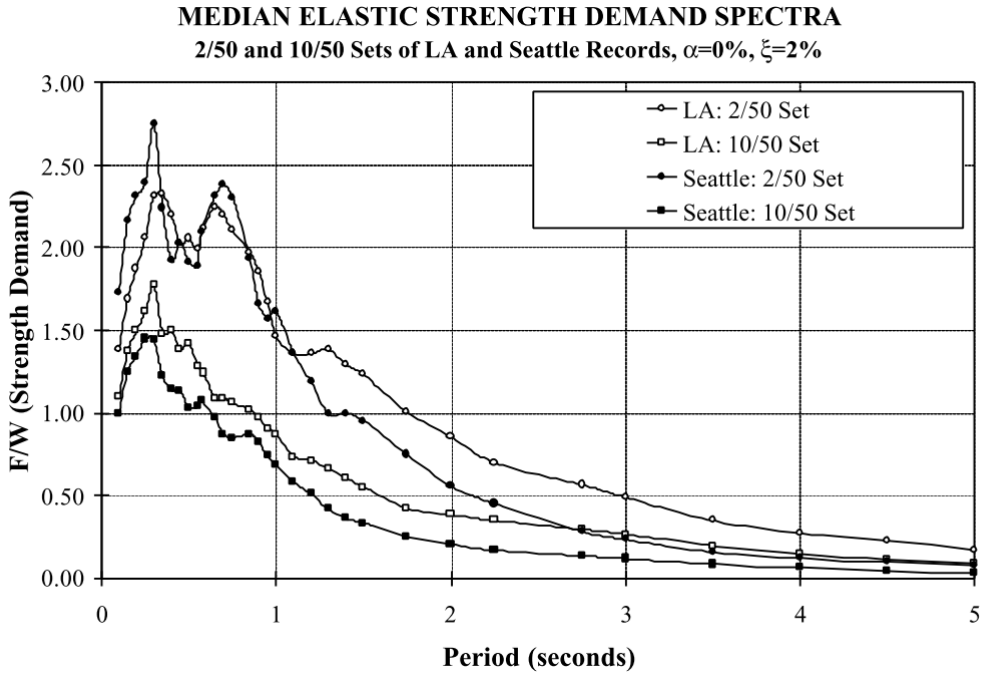

Figure 5-21 Comparison of median elastic spectra for medium and high suites of LA earthquakes (Gupta and Krawinkler, 1999)

Similar to the 9 story frame, flexible column splices increased drifts of the stories containing column splices. This sensitivity was mainly resulted from the column splice shear flexibility than the flexural flexibility. The change in the drift ratio response of the upper levels were more pronounced than lower floors, which could be a result of higher modes participation in the frame

response. Moment and shear demand in column splices vary with their location, geometry and stiffness properties. While the median of peak moment demands was smaller than the minimum strength requirement of $0.5\phi M_p$, the 86th percentile demand was larger than the minimum flexural strength requirement. Shear demands consistently exceeded the minimum shear strength requirement of $0.25\phi V_y$, stipulated in the New Zealand standard. This result means an increased risk of failure of flange splices after elimination of web splices in bolted column splice connections.

5.4. **Limitations**

In this study, no interaction between shear and flexural springs representing column splices was assumed. For wide flange column sections, this assumption is acceptable when there is no interaction between flange and web splices. As mentioned in Section 3.1.3, flange splices can contribute in transferring shear forces, which may reduce the ultimate flexural capacity of the connection. While the interaction of these components may reduce the ultimate capacity of these components in shear and moment, it may be reasonable to assume the interaction would not change the stiffness properties of these components, especially within the smaller linear ranges of moment and shear demands developed in the frames, as presented in the results.

In addition, it was assumed rotational behaviour of column splices were independent to axial load in columns. Realistically, axial loads could alter the flexural behaviour of column splices. However, the majority of building gravity loads are carried by gravity columns. Thus, perimeter moment frames mainly carry lateral loads, with small portion of building gravity loads. Therefore, ignoring the interaction of axial and flexural demands in column splices would not impact the results significantly.

5.5. **Summary**

This chapter discussed the effect of flexible column splices on the dynamic response of generic regular mid and high-rise moment frames. Nonlinear time history analyses were conducted incorporating nonlinear modelling and behaviour column splice flexural and shear hysteresis response. Gap models with incremental damage were utilized to simulate the flexural behaviour, while elsto-plastic models were used to present shear flexibility associate with bolted column splices. Parametric studies were undertaken to assess the performance of the frames with variation of parameters such as column splice stiffness and location. The effect of column splice location was investigated for two different arrangements through frame height, and the column height within the same story.

Results were compared with benchmark frames in which column splices were modelled as column section change with no introduced flexibility and a rigid splice. It was observed flexible splices can significantly increase drift ratios of the stories housing column splices, under both DBE and MCE level events. The increase in the drift response under MCE level events may spread to other stories, as well.

However, for the frames studied here, the increase was not significant or large enough to initiate a sway mechanism. Additionally, it was observed frame response may be sensitive to arrangement of column splices through the frame height. Higher modes appear to have been excited in the 20 story frame, resulting in a greater sensitivity of the frame response at higher levels due to column splices. It was also seen frame response is more sensitive to shear properties of column splices than their flexural properties. While zero flexural stiffness of column splices may not cause frame stability issues during an earthquake, a minimum column splice shear stiffness is required for the frame to remain stable.

Generally, the median values of moment demands at DBE level were smaller than the minimum prescribed design strength, $0.45M_p$, per (*NZS3404:Part 1, Steel Structures Standard*, 1997) for column splices in ductile moment frames. However, the median values of shear demands under DBE level were as large as $0.38V_y$, which is greater than the minimum prescribed shear strength for column splices of $0.225V_y$, in the New Zealand standard. Since no stiffness requirement has been defined for bolted column splice design in the design standard, it is likely bolted columns move relative to each other during earthquake motions. In this case, interaction of flange and web splices is inevitable. Thus, not only are bolted column splices designed for these minimum requirements at risk of shear failure, flange splices may also fail due to the interaction of shear and moment demands. The possibility of connection failure increases under MCE level demands. Hence, this analysis has uncovered a significant risk not previously delineated.

Moment and shear demand in column splices appear to be highly dependent on earthquake, frame and column splice properties. Generally, moment demands were smaller for flexible column splices, as opposed to rigid column splices, although there were geometry dependent exemptions. However, shear demands in column splices do not appear to be sensitive to the shear stiffness property of column splices. For the frames studied here, shear and moment demand ratios were generally larger at higher stories.

The practical implication of the results for use in design and analysis of moment frames will be discussed in Chapter 6.

Chapter 6. **Implications**

6.1. **Introduction**

The cyclic performance of different bolted splice connections under bending and shear loading was experimentally characterized in Chapter 3, and the fundamental governing mechanics were delineated and characterized in Chapter 4. In Chapter 5, the behaviour of column splice connections was explicitly modelled in two generic steel moment frames to understand the impact of these mechanical properties on overall frame dynamic response in major seismic events. This chapter ties the findings from these three chapters together in relation to column splice design, global frame analyses, and overall steel structural design.

6.2. **Column Splice Design and Specification**

6.2.1. ***Major Axis Bending and Shear***

Current design guidelines for lap splices assume bending actions are distributed between the tension and compression flange plates at a lever arm approximately equal to the depth of members being spliced. In addition, they assume the web splice is the primary component to transfer shear actions between the spliced members (Hogan and Munter, 2007). Although there is evidence these assumptions may satisfy the requirement for the connection to develop the design ultimate capacity, as observed in Chapter 3, it may result in undesirable stiffness characteristics for the connection.

As seen in Chapter 3, due to oversized holes in the web components, web splices may not get engaged in shear immediately, which means the shear force may be initially carried by flange

plates. If the web splice is only designed for strength, they may not have sufficient bolts to limit the initial slip in shear deformations. If the slip deformation is large, flange plates could yield along the central bolt rows, before the web plate is engaged (see Section 3.2.3), which would compromise the flexural capacity of the connection. In addition, large shear displacement would compromise the bearing area of bearing type connections. Thus, to improve seismic performance of bolted connections, a series of recommendations have been drawn from the findings of the experimental work in Chapter 3, which is limited to splice design where the bolts are the critical components. These recommendations include:

- **Web splices are recommended to be designed for stiffness, rather than strength as in current design codes.** Otherwise, flange splice capacity in current design approaches should be reduced to account for interaction of flange plates in shear.

- **It is recommended and important to check the inelastic buckling capacity of splice plates if inelasticity is expected in the plate.** Designing tension splice plates to their ultimate capacity (i.e. yielding over gross area or fracture capacity over the net area) may result in premature inelastic bucking when plates undergo compression loads (Observed in Section 3.2.2 Specimen #10). This mechanism is especially undesirable for non-bearing column splices.

- **It is recommended to use the same grade of material for lap splice plates as for column members.** This recommendation is a precaution to prevent connection designs with undesirable stiffness characteristics.

- **It is recommended to use unthreaded bolts in lap splices.** They are more desirable due to their higher shear stiffness, leading to a connection design with higher flexural and axial stiffness.

- **It is recommended to avoid loose fillers in bolted lap splice connections if possible.** Thick loose fillers in bolted lap splice connections allow larger slip rotations due to bolt tilting (See Section 3.2.1, Specimen #6). In addition, loose thick fillers can reduce bolt shear capacity due to bolt bending, as also indicated in NZS3404 clause C9.3.2.5.

- **It is recommended to consider reduced bolt shear strength and stiffness in designing non-bearing splices.** Unlike bearing lap splices in which bolts can only deform in one direction, bolts in non-bearing splices experience full cyclic loading when the connection undergoes cyclic flexural demands (See Section 3.2.1, Specimen #6). This loading could reduce bolt shear strength and stiffness in the reversed direction, which needs to be taken into account for ultimate capacity and stiffness predictions.

- **It is recommended to use stiffener plates in lap splice connections.** In lap splice connections, distortion in the free ends of flanges at the connection under bending moment and shear forces was observed in several cases. The defect could be improved using stiffener plates where possible.

- **It is recommended to mill end-plates in end-plate bolted connections after welding.** Good contact surfaces are essential to achieve the desired strength and stiffness performance.

6.2.2. *Minor Axis Bending in Wide Flange Sections*

There is not much literature available on the bending capacity of wide flange lap splices about the minor axis (Hamid and Cowie, 2015). A method to predict the capacity of lap splice connections about their minor axis is proposed in this study, and verified by the experimental results. The findings and recommendations useful for design practice are summarized:

- **It is recommended to use common plate analysis methods to analyse non-bearing lap splice connections about their minor axis.** The common plastic analysis method used in the LRFD manual to analyse bolted connections under eccentric shear may be applied to estimate bolt group capacity of non-bearing lap splices as long as beam/column ends do not meet each other due to rotations in the connection.

- **It is recommended splice plates be designed assuming there is no contact between spliced members for serviceability limit state.** Prior to slip in the bolt group, compression actions from bending moment are more likely to be transferred through splice plates and not column members, due to imperfect contact area in bearing splices.

- **For ultimate limit state design, it is recommended to minimize rotation at the required design capacity to avoid damage in column flanges**, as seen in the experiments (see Section 3.2.2, Specimens #9 & #10).

- **It is recommended to use stiffeners to restrain flange edges to delay flange bucking and improve overall flexural performance of the connection.**

6.3. Frame Analysis and Steel Design

Seismic demands in column splices as part of a moment frame appear to be dependent on the characteristics of ground motions and overall frame properties, as expected in general. Frame properties include geometrical parameters, such as number of bays and their span, height of stories, location of column splices within a story and through the height of building. In addition, seismic demands in column splices are a function of mechanical properties of the splices themselves. Splice details, such as different orientation of exterior columns and beam-column connection type would also alter column splice demands in the adjacent columns. Key implications of this research for analysis and design of steel frames include:

- **Column splices in seismic resisting frames are recommended to be specified as slip critical connections to ensure no damage to non-structural elements at the serviceability limit state.** Lap splice deformation associated with bolt slip due to 2-3mm oversized holes can have different behaviour depending on the specific detailing and design of the splice connection. For the specimens tested in this study, slip rotation was observed to be 1-3Rad (See Section 3.2.1) and shear distortions were as large as 1%. This amount of deformation would increase story drifts.

- **It is recommended, where possible, column splices not be placed at the ground story for buildings with basement.** Non-linear time history analysis of the 9 story moment frame with splices at different floors has shown drift response would be more sensitive to column splice properties if splices are located the ground story (see Section 5.3.1).

- **It is recommended column splices be designed for rigid performance in shear as a precursor of including shear flexibility of splices in frame analysis.** Non-linear time history analysis (see Section 5.3) indicates frame drift response are more sensitive to shear stiffness of column splices than their rotational stiffness.

- **It is recommended to model flexural properties of column splices in moment frame analysis.** A quick approach to investigate the sensitivity of frame responses to column splices is modelling column splices as perfect pins. Since bolted splices inherit characteristics of a gap system in bending, it is conservative to assume column splices represent perfect pins in a moment frame.

6.4. Summary

Column splice stiffness properties vary from completely rigid for welded splices to more flexible for bolted splices. Stiffness properties of column splices were observed to measurably alter the nonlinear dynamic response of steel moment frames. Similarly, steel frame response of other seismic resisting systems would be influenced by column splice stiffness properties. Simple approaches were proposed for practitioners to predict stiffness characteristics of splices and implement in frame analysis, where the sensitivity of frame response to these local flexibilities is in question. In addition, specific recommendations for column splice and frame design were proposed to mitigate undesirable behaviour of splices or due to splices.

Chapter 7. **Conclusion**

This thesis investigated seismic performance of bolted column splice connections in steel moment frames. The research comprises experimental and analytical phases to quantify, model, and analyse the cyclic performance of these connections, and to incorporate the results in non-linear time history analysis of moment frames. The thesis culminates with specific impacts and recommendations for professional practice based on the research presented.

Moment tests on bolted splice connections showed these connections represent a gap system. Lap bolted connections perform rigidly until moment actions overcome the friction between the splice plates and the member. Since the splice plates bend with the member, prying forces would be generated in the connecting bolts, reducing their efficacy and connection mechanical properties. In addition, cyclic shear deformations in bolts slacken off pretension. These phenomena diminish friction to a negligible amount, especially in large deformations. As long as bolts move freely in the bolt holes, the connection has zero to negligible stiffness impacting column and full structure response.

The stiffness of bolted lap splices is mainly due to bolt bearing stiffness, which involves series action of bolt shear stiffness and hole bearing stiffness. For bolted end-plate splices with relatively rigid end-plates, bolt axial stiffness dictates the stiffness of the connection. Once bolts enter their plastic state, gapping behaviour emerges in the connection. Thus, the impact is the same, with reduced mechanical properties and potentially altered seismic response.

Experimental results on splice connections in bending shows backbone stiffness can vary widely for these connections, adding further uncertainty in analysing structures with spliced

columns. Welded splice connections were found to be the most rigid and bolted lap splices were the most flexible, where stiffness was a function of factors such as whether the connection is bearing or non-bearing type, flange splice thickness, number of flange bolts, thickness of filler plates, presence or absence of a web splice. All of these factors were examined and quantified. Bolted end-plate splices were, in contrast, found to be the rigid in small range of deformation when the end-plates perform as relatively rigid components. There is thus, less variability in behaviour and impact.

Shear experiments on bolted lap splices with and without web splices demonstrated flange splices are instrumental in carrying shear when any shear deformation occurs. Flange splices bend in response to shear, which would cause yielding in the plates due to small bending capacity. In view of this result, web splices were recommended be designed for stiffness, rather than strength. Alternatively, thick flange splices may be required to satisfy the interaction, which may not be practical or cost-effective.

Models were developed to predict the behaviour of the splice connections. The models were developed based on the principles of equilibrium of forces acting on the connected members and geometrical compatibility of the moving parts. A generic shear force-deformation was used to model bolt shear behaviour mathematically. Overall, these predictive models showed good agreement with the experimental results despite relative simplicity. However, their simplicity and accuracy ensure they could be readily used by practitioners in designing new connections.

Non-linear time history analyses of moment frames with flexible column splices showed story drift profiles may change compared to the frame with rigid column splices. The difference in drift response was contingent on the pattern of splices over the frame height. Shear flexibility

of column splice plays a greater role than flexural flexibility in increasing story drifts. In addition, it was observed that flexibility of column splices did not change their shear demands compared to rigid splices, while moment demands would be limited by slip moment of the bolts.

Overall, it does not appear column splice flexibility leads to a significantly increased sway mechanism or increased collapse risk, provided column splices can develop the required strength. However, interaction of tension and shear forces in flange splice plates would significantly reduce the flexural capacity of column splices for subsequent events. For lap column splices designed for the minimum requirements set in NZS3404 clause 12.9.2.2, per the common design guidelines where flange splices are designed for tension and compression only, the connections appear at risk of failure for both DBE and MCE hazard level events. Hence, there is need to consider enhanced standards and design analyses.

In summary, this research has made a unique and novel contribution in the field of structural design of robust seismic resisting frames through:

- Describing cyclic behaviour of bolted column splice connections and quantifying stiffness and ductility characteristics of these connections.
- Developing simple predictive models for bolted column splice connections that would be implemented in global frame analysis.
- Evaluating the effect of shear and flexural flexibility of column splices in global frame response.
- Illustrating interaction of web and flange components under both shear and moment.
- Providing design recommendations for robust seismic design of steel frames.

Chapter 8. **Future Work**

This research presents a first experimental and analytical investigate of column splice stiffness characteristics and their effect on frame dynamic response. Several prospective areas of further experimental and analytical studies were identified during the course of this research, but were not explored due to limitations in time and resources. These areas are outlined here.

8.1. **Experimental Work**

8.1.1. ***Column Splices for Square Hollow Sections***

Square hollow sections are commonly used in steel buildings, especially at the corners. Bolted end-plate splices are the most common way of joining columns for hollow sections. However, this type of connection is not desirable architecturally and aesthetically. In addition, distortion or warping in the end plates could occur in the welding process, which could create tolerance issues with column verticality. Consequently, expensive procedures such as milling would be required to provide flat contact surfaces. With the advent and ubiquity of blind bolts, engineers and contractors would be interested in using bolted lap splices for this type of column section. Experimental studies would be required to characterize seismic performance of these connections, especially for varying section sizes, as would be expected for column splices.

8.1.2. ***Different Designs and Details of Column Splices***

The experiments conducted in this research were on splices with flange bolts being the critical flange components. In addition, web splice stiffness was small compared to stiffness of flange splices in shear. From the experiments, it was understood that the performance of bolted

connections is highly dependent to the specific design and detailing of the connection. Moment and shear testing on splices in which flange and web splice plates have a different detailing than tested here might result in unknown or unexpected failure mechanisms.

8.1.3. *Column Splices under Different Load Combinations*

Columns in different seismic resisting systems could experience a combination of different seismic demands. While interior columns in moment frames mainly experience bending and some axial compression, exterior columns (corner columns) would experience bidirectional bending and variable axial loading from compression to potentially tension. Moreover, columns in gravity frames mainly carry large axial compression while they could experience large axial compression or tension and some bending if placed in a braced frame. Research is proposed to characterize strength, stiffness, and ductility properties of column splices under a combination of loads.

8.1.4. *Bolt Shear-Deformation Relationship*

The formula used in Chapter 4 to express the relationship between bolt shear force and deformation is very generic. The data available in literature for bolt force-deformation relationship covers certain plate grades and thicknesses and bolt diameters. If splice components have different characteristics than those from which the formula was extracted, the formula may result in non-realistic performance predictions. Experimental work to extend the relationship for a wide range of plate thicknesses and grade, bolt diameter and grade, edge distance, bolt pre-tension, bolt single or double shear, bolt plane shank length under monotonic and cyclic loading would be of a great value.

8.2. Numerical and Analytical Work

8.2.1. *Bearing vs Non-bearing Column Splices in Moment Frames*

Research by Shen et al. and Hadjiyangou et al. have shown column splices in seismic resisting moment frames may experience larger moment demands than observed in this research. Subsequently, effect of splice flexibility on dynamic response of those frames (with smaller fundamental periods) is expected to be more significant. In addition, more studies are required to investigate the effect of bolted column splices in moment frames with irregular geometry. Moreover, bidirectional performance of column splices as part of a three dimensional frame is not well understood.

Interaction of bending moment and axial forces would change the location of neutral axis and demands in splice components. For non-bearing splices, ignoring the interaction of bending and axial actions would lead to non-conservative results. In order to model non-bearing splices, two linear springs in parallel can be used.

8.2.2. *Bearing vs Non-bearing Column Splices in Braced Frames*

Columns in braced frames may be required to carry significant axial tension or compression. Flexibility of column splices may compromise global lateral stiffness of the frame. In addition, with advances in building technology and new devices implemented in buildings, such as dampers, it is required to understand how flexibility and movement in these connections could affect the performance of the frame and its components, such as gusset plates.

8.2.3. *Finite Element Modelling of Column Splice Connections*

Finite element modelling of real scale columns with bolted lap splice connections would be useful to investigate overall capacity of column under bending. Flange splice plates could increase the flexural stiffness of a column locally and change the curvature in the column in bending. This issue could alter global and local buckling capacity of a column under a combination of bending and axial loads. Therefore, the effect of change in section size on overall column capacity is suggested to be investigated.

References

ACI Innovation Task Group 1, 2001. Acceptance Criteria for Moment Frames Based on Structural Testing (ACI T1.1-01). American Concrete Institute (ACI), Farmington Hills, Mich 13.

AISC 341–10. Seismic provisions for structural steel buildings, 2010.

Akbas, B., Doran, B., Sabol, T.A., Seker, O., Toru, P., Shen, J., 2014. Effect of various span lengths on seismic demand on column splices in steel moment frames. Engineering Structures 70, 94–105.

Akbas, B., Shen, J., Sabol, T. a., 2011. Estimation of seismic-induced demands on column splices with a neural network model. Applied Soft Computing 11, 4820–4829.

Allen, E., Iano, J., 2013. Fundamentals of building construction : materials and methods, Seventh ed. ed. John Wiley & Sons, Ltd.

Almufti, I., Hutt, C.M., Willford, M., Deierlein, G., 2012. Seismic Assessment of Typical 1970s Tall Steel Moment Frame Buildings in Downtown San Francisco. 15th World Conference on Earthquake Engineering.

Arno, L.D.I.S., Lnashai, A.S.E., 2002. Seismic Retrofitting of Steel and Composite Building Structures (Report).

Bedair, O., 2011. Cost-effective modeling strategies for the analysis of spliced steel connections. Applied Mathematical Modelling 35, 1881–1892.

Beedle, L.S., Christopher, R., 1963. Tests of steel Moment Connections (Report No. 205.79). Bethlehem, Pennsylvania.

Bjorhovde, R., Colson, A., Zandonini, R. (Eds.), 1996. Connections in Steel Structures III Behaviour, Strength and Design, Connections in Steel Structures III. Pergamon.

Blacks Fasteners, n.d. Blacks Fasteners Handbook.

Borello, D.J., Denavit, M.D., Hajjar, J.F., 2009. Behavior of Bolted Steel Slip-critical Connections with Fillers (Report No. NSEL-017).

Borello, D.J., Denavit, M.D., Hajjar, J.F., 2011. Bolted steel slip-critical connections with fillers: I. Performance. Journal of Constructional Steel Research 67, 379–388.

Borzouie, J., 2016. Low Damage Steel Base Connections (PhD Thesis). University of Canterbury.

Borzouie, J., Macrae, G.A., Chase, J.G., Rodgers, G.W., Clifton, G.C., 2015. Experimental studies on cyclic performance of column base weak axis aligned asymmetric friction connection. Journal of Constructional Steel Research 112, 252–262.

Borzouie, J., Macrae, G.A., Chase, J.G., Rodgers, G.W., Clifton, G.C., 2016. Experimental

Studies on Cyclic Performance of Column Base Strong Axis-Aligned Asymmetric Friction Connections. Journal of Structural Engineering (United States) 142, 1–10.

Bruneau, M., Mahin, S.A., 1991. Ultimate Behavior of Heavy Steel Section Welded Splices And Design Implications 116, 2214–2235.

Bruneau, M., Uang, C.-M., Whittaker, A., 2011. Ductile design of steel structures, 2nd editio. ed. McGraw-Hill, New York.

Carter, C., Murray, T., Thornton, W., 2000. Economy in steel. Modern Steel Construction Magazine (AISC).

Carter, C.J., Murray, T.M., Thornton, W.A., 2000. Cost-effective steel building design. Progress in Structural Engineering and Materials 2, 16–25.

Clough, R.W., Penzien, J., 1993. Dynamics of structures, 2nd editio. ed. McGraw-Hill, New York, New York.

Crawford, S.F., Kulak, G.L., 1971. Eccentrically Loaded Bolted Connections. Journal of the Structural Division (ASCE) 97, 765–783.

Denavit, M.D., Borello, D.J., Hajjar, J.F., 2011. Bolted steel slip-critical connections with fillers: II. Behavior. Journal of Constructional Steel Research 67, 398–406.

Design with Steel: Dimensions and Properties Handbook, 2013. . Steel&tube.

Douty, R.T., McGuire, W., 1965. High Strength Bolted Moment Connections. Journal of structural Division (ASCE) 91, 101–128.

Dusicka, P., Lewis, G., 2010. High strength steel bolted connections with filler plates. Journal of Constructional Steel Research 66, 75–84.

Edwards, J.H., Whittemore, H.L., Stang, A.H., 1929. Transverse tests of H-section column splices. Bureau of Standards Journal of Research 4, 395–413.

EN 1993-1-8: Eurocode 3: Design of steel structures - Part 1-8: Design of joints, 2005.

Eom, T.-S., Park, H.-G., 2010. Elongation of Reinforced Concrete Members Subjected to Cyclic Loading. Journal of Structural Engineering 136, 1044–1054.

Eurocode 3: Design of steel structures- part 1-8: Design of joints, 2005.

Fisher, J.W., 1965. Behavior of Fasteners and Plates with Holes. Journal of the Structural Division 91, 265–286.

Flores, F.X., Charney, F.A., Lopez-Garcia, D., 2014. Influence of the gravity framing system on the collapse performance of special steel moment frames. Journal of Constructional Steel Research 101, 351–362.

Galasso, C., Stillmaker, K., Eltit, C., Kanvinde, A., 2015. Probabilistic demand and fragility assessment of welded column splices in steel moment frames. Earthquake Engineering & Structural Dynamics 44, 1823–1840.

Girão Coelho, A.M., Simão, P.D., Bijlaard, F.S.K., 2010. Stability design criteria for steel column splices. Journal of Constructional Steel Research 66, 1261–1277.

Girão Coelho, A.M., Simão, P.D., Bijlaard, F.S.K., 2012. Guidance for the design of spliced columns. Journal of Structural Engineering (United States) 138, 1079–1088.

Green, D.L., Kulak, G.L., 1987. Design of web-flange beam or girder splices (Report No. 148).

Gupta, A., Krawinkler, H., 1999. Seismic Demands for Performance Evaluation of Steel Moment Resisting Frame Structures (Report No. 132).

Hadjiyiangou, M., 2017. Flexural demand of columns in Special Moment Frames (MSc Thesis). Iowa State University.

Hall, J.F., 1998. Seismic response of steel frame buildings to near-source ground motions. Earthquake Engineering and Structural Dynamics 27, 1445–1464.

Hamid, Z., Cowie, K., 2015. Bolted Column Splices with Minor Axis Bending (Report CON3102). Steel Construction New Zealand Inc., pp. 1–5.

Hoenderkamp, J.C.D., Snijder, H.H., 2008. Load bearing capacity of spliced columns with single row bolted butt-plates.

Hogan, T.J., Munter, S.A., 2007. Connection Design Guide 13. Australian Steel Institute.

Holbrow, C.H., Lloyd, J.N., Amato, J.C., Galvez, E., Parks, M.E., 2010. Modern introductory physics, 2nd ed. Springer.

Hutt, C.M., 2017. A Comparative Study on the Seismic Vulnerability of 1970s vs Modern Tall Steel Moment-Resisting Frame Building. In: 16th World Conference on Earthquake Engineering. pp. 1–13.

Hyland, C., Cowie, K., Clifton, C., 2003. HERA (Report R4-100.1).

Joints in Steel Construction; Simple Connections (Publication P212), 2002. . The Steel Construction Institute and The British Constructional Steelwork Association Limited.

Joints in Steel Construction: Moment Resisting Joints to Eurocode3 (Publication P398), 1995. , Steel Construction Institute.

Katta, A., 2019. Non-symmetrical column splice (MSc Thesis). Delft University of Technology.

Kaufmann, E., Kaufmann, E., Julio, R. Di, Gross, J., 1997. Failure analysis of welded steel moment frames damaged in the Northridge earthquake (Report NISTIR 5944). National Institute of Standards and Technology, Gaithersburg, MD.

Kulak, G.L., Fisher, J.W., Struik, J.H.A., 1987. Guide to Design Criteria for Bolted and Riveted Joints Second Edition, 2nd ed. American Institute of Steel Construction, Chicago, IL.

Lee, J.H., Fisher, J.W., 1968. Bolted joints With Rectangular or Circular Fillers (Report No. 318.6). Bethlehem, Pennsylvania.

Li, D., Uy, B., Aslani, F., Patel, V., 2017. Behaviour and design of demountable CFST column-column connections under tension. Journal of Constructional Steel Research 138, 761–773.

Li, D., Uy, B., Patel, V., Aslani, F., 2016. Behaviour and design of demountable steel column-column connections. Steel and Composite Structures 22, 429–448.

Limpert, E., Stahel, W.A., 2011. Problems with using the normal distribution - and ways to improve quality and efficiency of data analysis. PLoS ONE 6.

Limpert, E., Stahel, W.A., Abbt, M., 2001. Log-normal Distributions across the Sciences: Keys and Clues. BioScience 51, 341–352.

Lindner, J., 2008. Old and new solutions for contact splices in columns. Journal of Constructional Steel Research 64, 833–844.

Macrae, G.A., Kimura, Y., Roeder, C., 2004. Effect of Column Stiffness on Braced Frame Seismic Behavior. Journal of Structural Engineering 130, 381–391.

Mahin, S.A., 1998. Lessons from damage to steel buildings during the Northridge earthquake. Engineering Structures 20, 261–270.

Mann, A.P., Morris, L.J., 1984. Lack of fit in high strength bolted connections. Journal of Structural Engineering (United States) 110, 1235–1252.

Manual of Steel Construction, Load and Resistance Factor Design, 3rd ed, 2001. . American Institute of Steel Construction.

Mazzoni, S., Mckenna, F., Scott, M.H., Fenves, G.L., 2007. OpenSees Command Language Manual.

Miller, D.K., 1998. Lessons learned from the Northridge earthquake. Engineering Structures 20, 249–260.

Nakashima, M., Inoue, K., Tada, M., 1998. Classification of damage to steel buildings observed in the 1995 Hyogoken-Nanbu earthquake. Engineering Structures 20, 271–281.

Nudel, A., Marusich, S., Dana, M., Roufegarinejad, A., 2015. Evaluation and Remediation of Pre-Northridge Steel Moment Frame Column Splices. ATC & SEI 797–809.

NZS3404:Part 1, Steel Structures Standard, 1997. . Standards New Zealand.

Oberg, E., Jones, F.D., Horton, H.L., Ryffel, H.H., McCauley, C.J., 2016. Machinery's handbook, 30th editi. ed. Industrial Press, South Norwalk, CT.

Padilla, A.S., 2014. Full Scale Testing of HSS Column Splices under Combined Loading and Adapted Experimental Protocols (MSc Thesis). University of Colorado.

Park, R., Paulay, T., 1975. Reinforced concrete structures. J. Wiley & Sons.

Popov, E.P., Tsai, K., Engelhardt, M.D., 1989. On Seismic Steel Joints and Connections. Engineerinfg Structures 11, 148–162.

Portland Bolt, 2015. Washers for Structural Bolts. (https://www.portlandbolt.com/technical/faqs/washers-required-with-a325-or-a490/).

Priestley, M.J.N., Calvi, G.M., Kowalsky, M.J., 2007. Displacement-based seismic design of structures. IUSS Press.

Putkey, J.J., 1993. Common Steel Erection Problems and Suggested Solutions. Structural Steel Educational Council.

Ramhormozian, S., Clifton, G.C., MacRae, G.A., Davet, G.P., 2017. Stiffness-based approach for Belleville springs use in friction sliding structural connections. Journal of Constructional Steel Research 138, 340–356.

Ricker, david T., 2000. Value Engineering for Steel Construction. Modern Steel Construction.

SAC Joint Venture, 2000. The SAC Steel Project (https://www.sacsteel.org/). Redwood City, California.

Salmon, C.G., Johnson, J.E., Malhas, F.A., 2009. Steel structures : design and behavior : emphasizing load and resistance factor design. Pearson/Prentice Hall, Upper Saddle River, NJ.

Shaw, S.M., Stillmaker, K., Kanvinde, A.M., 2015. Seismic response of partial-joint-penetration welded column splices in moment-resisting frames. Engineering Journal 52, 87–108.

Shen, J.A.Y., Sabol, T.A., Akbas, B., Sutchiewcharn, N., 2010. Seismic Demand on Column Splices in Steel Moment Frames. Engineering Journal 223–240.

Simão, P.D., Coelho, A.M.G., Bijlaard, F.S.K., 2010. Influence of Splices on the Stability Beaviour of Columns and Frames. In: Stability and Ductility of Steel Structures. Rio de Janeiro, Brazil, pp. 619–626.

Simão, P.D., Girão Coelho, A.M., Bijlaard, F.S.K., 2012. Influence of splices on the buckling of columns. International Journal of Non-Linear Mechanics 47, 806–822.

Snijder, B.H.H., Hoenderkamp, H.J.C.D., 2006. Experimental Tests on Spliced Columns for Splice Strength and Stiffness Requirements. In: Stability and Ductility of Steel Structures. Lisbon, Portugal.

Snijder, H.H., Hoenderkamp, J.C.D., 2008. Influence of end plate splices on the load carrying capacity of columns. Journal of Constructional Steel Research 64, 845–853.

Somerville, P., Smith, N., Punyamurth, S., 1997. Development of Ground Motion Time Histories for Phase 2 of the FEMA/SAC Steel Project. Report No. SAC/BD-97/04, SAC Joint Venture, Richmond, VA. 2–4.

Stillmaker, K., Kanvinde, A., Galasso, C., 2015. Fracture Mechanics-Based Design of Column Splices with Partial Joint Penetration Welds. Journal of Structural Engineering 142, 04015115.

Stillmaker, K., Lao, X., Galasso, C., Kanvinde, A., 2017. Column splice fracture effects on the

seismic performance of steel moment frames. Journal of Constructional Steel Research 137, 93–101.

Stillmaker, K.R., 2016. Probabilistic Fracture Mechanics Based Assessment of Welded Column Splices in Steel Moment Frames (PhD Thesis). University of California Davis.

Thai, H.T., Uy, B., 2016. Rotational stiffness and moment resistance of bolted endplate joints with hollow or CFST columns. Journal of Constructional Steel Research 126, 139–152.

Tork Ladani, F., MacRae, G., Chase, G., 2015. Effects of Column Splice Location on Seismic Demands in Steel Moment Frames Considering Splice Flexibility. In: 8th International Conference on Behavior of Steel Structures in Seismic Areas. Shanghai, China.

Yura, J.A., Hansen, M.A., Frank, K.H., 1982. Bolted splice connection with undeveloped fillers. Journal of structural Division (ASCE) 108, 2837–2849.

Appendix A – Design Calculations for Test Specimens

Table 1- Universal Columns section and material properties (Steel&tube Handbook)

UNIVERSAL COLUMNS

DIMENSIONS AND PROPERTIES
AS/NZS 3679.1-300
AS/NZS 3679.1-300 SO (SEISMIC)

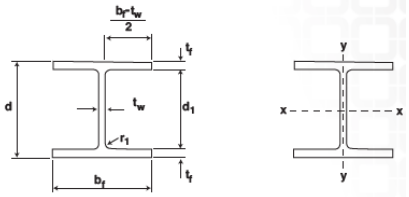

300PLUS

Designation	Mass per metre	Depth of section	Flange width	Flange thickness	Web thickness	Root radii	Depth between flanges	$\frac{d_1}{t_w}$	$\frac{(b_f-t_w)}{2t_f}$	Gross area of cross section	About x-axis				About y-axis				Torsion constant	Warping constant
		d	b_f	t_f	t_w	r_1	d_1			A_g	I_x	Z_x	S_x	r_x	I_y	Z_y	S_y	r_y	J	I_w
	kg/m	mm	mm	mm	mm	mm	mm			mm²	10^6mm⁴	10^3mm³	10^3mm³	mm	10^6mm⁴	10^3mm³	10^3mm³	mm	10^3mm⁴	10^9mm⁶
▲ 310UC	158.0	327	311	25.0	15.7	16.5	277	17.7	5.91	20100	388.00	2370.0	2680.0	139.0	125.00	807.0	1230.0	78.9	3810.0	2860.0
▲ 310UC	137.0	321	309	21.7	13.8	16.5	277	20.1	6.80	17500	329.00	2050.0	2300.0	137.0	107.00	691.0	1050.0	78.2	2520.0	2390.0
▲ 310UC	118.0	315	307	18.7	11.9	16.5	277	23.3	7.89	15000	277.00	1760.0	1960.0	136.0	90.20	588.0	893.0	77.5	1630.0	1980.0
▲ 310UC	96.8	308	305	15.4	9.9	16.5	277	28.0	9.58	12400	223.00	1450.0	1600.0	134.0	72.90	478.0	725.0	76.7	928.0	1560.0
▲ 250UC	89.5	260	256	17.3	10.5	14.0	225	21.5	7.10	11400	143.00	1100.0	1230.0	112.0	48.40	378.0	575.0	65.2	1040.0	713.0
▲ 250UC	72.9	254	254	14.2	8.6	14.0	225	26.2	8.64	9320	114.00	897.0	992.0	111.0	38.80	306.0	463.0	64.5	586.0	557.0
▲ 200UC	59.5	210	205	14.2	9.3	11.4	181	19.5	6.89	7620	61.30	584.0	656.0	89.7	20.40	199.0	303.0	51.7	477.0	195.0
▲ 200UC	52.2	206	204	12.5	8.0	11.4	181	22.7	7.84	6660	52.80	512.0	570.0	89.1	17.70	174.0	264.0	51.5	325.0	166.0
▲ 200UC	46.2	203	203	11.0	7.3	11.4	181	24.8	8.90	5900	45.90	451.0	500.0	88.2	15.30	151.0	230.0	51.0	228.0	142.0
150UC	37.2	162	154	11.5	8.1	8.9	139	17.1	6.34	4730	22.20	274.0	310.0	68.4	7.01	91.0	139.0	38.5	197.0	39.6
150UC	30.0	158	153	9.4	6.6	8.9	139	21.0	7.79	3860	17.60	223.0	250.0	67.5	5.62	73.4	112.0	38.1	109.0	30.8
150UC	23.4	152	152	6.8	6.1	8.9	139	22.8	10.70	2980	12.60	166.0	184.0	65.1	3.98	52.4	80.2	36.6	50.2	21.1
100UC	14.8	97	99	7.0	5.0	10.0	83	16.6	6.71	1890	3.18	65.6	74.4	41.1	1.14	22.9	35.2	24.5	34.9	2.3

▲ New Zealand Design Standard NZS 3404 Clause 12.4.1.1 requires steel in seismic-resisting systems to comply with this range – Steel 300 SO.

PROPERTIES FOR DESIGN
AS/NZS 3679.1-300
AS/NZS 3679.1-300 SO (SEISMIC)

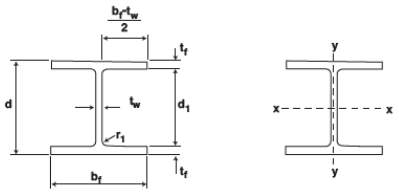

300PLUS					About x-axis		About y-axis		AS 3679.1-350				About x-axis		About y-axis	
Designation	Mass per metre	Flange f_y	Web f_y	Form factor	Compactness	Z_{ex}	Compactness	Z_{ey}	Designation	Flange f_y	Web f_y	Form factor	Compactness	Z_{ex}	Compactness	Z_{ey}
	kg/m	MPa	MPa	k_f		10^3mm³		10^3mm³		MPa	MPa	k_f		10^3mm³		10^3mm³
▲ 310UC	158.0	280	300	1	C	2680.0	C	1210.0	310UC	340	340	1	C	2680.0	C	1210.0
▲ 310UC	137.0	280	300	1	C	2300.0	C	1040.0	310UC	340	340	1	C	2300.0	C	1040.0
▲ 310UC	118.0	280	300	1	C	1960.0	C	882.0	310UC	340	340	1	N	1950.0	N	878.0
▲ 310UC	96.8	300	320	1	N	1560.0	N	694.0	310UC	340	360	1	N	1550.0	N	684.0
▲ 250UC	89.5	280	320	1	C	1230.0	C	567.0	250UC	340	360	1	C	1230.0	C	567.0
▲ 250UC	72.9	300	320	1	N	986.0	N	454.0	250UC	340	360	1	N	977.0	N	448.0
▲ 200UC	59.5	300	320	1	C	656.0	C	299.0	200UC	340	360	1	C	656.0	C	299.0
▲ 200UC	52.2	300	320	1	C	570.0	C	260.0	200UC	340	360	1	N	569.0	N	260.0
▲ 200UC	46.2	300	320	1	N	494.0	N	223.0	200UC	340	360	1	N	490.0	N	220.0
150UC	37.2	300	320	1	C	310.0	C	137.0	150UC	340	360	1	C	310.0	C	137.0
150UC	30.0	320	320	1	C	250.0	C	110.0	150UC	360	360	1	N	248.0	N	109.0
150UC	23.4	320	320	1	N	176.0	N	73.5	150UC	360	360	1	N	174.0	N	72.3
100UC	14.8	320	320	1	C	74.4	C	34.4	100UC	360	360	1	C	74.4	C	34.4

▲ New Zealand Design Standard NZS 3404 Clause 12.4.1.1 requires steel in seismic-resisting systems to comply with this range – Steel 300 SO.

Notes:
1. For 300PLUS sections the tensile strength (f_u) is 440 MPa.
2. For grade 350 sections the tensile strength (f_u) is 480 MPa.
3. C = compact section; N = non-compact section; S = slender section.
4. 300PLUS hot-rolled sections are produced to exceed the minimum requirements of AS/NZS 3679.1-300.
5. 300PLUS replaced grade 250 as the base grade for these sections in 1994.

Design Calculations for Specimen #1

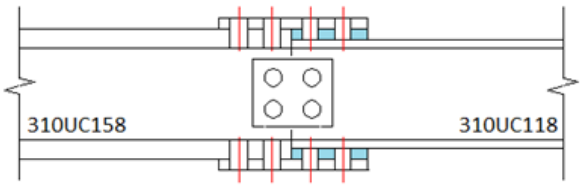

Figure 1- Schematic view of Specimen #1, (12mm flange plates and 6mm filler plates)

Moment Capacity of 310UC118:

$M_p = S_x * f_y = 1960 * 280 * 1000 = 548.8\ kNm$

$\phi M_p = \ 0.9 * 548.8 = 494\ kNm$

$M^* = \phi(0.5M_p) = \ 0.9 * 0.5 * 548.8 = 247\ kNm$ Targeting 50% of design moment capacity

$N_{ft}^* = N_{fc}^* = 247/(d - t_f) = 247/(315 - 18.7) = 833.5\ kN$ Tension & compression force in flanges

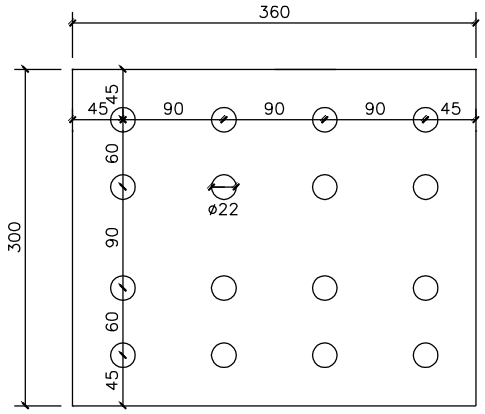

Figure 2- Flange splice with thickness of 12mm (dimensions in mm)

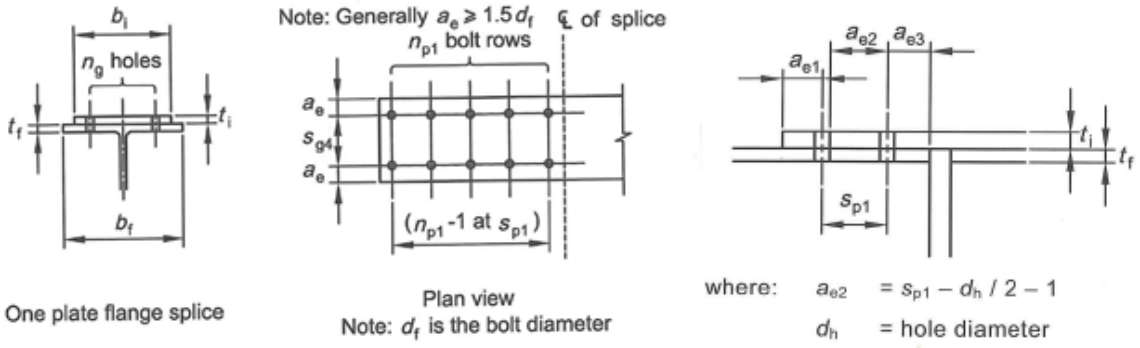

Figure 3- Definition of geometry of flange splice plates (Connection Design Guide 13)

Design check number 1: Design capacity of bolts at flanges

2*4 no* M20 bolts Class 8.8 per side of splice, threads included in shear plane. For filler thinner than 6mms there is no reduction factor for shear strength of bolts.

$\phi V_{fn} = 92.6\ kN$ Single bolt shear capacity including threads

$L_i = 90\ mm$ Distance between first to last bolt on each side of splice

$K_r = 1$ Reduction factor for length

$n_g = 4$ Number of bolts along width of splice

$n_{p1} = 2$ Number of bolts along length of splice per side

$a_{e1} = 45\ mm$

$a_{e2} = 90 - 22/2 = 79\ mm$

$a_{e3} = 45\ mm$

$t_f = 12mm$ Flange splice thickness

$a_{ep} = \min(a_{e1}, a_{e2})$, $a_{ef} = \min(a_{e1}, a_{e3})$

$$\phi V_{bi} = min\begin{cases} \phi * 3.2 * f_{ui} * t_i * d_f \\ \phi * f_{ui} * t_i * a_{ep} \\ \phi * f_{ui} * t_i * a_{e2} \end{cases}$$

Design capacity of splice plate

(local bearing/end plate tear-out)

$$\phi V_{bi} = min\begin{cases} 0.9 * 3.2 * 430 * 12 * 20/1000 = 297.2\ kN \\ 0.9 * 45 * 12 * 430/1000 = 209\ kN \\ 0.9 * 79 * 12 * 430/1000 = 366.9\ kN \end{cases}$$

$$\phi V_{bf} = min\begin{cases} \phi * 3.2 * f_{ui} * t_f * d_f \\ \phi * f_{ui} * t_f * a_{ef} \\ \phi * f_{ui} * t_f * a_{e2} \end{cases}$$ Design capacity of flange (local bearing/end plate tear-out)

$$\phi V_{bf} = min\begin{cases} 0.9 * 3.2 * 430 * 18.7 * 20/1000 = 463.2\ kN \\ 0.9 * 79 * 18.7 * 430/1000 = 571.7\ kN \\ 0.9 * 45 * 18.7 * 430/1000 = 325.7\ kN \end{cases}$$

$$\phi V_{df} = \min\left[\phi V_{bf}, \phi V_{bi}, \phi V_{fn}\right] = [92.6, 209, 325.7] = 92.6\ kN$$

$$\phi V_{fb} = 2 * 4 * 1 * 92.6 = 740.8\ kN$$ Capacity of bolt group

$$capacity\ of\ bolt\ group \approx \frac{740.8}{2 * 833.5} \approx 0.44\phi M_p$$

Design check number 2: Design capacity of flange cover plates (one plate splice)

$$\phi N_{pt} = min\begin{cases} 0.9 * f_{yi}\ t_i\ b_i \\ 0.9 * 0.85 * f_{ui}\ t_i\ (b_i\ -\ n_g d_h) \end{cases}$$

$$\phi N_{pt} = min\begin{cases} 0.9 * 300 * 310 * 12/1000 = 1004.4\ kN \\ 0.9 * 0.85 * 12 * 430/1000 * (300 - 4 * 22) = 836.8\ kN \end{cases}$$

$$capacity\ of\ splice\ plate \approx \frac{836.8}{2 * 833.5} \approx 0.5\phi M_p$$

Design check number 3: Design capacity of bolts on web

Thickness of the web cover plate is 6mm, Grade 350.

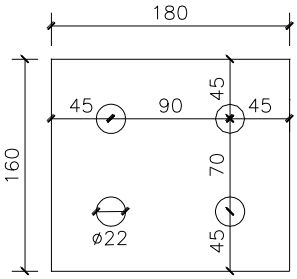

Figure 4- web splice with thickness of 6mm (Dimensions in mm)

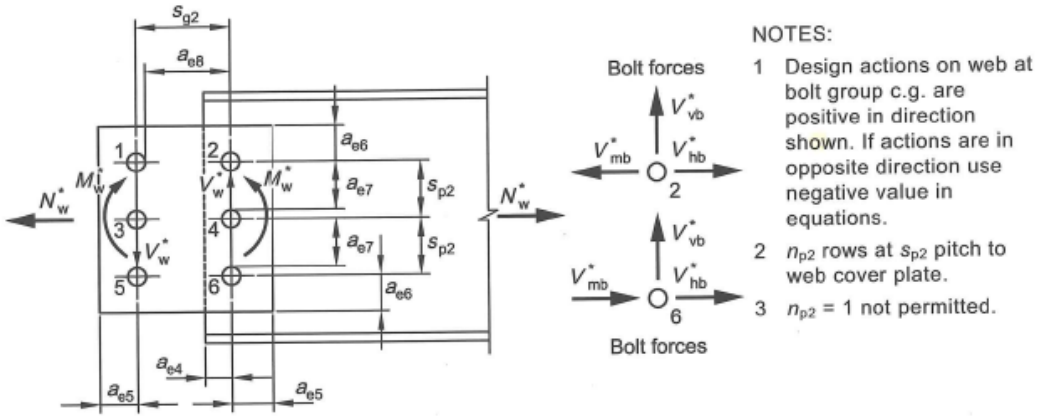

Figure 5- Web bolt forces with single line of bolts (Connection Design Guide 13)

$V_y = 0.6 * A_w * f_y = 0.6 * 300 * (315 - 2 * 18.7) * 11.9 = 594.6\ kN$

$V^* = 0.25 * \phi V_y = 0.25 * 0.9 * 594.6 = 133.8\ kN$ Targeting 25% of design shear capacity

2 No. M20 bolts Class 8.8 per side of splice, threads in shear plane, bolts in double shear

$\phi V_{fn} = 92.6\ kN$

$s_{p2} = 70mm$

$n_{p2} = 2$

$\phi V_{bi} = 0.9 * 3.2 * f_{ui} t_i d_f$ Capacity of web cover plate of thickness of t_i

$\phi V_{bw} = 0.9 * 3.2 * f_{uw} t_w d_f / 2$ Capacity of member web of thickness of t_w

$$\phi V_{bi} = 0.9 * 3.2 * 450 * 6 * \frac{20}{1000} = 155.5\ kN$$

$\phi V_{bw} = 0.9 * 3.2 * 430 * 11.9 * 10/1000 = 147.4\ kN$

$$\phi V_f = \min[92.6, 155.5, 147.4] = 92.6\ kN$$

$$\phi M_{dm} = 2 * \phi V_f * n_{p2} * (n_{p2} + 1) S_{p2}/6 = 2 * 92.6 * 2 * 3 * 70/6000 = 12.96$$

$$\approx 13\ kNm \qquad > M_w^* = 133.8 * 0.045 = 6.0\ kNm$$

$$\phi V_{dv} = 2 * 92.6 = 185.2\ kN > V_w^* = 133.8\ kN$$

$$capacity = \frac{185.2}{133.8 * 4} = 0.35 \phi V_y$$

$$(\frac{6}{12.96})^2 + (\frac{133.8}{185.2})^2 = 0.74 < 1$$ Interaction of shear and secondary moment

Additional requirement noting that $N^*_w = V_{hb}^* = 0$

$$a_{e4} = 45mm$$

$$a_{e8} = 90 - 11 = 79mm$$

$$a_{e5} = 45mm$$

$$a_{e6} = 45mm$$

$$a_{e7} = 70 - 11 = 59mm$$

$$a_{ey} = \min[45, 59] = 45mm$$

$$V_{vb}^* = 133.8/(2 * 2) = 33.5$$
$$< 0.9 * 59 * 6 * 450/1000 = 143.4\ kN$$
$$< 0.9 * 59 * 11.9 * 430/(2 * 1000) = 135.8\ kN$$

$$V_{mb}^* = 6\, M_w^*/2 n_{p2} S_{p2} (n_p + 1) = 6 * 6 * 1000/(2 * 2 * 3 * 70) = 42.8\ kN$$
$$< 0.9 * 45 * 6 * 450/1000 = 108.9\ kN$$
$$< 0.9 * 79 * 6 * 450/1000 = 196\ kN$$
$$< 0.9 * 45 * 11.9 * 430/2/1000 = 129.5\ kN$$

Design check number 4: Design capacity of web cover plate

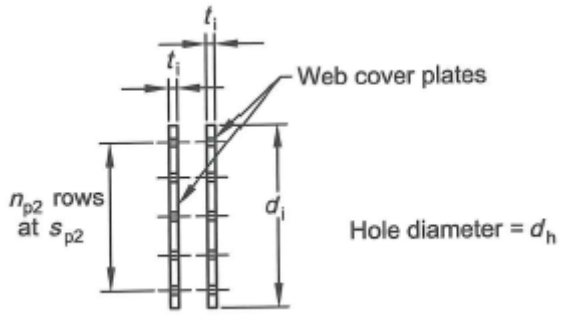

Figure 6- Geometry of web cover plates (Connection Design Guide 13)

$d_i = 45 * 2 + 70 = 160mm$

$t_i = 6mm$

$\frac{d_i}{t_i} = 160/6 = 80/3 < 82$

$Z_{ei} = S_i = t_i d_i^2/4 = \frac{6 * 160^2}{4} = 38400mm^3$

$\phi M_{wd} = 0.9 * 2 * 360 * 38400/10^6 = 24.9 > M_w^*$

$0.75\phi M_{wd} > M_w^* \Rightarrow$

$$\phi V_{wd} = \phi V_{vd} = 0.9 * 2 * \left(0.5 f_{yi} d_i t_i\right) = 0.9 * 2 * 0.5 * 360 * 160 * 6 = 311\ kN > V_w^*$$

$$capacity = \frac{311}{133.8 * 4} = 0.58\phi V_y$$

Design check number 5: Design capacity of flanges of spliced members

$$\phi N_{ft} = \min\left(0.9 * 280 * 18.7 * 307/1000 = 1447\ kN,\right.$$
$$\left. 0.9 * 0.85 * 430 * (307 - 4 * 22) * 18.7 = 1347.1\ kN\right)$$
$$= 1347.1 > N_{ft}^*$$

$\phi N_{fc} = 0.9 * 280 * 18.7 * 307/1000 = 1447KN > N_{fc}^*$

$$capacity\ in\ tension = \frac{1347.1}{833 * 2} = 0.81\phi M_p$$

$$capacity\ in\ compression = \frac{1447}{833 * 2} = 0.87\phi M_p$$

Design check number 6: Design capacity of spliced members at splice location

Since $N^* = 0, M_{rs} = M_s^{"}$

$$I_x' = I_x - 2n_h d_h t_f [\frac{d - t_f}{2}]^2 = 227 * 10^6 - 2 * 4 * 22 * 18.7(\frac{315 - 18.7}{2})^2$$

$$= 204.7 * 10^6 mm^4$$

$$Z_x' = \frac{I_x'}{d/2} = 204.7 * 2 * 10^6/315 = 1.3 * 10^6 mm^3$$

$$S_x' = S_x - 2n_h d_h t_f \left[\frac{d - t_f}{2}\right] = 1960 * 1000 - 2 * 4 * 22 * 18.7\left(\frac{315 - 18.7}{2}\right)$$

$$= 1472.4 * 10^3 mm^3$$

$$Z_e' = \min(1.5Z_x', S_x') = 1472400 mm^3$$

$$\phi M_{sx}^{"} = 0.9 * 280 * 1472400/10^6 = 371 kNm > M^*$$

$$capacity\ = \frac{371}{247 * 2} = 0.75\phi M_p$$

Serviceability Limit State – one plate flange splice

$$\phi V_{sf} = 0.7 \times (\mu\, n_{ei} \times N_{ti} \times k_h) = 0.7(0.35 \times 1 \times 101 \times 1) = 24.7\ kN$$

$$\phi V_{fs} = n_g \times n_p \times \phi V_{sf} = 2 \times 4 \times 24.7 = 198\ kN$$

$$capacity\ = \frac{198}{833.5 * 2} = 0.12\phi M_p$$

$$capacity\ without\ reduction\ factor\ (0.7) = \frac{0.12\phi M_p}{0.7} = 0.17\phi M_p = 0.19 M_p$$

Design Calculations for Specimen #2

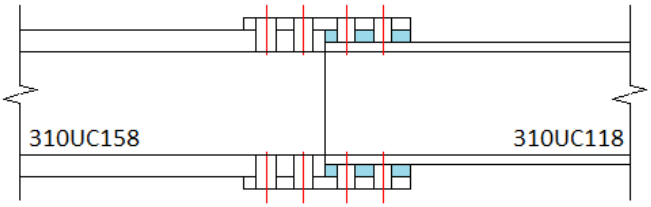

Figure 7- Schematic view of Specimen #2, (No web splice - 12mm flange plates and 6mm filler plates)

Design calculations for flange splice are identical to Specimen #1.

Design Calculations for Specimen #3

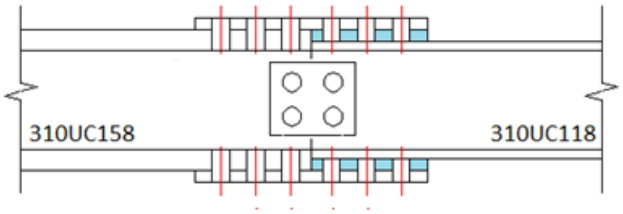

Figure 8- Schematic view of Specimen #3, (20mm flange plates and 6mm filler plates)

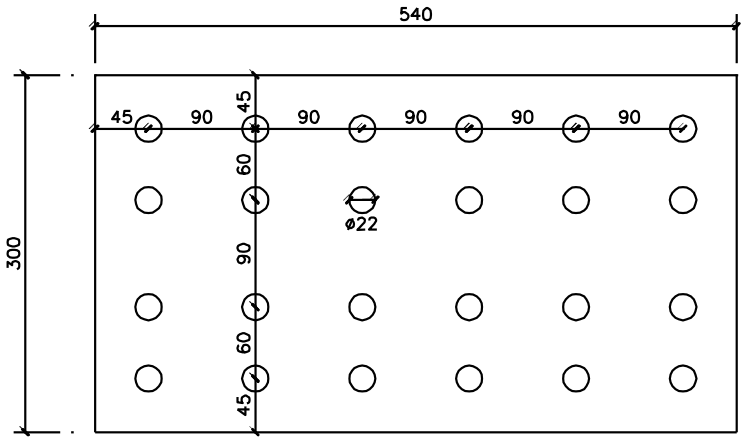

Figure 9- Flange splice with thickness of 20mm (dimensions in mm)

$M^* = 0.9 * 0.7 * 548.8 = 345.7\ kNm$ Targeting 70% of design moment capacity

$N_{ft}^{*} = N_{fc}^{*} = 345.7/(d - t_f) = 345.7/(315 - 18.7) = 1167\ kN$ Flange tension & compression force

Design check number 1: Design capacity of bolts at flanges

3*4 No. M20 bolts, Class 8.8 per side of splice, threads included in shear plane. For filler thinner than 6mms there is no reduction factor for shear strength of bolts.

$\phi V_{fn} = 92.6\ kN$

$L_i = 180mm$ Distance between first to last bolt on each side of splice

$k_r = 1$

$n_g = 4$ Number of bolts along width of splice

$n_{p1} = 3$ Number of bolts along length of splice per side

$a_{e1} = 45mm$

$a_{e^2} = 90 - 22/2 = 79mm$

$a_{e3} = 45mm$

$$\phi V_{bi} = min\begin{cases} 0.9 * 3.2 * 430 * 20/1000 = 495.4\ kN \\ 0.9 * 45 * 20 * 430/1000 = 348.3\ kN \\ 0.9 * 79 * 20 * 430/1000 = 611.5\ kN \end{cases}$$

$$\phi V_{bi} = min\begin{cases} 0.9 * 3.2 * 430 * 18.7/1000 = 463.2\ kN \\ 0.9 * 79 * 18.7 * 430/1000 = 571.7\ kN \\ 0.9 * 45 * 18.7 * 430/1000 = 325.7\ kN \end{cases}$$

$\phi V_{df} = min[92.6, 34.8, 325.7] = 92.6KN$

$\phi V_{fb} = 3 * 4 * 1 * 92.6 = 1111kN < 1167kN$

$$capacity \approx \frac{1111}{1167 * (10/7)} \approx 0.67\phi M_p$$

Design check number 2: Design capacity of flange cover plates(one plate splice)

Thickness of the flange cover plate is 20mm, Grade 300.

$$\phi N_{pt} = min\begin{cases}0.9 * 300 * 300 * 20/1000 = 1458\ kN \\ 0.9 * 0.85 * 20 * 430/1000 * (300 - 4 * 22) = 1394.7\ kN\end{cases}$$

$$capacity \approx \frac{1394.7}{\left(\frac{10}{7}\right) * 1167} \approx 0.84\phi M_p$$

Design check number 3: Design capacity of bolts on web (same as Specimen#1)

Design check number 4: Design capacity of web cover plate (same as Specimen#1)

Design check number 5: Design capacity of flanges of spliced members (same as Specimen#1)

Design check number 6: Design capacity of spliced members at splice location (same as Specimen#1)

Serviceability Limit State – one plate flange splice

$$\phi V_{sf} = 0.7 \times (\mu\, n_{ei} \times N_{ti} \times k_h) = 0.7(0.35 \times 1 \times 101 \times 1) = 24.7\ kN$$

$$\phi V_{fs} = n_g \times n_p \times \phi V_{sf} = 3 \times 4 \times 24.7 = 296\ kN$$

$$capacity\ = \frac{198}{833.5 * 2} = 0.18\phi M_p$$

$$capacity\ without\ reduction\ factor\ (0.7) = \frac{0.12\phi M_p}{0.7} = 0.25\phi M_p = 0.28 M_p$$

Design Calculations for Specimen #4

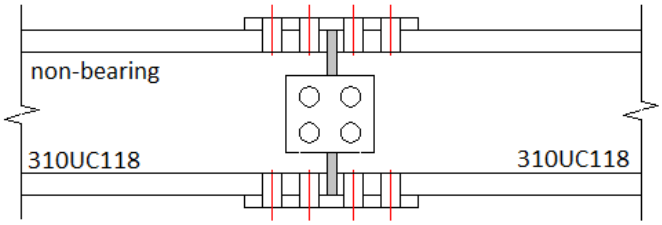

Figure 10- Schematic view of Specimen #4, (Non-bearing with 10mm gap, no fillers, 12mm flange plates)

Design calculations are identical to Specimen #5.

Design Calculations for Specimen #5

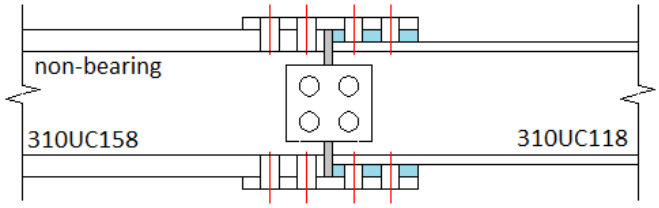

Figure 11- Schematic view of Specimen #5, (Non-bearing with 10mm gap, 6mm fillers, 12mm flange plates)

Design check number 1: Design capacity of bolts at flanges (Same as Specimen #1)

Design check number 2: Design capacity of flange cover plates (Same as Specimen #1)

Design check number 3: Design capacity of bolts on web

Thickness of the web cover plate is 6mm, Grade 350.

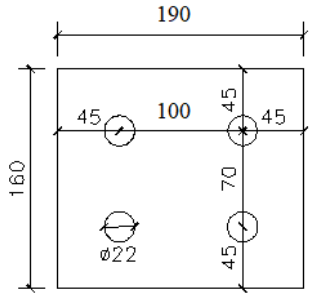

Figure 12- web splice with thickness of 6mm (Dimensions in mm)

$V_y = 0.6 * A_w * f_y = 0.6 * 300 * (315 - 2 * 18.7) * 11.9 = 594.6\ kN$

$V^* = 0.25 * \phi V_y = 0.25 * 0.9 * 594.6 = 133.8\ kN$

2 No. M20 bolts Class 8.8 per side of splice, threads in shear plane, bolts in double shear

$\phi V_{fn} = 92.6\ kN$

$s_{p2} = 70mm$

$n_{p2} = 2$

$\phi V_{bi} = 0.9 * 3.2 * f_{ui} t_i d_f$ Capacity of web cover plate of thickness of t_i

$\phi V_{bw} = 0.9 * 3.2 * f_{uw} t_w d_f / 2$ Capacity of member web of thickness of t_w

$\phi V_{bi} = 0.9 * 3.2 * 450 * 6 * \frac{20}{1000} = 155.5\ kN$

$\phi V_{bw} = 0.9 * 3.2 * 430 * 11.9 * 10/1000 = 147.4\ kN$

$\phi V_f = \min[92.6, 155.5, 147.4] = 92.6\ kN$

$\phi M_{dm} = 2 * \phi V_f * n_{p2} * (n_{p2} + 1) S_{p2}/6 = 2 * 92.6 * 2 * 3 * 70/6000 = 12.96$

$\approx 13\ kNm \quad > M_w^* = 133.8 * 0.050 = 6.7\ kNm$

$\phi V_{dv} = 2 * 92.6 = 185.2\ kN > V_w^* = 133.8\ kN$

$capacity = \frac{185.2}{133.8 * 4} = 0.35 \phi V_y$

$(\frac{6.7}{12.96})^2 + (\frac{133.8}{185.2})^2 = 0.78 < 1$ Interaction of shear and secondary moment

Additional requirement noting $N^*_w = V_{hb}^* = 0$

$a_{e4} = 45mm$

$a_{e8} = 100 - 11 = 89mm$

$a_{e5} = 45mm$

$a_{e6} = 45mm$

$a_{e7} = 70 - 11 = 59mm$

$a_{ey} = \min[45, 59] = 45mm$

$$V_{vb}^* = 133.8/(2 * 2) = 33.5 < 0.9 * 59 * 6 * 450/1000 = 143.4\ kN < 0.9 * 59 * 11.9 * 430/(2 * 1000) = 135.8\ kN$$

$$V_{mb}^* = 6\,M_w^*/2n_{p2}S_{p2}(n_p + 1) = 6 * 6 * 1000/(2 * 2 * 3 * 70) = 42.8\ kN < 0.9 * 45 * 6 * 450/1000 = 108.9\ kN < 0.9 * 89 * 6 * 450/1000 = 220\ kN < 0.9 * 45 * 11.9 * 430/2/1000 = 129.5\ kN$$

Design check number 4: Design capacity of web cover plate

$d_i = 45 * 2 + 70 = 160mm$

$t_i = 6mm$

$\frac{d_i}{t_i} = 160/6 = 80/3 < 82$

$Z_{ei} = S_i = t_i d_i^2/4 = \frac{6 * 160^2}{4} = 38400mm^3$

$\phi M_{wd} = 0.9 * 2 * 360 * 38400/10^6 = 24.9 > M_w^*$

$0.75\phi M_{wd} > M_w^* \Rightarrow$

$$\phi V_{wd} = \phi V_{vd} = 0.9 * 2 * (0.5 f_{yi} d_i t_i) = 0.9 * 2 * 0.5 * 360 * 160 * 6 = 311\ kN > V_w^*$$

$$capacity = \frac{311}{133.8 * 4} = 0.58\phi V_y$$

Design check number 5: Design capacity of flanges of spliced members (Same as Specimen #1)

Design check number 6: Design capacity of spliced members at splice location (Same as Specimen #1)

Design Calculations for Specimen #6

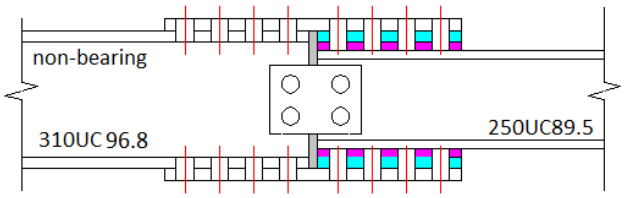

Figure 13- Schematic view of Specimen #6, (Non-bearing with 10mm gap, 2x12mm fillers, 12mm flange plates)

Moment Capacity of 250UC89.5:

$M_p = S_x * f_y = 1230 * 280 * 1000 = 344.4\ kNm$

$M^* = 0.9 * 0.5 * 344.4 = 155\ kNm$ Targeting 50% design moment capacity

$N_{ft}^* = N_{fc}^* = 155/(d - t_f) = 155/(260 - 17.3) = 638.6\ kN$ Flange tension and compression force

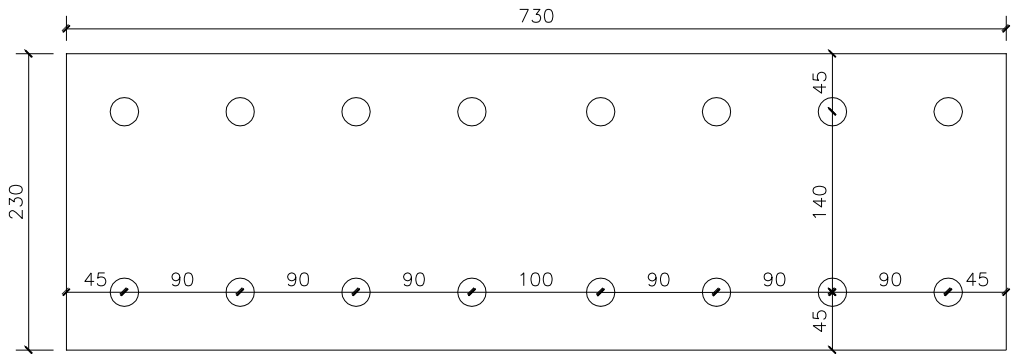

Figure 14- Flange Splice plate with 12mm thickness (Dimensions in mm)

Design check number 1: Design capacity of bolts at flanges

4*2 no* M20 bolts per side of splice, 8.8 category, threads included in shear plane, for filler thicker than 6mms (15% reduction factor for shear strength of bolts should be applied.)

$\phi V_{fn} = 92.6kN$

$L_i = 270mm$ Distance between first to last bolt on each side of splice

$K_r = 1$

$n_g = 2$ Number of holes along width of splice

$n_{p1} = 4$ Number of holes along length of splice per side

$a_{e1} = 45mm$

$a_{e2} = 90 - 22/2 = 79mm$

$a_{e3} = 45mm$

$$\phi V_{bi} = min\begin{cases} 0.9 * 3.2 * 440 * 12 * 20/1000 = 304.1\ kN \\ 0.9 * 45 * 12 * 440/1000 = 213.8\ kN \\ 0.9 * 79 * 12 * 430/1000 = 375.4\ kN \end{cases}$$

$$\phi V_{bf} = min\begin{cases} 0.9 * 3.2 * 410 * 17.3 * 20/1000 = 408.5\ kN \\ 0.9 * 79 * 17.3 * 410/1000 = 504.3 \\ 0.9 * 45 * 17.3 * 410/1000 = 287.3 \end{cases}$$

$\phi V_{df} = [92.6, 213.8, 287.3] = 92.6kN$

$\phi V_{fb} = 0.85 * 2 * 4 * 1 * 92.6 = 629.3\ kN < 638.6kN$

$$capacity \approx \frac{629.3}{2 * 638.6} \approx 0.49\phi M_p$$

Design check number 2: Design capacity of flange cover plates (one plate splice)

Thickness of the flange cover plate is 12mm, Grade 300.

$$\phi N_{pt} = min\begin{cases} 0.9 * 310 * 230 * 12/1000 = 770\ kN \\ 0.9 * 0.85 * 12 * 430/1000 * (230 - 2 * 22) = 734.2\ kN \end{cases}$$

$$capacity \approx \frac{734.2}{2 * 638.6} \approx 0.57\phi M_p$$

Design check number 3: Design capacity of bolts on web

Thickness of the web cover plate is 6mm, Grade 350.

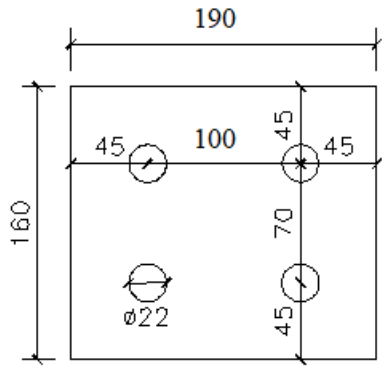

Figure 15- Web splice plate (Dimensions in mm)

$V_y = 0.6 * A_w * f_y = 0.6 * 320 * (260 - 2 * 17.3) * 10.5 = 454.4\ kN$

$V^* = 0.25 * \phi V_y = 0.25 * 0.9 * 454.4 = 102.2\ kN$

2 No. M20 bolts Class 8.8 per side of splice, threads in shear plane, bolts in double shear.

$\phi V_{fn} = 92.6\ kN$

$s_{p2} = 70mm$

$n_{p2} = 2$

$\phi V_{bi}^* = 0.9 * 3.2 * 450 * 6 * 20/1000 = 155.5\ kN$

$\phi V_{bw}^* = 0.9 * 3.2 * 430 * 10.5 * 10/1000 = 130\ kN$

$$\phi V_f = \min[92.6, 126.7, 133] = 92.6\ kN$$

$$\phi M_{dm} = 2 * \phi V_f * n_{p2} * \left(n_{p2} + 1\right) S_{p2}/6$$
$$= 2 * 92.6 * 2 * 3 * 70/6000 = 12.96\ kNm$$
$$> M_w^* = 102.2 * 50 = 5.3\ kNm$$

$$\phi V_{dv} = 2 * 92.6 = 185.2KN > V_w^* = 102.2\ kN$$

$$capacity = \frac{185.2}{102.2 * 4} = 0.45\phi V_y$$

$$\left(\frac{5.3}{12.96}\right)^2 + \left(\frac{102.2}{185.2}\right)^2 = 0.47 < 1$$ Interaction of shear and secondary moment

Additional requirement noting $N^*_w = V_{hb}^* = 0$

$$a_{e4} = 45mm$$

$$a_{e8} = 100 - 11 = 89mm$$

$$a_{e5} = 45mm$$

$$a_{e6} = 45mm$$

$$a_{e7} = 90 - 11 = 79mm$$

$$a_{ey} = \min[45, 79] = 45mm$$

$$V_{vb}^* = 102.2/(2 * 2) = 25.5$$
$$< 0.9 * 45 * 6 * 450/1000 = 109.3\ kN$$
$$< 0.9 * 45 * 11.9 * 430/(2 * 1000) = 103.6\ kN$$

$$V_{mb}^* = 6\, M_w^*/2n_{p2}S_{p2}\left(n_p + 1\right) = 6 * 5.3 * 1000/(2 * 2 * 3 * 90) = 29.4\ kN$$
$$< 0.9 * 45 * 6 * 450/1000 = 108.9\ kN$$
$$< 0.9 * 89 * 6 * 450/1000 = 215.8\ kN$$
$$< 0.9 * 45 * 11.9 * 430/2/1000 = 103.6\ kN$$

Design check number 4: Design capacity of web cover plate

$d_i = 160mm$

$t_i = 6mm$

$\frac{d_i}{t_i} = 160/6 = 80/3 < 82$

$Z_{ei} = S_i = t_i\, d_i^2/4 = 38400mm^3$

$\phi M_{wd} = 0.9 * 2 * 360 * 384200/10^6 = \ 24.9 > M_w^*$

$0.75\phi M_{wd} > M_w^* \Longrightarrow \ \phi V_{wd} = \phi V_{vd} = 0.9 * 2 * \left(0.5 f_{yi} d_i t_i\right)$
$= 0.9 * 2 * 0.5 * 360 * 160 * 6 = 311KN > V_w^*$

$capacity = \frac{311}{4 * 102.2} = 0.76\phi V_y$

Design check number 5: Design capacity of flanges of spliced members

$\phi N_{ft} = \min(0.9 * 280 * 17.3 * 256/1000 = 1116KN,$
$0.9 * 0.85 * 410 * (256 - 4 * 22) * 17.3 = 1150.3KN)$
$= 1116 > N_{ft}^*$

$\phi N_{fc} = 0.9 * 280 * 17.3 * 256/1000 = 1116KN > N_{fc}^*$

Design check number 6: Design capacity of spliced members at splice location

Since $N^* = 0, M_{rs} = M_s''$

$I_x' = I_x - 2n_h d_h t_f \left[\frac{d - t_f}{2}\right]^2 = 143 * 10^6 - 2 * 2 * 22 * 17.3 \left(\frac{260 - 17.3}{2}\right)^2$

$= 120.6 * 10^6 mm^4$

$Z_x' = \frac{I_x'}{d/2} = 120.6 * 2 * 10^6/260 = 0.93 * 10^6 mm^3$

$S_x' = S_x - 2n_h d_h t_f (\frac{d - t_f}{2}) = 1230 * 1000 - 2 * 2 * 22 * 17.3 (\frac{260 - 17.3}{2})$

$= 1045.2 * 10^3 mm^3$

$Z'_e = \min(1.5Z'_x, S'_x) = 1045200mm^3$

$\phi M''_{sx} = 0.9 * 280 * 1045200/10^6 = 263\ kNm > M^*$

Design Calculations for Specimen #7

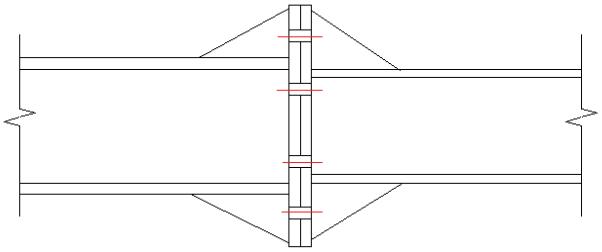

Figure 16- Schematic view of Specimen #9, (32mm end-plates with 14mm gussets)

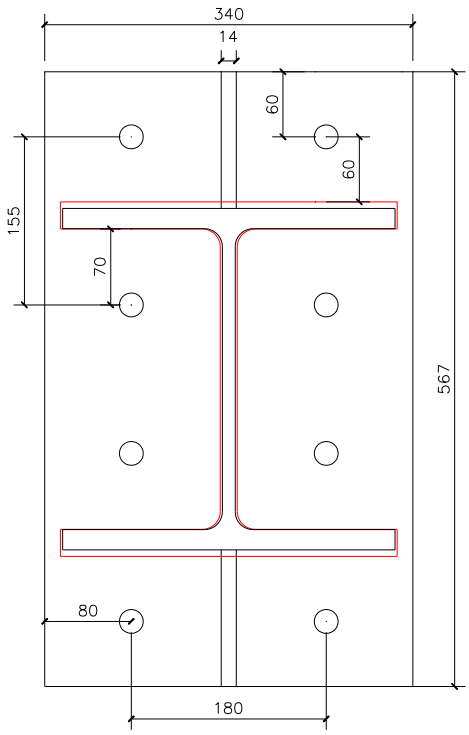

Figure 17- End-plate with thickness of 32mm, Grade 350 (Dimensions in mm)

$M_p = S_x * f_y = 1960 * 280 * 1000 = 548.8\ kNm$

$M^* = 0.9 * 0.5 * 548.8 = 247\ kNm$

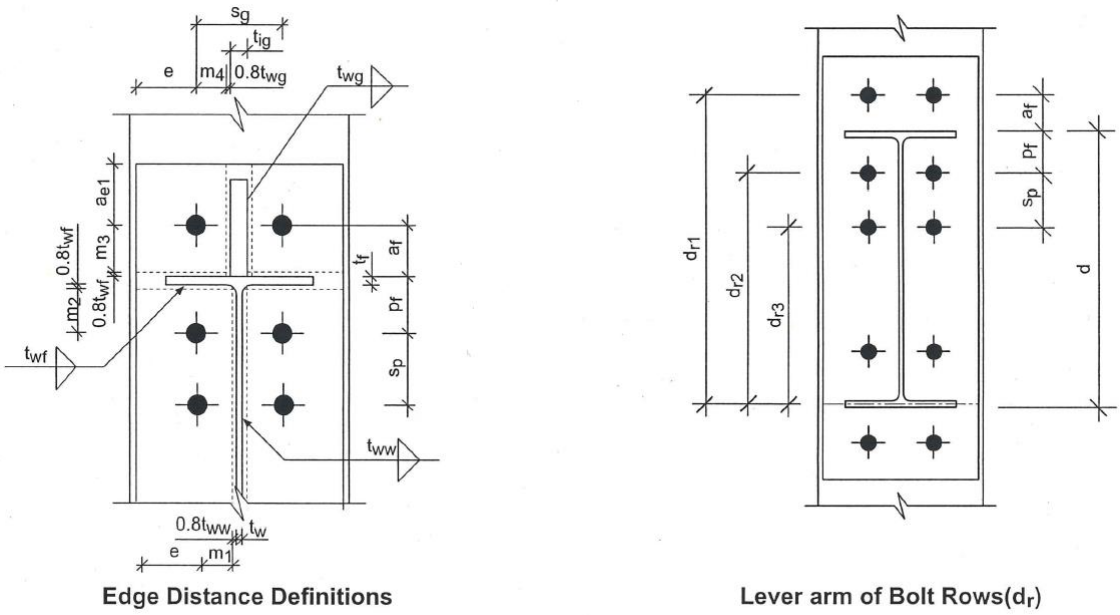

Figure 18- Definitions of edge distance and level arm of bolt row (HERA report R4-100.1:2003)

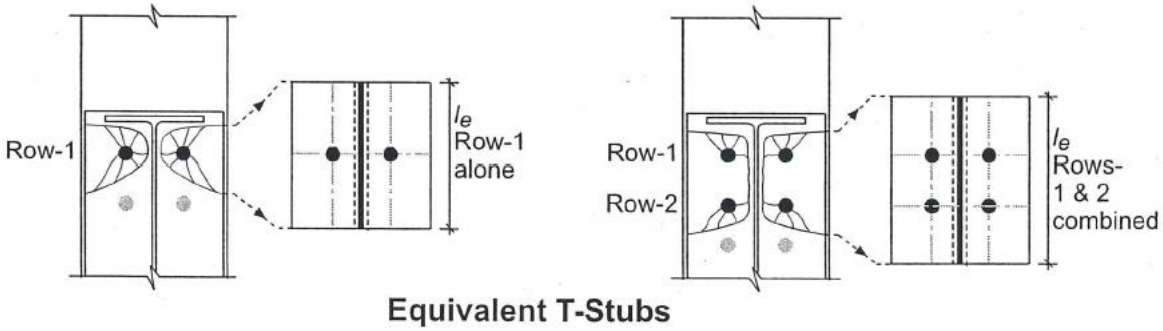

Figure 19- Equivalent T-stubs (HERA report R4-100.1:2003)

End plate bolt row design capacities:

$\phi N_{rx} = \min(\phi N_1, \phi N_2, \phi N_3, \phi N_v)$ Bolt row x capacity

$\emptyset N_1 = \frac{\phi_s f_{yi} l_{erx} t_i^2}{m}$ Mode 1: 4 plastic hinges in T stub

$\emptyset N_2 = \frac{0.5\phi_s f_{yi} l_{erx} t_i^2 + n2\phi_b N_{tf}}{m+n}$ Mode 2: 2 plastic hinges in T stub

$\emptyset N_3 = 2\phi_b N_{tf}$ Mode 3: Bolt only mode

$\emptyset N_v = 0.6\phi_s f_{yi} 2 l_{erx} t_i$ Moment interaction pull-out shear

$a_{e1} = 61.5mm$

$d_f = 24mm$

$d_h = 26mm$

$a_f = 67.8mm$

$d_{r1} = 373mm$

$d_{r2} = 217mm$

$\phi_w = 0.8$

$\phi_b = 0.8$

$\phi_s = 0.9$

$e = \frac{b_i}{2} - \frac{s_g}{2} = (340 - 180)/2 = 80mm > 2d_f$

Effective T stub length: First row of bolts in extension with gusset

With gusset thickness, t_{ig} = 14mm and fillet weld of t_w = 8mm all around:

$m_3 = a_f - 0.8t_{wf} = 61mm$	Bolt distance from flange weld
$m_4 = s_g/2 - t_{ig}/2 - 0.8t_{wg} = 76.6mm$	Bolt distance from gusset weld
$m = m_4 = 76.6mm$	Rows adjacent to end plate gusset
$n = \min(1.25m, a_{e1}) = 80mm$	Effective edge distance adjacent to gusset
$\lambda_1 = \frac{m_4}{m_4 + e} = 0.49$	Edge distance ratio
$\lambda_2 = \frac{m_3}{m_4 + e} = 0.39$	Edge distance ratio
$\alpha = 6.1$	Stiffened end-plate factor function of λ_1, λ_2

$l_{e1} = 2\pi m_4 = 481mm$	Circular yielding pattern
$l_{e2} = 4m_4 + 1.25e = 406mm$	Side yielding pattern

$l_{e3} = \alpha m_4 = 470mm$ Side yielding near flange pattern

$l_{e5} = 2m_4 + 0.625e + a_{e1} = 265mm$ Corner yielding pattern

$l_{e6} = \alpha m_4 - (2m_4 + 0.625e) + a_{e1} = 328mm$ Corner yielding near stiffener pattern

$l_{er1} = \min(l_{e1}, (l_{e2}, l_{e3})_{max}, (l_{e5}, l_{e6})_{max}) = 328mm$ Top bolt row effective T-stub length

Effective T stub length: Second row of bolts

$m_1 = s_g/2 - t_w/2 - 0.8t_{ww} = 77.6mm$ Bolt distance from web weld

$m_2 = p_f - t_f - 0.8t_{wf} = 63.6mm$ Bolt distance from flange weld

$m = m_1 = 77.6mm$ Rows adjacent to web

$n = \min(1.25m, e) = 80mm$ Effective edge distance adjacent to web

$\lambda_1 = \frac{m_1}{m_1 + e} = 0.49$ Edge distance ratio

$\lambda_2 = \frac{m_2}{m_1 + e} = 0.40$ Edge distance ratio

$\alpha = 6.1$ Stiffened end-plate factor function of λ_1, λ_2

$l_{e1} = 2\pi m_1 = 488mm$ Circular yielding pattern

$l_{e2} = 4m_1 + 1.25e = 410.6mm$ Side yielding pattern

$l_{e3} = \alpha m_1 = 473$ Side yielding near flange pattern

$l_{er2} = \min(l_{e1}, (l_{e2}, l_{e3})_{max}) = 473mm$ Effective T-stub length for second row of two bolts

For first row of bolts we have:

$$\left.\begin{array}{l}\phi N_1 = 1343kN \\ \phi N_2 = 568kN \\ \phi N_3 = 468kN\end{array}\right\} \Rightarrow \phi N_{r1} = 468kN$$

For second row of bolts we have:

$$\left.\begin{matrix}\phi N_1 = 1909kN \\ \phi N_2 = 708kN \\ \phi N_3 = 468kN\end{matrix}\right\} \Rightarrow \phi N_{r2} = 468kN$$

$$\phi M_{con} = \phi N_{r1} d_{r1} + \phi N_{r2} d_{r2} = 276\ kNm$$

$$capacity = \frac{276}{2 * 247} = 0.56\phi M_p$$

$$V_v = 0.6 * A_w * f_y = 0.6 * 300 * (315 - 2 * 18.7) * 11.9 = 594.6kN$$

$n_{bb} = 4$ Number of bolts at bottom flange bolt group

$\phi V_b = n_{bb}\phi_b V_{fn} = 532\ kN$ Bolt group shear capacity

$\phi V_i = \min(\phi V_{bi}, \phi V_{tti}, \phi V_{gsi})$ Plate shear

$\phi V_{bi} = n_{bb}\phi_s * 3.2 f_{ui} d_f t_i = 3981\ kN$ Bolt hole 1st bearing

$\phi V_{tti} = n_{bb}\phi_s * a_{e1} f_{ui} t_i = 3188\ kN$ Bolt hole 1st transverse tearing

$\phi V_{gsi} = 2\phi_s * 0.5 f_{yi} d_i t_i = 5581\ kN$ Gross transverse shear yield

$\phi V_{con} = \min(\phi V_b, \phi V_i, \phi V_{gsb}, \phi V_{ww}) = 532\ kN$ Connection design shear capacity

$$capacity = \frac{532}{0.9 * 594.6} = 0.99\phi V_y$$

Design Calculations for Specimen #10

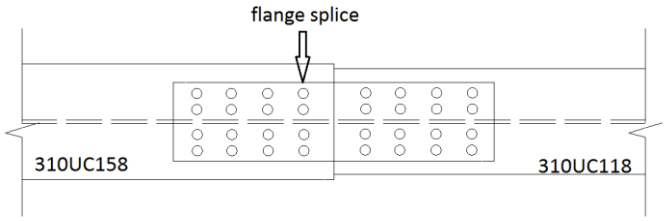

Figure 20- Schematic view of Specimen #7 tested about minor axis, (6mm fillers, 12mm flange plates)

Plastic moment capacity of 310UC118 about weak axis:

$M_{p(y)} = S_x * f_y = 893 * 280 * 1000 = 250\ kNm$

$M^* = 0.9 * 0.5 * 250 = 112.5\ kNm$ Targeting 50% of design moment capacity

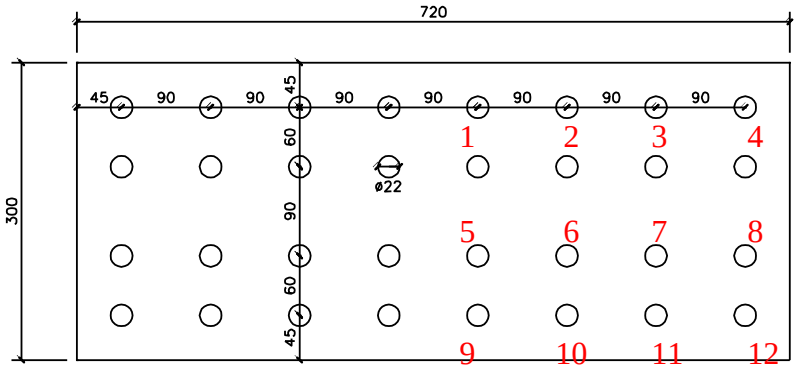

Figure 21- Flange splice with thickness of 12mm (Dimensions in mm)

Splice plate design for bending moment:

$d_i = 300mm$

$t_i = 12mm$

$\frac{d_i}{t_i} = 300/12 = 25 < 82 \Rightarrow compact\ plate \Rightarrow Z_{ei} = S_i = t_i\, d_i^2/4 = 270000mm^3$

$\phi M_p = 0.9 * 2 * 310 * 270000/10^6 = 150.7$

$$capacity = \frac{150.7}{2 * 112.5} = 0.67\phi M_{py}$$

Traditional elastic/vector analysis for bolts

Bolt number	x_i	y_i	r_i	V_i(KN)
1	-135	105	171	92.6
2	-45	105	114	61.7
3	45	105	114	61.7
4	135	105	171	92.6
5	-135	45	142	76.9
6	-45	45	64	34.6
7	45	45	64	34.6
8	135	45	142	76.9
9	-135	-45	142	76.9
10	-45	-45	64	34.6
11	45	-45	64	34.6
12	135	-45	142	76.9
13	-135	-105	171	92.6
14	-45	-105	114	61.7
15	45	-105	114	61.7
16	135	-105	171	92.6

$$J = \sum r_i^2 = 266308\ mm^2$$

$$\phi M_{bolt\ group} = \phi V_{fn} \times \frac{J}{r_i} = 144\ kNm \text{ Per cover plate}$$

$$Bolt\ group\ capacity = \frac{2 * 144}{2 * 112.5} = 1.28\phi M_{py}$$

Appendix B – Additional Information for Component testing

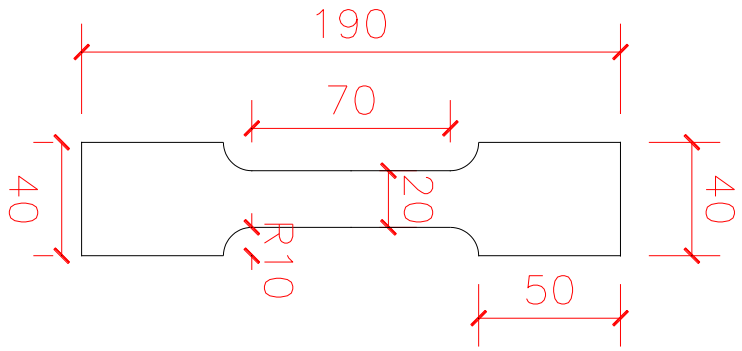

Figure 1- Steel coupon used to test splice plates

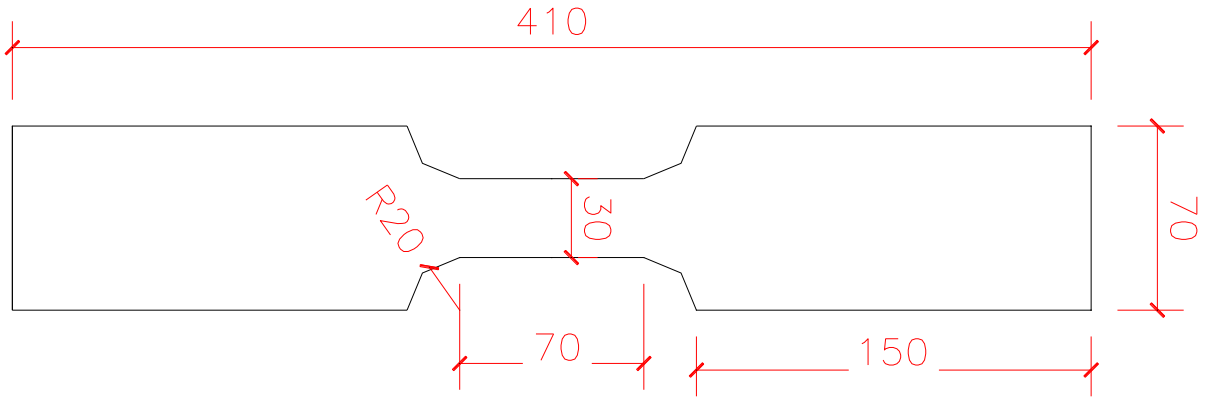

Figure 2- Steel coupon used to test column flange and web plates

Figure 3- Steel coupon showing necking after tensile test

Figure 4- Fracture of the steel coupon after testing, two fracture planes in the necking area

Figure 5- Fracture of the steel coupon after testing, one fracture plane at approximately 45-degree angle

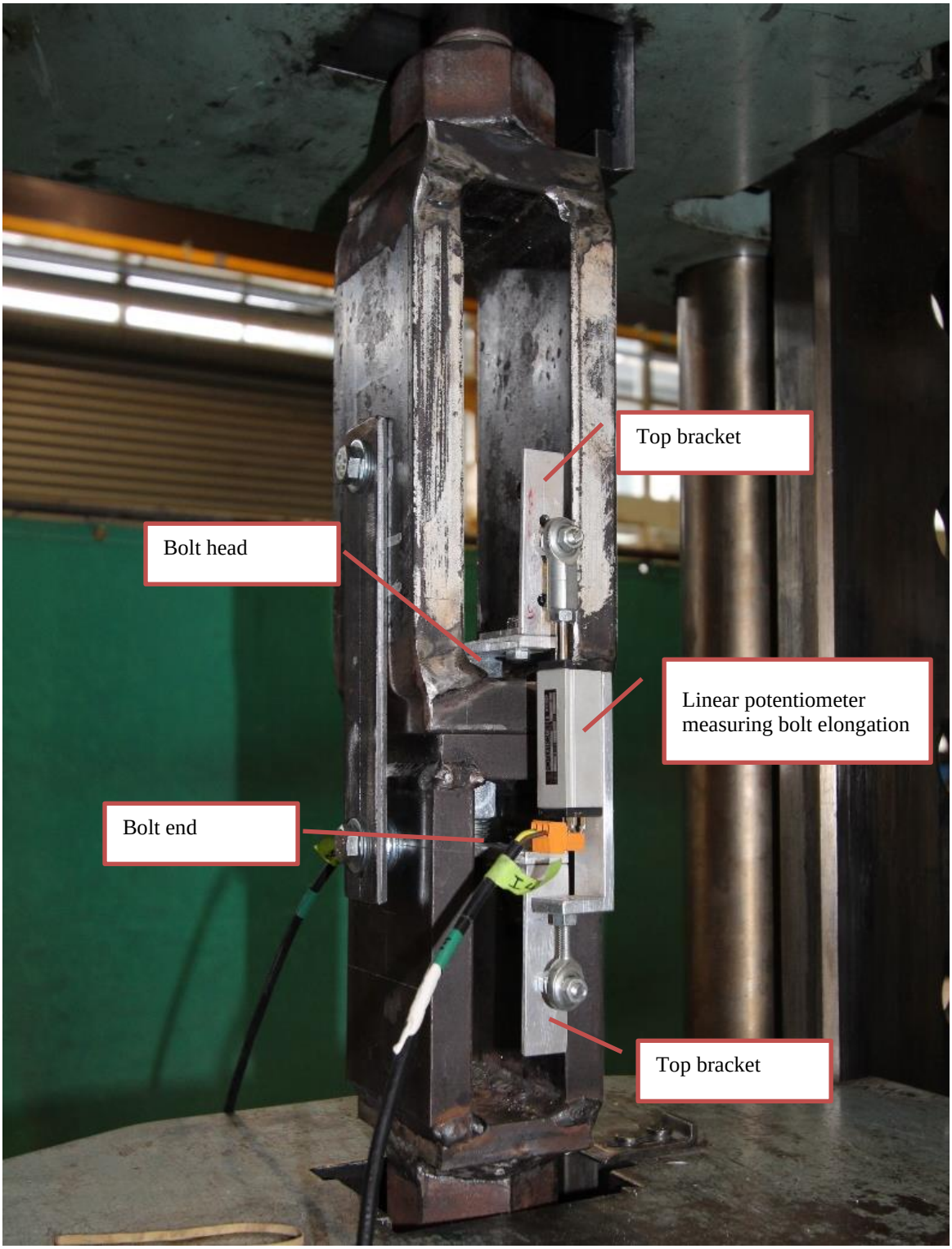

Figure 6- Bolt tensile test rig. Two linear potentiometers were used to measure elongation of the bolt. The potentiometers are connected to the two brackets glued to the bolt head and end.

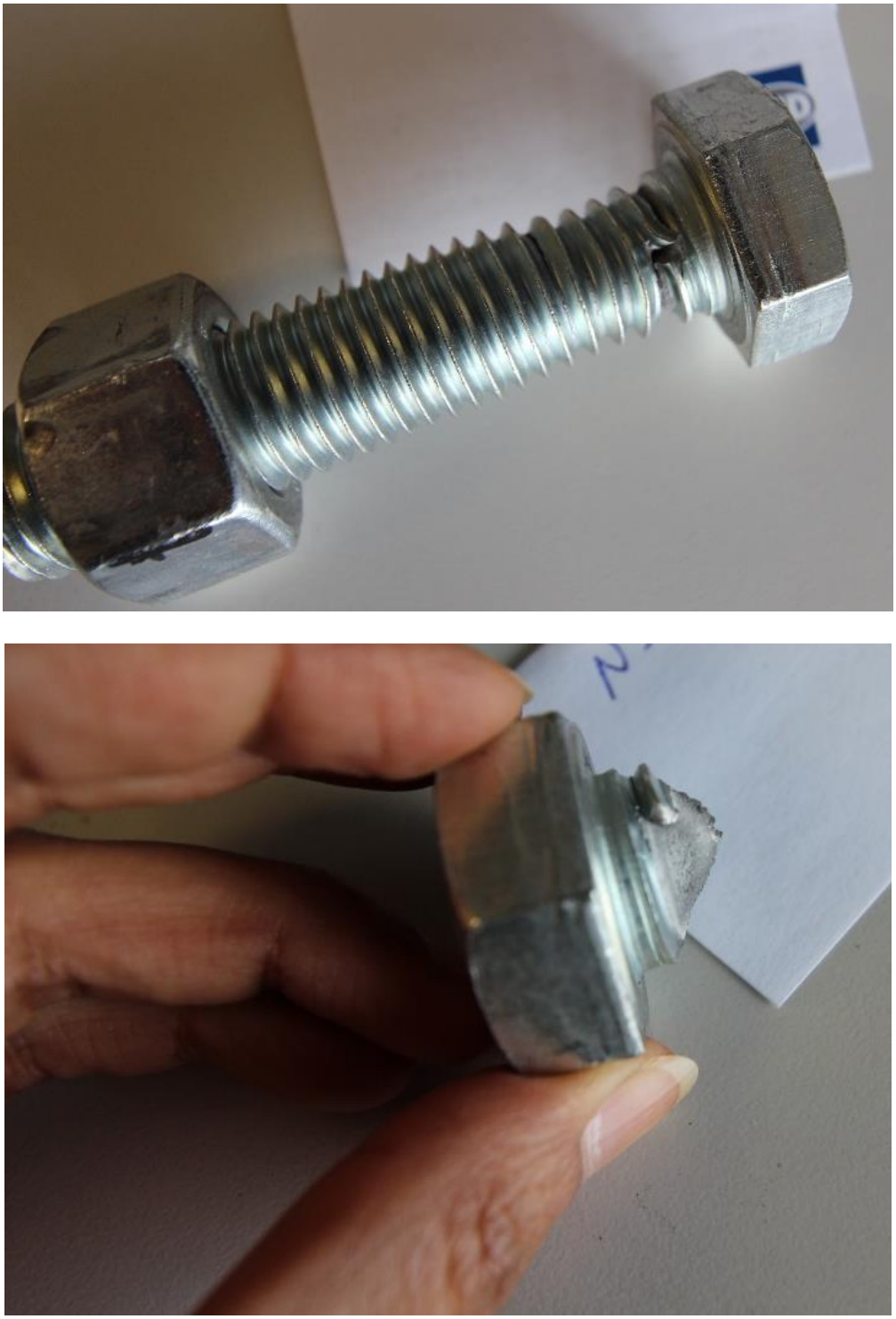

Figure 7- Necking and fracture near bolt head in fully threaded bolt

Figure 8- Necking at mid length of fully threaded bolt

Figure 9- Necking and fracture at the intersection of threaded and unthreaded length, in partially threaded bolts

Appendix C – Verification of Time History Results

To date, no research has been conducted to study seismic behaviour of moment frames which incorporates flexible column splice connection behaviour in the analysis. This lack of study limits the possibility of full verification of the results in this chapter by previous literature. However, indirect verification of frame responses are possible through comparing the previous study by (Gupta and Krawinkler, 1999) with frames including rigid column splice connections. The geometry of the frames studied in this chapter are identical to model M1 in (Gupta and Krawinkler, 1999), in which beams and columns extend from centreline to centreline and panel zones were not modelled. This model is recognized as the most commonly used model in structural engineering analyses.

Two main differences of the models here with the ones in (Gupta and Krawinkler, 1999) are use of concentrated plastic hinges and P-delta effect modelling. In model M1, P-delta effects were defined through attaching an imaginary elastic column to the moment frame with link elements. Large axial stiffness and negligible flexural stiffness was defined for the column so the column could bend with the moment frame without attracting bending moment. All tributary gravity loads were allocated to the P-delta column.

The first and second mode periods of the 9 story frame are 2.37Sec and 0.89Sec, respectively, which are consistent with the 2.34Sec and 0.88Sec values in the research conducted by (Gupta and Krawinkler, 1999). Similarly, the first and second mode periods of the 20 story frame are 4.01Sec and 1.38Sec, respectively, which are consistent with the 3.98Sec and 1.36Sec values in the research conducted by (Gupta and Krawinkler, 1999). Also, the median of peak story drift profiles for DBE and MCE levels, show very good agreement between the two models.

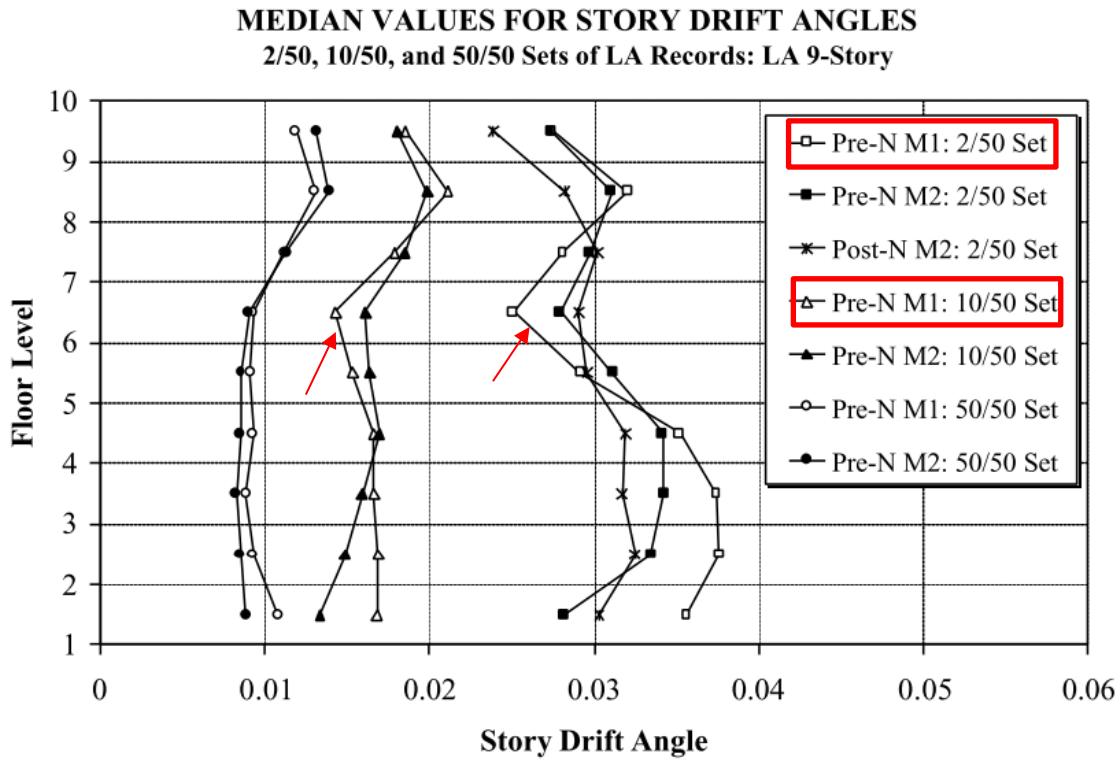

Figure 1- Story drift angle for 9 story moment frame, pre-Northridge design (Gupta and Krawinkler, 1999)

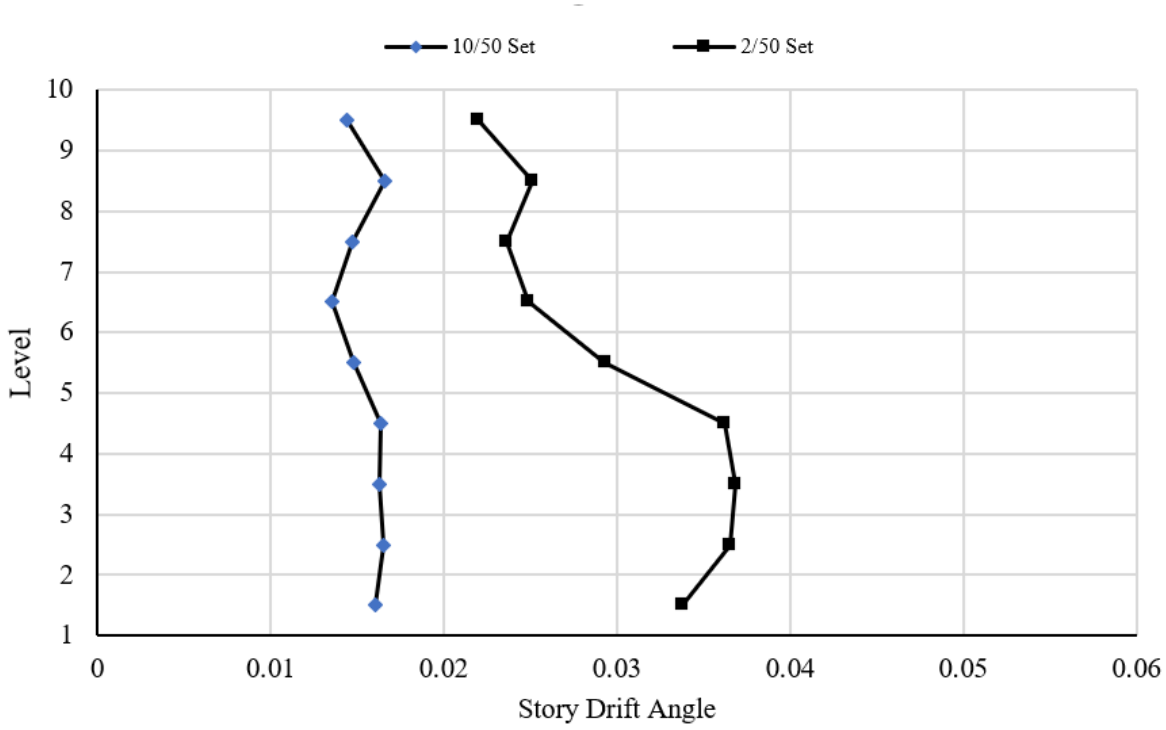

Figure 2- Story drift angle for 9 story moment frame, pre-Northridge design in this research

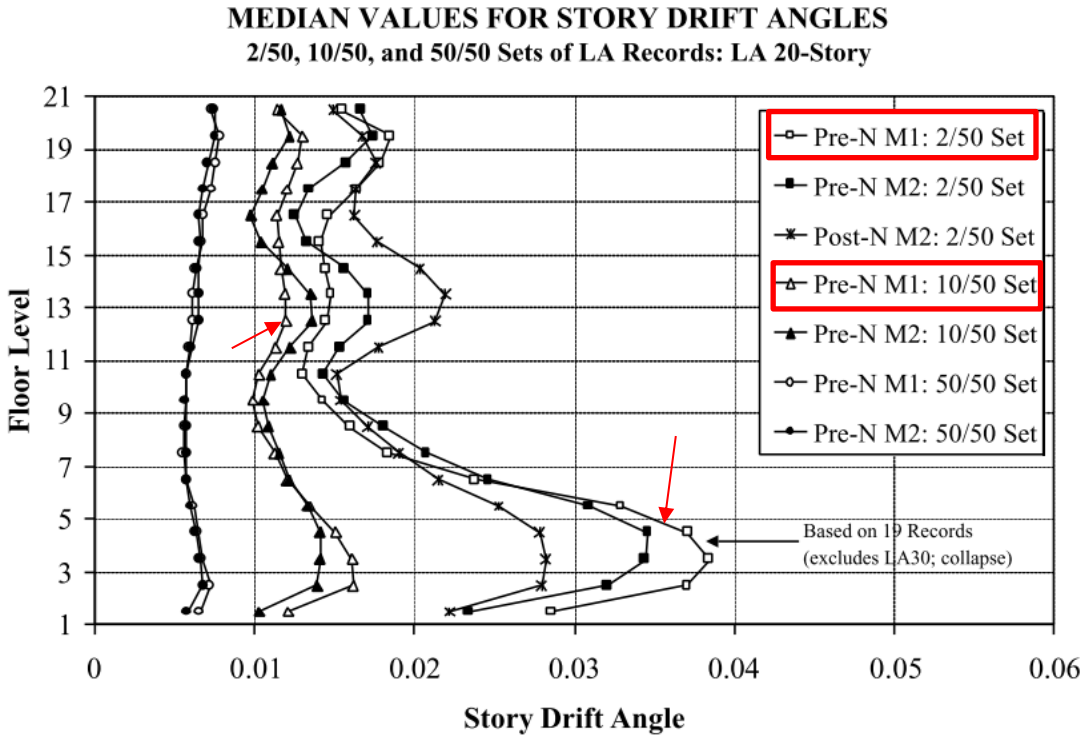

Figure 3- Story drift angle for 20 story moment frame, pre-Northridge design (Gupta and Krawinkler, 1999)

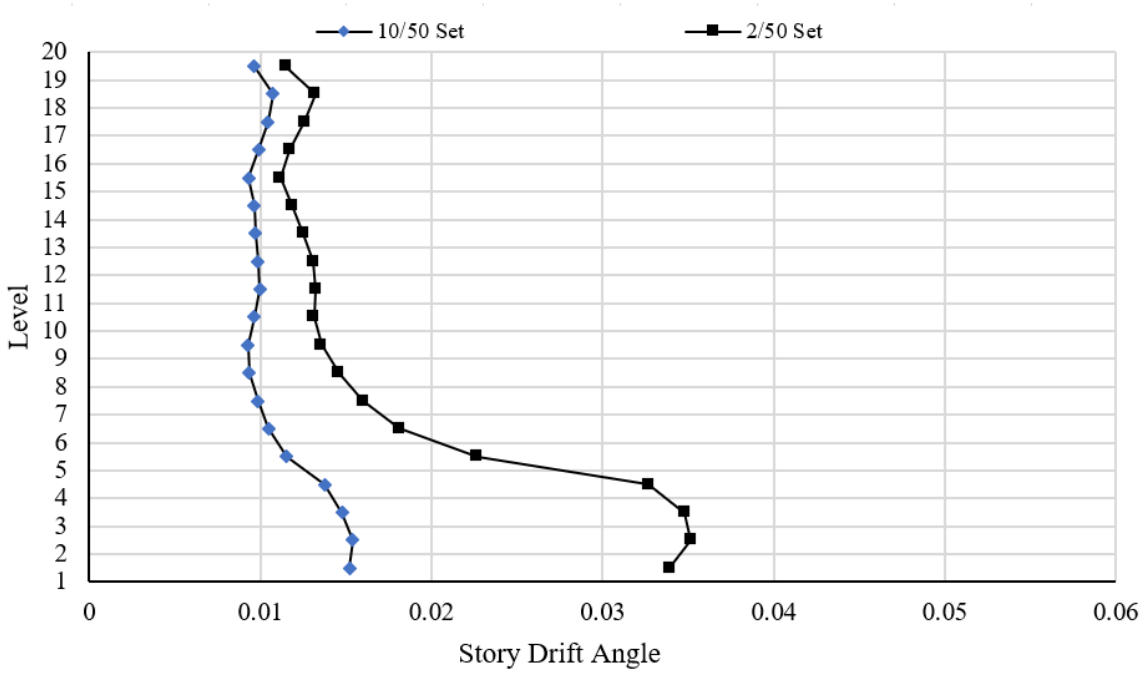

Figure 4- Story drift angle for 20 story moment frame, pre-Northridge design in this research